David Schweinzer, BA BSc

Optimization of the partial cooling process for the economic production of hot-formed ultra-high strength steel blanks in the automotive industry

MASTER'S THESIS

to achieve the university degree of

Diplom-Ingenieur

Master's degree programme: Production Science and Management

submitted to

Graz University of Technology

Supervisors

Univ.-Prof. Dipl.-Ing. Dr.techn., Christof Sommitsch

Ass.Prof. DDDipl.-Ing. Dr.mont., Josef Domitner

Institute of Materials Science, Joining and Forming

Research Group Tools & Forming

Graz, May 2019

Affidavit

I declare that I have authored this thesis independently, that I have not used other than the declared sources/resources, and that I have explicitly indicated all material which has been quoted either literally or by content from the sources used. The text document uploaded to TUGRAZonline is identical to the present master's thesis.

....

Date Signature

Eidesstattliche Erklärung

Ich erkläre an Eides statt, dass ich die vorliegende Arbeit selbstständig verfasst, andere als die angegebenen Quellen/Hilfsmittel nicht benutzt, und die den benutzten Quellen wörtlich und inhaltlich entnommenen Stellen als solche kenntlich gemacht habe. Das TUGRAZonline hochgeladene Textdokument ist mit der vorliegenden Diplomarbeit identisch.

....

Datum Unterschrift

Acknowledgement

First, I want to thank Univ.-Prof. Dipl.-Ing. Dr.techn. Christof Sommitsch for his supervision and evaluation of my master's thesis. In addition, I want to thank my supervisor Dr. Josef Domitner for his support and for the possibility to write my master's thesis at the Institute of Materials Science, Joining and Forming, Research Group Tools & Forming. I also want to highlight, that this work would have never been possible without the excellent expertise of Dipl.-Ing. Vladimir Bošković.

Furthermore, I want to point out that this thesis would have never been possible without the company EBNER Industrieofenbau GmbH and I would also like to express my gratitude to all their employees, especially Dipl.-Ing. Peter Seemann who gave me the possibility to write my thesis in collaboration with this company. I would also thank Mr. Lukas Heitzmann, Mr. Harald Humer, Mr. Daniel Schatz, Mr. Mustafa Musič, Dipl.-Ing. Carsten Broermann, Ing. Sandra Intering, and Mr. Anton Oppermann MSc for their pathbreaking and supportive way in every section of this project.

Additional thanks go to all the other colleagues working at the Institute of Materials Science, Joining and Forming for their excellent cooperation and which continuously supported and guided me with all their knowledge and experience during the whole time of conducting my thesis.

Furthermore, a special thank you goes to my parents and my girlfriend, who showed loads of empathy, patience, and support during that journey.

Without the support of the people listed above the encouraging outcome of this thesis would have never been possible.

Abstract

The growing number of vehicles on our roads will result in new laws and regulations to reduce greenhouse gas emissions and to make driving cars more safely. Besides increasing material mixes and even more complex part geometries the stiffness requirements and especially tailored parts will get a high focus in developing new body-in-white applications in the future. In fact, the decrease of car body weight leads to a significant reduction of the carbon footprint due to lower fuel consumption. Therefore, the big challenge for car manufacturers is to find a balance between increasing weight and the need for weight reduction of vehicles regarding safety, comfort, driving performance and fuel consumption. In other words, the safety of car occupants and the weight of vehicles play a significant role when developing modern car bodies.

Press hardening is the solution for the economic production of contemporary automobile components. Tailored tempering represents a special form of this technology enabling the creation of light-weight parts with customized workpiece properties regarding strength, hardness and ductility. This method combines ideal stiffness in order to obtain minimal deformation of the passenger cabin and the ability to absorb energy. Thus, the crash safety of passengers will be drastically improved while the weight of cars simultaneously will be reduced when using thinner high strength steel blanks.

Besides conducting a branch analysis, the theoretical part of this thesis demonstrates which state-of-the-art technologies currently exist in the field of tailored tempering having a strong focus on the automotive industry.

The focus of the practical part is to conduct various experiments with regard to EBNER's partial cooling technology used for the thermal treatment of blanks. The outcome of changed process parameters is studied and continuously improved in order to get customized safety components with different material properties in one piece.

Kurzfassung

Aufgrund der Tatsache, dass die Anzahl der Autos auf unseren Straßen in den folgenden Jahren drastisch ansteigen wird, werden neue Gesetze und Vorschriften notwendig sein, um die Treibhausgasemissionen reduzieren zu können, und auch um das Autofahren sicherer zu machen. Neben dem zunehmenden Materialmix und den komplexeren Teilegeometrien, werden die Steifigkeitsanforderungen, und im Speziellen maßgeschneiderte Teile einen hohen Fokus bei der Entwicklung von zukünftigen Body-in-White-Applikationen erhalten. Tatsächlich führt die Verringerung des Karosseriegewichts zu einer signifikanten Verringerung des CO_2-Fußabdrucks, da dann weniger Treibstoff verbraucht wird. Daher besteht die große Herausforderung für Automobilhersteller darin, ein Gleichgewicht zwischen einerseits zunehmendem Gewicht, und andererseits der Notwendigkeit einer Gewichtsreduzierung von Fahrzeugen in Bezug auf Sicherheit, Komfort, Fahrleistung und Treibstoffverbrauch zu finden. Mit anderen Worten, die Sicherheit der Fahrzeuginsassen und das Gewicht der Fahrzeuge spielen eine wichtige Rolle bei der Entwicklung moderner Fahrzeugkarosserien.

Das Presshärten ist die Lösung für die wirtschaftliche Herstellung zeitgemäßer Automobilkomponenten. Tailored Tempering stellt eine Sonderform dieser Technologie dar, welche die Herstellung von Leichtbauteilen mit angepassten Werkstückeigenschaften hinsichtlich Festigkeit, Härte und Verformbarkeit ermöglicht. Diese Methode kombiniert ideale Steifigkeit, um eine minimale Verformung der Fahrgastzelle und des Fahrzeugs zu erreichen, mit der Fähigkeit, Energie zu absorbieren. Somit verbessert sich die Aufprallsicherheit der Passagiere drastisch, während gleichzeitig durch den Einsatz von dünneren hochfesten Stahlblechen das Gewicht der Automobile reduziert wird.

Neben der Durchführung einer Branchenanalyse wird im theoretischen Teil dieser Arbeit gezeigt, welche Technologien am aktuellen Stand der Technik im Bereich des Tailored Tempering, mit einem starken Fokus auf die Automobilindustrie existieren.

Der Schwerpunkt des praktischen Teils besteht in der Durchführung verschiedener Experimente bezüglich der partiellen Kühltechnologie von EBNER, die bei der thermischen Behandlung von Platinen eingesetzt wird. Das Ergebnis geänderter Prozessparameter wird untersucht und kontinuierlich verbessert, um kundenspezifische Sicherheitskomponenten mit unterschiedlichen Materialeigenschaften in einem Stück zu erzeugen.

Symbols and acronyms

List of symbols

$\dot{v}_N$	Nitrogen flow in the upper area of the contact cooler [m^3/h]
$\dot{v}_w$	Cooling medium flow in the contact cooler [lpm]
A_{50}	Elongation at fracture [%]
A_{c1}	Blank austenitization start temperature [°C]
A_{c3}	Blank austenitization finish temperature [°C]
$CR_{fqt\_750\text{-}200}$	Cooling gradient between 750 and 200°C of the flat quenching tool [°C/sec]
Fe_3C	Cementide
F_p	Press force of the flat quenching tool [kN]
I_i	Input
l_b	Blank length [mm]
M_f	Martensite finish temperature [°C]
M_s	Martensite start temperature [°C]
O_i	Output
R_m	Ultimate tensile strength [MPa]
R_{m_ad}	Ultimate tensile strength as-delivered [MPa]
R_{m_h}	Ultimate tensile strength of the hard zone [MPa]
R_{m_hf}	Ultimate tensile strength after quenching [MPa]
R_{m_s}	Ultimate tensile strength of the soft zone [MPa]
$R_{p0,2}$	Yield strength [MPa]
s_b	Blank thickness [mm]
s_{tz}	Size of the transition zone [mm]
$t_{700\_crit\_i}$	Critical transfer times until a minimum allowable hot zone insertion temperature of approximately 700°C is reached [sec]
$t_{700\_i\_j\_av}$	Actual values of lower and upper transfer times [sec]
$t_{700\_i\_j\_sv}$	Set values of lower and upper transfer times [sec]
T_a	Room temperature [°C]
T_{bi_h}	Insertion temperature of the hard zone before quenching [°C]
T_{bi_s}	Insertion temperature of the soft zone before quenching [°C]
t_{c_cc}	Contact time of the contact cooler [sec]
T_f	Furnace temperature [°C]
t_{fqt}	Quenching time of the flat quenching tool [sec]
t_h	Blank heating time [sec]
$t_{i\_j\text{-}pt}$	Ideal contact times of the contact cooler [sec]
$t_{i\_pt\text{-}700}$	Ideal furnace dwell times after the contact cooler [sec]
T_{m_al}	Melting point of aluminum [°C]
T_{m_cu}	Melting point of copper [°C]
$T_{max\_nail\ i}$	Maximum temperature of the nails [°C]
T_{out_TC1}	Temperature of the pre-cooled zone before moving out of the furnace [°C]
T_{out_TC2}	Temperature of the hot zone before moving out of the furnace [°C]
T_{pt}	Temperature when the phase transformation starts [°C]
T_{tool_i}	Quenching temperature in the end of the quenching process [°C]
w_b	Blank width [mm]
X_i	Controllable factors

YS_{ad}	Yield stress as-delivered [MPa]
YS_{hf}	Yield stress after hot forming [MPa]
Z_i	Uncontrollable factors
α‘-Fe	Martensite
α-Fe	Ferrite
γ-Fe	Austenite
λ	Heat conductivity [W/(m*K)]

List of acronyms

AHSS	Advanced high strength steels
AS	Aluminum-silicon
ASS	Austenitic stainless steels
BCT	Body-centered tetragonal
BE	Backscatter electron
BH	Bake hardenable
BiW	Body-in-white
CAFE	Corporate average fuel economy
CCT	Continuous cooling transformation
CFB	Carbide-free bainitic
CMn	Carbon-manganese
CP	Complex phase
CR_i	Cooling rates
DMF	Direction of material flow
DoE	Design of experiment
DP	Dual phase
DPH	Direct press hardening
EDX	Energy-dispersive X-ray spectrometer
FCC	Face-centered cubic
GHG	Greenhouse gas
HPH	Hybrid press hardening
HSLA	Low alloyed high strength
HSS	High strength steels
HV	Vickers hardness
HZ	Hard zone
ID	Identification
IF	Interstitial free
IPH	Indirect press hardening
LDV	Light-duty commercial vehicle
LME	Liquid metal embrittlement
LSS	Low strength steels
MS	Mild steels
MSPH	Multi-step press hardening
N.i.	No information available
OEM	Original equipment manufacturer
OM	Optical microscopy
PE	Primary electron
PHS	Press hardened steels
Q&P	Quenching and partitioning
SE	Secondary electron
SEM	Scanning electron microscope
SimCAL 3.0	Simulator for continuous heat treatments of blanks
SZ	Soft zone
TC	Thermocouple
TE	Total elongation
TPP	Tailored property part

TRBs	Tailor rolled blanks
TRIP	Transformation-induced plasticity
TWBs	Tailor welded blanks
TWIP	Twinning induced plasticity
UHSS	Ultra-high strength steels
ULSAB	Ultra-light steel auto body
UTS	Ultimate tensile strength
YS	Yield stress

Table of contents

1 Introduction

This chapter provides an overview of the major trends influencing the automotive industry and which challenges car manufacturers have to face regarding the production of regulations-fulfilling state-of-the-art vehicles.

Trends influencing the automotive sector

Analysts within the automotive industry have calculated that the total amount of vehicles has already reached the number of 1.2 billion worldwide. In addition, this number is rapidly growing because of suggested rising annual sales from 84 million in 2017 up to 127 million by 2035. In other words, we will hit the number of two billion cars on the roads around the globe by 2035. [1] These facts play a major role for developing new cars because upcoming decarbonization commitments and emission targets become more stringent and have to be fulfilled to avoid penalties. One of these targets is set by the European Union aiming to reduce road transport emissions being a trend setting nation concerning this topic. [2] An outstanding point of the European Climate Change Program is that the carbon dioxide emission target of 95g CO_2/km has to be met by all new cars on the European market by 2021. This represents a reduction of approximately 40% compared to the average CO_2 emissions of 158.7g CO_2/km of the same car fleet back in 2007. [3, 4] Similar actions regarding the reduction of CO_2 emissions are set by the United States of America with their target to achieve 99g CO_2/km by 2025 and other nations displayed in figure 1. [5]

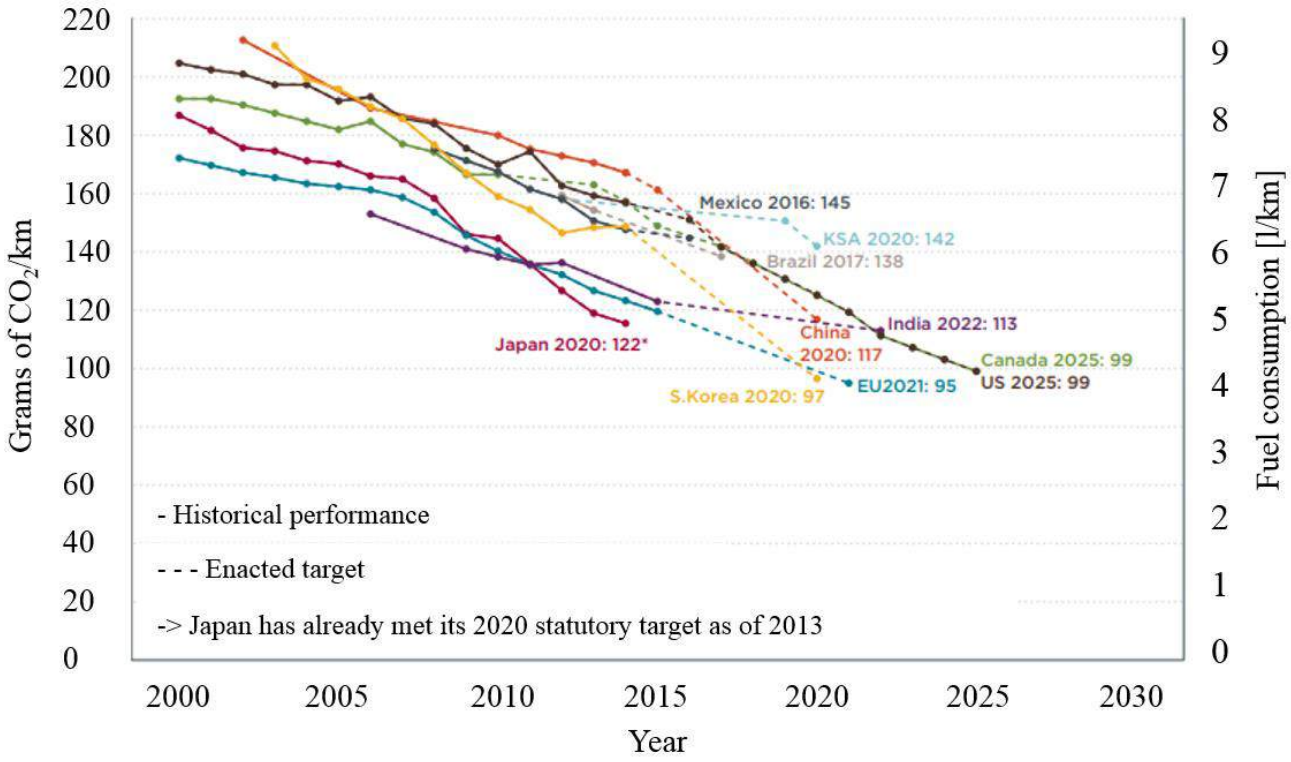

Figure 1: Decreasing international CO_2 emission trends in different countries (based on: [5])

Another example for being a driving factor for vehicle manufacturers is the so-called Corporate Average Fuel Economy (CAFE) regulation enforced by the United States affecting light trucks and cars. New regulations are forcing light-duty commercial vehicles (LDVs) to have a fuel consumption of about 54.5mpg by 2025. [3, 6, 7] Therefore, the ability to meet upcoming emission regulations and fuel efficiency standards is a driving factor for the rapid development of cost-efficient ultra-high strength steel (UHSS) parts for the automotive industry. Then, it is possible to produce light-weight parts with lower blank thicknesses whilst generating the same or even higher strength values. Light-weight design of cars even has the potential to trim overall body-in-white (BiW) mass by about 50%. In fact, these were only some of numerous activities pushing the development of press hardened manganese-boron steel parts in the automotive sector due to their high potential of saving vehicle mass. This technology especially provides the possibility to produce light-weight tailored part geometries without neglecting collision safety. Summing up, the reduced overall vehicle mass then leads to fewer fuel consumption and in addition to other positive side effects, such as lower greenhouse gas (GHG) emissions. [3, 8]

Challenges

Conventional press hardening methods do not provide the production of BiW parts with varying mechanical properties looking at one and the same steel blank. This leads to an insufficient crash performance because these martensitic steels then provide inadequate properties to ensure high energy absorption in case of a car accident. Furthermore, problems with mechanical joining techniques arise if the whole part has an ultra-hard martensitic microstructure. There exist many different press hardening methods to locally adapt mechanical properties. Nonetheless, most of them are insufficient because of not providing flexible part geometries and because of producing too big transition zones which then have a negative impact on the crash performance of cars. Therefore, the challenge is to develop a flexible tailored tempering technology offering minimal transition zones whilst fulfilling the mechanical requirements regarding ductile and hard zones expected of car manufacturers. The positive effects regarding different material properties of BiW parts is demonstrated by the hot stamped B-pillar in the 2017 Chrysler Pacifica. Besides of a total weight reduction of 8.64kg and reduced costs of material, a better collision performance was achieved. [9, 19]

Figure 2 shows the increased crash performance that can be achieved by using a press hardened component.

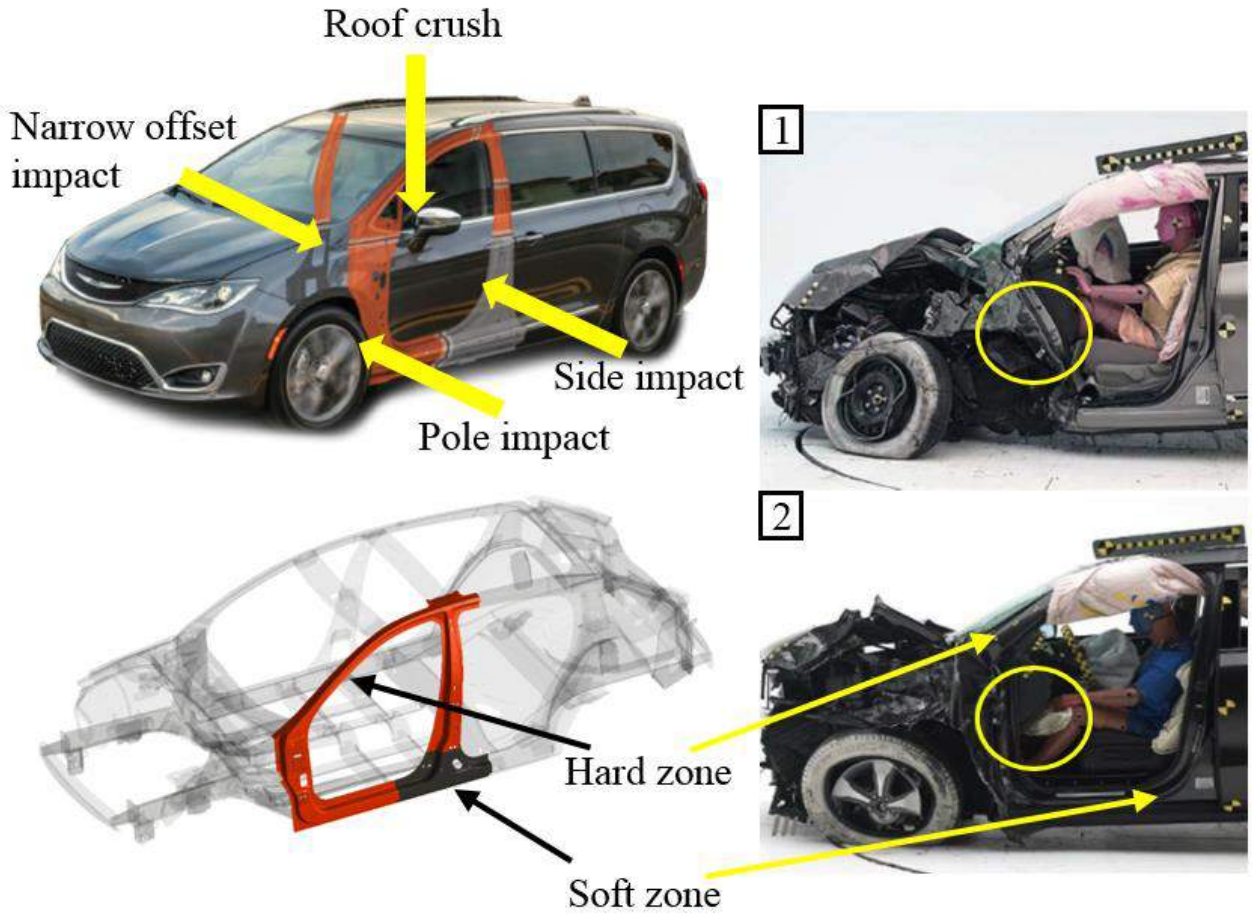

Figure 2: 2017 Chrysler Pacifica with different collision performances (1: conventional door ring, 2: door ring with hot-formed components (based on: [9]))

In fact, a state-of-the-art press hardening method should be able to meet upcoming technological challenges related to heat treatment and forming processes within the automotive industry which are listed within table 1.

Challenges	
• improved cycle times • higher complexity of components with reduced weight • systems enabling TPP • process control/ monitoring • high quality mass production with high output rates	• better cost-benefit ratio per part • better lead times • high availability and reliability of the production system • pre-coating to avoid scale formation above furnace temperatures of T_f = 600°C • output rates-dependent cooling time

Table 1: Challenges in the automotive industry regarding the production of BiW parts (based on: [4, 8, 10, 11])

2 State-of-the-art

A short introduction to high strength materials which are commonly used in the automotive sector will be discussed in the context of chapter 2. In addition, special attention is paid to the most commonly used steel grades used for press hardening. The process-specific features of press hardening will be explained before local adaptation strategies regarding partial press hardening and the branch structure analysis will be discussed in detail.

2.1 High strength materials in the automotive industry

There are numerous ways to categorize steels which are relevant for the production of automobiles. One prevalent designation is done according to figure 3 showing the total elongation (TE) as a function of the ultimate tensile strength (UTS) with the so-called "banana curve". Low strength steels are placed on the left side of the graphic representing traditional steel grades, such as interstitial free (IF) and mild steels (MS). These grades are known for their high ductility and for their low UTS levels below 270MPa. According to Billur et al., these types of steel were mostly applied in cars until the 1990s. [12, 13]

The need for lower fuel consumption of cars and the Ultra-Light Steel Auto Body (ULSAB) project lead engineering efforts towards the production of steels with higher strength values. This was provided by conventional high strength steels (HSS) marked in brown in figure 3. HSS are placed between UTS levels starting from 270MPa reaching up to 700MPa whereas ultra-high strength steels have UTS levels greater than 700MPa. [6, 14] The development of UHSS focuses on meeting increasing passenger safety requirements by enabling the production of complex and low weight safety components for cars. In fact, these advanced high strength steel (AHSS) blanks are no longer indispensable when producing high strength parts with improved formability behavior providing optimal absorption of energy in case of a car crash. Some representatives of this steel grade can be seen in the right area of figure 3. [6] The development trends of AHSS go towards the achievement of steel grades with at least the same elongation - but higher strength-levels (considering the yield stress (YS) and the UTS) compared to the already existing conventional HSS and UHSS types. Current examples for such steel grades are highlighted in gray. [14, 6]

Press hardenable steel (PHS), such as 22MnB5, is the most important steel grade for this thesis. The growing demand for PHS is based on multiple advantages generated by hot forming. This allows to overcome the poor formability behavior compared to cold form steels and offers the possibility to produce thinner and more complex car components with UTS levels ranging between 1500 and 2000MPa. Furthermore, this leads to tremendous cuts in weight of the BiW and especially assures meeting the same crash safety requirements as thicker blanks do. It must be noted, that 22MnB5 is the most commonly used cold-rolled boron-alloyed manganese press hardening steel grade which has more than 1500MPa UTS and up to 1000MPa YS after being quenched. [6, 15, 14, 16, 17]

The different steel grades available on the market are illustrated in figure 3.

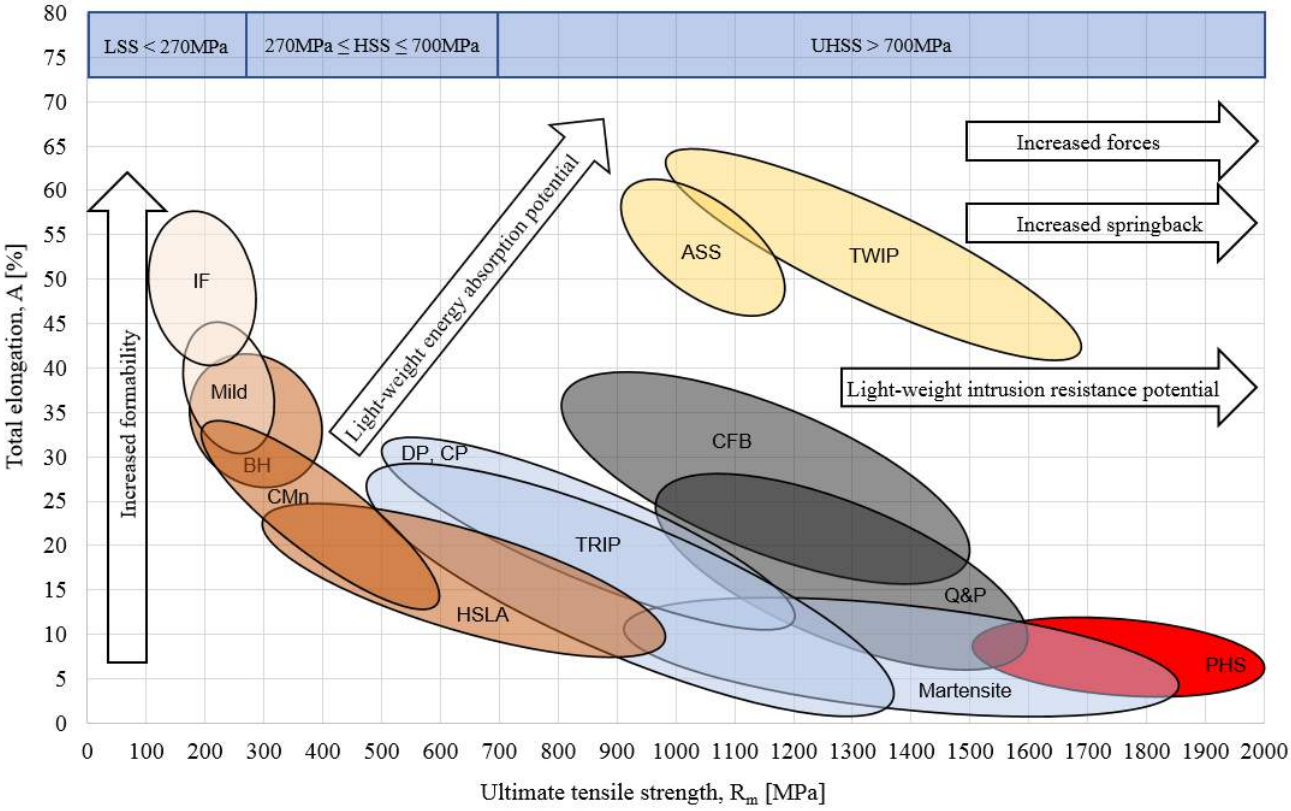

Figure 3: Schematic illustration of steel grades used in the automotive industry (based on: [12, 14, 20, 21])

Press hardening

The history of press hardening starts in the early 1970s when a company named Plannja HardTech AB, which was a tier 1-part manufacturer for construction and agricultural industries and a subsidiary of the Swedish steel manufacturer Norbottens Järnverk AB developed a process for the production of lawn mower- and saw-blades, forks, spades, plough shares, and disc harrows. This technology also got patented in 1974 and the patent GB1490535 got published afterwards in 1977. [22] After 1975 carmakers also got interested in this upcoming hot stamping technology leading to collaborative research and numerous activities in that field, continuously pushing the development of press hardening. [23] ThyssenKrupp Steel AG enabled the production of hot stamped B-pillars for the 2006 VW Tiguan by making use of the first commercialized tailored heating technology meeting increasing quality in crashworthiness in a better way compared to conventional press hardening. Another milestone in press hardening history was the usage of tailor welded blanks (TWBs) for hot-formed B-pillars of the 2007 Audi A4. [24] It is also worth noting, that these multiple activities in the area of press hardening increased the production of press hardened components up to 20 times more than in 1997 which stands for 124 million produced parts per year in 2010. [20] The B-pillar of 2011's Audi A6 was the first commercialized hot forming application making use of the tailored quenching technology invented five years before in 2006. [24] The worldwide production of hot-formed components in 2015 rose up to approximately 300 million parts per year. This seems to have an enormous potential for the company EBNER to emphasize in

the continuous improvement process with special regard to their press hardening furnace solutions. [25] Therefore, EBNER tries to meet specific customer requirements whilst pushing the development of a flexible tailored tempering process. This approach has various benefits explained in detail within this work.

The following graphic illustrates the major evolutionary milestones in the development of the hot forming technology from its start until now.

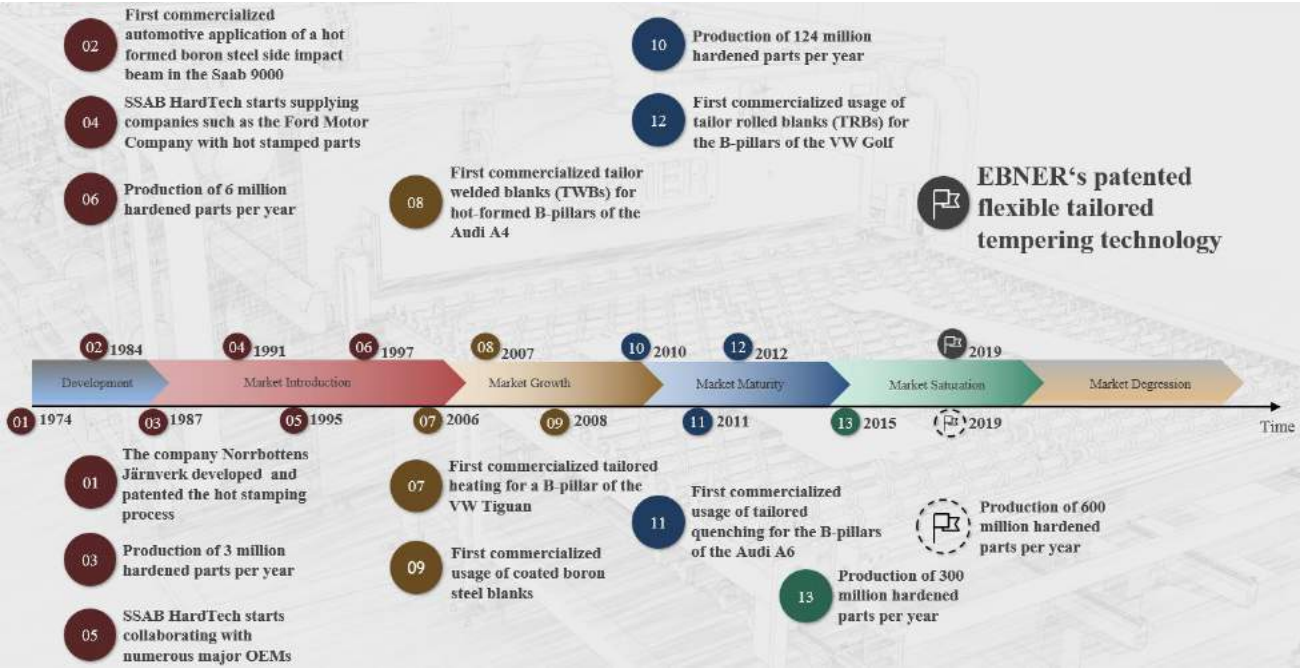

Figure 4: Milestones in the hot forming technology (based on: [20, 24, 25])

Press hardening methods

Press hardening can also be found in literature named hot stamping or hot press forming. It enables the production of complex part geometries by using manganese-boron steel blanks. According to Billur, press hardening can be differentiated between four different processes:

- indirect press hardening (IPH)
- direct press hardening (DPH)
- hybrid press hardening (HPH), and
- multi-step press hardening (MSPH). [14]

The DPH method will be explained in detail because this type of process represents the base for the economic production of tailored part properties which will be investigated in context of this thesis.

Direct press hardening

The DPH method provides various advantages compared to the IPH method, such as a low number of process steps, simple furnace technologies, cost efficiency for simple part geometries, optimized material usage etc. Therefore, according to Veit et al., DPH is preferred within the automotive industry offering typical cycle times between 10 and 20 seconds. [14, 38, 60] It is important to understand the DPH method, which is the base for improving the partial cooling process the practical part of this thesis deals with. Figure 5 illustrates the entire DPH process chain in detail, with numerous strategies currently being used to tailor the final part properties. Chapter 2.2 then provides more information about the pre-processing techniques being the most relevant ones for this thesis.

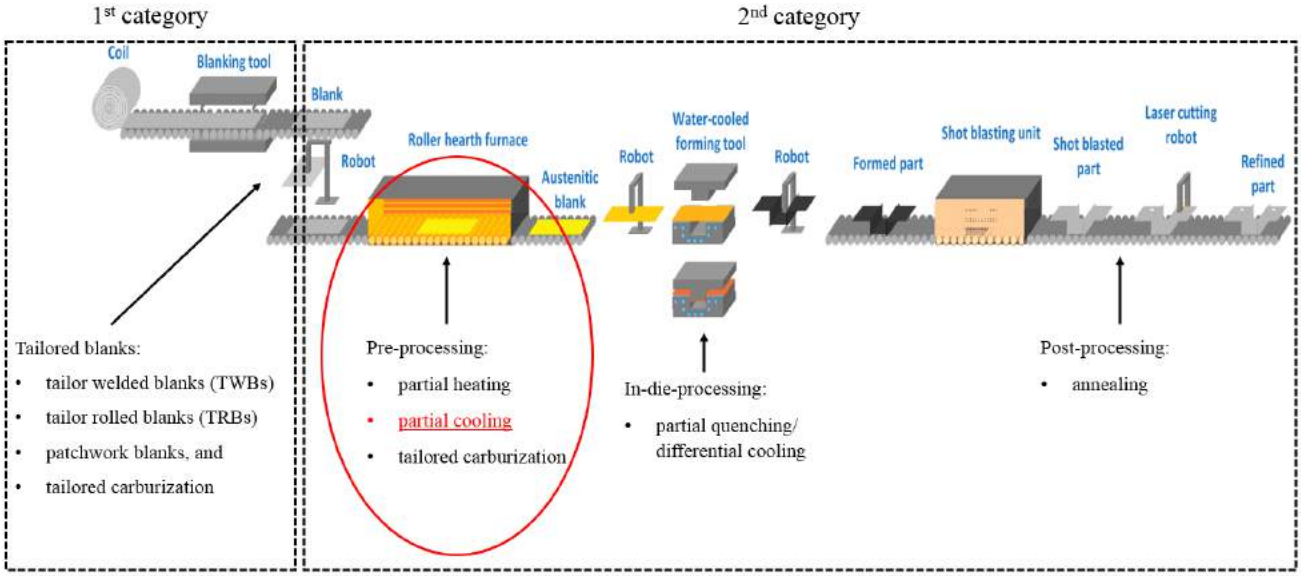

Figure 5: DPH and methods for locally adjusting mechanical properties of steel blanks (based on: [20, 61, 63])

First, the blanks are trimmed from a coil. The initial ferritic-pearlitic condition of the blanks has a body-centered cubic (BCC) crystal structure with UTS- and ductility-levels of about 600MPa respectively 25%. Then, the parts are homogenously austenitized at a furnace temperature ranging between $880 \leq T_f \leq 950°C$ for achieving a fully austenitic state (γ-Fe). The optimal soak time which ensures complete austenitization is set between one to eight minutes, primarily depending on the coating and the sheet thickness. This then leads to a face-centered cubic (FCC) structure of the steel. In addition, this process step helps permitting interlayer coating, dissolving carbides, and ensuring the creation of required austenitic grain growth to achieve hardenability in the end of the process chain. After the blank gets transferred and settled in the water-cooled tool, forming and quenching follow until the quenching temperature in the end of the quenching process T_{tool_i} is reached before the shot blasting and laser cutting parts of the process follow. [20, 50, 52]

Figure 6 represents a conventional blank heat treatment process using a conventional roller-hearth furnace.

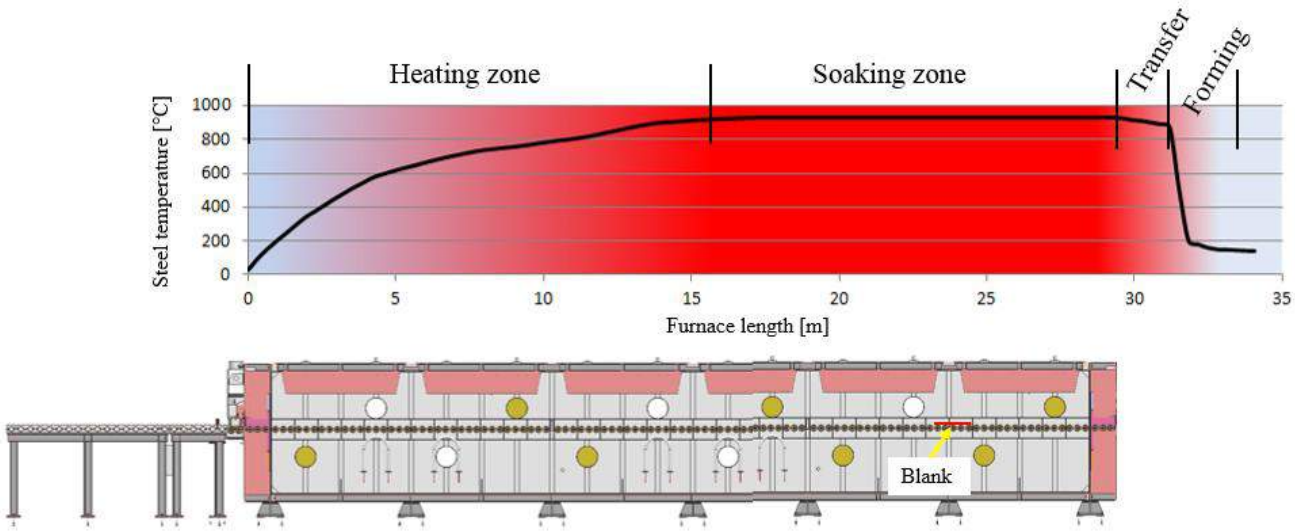

Figure 6: Blank heat treatment process [courtesy of EBNER Industrieofenbau GmbH]

Figure 7 demonstrates three cooling rates (CR_1, CR_2, and CR_3) leading to different mechanical properties of the blank after the water-cooled tool gets closed. Crucial for the outcome are the cooling rates (CR_i) and the quenching temperature in the end of the quenching process T_{tool_i}. The cooling rate CR_1 illustrates the rapid cooling of a blank enabling the generation of a fully martensitic microstructure (α‘-Fe), where carbon atoms of the austenite are caught in octahedral interstitial zones between the Fe atoms, being the hardest form of steel with UTS levels above 1500MPa and low TE levels of approximately 6%. In fact, a higher cooling rate above 27°C/sec for 22MnB5 steels hinders the solid-state carbon diffusion, leading to a body-centered tetragonal (BCT) crystal structure which is more expanded compared to a ferritic microstructure. [44, 50, 53, 54, 55] Lower cooling rates are also displayed in figure 7 by using the variants CR_2 and CR_3. The first one mentioned leads to the formation of a bainite which is a microstructural composition of ferrite (α-Fe) and cementite (Fe_3C) phases. [53, 56] CR_3 points out the slowest cooling rate of a blank. This especially results in α-Fe and pearlite. Pearlite is a lamellar composition of α-Fe, Fe_3C, and a proeutectoid phase. [53, 56]

The different variants of in-die cooling rates described above are displayed within figure 7.

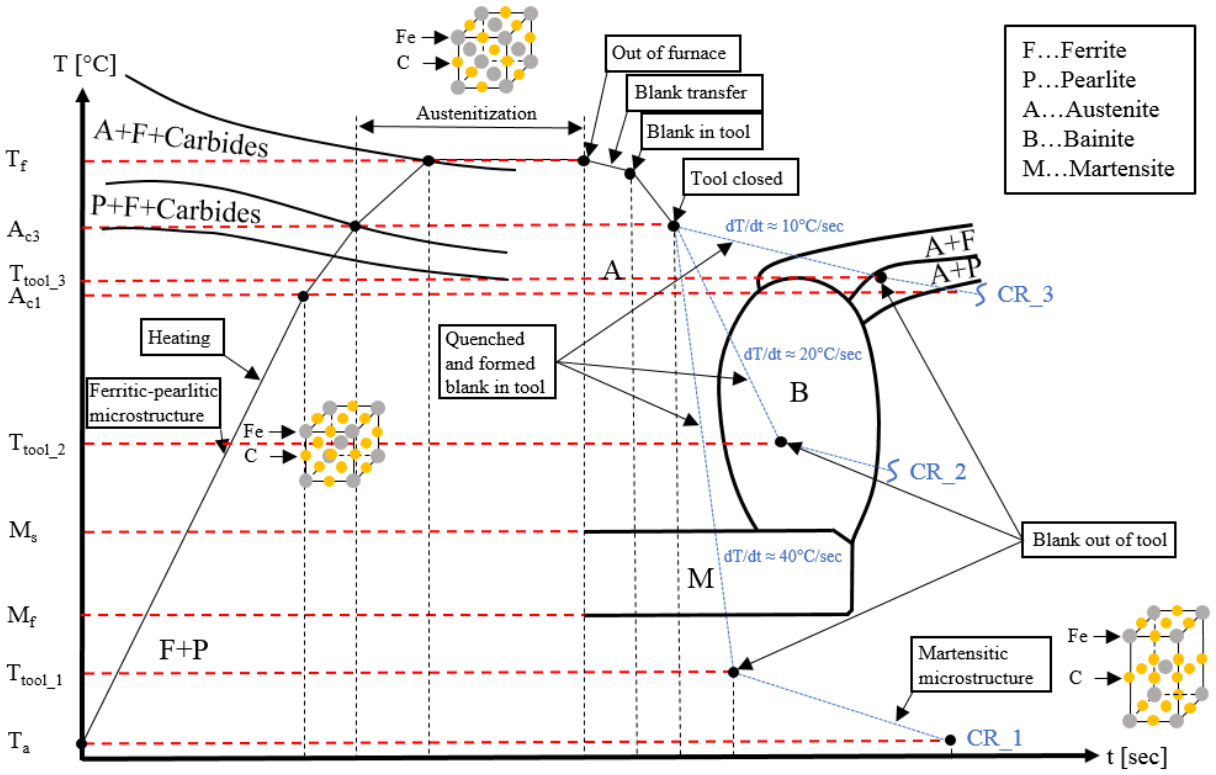

Figure 7: Schematic illustration of different in-die cooling rates (based on: [20, 42, 53, 57, 58])

Continuous cooling transformation (CCT) diagram

Modern heat treatment methods allow continuous improvements of mechanical properties whilst precisely influencing the DPH process. Therefore, the knowledge of the exact phase transformation by making use of the CCT diagram is crucial for specific adjustments of sheet metal blanks. Using different cooling rates result in hardness values ranging between 160 and 475HV. This know-how enables strategies for tailoring final material properties which are going to be discussed later in this thesis. [31]

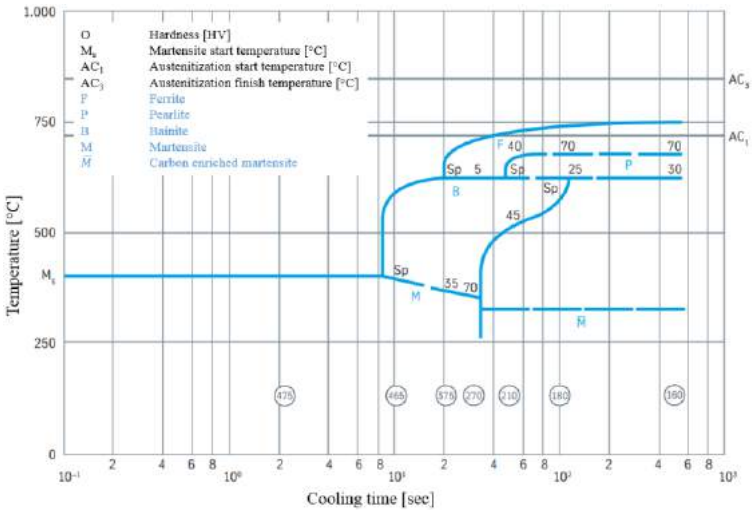

Figure 8: CCT diagram for 22MnB5 (based on: [31])

Semi-finished materials suitable for press hardening

A fine selection of various boron steels which are suitable for the production of light-weight parts is provided next. Table 2 tabulates the mechanical properties of conventional boron steels available on the market.

Steel grade	YS_{ad}	YS_{hf}	R_{m_ad}	R_{m_hf}
[-]	**[MPa]**	**[MPa]**	**[MPa]**	**[MPa]**
20MnB5	505	967	637	1354
22MnB5	457	1010	608	1478
28MnB5	420	1135	620	1740
30MnB5	510	1230	700	1740
34MnB5	600	1225	820	1919
27MnCrB5	478	1097	638	1611
33MnCrB5	420	1290	620	1850
37MnB4	580	1378	810	2040

Table 2: Mechanical properties of boron steels (based on: [26, 27, 28, 29])

The figures in table 2 show that the hot stamping process leads to significant advantages in material properties regarding YS and UTS levels. Due to excellent mechanical properties achieved from the steel grade 22MnB5 (EN 1.5528) during hot forming, this grade is preferred as the base material for light-weight vehicle construction. It is proven to be particularly suitable for the production of structural and safety-related components for anti-intrusion parts. [30]

22MnB5

As already mentioned, 22MnB5 has become the benchmark steel for hot forming procedures in industrial matters. The 608MPa UTS deriving from its initial ferritic-pearlitic grain structure reaches up to a total of 1478MPa having a fully martensitic state, whereas the YS levels reach from 457MPa to 1010MPa after the quenching process is completed. [26] There exist various steel manufacturers around the globe which produce cold- and hot-rolled annealed 22MnB5 steels having low amounts of carbon. [20, 28]

The following table gives an overview of the chemical compositions of some 22MnB5 blanks from different steel manufacturers having similar chemical specifications.

Producer	Product name	C max.	Mn max.	Si max.	P max.	Al max.	Cr+Mo max.	Ti+Nb max.	B max.	S max.
[-]	[-]	[wt-%]	[wt-%]	[wt-%]	[wt-%]	[wt-%]	[wt-%]	[wt-%]	[wt-%]	[wt-%]
ArcelorMittal	Usibor®1500	0.250	1.400	0.400	0.030	0.010 - 0.100	1.000	0.120	0.005	0.010
ThyssenKrupp Steel AG	MBW®1500	0.250	1.400	0.400	0.025	0.015	0.500	0.050	0.005	0.010
Swedish Steel AB	Docol®PHS1500	0.250	1.350	0.350	0.025	-	0.350	-	0.005	0.005
Voestalpine	phs-ultraform1500	0.250	2.000	0.500	0.020	0.100	0.500	0.050	0.005	0.005

Table 3: Steel producers offering 22MnB5 with different chemical compositions (based on: [30, 31, 32, 33])

The austenite stabilizer C is added to enable hardenability and interstitial solid solution strengthening which directly determines the UTS of the final product. Mn, Si and Cr also offer hardenability and substitutional solid solution strengthening whereas Si acts as a deoxidizing agent but needs to be minimized to keep surface-bound silicon oxide formation at a minimum having the ability to hamper adherence of metallic coatings as one major negative side effect. Ti nitride is formed after residual nitrogen combines with the element Ti. This prevents losing B in the interstitial solid solution which is required to reach hardenability because the formation of boron nitride is inhibited. Ti carbide leads to the problem of decreased hardenability because carbon gets removed from the solid solution. The element B influences hardenability the most. [20, 50] Besides high hardness deriving from the minute boron addition also tensile strengths of heat-treated 22MnB5 steel blanks reach up values which are comparable to steels having much higher alloy or carbon contents. In fact, dissolved solute boron in solid austenite solution boosts the reconstructive phase transformation activation energy, rises the energy of the austenite grain boundary surface, decreases the driving force which is needed for a reconstructive phase transformation, reduces ferrite nucleation and enables better hardening effects because the chance of a displacive phase transformation is much higher. [34]

Furthermore, the coating possibilities with their different advantages and disadvantages followed by the heating and cooling typologies of the base material 22MnB5 will be described in detail within the next paragraphs.

Variations of coatings

The primary goal for using coatings on sheet metal blanks is to produce high quality parts without any formation of rough and brittle scale during the heat treatment in the furnace. A proper surface of the blank then leads to lower friction coefficients and wear during the forming process in the tool where even paintability is guaranteed. In addition, this results in increased production efficiency due to lower maintenance activities of the stamping tool. This can also be achieved if uncoated blanks are heated using a protective gas atmosphere, whereas coated

blanks do not need any protective gas during the whole process. Nonetheless, scale formation of uncoated blanks appears due to oxidation of the blank while being transferred from the furnace to the press because of being exposed to air. [35, 17] Besides the already mentioned scaling prevention necessity, coatings should also provide an adequate corrosion barrier, a good formability at various temperatures, an oxidation resistance, weldability, and satisfactory paint adhesion. The classification of coatings is done according to three main types:

- Al-coated e.g. Usibor®1500-AS
- Zn-coated e.g. Usibor®1500-GI
- Varnish coated e.g. x-tec®

Numerous coatings have been tested by researchers in the past to investigate their ability to provide adequate protection for sheet metal blanks. It must be noted, that AlSi coatings are dominantly used because of being suitable for the DPH process whilst providing numerous advantages. [17, 28, 38, 50]

In addition to uncoated blanks, table 4 also lists other major types of coatings used for press hardening applications.

Type of coating	Process	Advantages	Disadvantages
Uncoated **e.g. 22MnB5**	direct	• cheaper than coated blanks	• protective gas atmosphere needed • missing corrosion barrier • scale formation • decarburization
Al-coated (AS) **e.g. Usibor®1500-AS**	direct	• scale formation protection • bigger process window than Zn • weldable without any shot blasting • no protective gas atmosphere needed • no decarburization • better heat resistance than Zn-coated blanks • more experience of stampers with Al-coated blanks • sufficient oxidation resistance	• hydrogen embrittlement • longer furnaces required than for uncoated blanks • Al-accretions on rollers • no cathodic corrosion protection • mostly used for dry-zone-BiW-parts • highly monopolized market by ArcelorMittal
Zn-coated **e.g. Usibor®1500-GI**	indirect (GI)/ direct and indirect (GA)	• excellent cathodic corrosion protection • lower friction coefficient than AlSi and uncoated blanks	• post-surface cleaning for better paint adherence • low experience with Zn • problems with direct process e.g. macro cracks (LME), micro cracks, and Zn-vaporization • costly process (need for pre-cooling to avoid LME during direct process) • lower process window than AlSi
Varnish-coated **e.g. x-tec®**	direct/ indirect	• no scale formation during heating • additional active corrosion protection • lower friction coefficient compared to uncoated- or AlSi-coated blanks • reduced cracks during direct process • no decarburization • weldability guaranteed without removing coating after hot stamping • suitable for conductive, inductive, and infrared heating	• limited corrosion resistance • not widely used

Table 4: Coatings for protection and wear reduction of tools (based on: [4, 20, 28, 30, 35, 36, 37, 38, 39, 40, 41, 42, 43, 44, 44, 45, 46, 47, 48, 49, 50])

2.2 Strategies for tailoring final part properties

Figure 9 gives an overview of components in the BiW where the conventional hot forming process and especially the tailoring of final material characteristics have already been used for producing bumpers, pillars, tunnels, rails, and other parts. The areas of the BiW with higher ability to absorb crash deformation energy are marked with "AAIE".

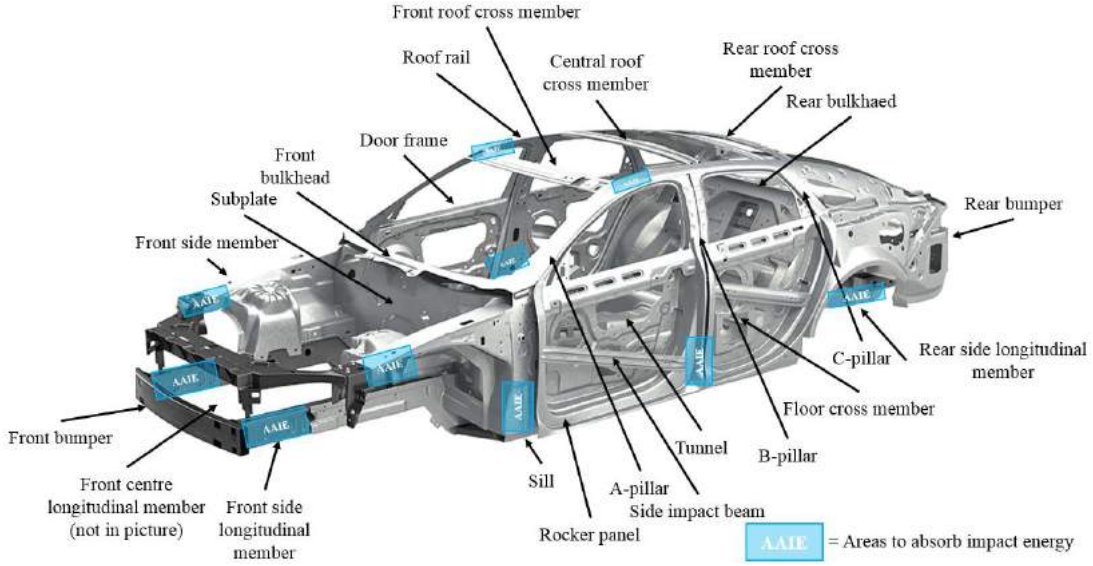

Figure 9: Schematic illustration of some examples for press hardened parts used in the BiW (based on: [2, 11, 20, 43, 62])

Strategies for tailoring final material characteristics are basically classified in two main categories being both integrated in the common hot forming process with regard to figure 5. Tailored blanks are part of the first category, where sheet metal blanks are taken which differ in their thickness and/or their chemical composition to produce a final part with varying mechanical properties. The other category includes process variants where different mechanical properties are achieved through thermal heat treatment procedures using one and the same blank. [20] A finer categorization of the production of tailored part properties is done according to their time of appearance. In recent years, a lot of research has been done to develop locally adjusted mechanical properties of hot stamped components. This especially enables the production of automotive parts, such as B-pillars with custom-designed hard and soft zones through making use of different variants already mentioned in figure 5. On the one hand, the avoidance of intrusion is desired with very hard regions on the upper side of the B-pillar. These high strength martensitic areas are keeping enough survival space after deformation occurs during an impact. On the other hand, vehicle manufacturers try to enforce the ability to absorb the impact energy by developing soft zones consisting of ferritic, pearlitic, and bainitic phases in the bottom area of the B-pillar. The development of tailored crumple zones also improves the protection of car occupants in case of a crash. These crumple zones have the ability to absorb the deformation energy occurring during a crash in an excellent and controlled way whilst decreasing the maximum load of car passengers and increasing the deceleration time during the impact. [20, 42, 63, 64]

Figure 10 shows practical examples of the aforementioned tailored B-pillar and of crumple zones being used for rear frames with distinctive customized crystallographic disparities.

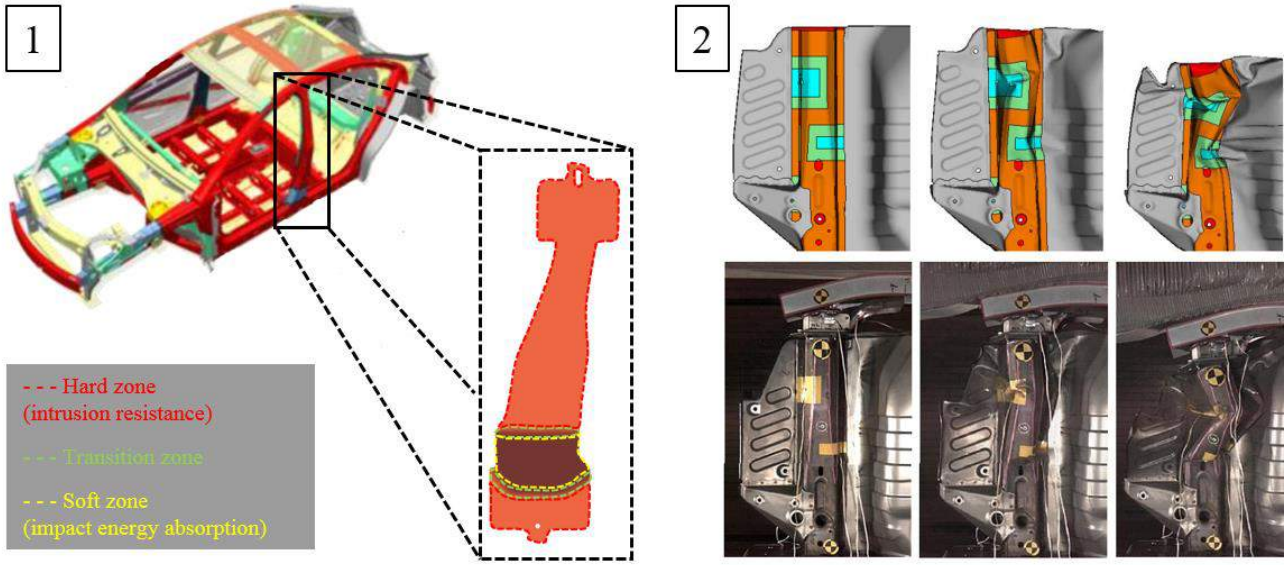

Figure 10: 1: tailored B-pillar, 2: tempered crumple zones of a rear frame (based on: [66])

The production of components with unique tailored properties is typically done with cooled dies although this is a challenging task regarding e.g. non-stable temperature gradients in the die, unknown heat transfer coefficients during the forming takes place etc. Therefore, a lot of interest is directed towards the development of alternative furnace solutions, such as partial heating, partial cooling, and tailored carburization strategies providing numerous advantages compared to in-die solutions. [65]

Production type for tailor tempered blanks	Characteristics
In-die solution	• very small transition area • small local zones possible e.g. flanges, spots etc. • standard roller-hearth furnace can be used • unique solution for every single project
Furnace solution	• highly reduced energy consumption • less die wear • extended lifetime of die • more stable results

Table 5: In-die solution vs. furnace solution (based on: [72])

Partial heating

The relatively simple partial heating methodology is used to achieve adjustable local austenitization in a single blank during the heating process. One way of partial heating is done by dividing furnace areas. One part of the blank is kept in a cooler furnace chamber to achieve soft regions with better ductility after the press hardening process is completed, while the other part is fully austenitized above A_{c3}. Another partial heating approach for achieving tailored properties is done by cooling masses or heat shields, such as ceramic insulating materials placed on the blanks inside the furnace. During subsequent quenching, no martensitic transformation takes place in those cooled areas. The fact, that the temperature before quenching has a major influence on the final hardness values of blanks has already been proved by Stöhr et al. in 2009. [19, 61, 63, 67]

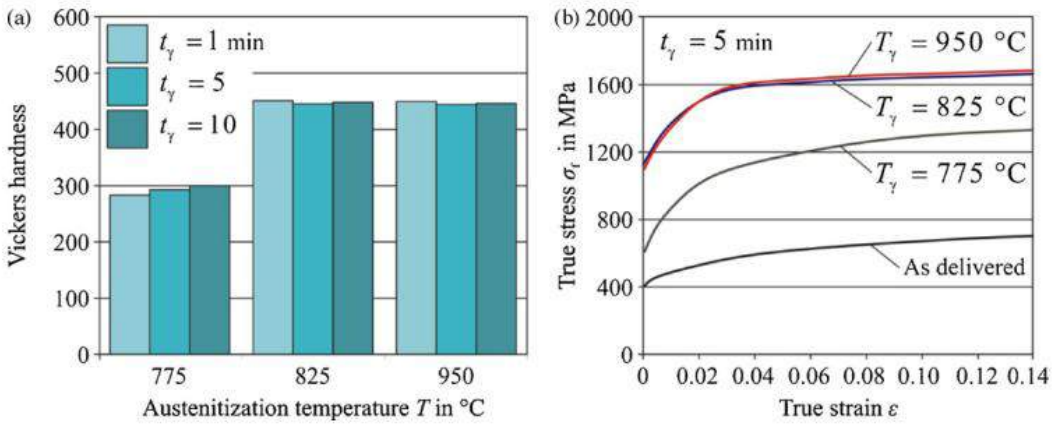

Figure 11: Temperature-dependent hardness values [70]

Table 6 illustrates the main advantages and disadvantages between the two types of partial heating.

Partial heating type	Advantages	Disadvantages
Divided furnace	• simple • adjustable local austenitization • well reproducible transition zones • relatively constant surface properties in different areas of blank	• only two different areas possible • large transition areas (25-50mm) • inconsistent material characteristics
Cooling masses or heat shields	• simple • adjustable local austenitization	• expensive and complex design • difficult implementation in roller-hearth furnace • withdrawing of heating energy from cooling object • only two different areas possible • large transition areas (25-50mm) • reproducibility of same transition areas • inequality of surface properties • inconsistent material characteristics

Table 6: Pros and cons of common partial heating techniques (based on: [19, 61, 63, 65, 67])

This highlights, that these methods are insufficient in fulfilling nowadays customer requirements regarding a flexible production of tempered zone layouts.

Partial cooling

For the highly innovative partial cooling technique, the blanks are first fully austenitized while remaining in the furnace in contrast to the partial heating method where selected regions are not austenitized at all. After being austenitized, selected areas are pre-cooled to create soft material characteristics in the same part after getting hot stamped. An already existing air/jet-system enables a flexible production of areas with diverse material properties developed by Schwartz GmbH. EBNER is also present in the field of partial cooling technologies currently offering a fully-automated system. This multi-level chamber furnace allows a flexible and small-space-production of automotive parts with a maximum throughput of about 5.1t per hour compared to conventional roller-hearth furnaces with lengths of approximately 30 to 50m and maximum throughput levels ranging between 3.5 and 6t per hour. An electric heated transfer box makes also use of an air/jet-system to generate local mechanical properties of only coated material and even ensures that heated blanks always have the same temperature before being fixed in the press. The transition zones of produced components are normally less than 60mm, whereas the variation of the starting- and ending-point of these areas is lesser than ±10mm. For both partial heating and cooling strategies, unwanted transition zones with dimensions of approximately 30 up to 150mm are created due to heat conduction which can be considered to be minimized using improved thermal controlling techniques. [4, 19, 61, 69, 71, 72, 73, 74, 88]

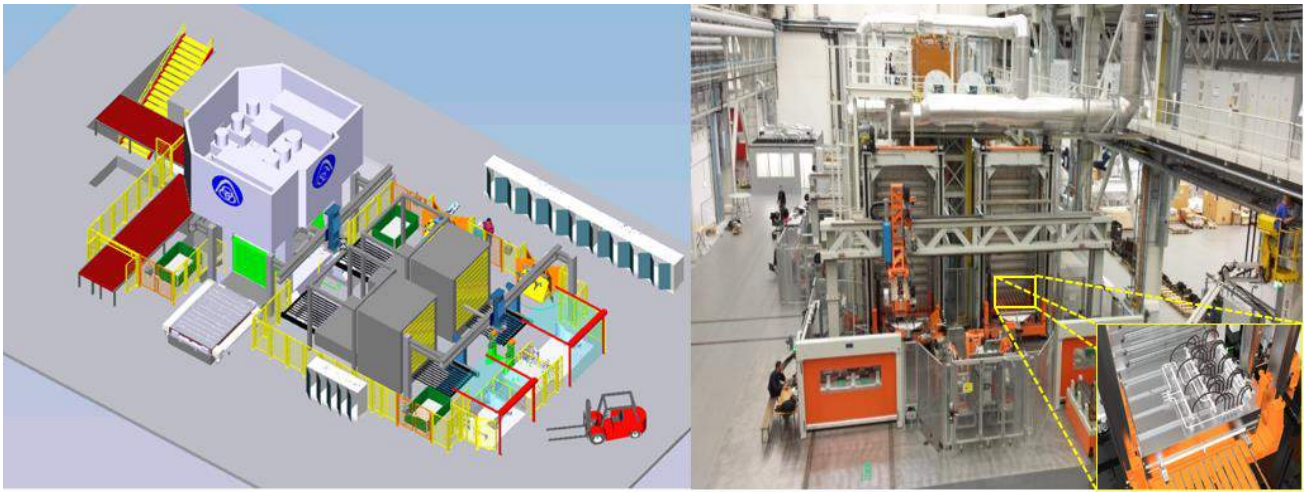

Figure 12: Multi-level chamber furnace with twelve layers (based on: [72, 73])

Figure 13 shows a B-pillar which just came out of the furnace with remarkably different blank temperatures.

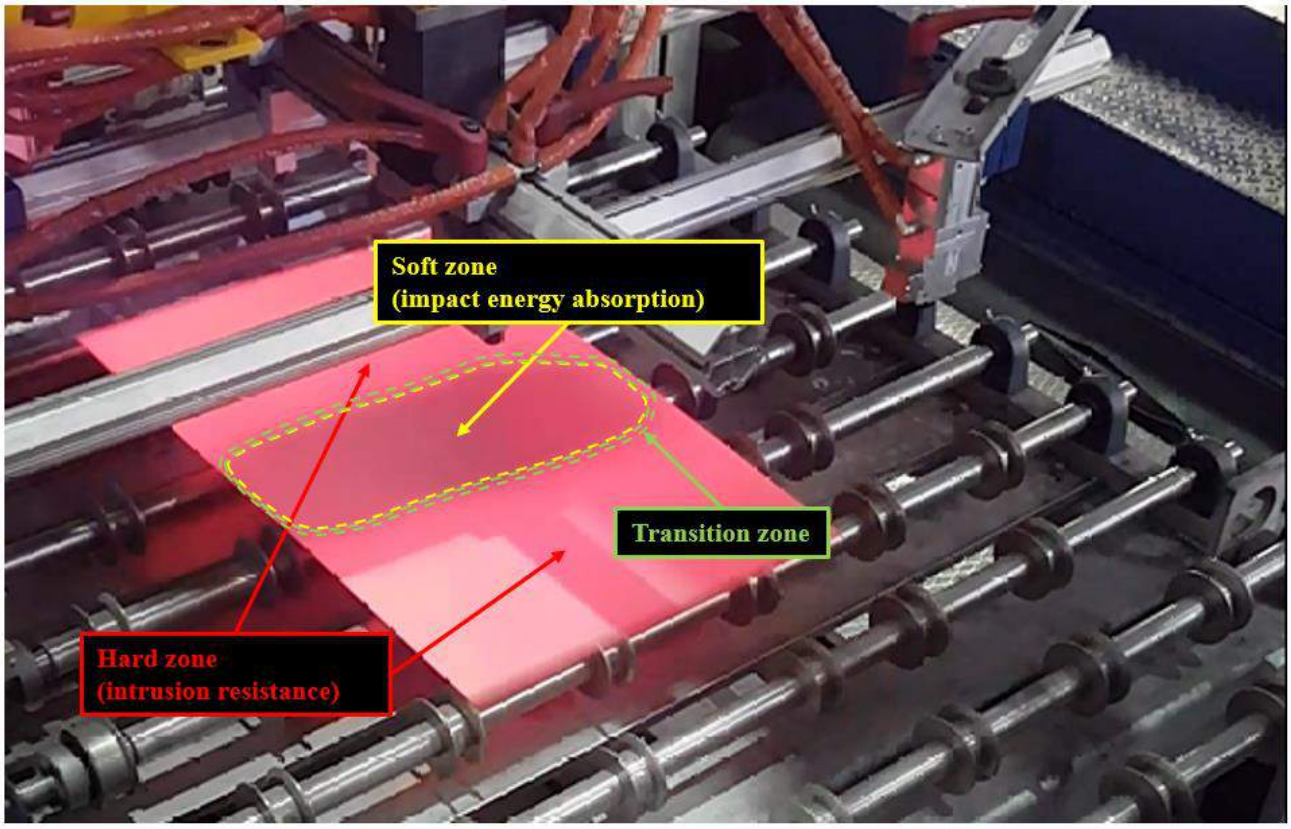

Figure 13: Blank with temperature gradient [courtesy of EBNER Industrieofenbau GmbH]

Tailored carburization

Tailored carburization is a totally new approach for achieving custom-designed material characteristics using the uncoated complex phase steel CP-W-800 instead of the commonly used press hardening steel 22MnB5. This steel grade has a reduced carbon content of about 0.12wt-%, which especially allows local carburization when selected areas are covered with graphite before being heat-treated. This finally leads to higher strength values in those graphite-treated zones. [75]

2.3 Structural analysis of the TPP branch

Beside of the technical point of view discussed within the previous chapters, the following paragraphs focus on the economic aspects regarding tailored tempering. Comprehensive knowledge of the branch structure is the basis for formulating competitive strategies for new or currently existing companies in a specific field. In fact, the structure of the whole industry has a direct impact on the profitability of a business and thus influences decisions made by enterprises in a significant way. Apart from the competitive intensity, also structural characteristics within the industry are identified by using Porter's Five Forces. The model is basically divided in the following parts which are illustrated in figure 14.

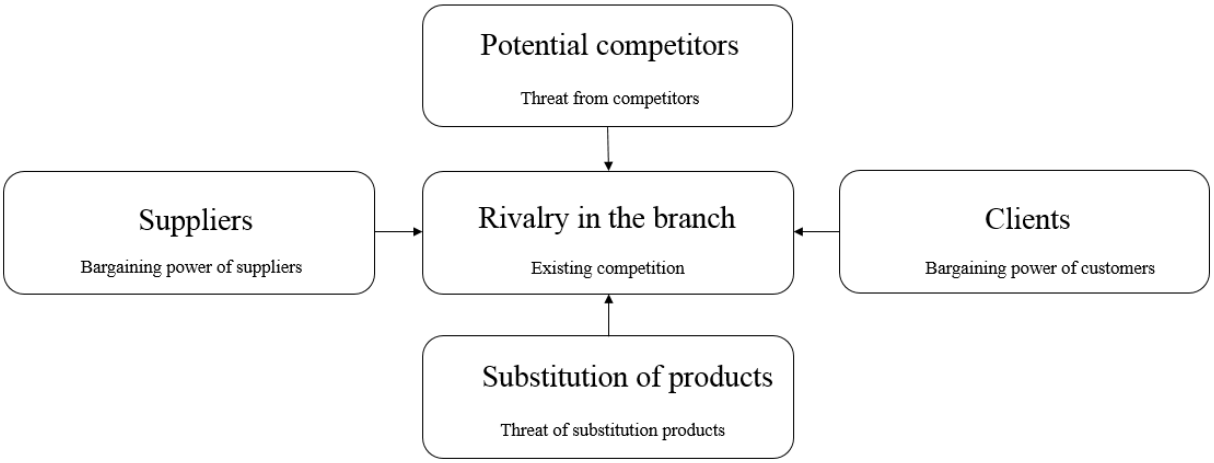

Figure 14: Porter's Five Forces determining the profitability of a branch (based on: [18])

A structural analysis based on Porter's concept is done to estimate the market potential and the profitability, especially for tailored tempering furnace solutions. The results of this analysis are primarily generated through market research activities, where a questionnaire, the internet, patents, and internal databases at the headquarters of EBNER were used and checked. Furthermore, personal interviews were held with EBNER's staff members, such as product managers, product development specialists and, above all, experts of the Graz University of Technology to make the results as complete as possible. Based on the gained information, strengths or weaknesses of the single forces are evaluated which helps in identifying possible market opportunities and threats. [18]

Rivalry in the branch

Table 7 summarizes the most important companies currently acting in the field of press hardening. Schwartz GmbH/Hütte GmbH, Benteler, and AP&T are considered as main competitors of EBNER. Besides showing the most relevant organizations it was investigated whether these enterprises currently sell press hardening furnaces respectively any tailored tempering solutions. [69]

Institution	Head-quarters	Website	Press hardening furnace	Tailored tempering solutions	Tailored tempering solution in a roller-hearth furnace
Schwartz GmbH **Hütte GmbH**	DE DE	www.schwartz-wba.com www.huette-tpt.de	yes	yes	yes
Benteler	DE	www.benteler-mechanicalengineering.com	yes	yes	yes
AP&T	SE	www.aptgroup.com	yes	yes	no
Shinsung Co., Ltd.	KR	www.ssung.co.kr	yes	n.i.	n.i.
EBNER Industrieofenbau GmbH	AT	www.ebner.cc	yes	yes	no
Aichelin Holding GmbH **BSN Thermoprozesstechnik GmbH**	AT DE	www.aichelin.com www.bsn-therm.de	yes	yes	no
Eisenmann SE **Telos Global** **Ruhstrat GmbH**	DE US DE	www.eisenmann.com www.telosphs.com www.ruhstrat.com	yes	yes	no
LOI Thermprocess GmbH	DE	www.loi.tenova.com	yes	yes	yes
Meapforni srl	IT	www.meapforni.com	yes	yes	yes

Table 7: Companies acting in the field of press hardening (based on: [69])

The approximate number of press hardening furnaces sold worldwide is estimated to be between 500 and 550 based on data generated through market research activities of EBNER. Schwartz/Hütte can be seen as the market leader in developing heating technologies for the press hardening industry, having a market share of approximately 60% and counting about 290 furnaces being totally sold in 2018. The relative market share of EBNER is about 9%. Schwartz/Hütte are primarily selling furnaces for press hardening applications for about 35 years, whereas EBNER has a wide range of experience in developing heat treatment technologies for more than seven decades, which sets this company apart from other competitors. EBNER and Schwartz/Hütte are currently enforcing active collaborations with universities and competence centers, which enables the publication of various scientific documents in the area of heat treatment technologies. Furthermore, active presence at trade fairs is forced in order to attract new suppliers' and/or customers' attention. Other enterprises listed within table 7 also are, similar to EBNER, developing heating systems for other industries. In addition, only eight different noteworthy enterprises are offering tailored tempering solutions. This means, that the current

competition between competitors in the press hardening sector respectively the tailored tempering industry can be considered as low, since there is only one clear market leader and a lack of competition, especially in the field of tailored tempering. [69]

Potential competitors

Chapter 1 already mentioned the generally increasing demand of economically priced UHSS components within the last decades, which makes it attractive for companies to enter the press hardening market whilst additionally offering solutions fulfilling the tailored tempering trend. Nonetheless, the automotive industry is currently witnessing a general decreasing trend in demand. According to Mr. Koestler – Senior Vice President of Continental AG – the annual sales of vehicles in the following years will reach 110 million but remain constant thereafter. The continuously growing range of means of transport contributes significantly. Car sharing, public transportation, and the light e-mobility are becoming increasingly important these days, with the result, that sales of automobiles will stagnate as soon as the previously mentioned peak is reached. [69]

First, a clear differentiation has to be made between companies who want to offer in-roller-hearth furnace tailored tempering solutions and between companies who have the ability to develop and sell other technologies enabling the production of tailor tempered sheet metals. Table 8 shows various potential competitors regarding tailored tempering, whereas institutions fulfilling the second category are underlined. The total threat of potential competitors is evaluated of being low because the development of an in-roller-hearth furnace tailored tempering solution requires high financial capacities and, in addition, a lot of experience in furnace technologies. [69]

Institution	Headquarters	Website
Eisenmann SE	DE	www.eisenmann.com
Telos Global	US	www.telosphs.com
Ruhstrat GmbH	DE	www.ruhstrat.com
EBNER Industrieofenbau GmbH	AT	www.ebner.cc
AP&T	SE	www.aptgroup.com
SMS Elotherm GmbH	DE	www.sms-elotherm.com
AjaxTOCCO Magnethermic GmbH - Intec Induction	DE	www.ajaxtocco.de
ITG INDUKTIONSANLAGEN GMBH	DE	www.itg-induktion.de
SMS Elotherm GmbH	DE	www.sms-elotherm.com
Neue Materialien Bayreuth GmbH	DE	www.nmbgmbh.de
Daimler AG	DE	www.daimler.com
IHT Infrared Heating Technologies	US	www.infraredheating.com
SCHWING Technologies GmbH	DE	www.schwing-technologies.com

Table 8: Potential competitors regarding tailored tempering (based on: [69])

Substitution of products

Table 9 shows possible technologies which can be used to produce automotive parts with diverging material properties. Therefore, these technological approaches can be seen as potential substitutes because of having the ability to replace in-roller-hearth furnace tailored tempering methods. The highest potential as a substitute has the multi-level chamber furnace solution with a tailored tempering function developed by AP&T. [59]

Both induction-based heating and contact heating systems also have the ability to produce parts with customized material properties. On the one hand, a much higher energy efficiency rate is the main advantage of these two systems compared to conventional roller-hearth furnaces with their high amounts of energy loss during operation times. On the other hand, induction-based heating and contact heating systems have problems in producing homogeneous material properties of parts with high sheet thicknesses and larger dimensions. [69]

Furthermore, fluidized bed systems also are suitable for partial annealing procedures of autobody components according to statements on the website of SCHWING Technologies GmbH and, therefore, also have to be considered when evaluating potential substitutes. [51]

Summing up, the threat of substitution products can also be seen as being low because the alternatives available on the market are not as suitable for series production as EBNER's approach with the in-roller-hearth furnace tailored tempering solution. [69]

Institution	Headquarters	Website	Substitution product
AP&T	SE	www.aptgroup.com	Multi-level chamber furnace
SMS Elotherm GmbH	DE	www.sms-elotherm.com	Induction-based heating
AjaxTOCCO Magnethermic GmbH - Intec Induction	DE	www.ajaxtocco.de	Induction-based heating
ITG INDUKTIONSANLAGEN GMBH	DE	www.itg-induktion.de	Induction-based heating
SMS Elotherm GmbH **Neue Materialien Bayreuth GmbH** **Daimler AG**	DE DE DE	www.sms-elotherm.com www.nmbgmbh.de www.daimler.com	Contact heating
IHT Infrared Heating Technologies	US	www.infraredheating.com	Infrared heating
SCHWING Technologies GmbH	DE	www.schwing-technologies.com	Fluidized bed system

Table 9: Substitution products (based on: [69])

Suppliers

According to information gained through personal interviews at EBNER, the press hardening branch seems to have high attractiveness for companies to supply furnace manufacturers and end customers. The main business for these suppliers is the after-sales service, which ensures a secure supply of equipment, such as rollers (if they are broken). [69]

The bargaining power of suppliers is estimated to be low due to strong competition in the supplier industry. In particular, there is a high price pressure as many of the standard components are manufactured in low-cost countries. Therefore, it is difficult for furnace manufacturers to get any discounts from their suppliers. An exception, for example, are special solutions, such as low-NOx burner systems from WS-Wärmeprozesstechnik GmbH. Companies such as WS-Wärmeprozesstechnik GmbH, which offer products that require special expertise, have a much higher bargaining power that allows them to differentiate themselves from standard suppliers. [69]

The whole market situation for furnace manufacturers can be classified as a buyer's market where supply is bigger than demand. Some suppliers currently being present in the press hardening branch are summarized in table 10. The enterprises are classified according to the parts which are needed for the construction of the trial furnace from EBNER. [69]

Type of product	Company	Website
22MnB5 AlSi steel blank	ArcelorMittal	corporate.arcelormittal.com
	ThyssenKrupp Steel AG	www.thyssenkrupp-steel.com
	Swedish Steel AB	www.ssab.de
	Voestalpine Metal Forming Division	www.voestalpine.com
	BILSTEIN GmbH & Co. KG	www.bilstein-kaltband.de
Heating device	Honeywell Kromschröder	www.kromschroeder.de
	CombuTec GmbH & Co. KG	www.combutec.de
	ANDRITZ FBB GmbH	www.andritz.com/metals-en/about-us/locations/fbb-gmbh
	IBS Industrie-Brenner-Systeme GmbH	www.ibs-brenner.de
	WS-Wärmeprozesstechnik GmbH	flox.com
	NOXMAT GmbH	www.noxmat.com
Insulation	Promat GmbH	www.promat-hpi.com
	Silca Service- und Vertriebsgesellschaft für Dämmstoffe mbH	www.silca-online.de
	THERMO Feuerungsbau-Service GmbH	thermo-fb.de
	Unifrax GmbH	www.unifrax.com
	Merkel Feuerfest	www.merkel-feuerfest.de
	G&L Feuerfesttechnik GmbH	www.gl-ff-tech.at
	RATH AG	www.rath-group.com
Roller drive unit	Morgan Advanced Materials Haldenwanger GmbH	www.morgantechnicalceramics.com
	EmcoTherm GbR	www.emcotherm.com

	Vesuvius plc	www.vesuvius.com
	Saint-Gobain IndustrieKeramik Rödental GmbH	www.saint-gobain.de
	Sirtec s.r.l.	www.sirtecgroup.it
	Freedom Ceramics Suzhou Limited	www.freeceram.com
	ESTIVA Refratários	www.estivarefratarios.com.br
	Diamorph Hob Certec, s.r.o.	www.certec.cz
Power unit	Lenze SE	www.lenze.com
	ROLLMOD GmbH	www.rollmod.de
	SEW-EURODRIVE Ges.m.b.H.	www.sew-eurodrive.at
	Saint Gobain	www.saint-gobain.de
Chain guiding device	Ebner Industrieofenbau GmbH	www.ebner.cc
	Murtfeldt Kunststoffe GmbH & Co. KG	www.murtfeldt.de
Bearing	Svenska Kugellagerfabriken - SKF	www.skf.com
	Nippon Seikō K.K. - NSK	www.nskeurope.de
	Schaeffler-Gruppe	www.schaeffler.at
CPU unit	Siemens AG	new.siemens.com
	Mitsubishi Electric Europe B.V.	de3a.mitsubishielectric.com
Software	Ebner Industrieofenbau GmbH	www.ebner.cc
Centering device	Ebner Industrieofenbau GmbH	www.ebner.cc
	WITTENSTEIN alpha GmbH	alpha.wittenstein.de
	Bosch Rexroth AG	www.boschrexroth.com
	Lenze Austria Holding GmbH	www.lenze.com
	AVENTICS GmbH	www.aventics.com
	KAINDL Technischer Industriebedarf GmbH	www.kaindltech.at
	Festo Gesellschaft m.b.H.	www.festo.com
Cooling device	Ebner Industrieofenbau GmbH	www.ebner.cc
	ZIMM Maschinenelemente GmbH + Co KG	zimm-hubgetriebe.com
	Karl Mertl Handelsges.m.b.H.	www.mertl.com
	WERZ Vakuum-Wärmebehandlung GmbH & Co. KG	www.werz.de
	Bosch Rexroth AG	www.boschrexroth.com
	Morgan Advanced Materials Haldenwanger GmbH	www.morgantechnicalceramics.com
	B&T Metall- und Kunststoffhandel GmbH	www.metall-kunststoffhandel.de

Table 10: Suppliers in the branch (based on: [69])

Clients

The main customers of hot forming furnaces can be divided into three groups consisting of Original Equipment Manufacturers (OEMs), Tier 1 suppliers, and suppliers of complete press hardening lines (press makers). In fact, some press makers operate as full-line suppliers with OEMs and Tier 1 suppliers as their end customers. The risk of backward integration is therefore considered high, as press makers also know many details about furnace technologies when selling complete press hardening equipment to OEMs and Tier 1 suppliers. [69]

Figure 15 gives a brief overview of the various customers of blank heating systems.

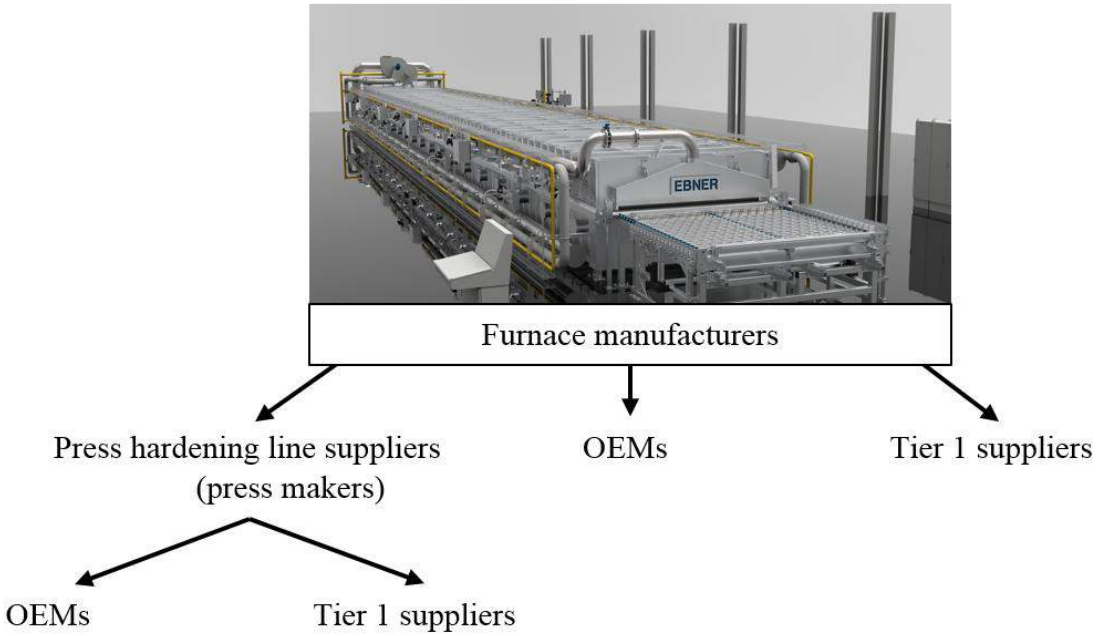

Figure 15: Clients of EBNER (based on: [69, 78])

Table 11 shows some examples of clients mentioned in figure 15.

Type of client	Company	Website
Tier 1 suppliers	Magna International Inc.	www.magna.com
	Muhr und Bender KG	www.mubea.com
	Karmax Heavy Stamping	www.karmax.com
	Gestamp Servicios S.A.	www.gestamp.com
	Benteler International AG	www.benteler.com
OEMs	Volkswagen AG	www.volkswagenag.com
	Fiat S.p.A.	www.fiat.com
	Audi AG	www.audi.de
	Seat S.A.	www.seat.com
	Proton AG	www.proton.com/
	Volvo AB	www.volvocars.com
	Honda Motor Co., Ltd.	world.honda.com
	Renault S.A.	www.renault.com
Press hardening line suppliers	Loire Gestamp	loire.gestamp.com
	AP&T	www.aptgroup.com
	Walter Neff GmbH Maschinenbau	www.neff-pressen.de
	Schuler AG	www.schulergroup.com

Table 11: Exemplary clients in the branch (based on: [69, 77, 78])

Loads of press hardened parts are bought from Tier 1 suppliers because of various reasons. First, the acquisition of entire press hardening lines is associated with high investment and operating costs. Furthermore, the production of press hardened components requires a lot of experience and know-how. Referring to an interview with one of EBNER's product managers, nowadays press hardening market situation can be identified as a buyer's market where the bargaining power of clients is high. In addition, there is currently a surplus of spare capacity in the production of press hardened components, especially in the Asian economic area. This also leads to falling prices for products from furnace manufacturers. Therefore, focusing on highly innovative product differentiation strategies, such as a customizable tailored tempering solution in a roller-hearth furnace has a very high potential to create a long-term competitive advantage. That can help overcoming the currently stagnant conventional press hardening industry. In addition, it makes sense to search for new application areas for press hardening in order to evade the current decline in demand for press hardened components. The defense industry, shipbuilding, agricultural engineering, and safety technology are, in addition to the automotive branch, industries with high potential for the use of press hardened components. [8, 78]

3 Goals of the thesis

The production of automotive parts with customized tailored mechanical properties in one single component with additionally sharp transition lengths of $s_{tz} \leq 30$mm still represents a challenging task for vehicle- as well as press- and furnace-manufacturers.

Besides providing a theoretical background of press hardening, the primary goal of this thesis is held on thermal controlling strategies for tailoring final material characteristics. In addition, a comprehensive branch analysis is conducted referring to press hardening respectively tailored tempering solutions based on the Porter's Five Forces framework. Special attention will also be paid to EBNER's partial cooling technology enabling the production of flexible material properties in one and the same steel blank.

The target of the practical part of this thesis deals with the optimization of EBNER's tailored tempering technology which enables the production of custom-designed soft zones and transition areas with a contact cooling device. AlSi-coated 22MnB5 steel blanks are going to be taken for a set of experiments using EBNER's heat treatment simulation tool called SimCAL 3.0 and a trial furnace. A systematically iterative approach is going to be conducted by varying controllable factors X_i to achieve the most encouraging outcome O_i regarding the required mechanical properties of the blanks. Figure 16 overviews this general process which is based on the design of experiment (DoE) tool.

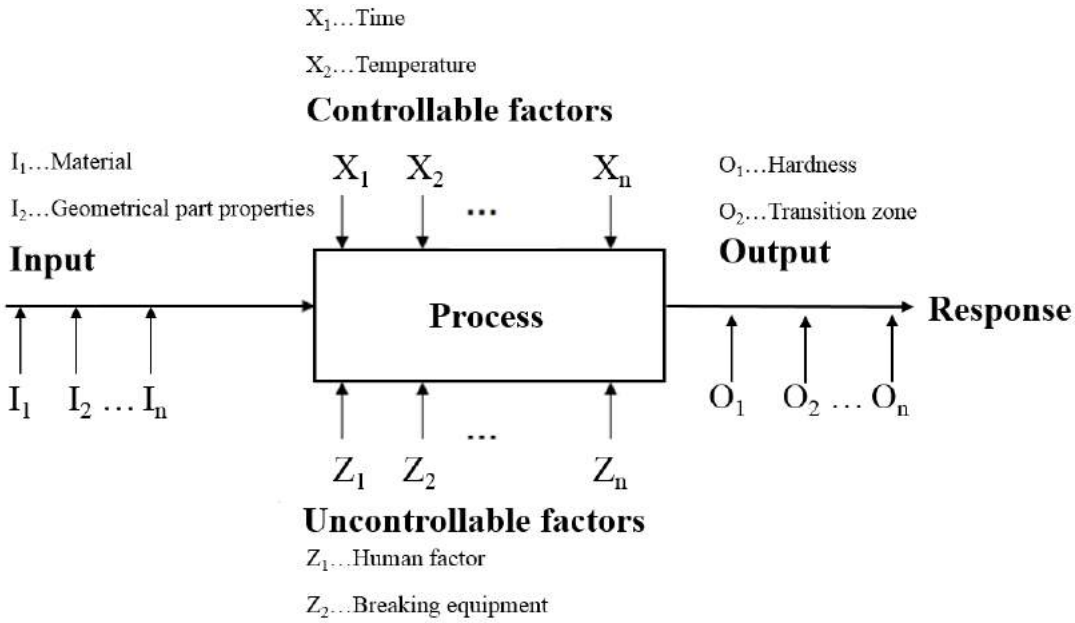

Figure 16: General process model for experimental investigations (based on: [76])

The resulting temperature curves conducted with EBNER's SimCAL 3.0 are going to be taken to create a material-dependent CCT diagram showing the different phase boundaries of the steel grade. The knowledge of the exact position of the different phases allows an accurate optimization of the partial cooling process. Besides investigating different cooling concepts, the optimal furnace temperature T_f, the shortest cooling times of the

contact cooler $t_{i\_j\text{-}pt}$, the necessary dwell times after the cooling device $t_{i\_pt\text{-}700}$, and the critical transfer times $t_{700\_crit\_i}$ are going to be determined which makes it possible to achieve the required mechanical properties. Furthermore, a mechanical examination of the samples is going to be carried out by means of hardness tests and tensile tests. An EDX-analysis and a microstructural observation are also going to be performed to allow an accurate optical inspection of critical areas. The scientific documentation of all procedures is indispensable to be able to reproduce the results as precisely as possible.

The performance specifications for all investigations are listed as followed:

- Usibor1500 AS150 (22MnB5) represents the steel grade for all tests to be carried out
- In order to ensure better reproducibility, all blanks are going to be degreased and cleaned before the experiments are conducted to reduce undesired influencing factors
- The dimensions of the sheet metal blanks are going to vary between 450x20x2mm (SimCAL 3.0), and 250x250x1mm, 250x250x2mm, and 750x250x2mm (trial furnace)
- Depending on the type of experiment, all saturated thermocouples (TCs) of type N and sheath thermocouples for repetitive tests with EBNER's SimCAL 3.0 and the trial furnace are going to be placed in the same positions to make the results as comparable as possible
- Consistent positioning and uniform dimensions of the cooled area are guaranteed
- Creation of a batch-dependent CCT diagram with the SimCAL 3.0
- Proof of the temperature uniformity of the trial furnace
- Investigation of the cooling performance of the contact cooler during the simulation of realistic cycle times
- Hardness measurements and tensile tests are going to be executed to determine the mechanical properties of the specimens
- The insertion temperature of the hard zone before quenching T_{bi_h} should not be lower than 700°C
- The hardness values of the soft areas are set to be between 180 and 220HV10 ($575 \leq R_{m_s} \leq 705$MPa), whereas the values of the hard zones should be between 420 and 520HV10 ($1350 \leq R_{m_h} \leq 1700$MPa)
- The size of the transition zone s_{tz} should not exceed a maximum of 30mm

The next milestone is to realize and prove the series maturity of this system. Results gained through this work are going be taken under consideration when conducting further pilot tests at manufacturing sites of EBNER's customers. This then helps evaluating the optimized tailored tempering technology whilst producing bodywork parts under realistic conditions.

At the end of this thesis, further recommendations for action are going to be given for the company EBNER. All experimental results from the practical part of this thesis are attached in the Appendix.

4 Equipment

The practical part of this work deals with the elaboration of numerous experiments with the aim of optimizing the partial cooling process of EBNER's press hardening furnace. Beforehand, the chosen steel grade with its own specifications and the testing equipment will be discussed. Afterwards, the relevant measurement and evaluation systems will be presented.

4.1 Chosen steel grade

For the practical part of this thesis, ArcelorMittal's 22MnB5 is chosen as the base material for the entire experimental investigation. This boron steel grade, which is popular for hot stamping procedures, has an as-delivered ferritic-pearlitic microstructure known for its low initial mechanical characteristics. The chemical components of this steel grade with its own trade name Usibor®1500 AS150 is shown in table 12.

Producer	Product name	C max.	Mn max.	Si max.	P max.	Al max.	Cr+Mo max.	Ti+Nb max.	B max.	S max.
[-]	[-]	[wt-%]	[wt-%]	[wt-%]	[wt-%]	[wt-%]	[wt-%]	[wt-%]	[wt-%]	[wt-%]
ArcelorMittal	Usibor®1500 AS150	0.250	1.400	0.400	0.030	0.010 - 0.100	1.000	0.120	0.005	0.010

Table 12: Chemical Components of the Usibor®1500 AS150 [30]

The abbreviation AS150 stands for being continuously aluminized with a metallic coating. In this case, a layer thickness of 150g/m^2 is applied using a hot-dipping procedure. This widely used type of coating with its various advantages, tabulated in table 4, is applied at 675°C and typically consists of 3wt-% Fe, 9wt-% Si, and 88wt-% Al. Si is added to primarily hinder the formation of Fe-Al intermetallic phases resulting in better properties of the coating. The layer thickness normally varies between 25-30µm consisting of two different zones after press hardening. The outer layer consists of Al and Si whereas the inner layer is an intermetallic Fe-Al-Si compound. [17, 38, 50]

The sheet metal blanks for the practical tests with EBNER's SimCAL 3.0 and the trial furnace are cut out of raw blanks according to the desired dimensions. As displayed in table 13, two thicknesses and three different geometries are used.

Product name	Testing apparatus	l_b	w_b	s_b
[-]	[-]	[-]	[-]	[-]
Usibor®1500 AS150	SimCAL 3.0	450	20	2
Usibor®1500 AS150	Trial furnace	250	250	1
Usibor®1500 AS150	Trial furnace	250	250	2
Usibor®1500 AS150	Trial furnace	750	250	2

Table 13: Required blank geometries for EBNER's SimCAL 3.0 and the trial furnace

It is important to note, that the blank's dimensions have a significant influence on the heating rate in the furnace respectively the cooling rate when the blanks are transferred to the flat quenching tool. Blanks with a thickness of 1mm have a much higher cooling rate compared to blanks with a thickness of 2mm. This can be problematic if the required forming temperature of the blank is too low when being positioned in the press. Therefore, it is important to simulate the entire press hardening process, consisting of the 'furnace part-phase 1' and the 'outside of the furnace part-phase 2', in order to optimize EBNER's entire tailored tempering process.

EBNER's trial furnace, which will be introduced within chapter 4.2.2, is also used to produce of a fully hardened Usibor®1500 AS150 blank. The mechanical properties of this sample serve as reference values for further tests. First, the sample with a sheet dimension of 250x250x2mm is heated up to a temperature of T_f = 900°C. Then, the blank is transported through the furnace for about 32 seconds until the probe gets transferred to the flat quenching tool within 8 seconds. The blank finally gets quenched with an average cooling rate of about $CR_{fqt\_750\text{-}200} \approx 102.16$°C/sec. Afterwards, tensile tests are conducted to determine the final mechanical values of the sample as illustrated in table 14.

States	**R_m**	**$R_{p0,2}$**	**A_{50}**
[-]	**[MPa]**	**[MPa]**	**[%]**
As-delivered	581	411	22.3
Hardened	1516	871	6.3

Table 14: Mechanical properties of used steel grade

The test protocols can be found in Appendix A8.

4.2 Testing apparatus

Chapter 4.2 describes the two apparatus which are used for identifying the optimal process parameters regarding tailor tempered blanks. This is crucial for achieving the desired material properties of the hard and soft zones of the selected steel grade.

4.2.1 EBNER's SimCAL 3.0

SimCAL 3.0 is a continuous heat treatment simulation apparatus which was developed by EBNER. The information gained by preliminary experiments with the SimCAL 3.0 is essential for further investigations as it is more time saving as well as cost efficient compared to tests with the trial furnace. This drastically reduces the total trial period of developing a new product. Figure 17 shows the SimCAL 3.0 in the Research and Development Department of EBNER's headquarters.

Figure 17: Continuous heat treatment simulation apparatus – SimCAL 3.0

This simulator is able to heat and cool steel stripes with a sheet width of up to 30mm and sheet thicknesses of up to 3mm. This means, that this simulator can reproduce any heat treatment process using a different heating respectively cooling technology compared to the trial furnace, which will be explained within chapter 5.3.

4.2.2 EBNER's trial furnace

The trial furnace from EBNER is used for the main part of the test series. This trial furnace is developed to perform realistic process cycles regarding tailored tempering under laboratory conditions. The main components are illustrated in figure 18 and discussed within the following lines. A computer (position a) is used for process monitoring, recording, and setting of relevant process parameters. The control unit (position e) enables, for example, the actuation of the centering devices. The heating (position c) and pre-cooling (position d) of blanks takes place in the trial furnace (position b). The flat quenching tool (position f) is used to simulate realistic cooling rates whilst considering crucial transfer times between the trial furnace and the flat tool. Realistic

material properties can be achieved by simulating the aforementioned process sequences, whereby the performance specifications already discussed in chapter 3 must be fulfilled.

As shown in figure 18, the geometry of the trial furnace is reduced in comparison to standard EBNER press hardening furnaces on a scale of 1:6.

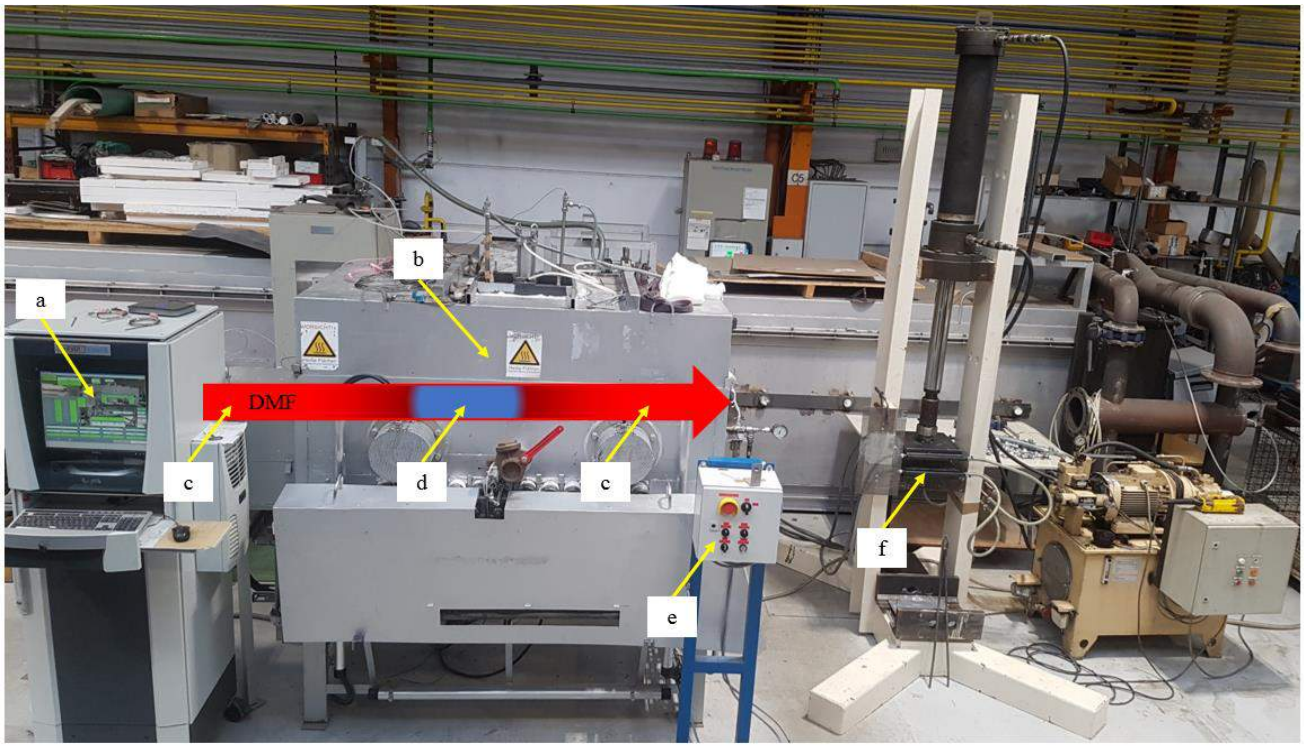

Figure 18: Illustration of EBNER's entire trial system with the direction of material flow (DMF)

Heating concept

The hybrid heating system consists of two built-in gas heated SiSiC radiant tubes and an electric heating coil. The total furnace heating capacity is about 23kW. The recuperative burners, placed on the left and right side of the contact cooler, are encapsulated in ceramic jacket tubes in order to not change the furnace atmosphere during operation mode. Furthermore, this ensures keeping the dew point at a desired level to avoid any hydrogen embrittlement of the steel blanks. The heating coil is placed in the area of the contact cooler directly under the rollers to produce a more realistic process condition with respect to the heat uniformity of a normal press hardening furnace. This then reduces unwanted pre-cooling of the blanks before the contact cooling takes place.

Contact cooler

Figure 19 illustrates a schematic drawing of the contact cooler and the contact cooler during assembly and operating modes. One of the main advantages of this trial system is the production of flexible soft shapes via contact cooling (position 2a) of sheet metal blanks (position 2f). This is done by making use of a module-based cooling system having a high influence on the final part properties. It is centered by bolts (position 2g) during assembly, which especially allows short setup times. The entire system is installed in the roof section of the

furnace with insulating material (position 1a, 2e) to protect the cooling device from high temperatures occurring inside of the furnace. The insulation under the cooler is designed by using a tongue and groove system to prevent possible cracks during operation. Preliminary tests between St nails, Al nails, and Cu nails are conducted to find the material with the best properties. Cu is finally chosen as the base material for the cooling nails (position 1b, 2c) because of its very high heat conductivity of λ = 380W/m*K [79]. Another reason for this decision is, that Cu has the highest density of approximately 8.92g/cm^3 compared to conventional mild steel with 7.85g/cm^3 or Al with a density of about 2.7g/cm^3. [80, 81, 82] Light-weight Al nails are often stuck in the nail holding application and may not cool the blank properly. In addition, Al has a much lower melting point of T_{m_al} = 660.32°C compared to Cu with a melting point of T_{m_cu} = 1084°C, which also may lead to additional problems regarding mass production. [83] These Cu nails get cooled whilst being in the upper position (position 2b), whereas they act as a perfect heat conductor when being in contact with the austenitized blank in the lower position (position 2a). Through the vacuum-brazed cooler (position 1c, 2d) flows constantly cold water with $\dot{v}_w$ = 11 l/min, in order to dissipate the heat from the nails optimally. All nails are held in position in the perforated plates (position 2h) by cutting rings (position 1e) attached at the top of each nail. A brightly polished stainless-steel plate (position 2i) is placed on the perforated plate to cover the free holes and to reduce the undesired skid mark on the heated blanks. In addition, gaseous N is continuously purged in the upper area of the contact cooler (position 1d) to avoid any condensation on the nail cooler. This ensures constant cooling rates during all experiments.

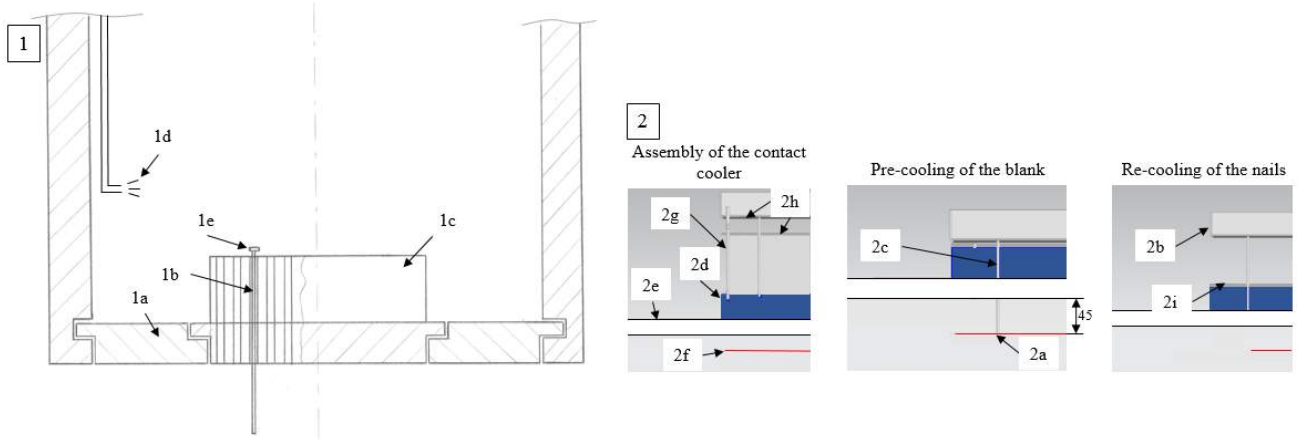

Figure 19: Drawing and schematic illustration of the different operating modes of EBNER's contact cooler

Centering devices

Another important point is the centering of the blanks before they are pre-cooled with the contact cooler. Therefore, three centering devices installed in the trial furnace are used to guarantee that the blanks are positioned the same for each test cycle. Figure 20 shows the outside and inside views of the trial furnace and the exact location of the centering devices.

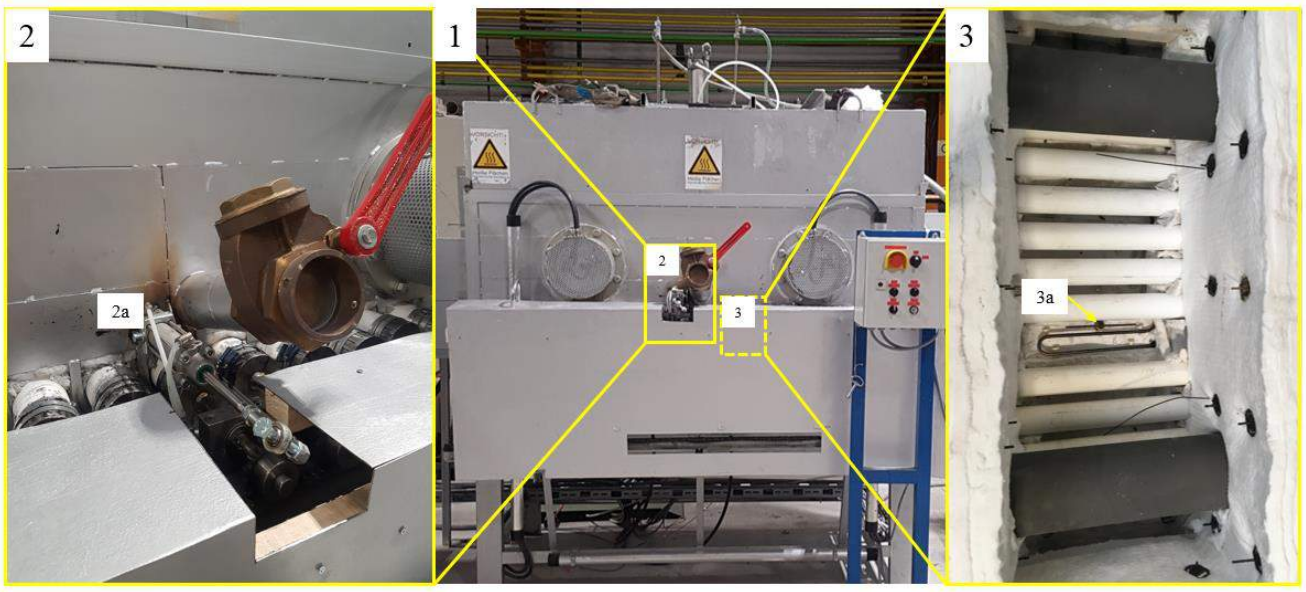

Figure 20: Centering devices (1: trial furnace, 2a: transverse centering, 3a: longitudinal centering)

Detail 2 of figure 20 shows one of the two transverse centering devices (position 2a) arranged on both sides of the trial furnace. Detail 3 displays the inner part of the furnace with its longitudinal centering device (position 3a) which is placed next to the electric heating coil.

The excellent centering of the blank during operation mode is shown in figure 21.

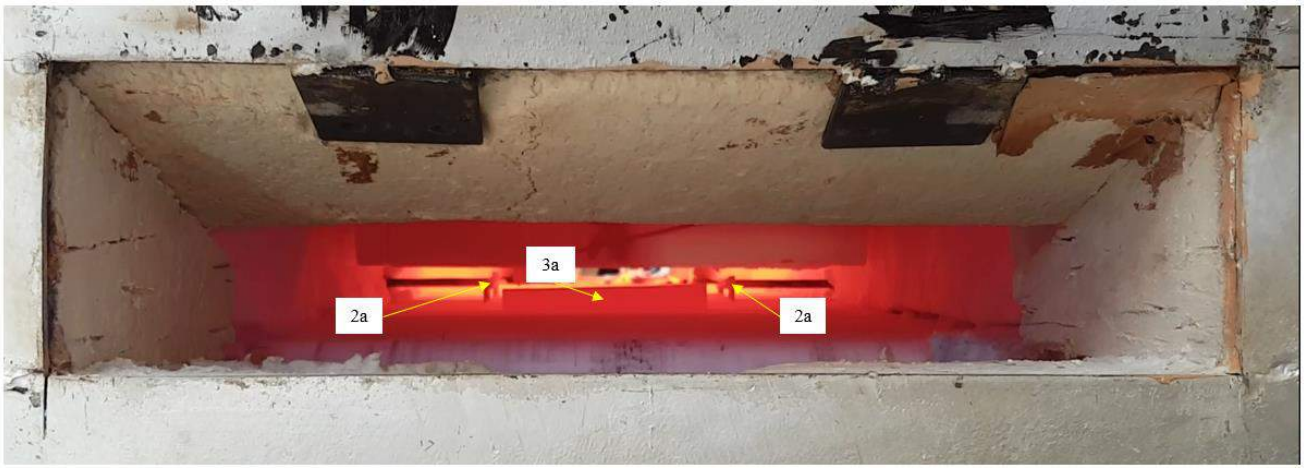

Figure 21: Blank centering

Roller drive unit

As shown in figure 22, a total of twelve ceramic solid rollers of fused silica (position a) are installed at the trial furnace, which are equipped with high temperature resisting sealings. It should be noted, that the bearings (position b) are located on the outside of the furnace to protect them from high temperatures. [17]

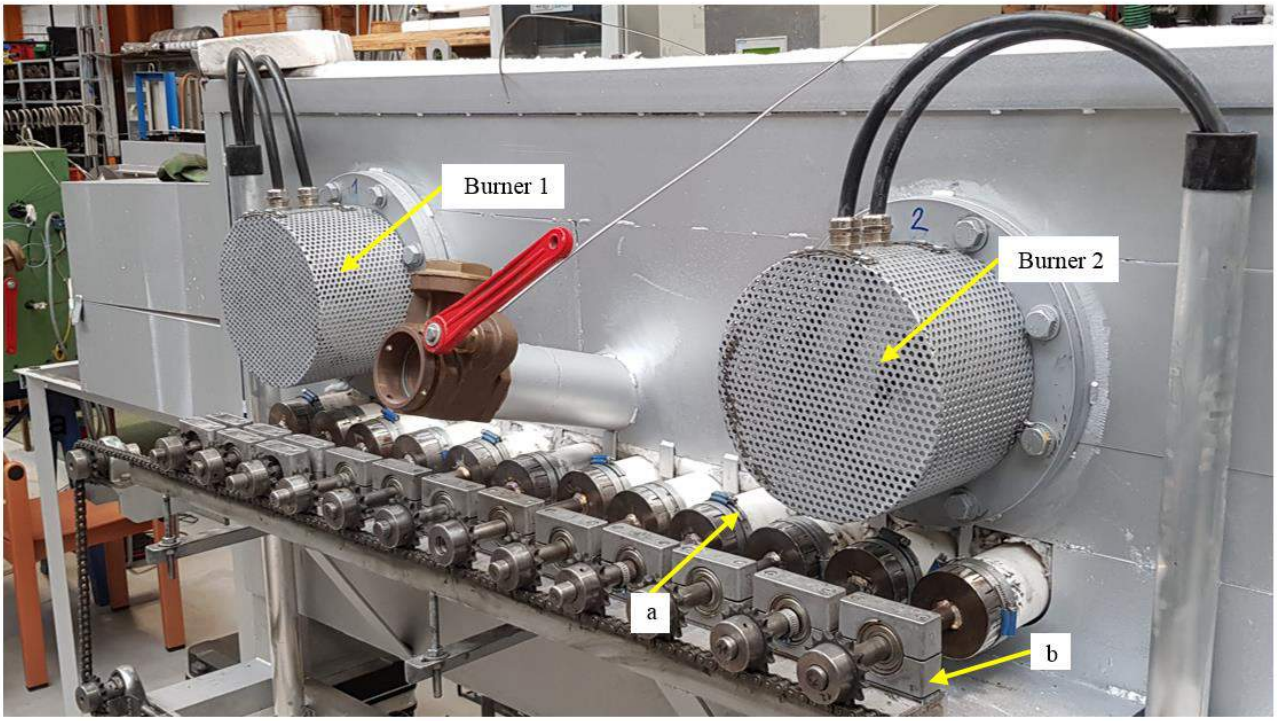

Figure 22: Roller drive unit of the trial furnace

4.3 Measurement and evaluation tools

The measurement and evaluation instruments used for this work are listed and explained herein. It is very important that all experimental procedures are measured and recorded during the execution to ensure the adjustment and optimization of any test settings. The analysis was mainly carried out at the Materials Testing Department of EBNER and additionally at the Institute of Materials Science, Joining and Forming of Graz University of Technology.

4.3.1 Temperature mensuration

Several thermocouples are arranged to detect and record varying temperatures during the heat treatment in various regions of the blanks and the testing apparatus. The thermocouples are connected to the portable laboratory data acquisition and recording device ‘Touch Screen GP20’. This multi-point touch panel from ‘Yokogawa’ is illustrated in figure 23.

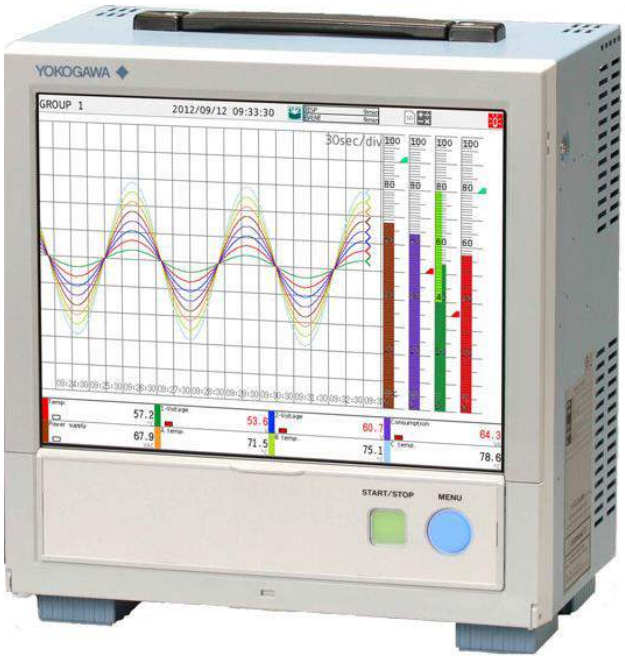

Figure 23: OpreX^{TM} data acquisition and recording system [68]

4.3.2 Temperature evaluation

The data generated by the Yokogawa recorder is analyzed using EBNER’s evaluation software ‘GLdat NT’. The archived process parameters and time-temperature curves then help accurately identifying and changing important setpoints.

Figure 24 schematically shows a time-temperature curve generated by a thermocouple in the middle of a 250x250x2 boron steel blank and two thermocouples on the inside of the Cu nails of the cooling system. As shown, the maximum temperature of one Cu nail rises to about 195°C while the blank gets pre-cooled.

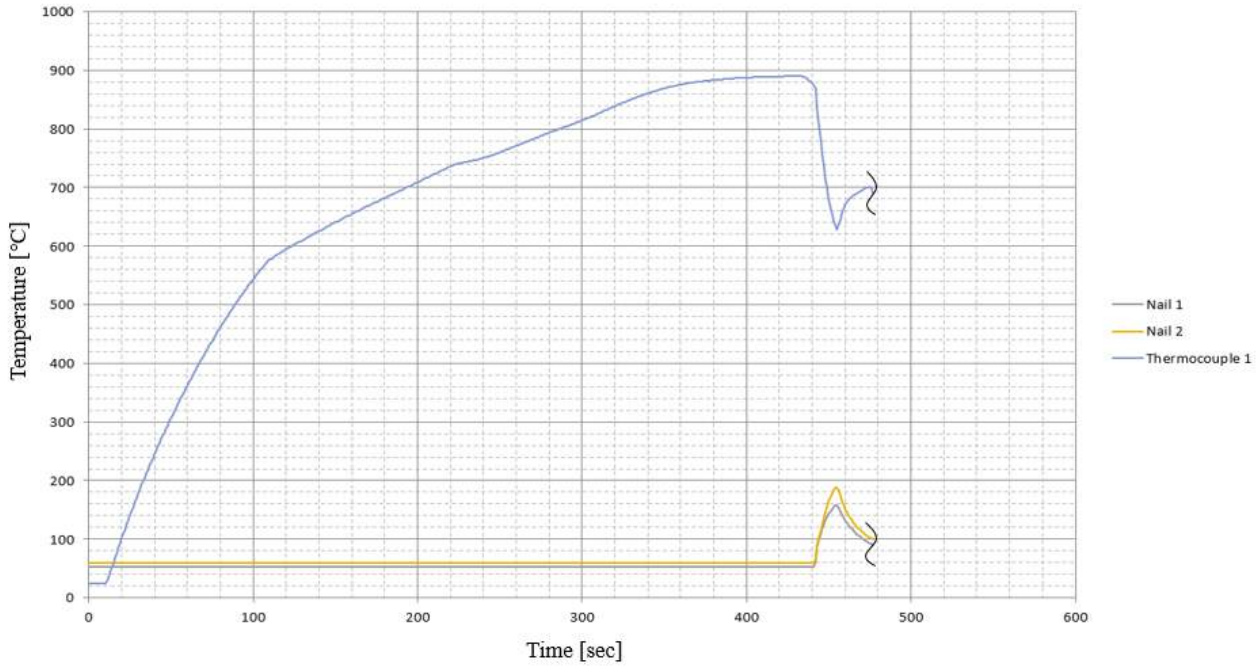

Figure 24: Process evaluation with 'GLdat NT'

4.3.3 Tensile tests

Tensile tests are performed to determine the stress-strain relationships of the blanks in the as-delivered and heat-treated conditions. After the controlled quenching in the flat tool, the test pieces are cut out by using the waterjet cutter 'ProtoMAX'. This is done to obtain reliable stress-strain relationships, whilst considering the rolling direction of each blank.

In addition, this type of sample preparation minimizes the unwanted heat affected zone and does not alter the microstructural properties of each probe to ultimately obtain valid results.

Figure 25: Sample preparation with the waterjet cutter built by OMAX [84]

Flat dog bone specimens are prepared according to DIN EN ISO 6892-1 with a gauge length of 50mm (A_{50}). The sample thicknesses are 1 and 2mm. All tensile tests are carried out with the material testing device ‘RetroLine’ from the company Zwick/Roell.

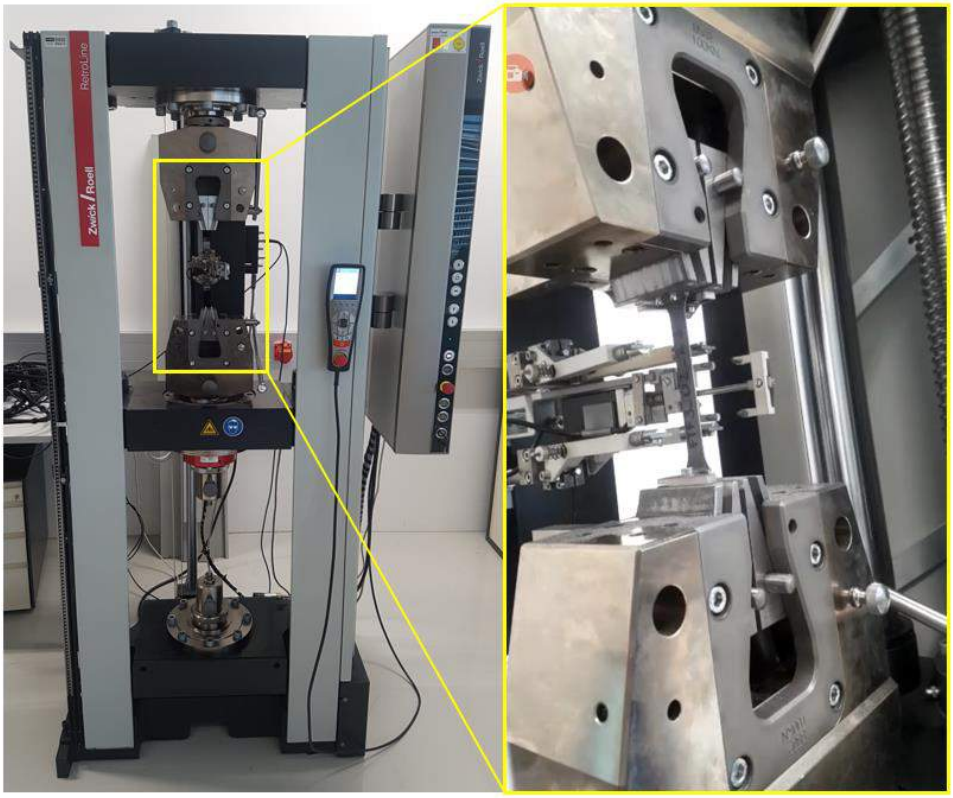

Figure 26: Zwick/Roell materials testing machine

The geometric characteristics and the exact position of the specimens for the tensile tests are illustrated in Appendix A1.

4.3.4 Hardness tests

First, the samples are cut out from each heat-treated blank using the waterjet cutter ‘ProtoMAX’. Then, hardness curves are obtained by measuring the cross-section of the polished specimens. Before the hardness mapping can be done, the probes have to be embedded with Struers’ electro-hydraulic dual cylinder mounting press using the embedding agent ‘DuroFast’. After curing, the specimens are ground and polished to 1µm with the ‘Tegramin-30’ grinding and polishing machine from Struers to achieve the surface quality required for the tests. Finally, the ‘EMCO-TEST’ hardness testing machine is used, where indentations are held at a constant distance of 1mm to obtain the most accurate hardness mapping throughout all samples. In the present work, the Vickers hardness test is used, which is standardized according to DIN EN ISO 6507-1. During the measurement, the indenter is pressed into the sample with a defined test load. With this optical non-destructive and static measurement system, the indentations (diagonals) created by the equilateral diamond pyramid are measured to determine the hardness values. This square-based pyramid has an aperture angle of 136°. [87] The yellow square (position 3) of figure 27 shows the area in which HV10 hardness measurements are carried out.

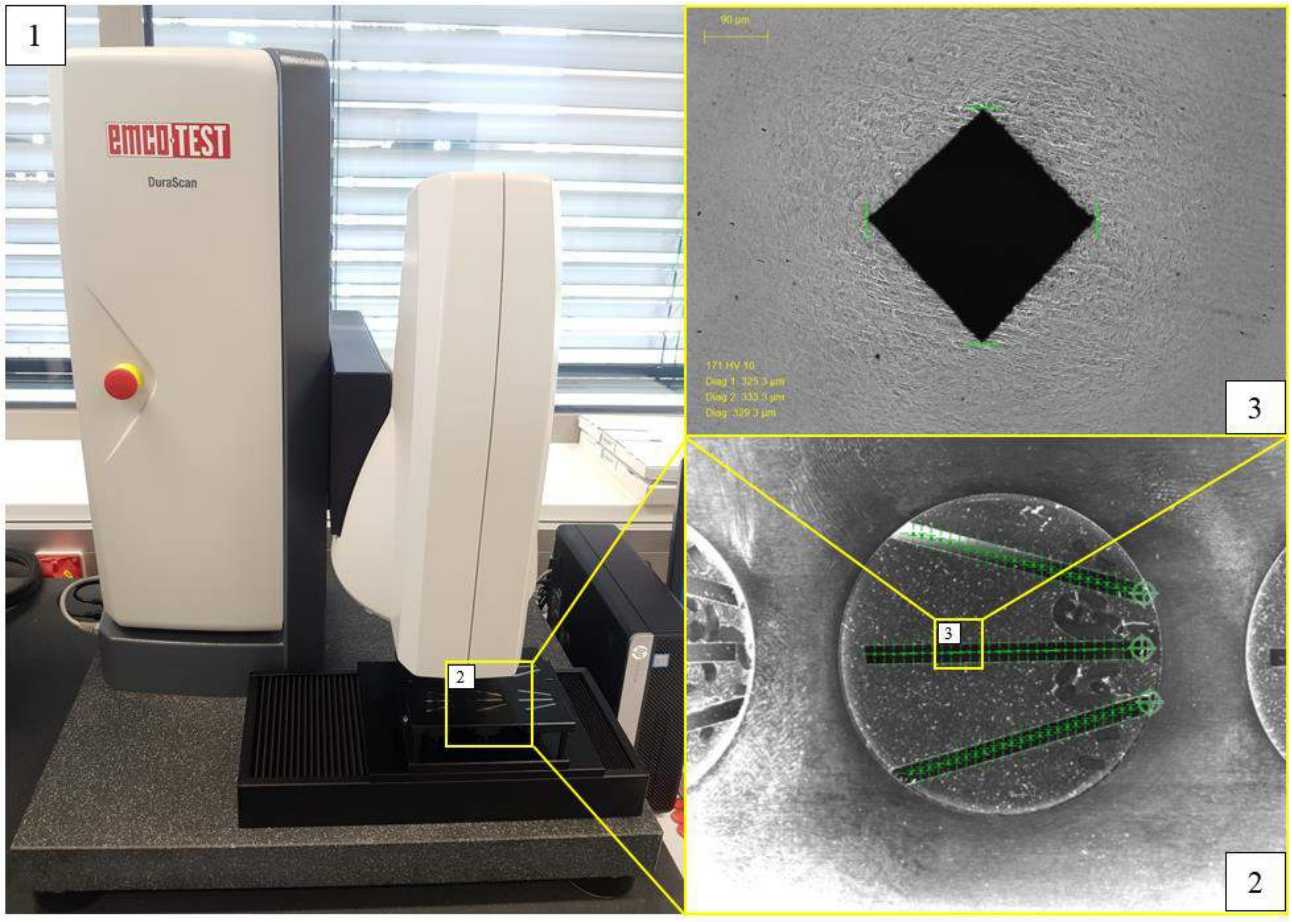

Figure 27: Hardness measurements (1: hardness testing machine ‘DuraScan’, 2: setting of the distance between the indentations, 3: thumbnail of an indentation)

As already noted in chapter 4.2.1, EBNER’s SimCAL 3.0 is used to execute time and cost saving experiments. Figure 28 illustrates the top view of the geometric properties of heat-treated samples from EBNER’s

SimCAL 3.0. The red cross on the right side of the blank indicates the position of the thermocouple, which is used as the temperature reference throughout the entire tempering process.

The arrow in figure 28 indicates the side on which the hardness measurements are made to get an overview of the different hardness distributions. In addition, the analysis of the time-temperature curves allows the exact definition of each phase transformation occurring during all experiments. Knowing the exact position of the phase boundaries allows the creation of a batch-dependent CCT diagram.

The resulting CCT diagram will be explained in chapter 6.1.

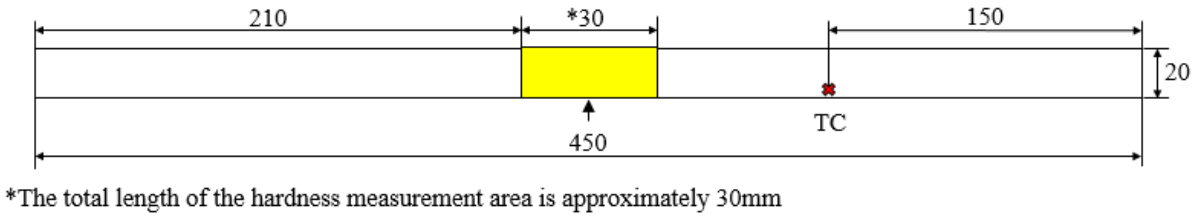

Figure 28: Range for HV10 hardness measurements of SimCAL 3.0 samples

The trial furnace is used to determine the exact size of the transition zones between the hard and soft areas of the blanks. Therefore, the selected cross-sections of the samples from the trial furnace are in the areas between the hard and soft zones. The exact geometric properties of the samples for the hardness measurements can be seen in Appendix A1 which are also cut out by using the waterjet cutter.

4.3.5 Energy dispersive X-ray spectrometer (EDX)

The detection of any Cu residues on the blanks and/or any AlSi residues on the nails as a result of contacts between the contact cooler and the austenitized blanks is carried out with an EDX-analysis. This method is widely used and is able to detect various elements or substance quantities of less than 0.1 picogram. Various signals, such as X-rays, are emitted when the samples are exposed to a primary electron (PE) beam. [85]

The whole procedure is shown in figure 29.

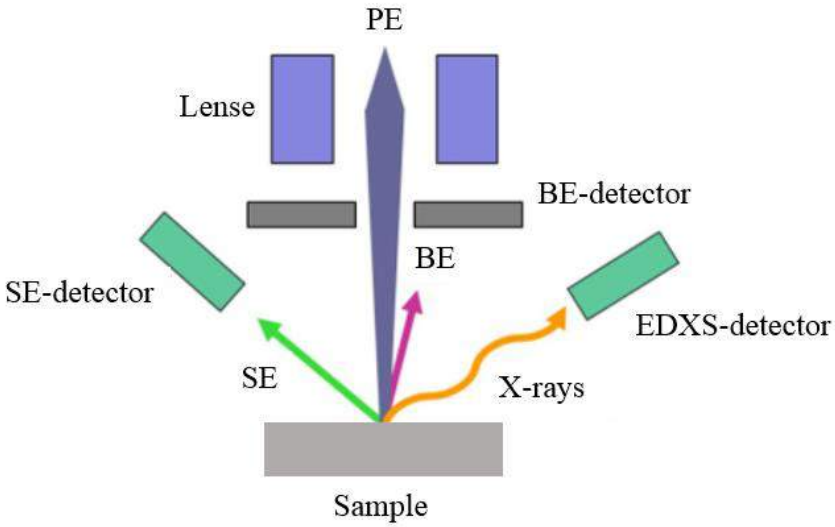

Figure 29: Principal sketch of the signals created by PEs (based on: [86])

4.3.6 Microstructural analysis

Polished specimens can be used to perform microscopic examinations that provide information about the microstructure and the resulting layer thickness of the AlSi coating. Similar to the sample preparation for the hardness measurements in the cross-sectional areas, the probes must also be embedded, ground and polished to 1µm for the microstructural analysis. Thereafter, the samples are etched with an etchant consisting of 3% HNO_3 for approximately three seconds before being analyzed according to their microstructural properties. The microstructural observation is done using an optical microscopy (OM) as illustrated in figure 30.

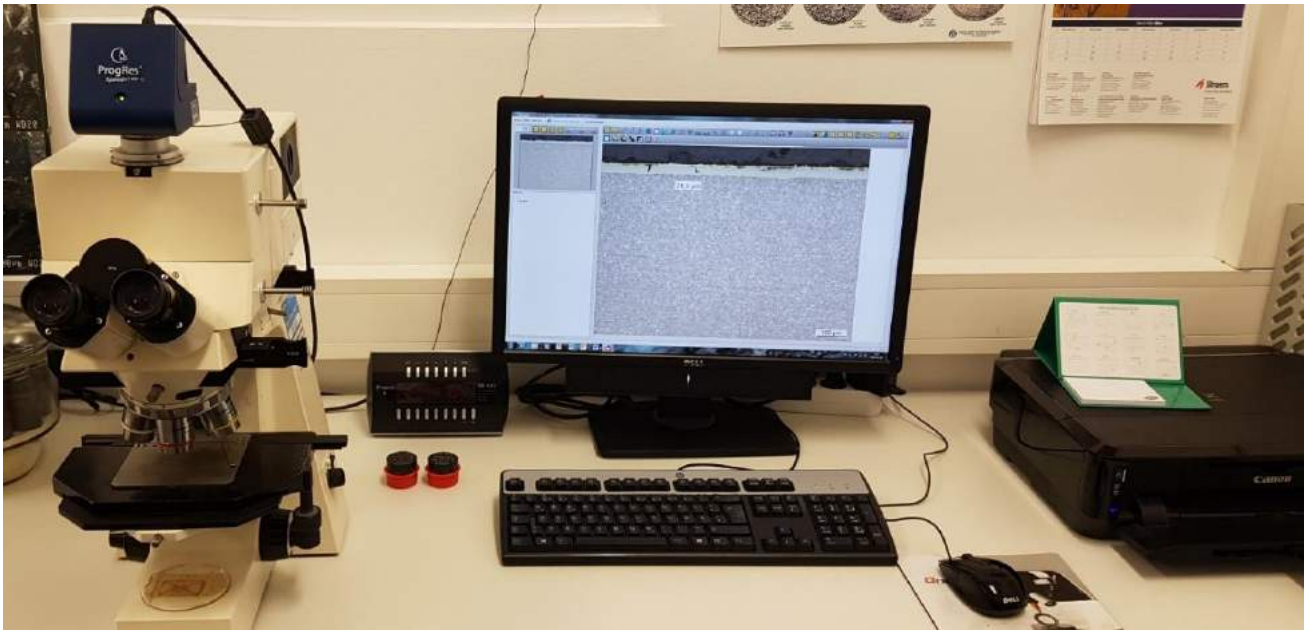

Figure 30: Photomicroscope ‘Axiophot’

5 Experimental procedure

In the following sections of chapter 5, various process steps and the required equipment for all tests are described in detail to understand the entire experimental design in a better way. In addition to determining the preparatory steps for the experiments, the execution of the tests is also explained whilst considering various process parameters.

5.1 Design of experiment

The design of experiment (DoE) identifies important phases of the entire experimental procedure. This helps creating a robust process by keeping unwanted variation at a minimum level. Figure 31 gives an overview of the experimental flowchart, which represents the main phases during the test enforcement and the results evaluation.

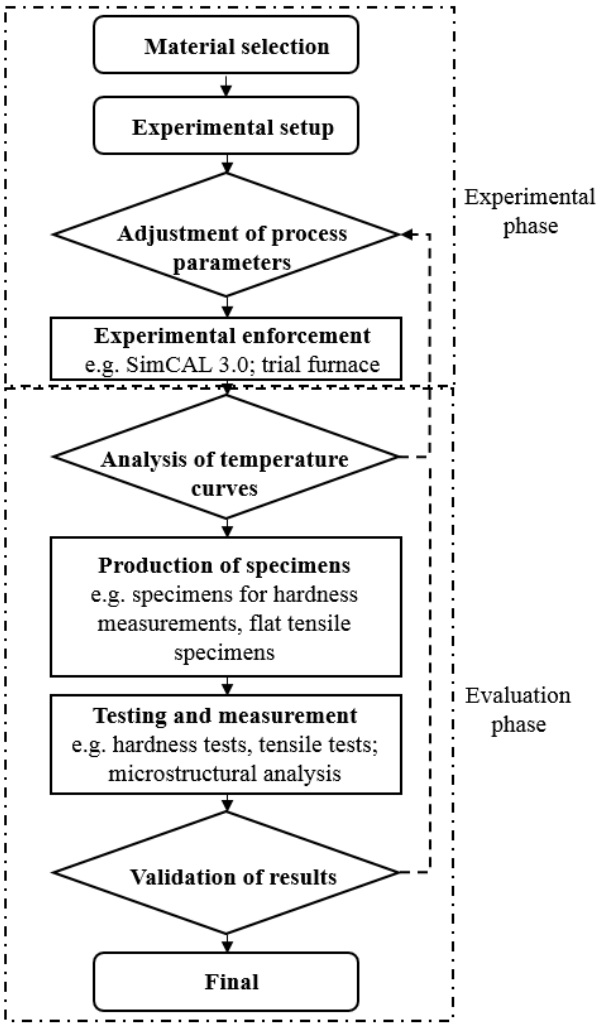

Figure 31: Experimental flowchart

5.2 Experimental setup

The preparation phase is a crucial part to eliminate errors during the experimental procedure. The main purpose of doing these time-consuming preparation activities is to ultimately generate valid results. The blanks used for the practical part of the thesis are cut out of the same batch according to the dimensions given in table 13, paying particular attention to the rolling direction of the entire batch. Then, the flat steel blanks are cleaned with a special cleaning agent before starting the test series in order to remove possible impurities, such as dust, lubrication, dirt, etc. on the surface of the blanks. Guaranteeing a flawless and clean surface condition, the thermocouples for tests with the SimCAL 3.0 and the trial furnace are always, depending on the type of test, placed in the same position on the surface of the blanks to obtain comparable results. This then helps in monitoring, recording, analyzing, and optimizing the heat treatment of steel blanks during and after the tests.

The areas of the blanks, which are pre-cooled with the contact cooler, are pre-marked before heating the furnace. For this purpose, the entire process is simulated in cold condition by using the external and internal centering devices already described in chapter 4.2.2. The benefit of doing so, is to ensure the specimens for the tensile tests and the hardness measurements are cut out of the correct positions.

It has to be mentioned, that it is of utmost importance that these preparatory steps are carried out in the most accurate way in order to obtain the most reliable and comparable results.

5.3 Process parameters

The practical part of this thesis is carried out with special consideration of the DoE, which guarantees an adequate selection and compliance of the process parameters, as these have a direct influence on the final quality of the sheet metal blanks. The variation of these process parameters, which are explained in this chapter, allow the realization of widely diverging material properties.

The entire process can be divided into two different phases. Phase 1 covers the period in which the blanks are transported through the furnace, while phase 2 covers the period of time in which the blanks are transferred from the furnace to the water-cooled dies.

Finally, the blanks get quenched in the flat tool. Both phases are illustrated in figure 32.

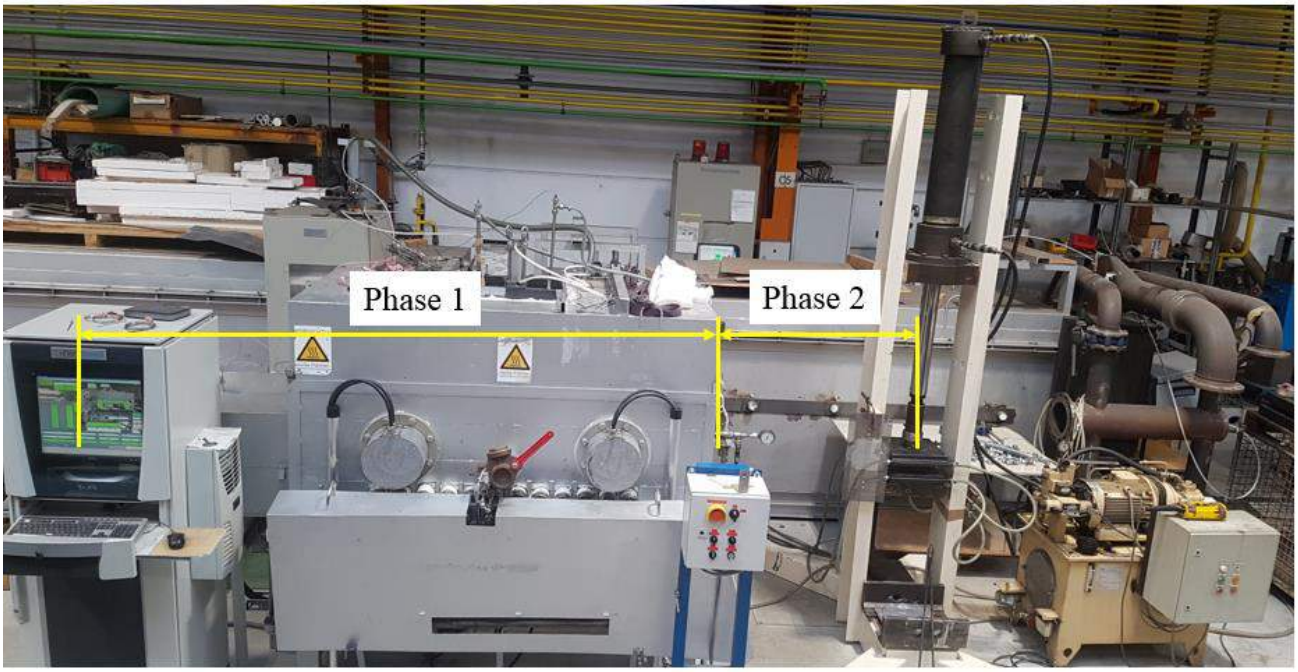

Figure 32: Illustration of the two relevant phases of the entire tailored tempering process

The information regarding relevant process parameters, such as the blank thickness-dependent ideal contact times of the contact cooler $t_{i\_j\text{-}pt}$, the ideal furnace dwell times after the contact cooler $t_{i\_pt\text{-}700}$, the critical transfer times $t_{700\_crit\_i}$, the cooling rates in the flat quenching tool $CR_{fqt\_750\text{-}200}$ etc. are taken from data generated through various tests that have been conducted using the trial furnace which will be explained within the following lines.

An important step of the whole experimental procedure is the determination of the process parameters of phase 1. This is done according to the figures listed in the tables 15 and 16.

ID	s_b	T_f	t_{c_cc}	$t_{i\_j\text{-}pt}$	T_{pt}
[-]	[mm]	[°C]	[sec]	[sec]	[°C]
1.1_890-pt	1	890	30	14	524
2.1_890-pt	2	890	30	12	666
3.1_930-pt	1	930	30	21	455
4.1_930-pt	2	930	30	20	605

Table 15: Preliminary tests to determine the ideal contact times of the contact cooler $t_{i\_j\text{-}pt}$

The blanks are heated to about 890°C respectively 930°C whilst lying exactly under the first burner, where a temperature of T_f = 890°C respectively T_f = 930°C is set, before the test pieces get pre-cooled with the contact cooler for about 30 seconds. All samples listed in table 15 are heated until a blank temperature of 870C° is reached before the austenitization-time-limiting countdown starts.

Then, the samples 1.1_890-pt and 2.1_890-pt are austenitized for approximately 85 seconds, whereas the probes 3.1_930-pt and 4.1_930-pt are austenitized for about 100 seconds before the pre-cooling process begins.

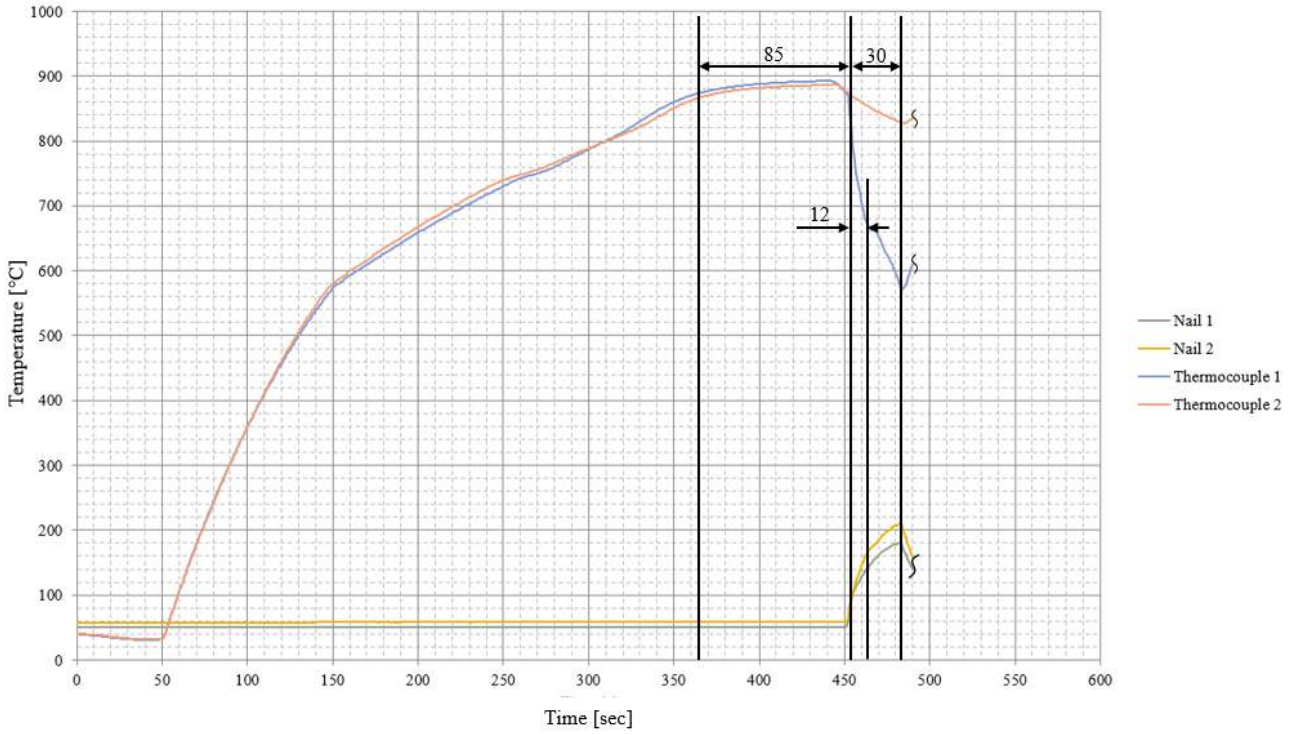

Figure 33: 30 seconds of pre-cooling of the sample 2.1_890-pt

All time-temperature curves, during which the sheet metal blanks are pre-cooled for 30 seconds, can be looked up in Appendix A2.

The electric heating coil, which is placed below the rollers in the area of the contact cooler, is set to a temperature of about 845°C for all tests to minimize the undesired skid mark as the blank moves in this zone. Nevertheless, the temperature in this area varies between 775°C and 812°C during all experiments.

The time-temperature curves are analyzed according to the time elapsed until the phase transformation starts during the pre-cooling process with the contact cooler. The results then are taken as the ideal contact times $t_{i\_j\text{-}pt}$ for each blank. Table 15 also tabulates the temperatures T_{pt} at which the phase transformations begin. It can be seen, that the starting point of the phase transformation decreases with an increasing furnace temperature T_f.

The four pre-cooling times $t_{i\_j\text{-}pt}$ are examined by using two thermocouples on the blank's surface as shown in figure 34. It must be noted, that the positions of the two thermocouples are exactly located between the rollers while the blank is pre-cooled, ensuring the temperature influence of surrounding rollers is minimized.

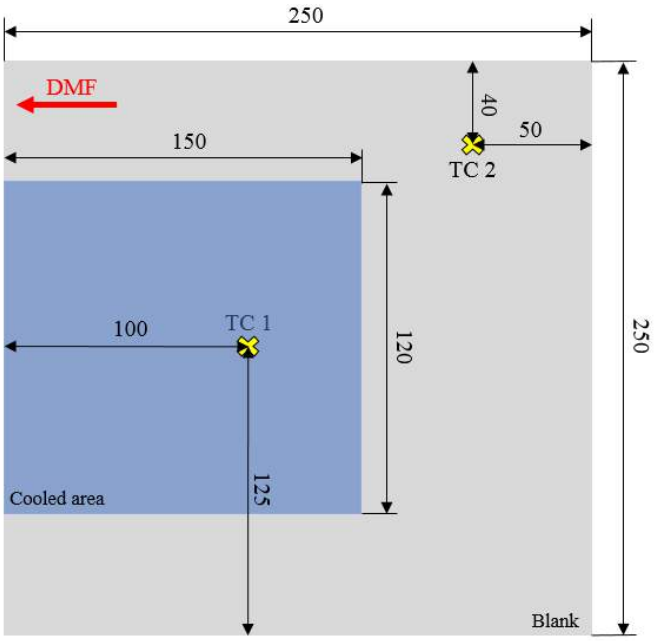

Figure 34: Thermocouples for investigating the ideal contact times of the contact cooler $t_{i\_j\text{-}pt}$

The time periods $t_{i\_j\text{-}pt}$ are subsequently used for further tests determining the ideal furnace dwell times after the contact cooler $t_{i\_pt\text{-}700}$. The determination of $t_{i\_pt\text{-}700}$ is also done using two thermocouples placed on the blanks according to figure 34. After the pre-cooling step is carried out, the test pieces are conveyed to the second burner which is set to a constant temperature of 750°C for all tests. The boron steel samples remain at this position until the pre-cooled area is reheated to a temperature of T_{out_TC1} = 700°C. The experimental setup with the investigated ideal dwell times after the contact cooler $t_{i\_pt\text{-}700}$ and the diverging temperatures in the hot region T_{out_TC2} are illustrated in table 16.

ID	s_b	T_f	$t_{i\_j\text{-}pt}$	$t_{i\_pt\text{-}700}$	T_{out_TC1}	T_{out_TC2}
[-]	[mm]	[°C]	[sec]	[sec]	[°C]	[°C]
1.2_pt-700	1	890	14	32	700	757.8
2.2_pt-700	2	890	12	19	700	806.5
3.2_pt-700	1	930	21	35	700	764.1
4.2_pt-700	2	930	20	29	700	805.1

Table 16: Preliminary tests to determine the ideal furnace dwell times after the contact cooler $t_{i\_pt\text{-}700}$

Figure 35 shows an exemplary time-temperature curve of the sample 2.2_pt-700. As illustrated, the blank gets reheated for about 19 seconds until a temperature of 700°C in the pre-cooled area is reached again.

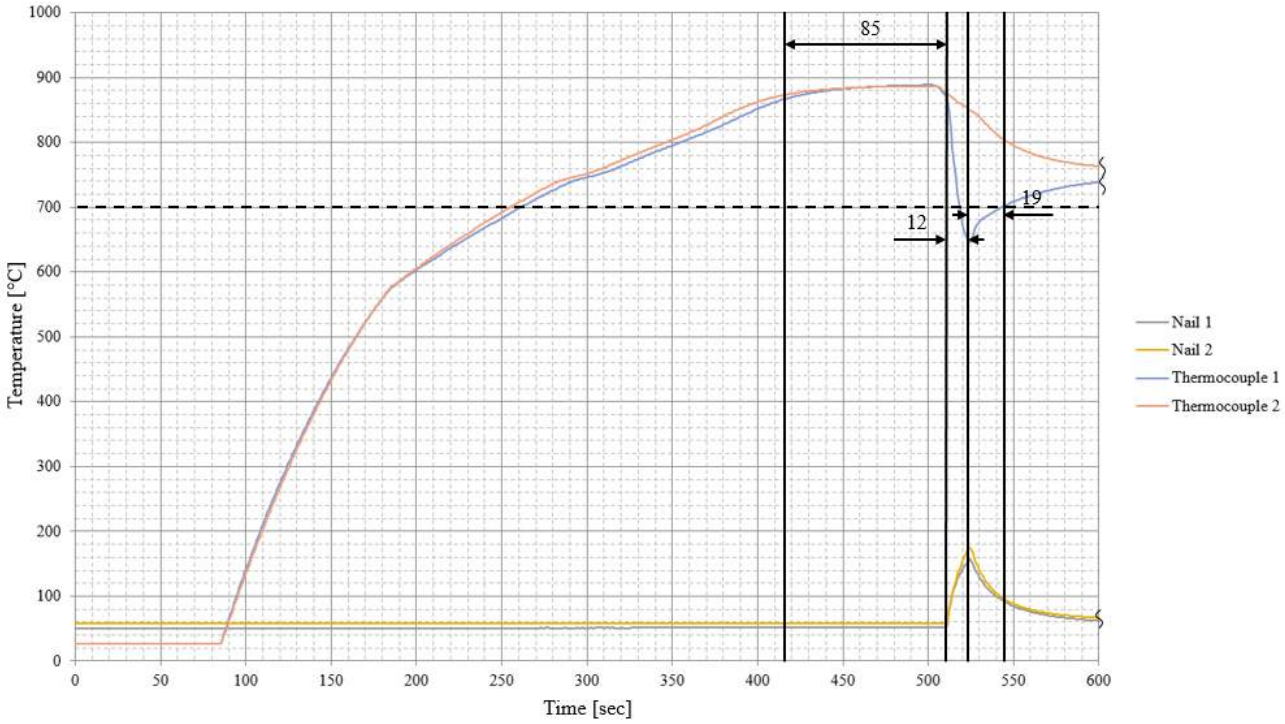

Figure 35: Ideal furnace dwell time of the sample 2.2_pt-700

All tests performed to determine the ideal furnace dwell times after the contact cooler $t_{i\_pt\text{-}700}$ are illustrated in Appendix A3.

After all relevant process parameters of phase 1 are fixed, the investigation of the process windows of phase 2 remains. For these tests, eleven thermocouples are spot-welded on the blank's surface, covering the entire transition zone, which are prepared as shown in figure 36. The thermocouple TC10 is used as a reference for the heated area of the blank where no skid mark of the contact cooler appears.

The transverse and longitudinal centering of the blank before the pre-cooling step is carried out according to the details 1 and 2 as displayed in figure 36.

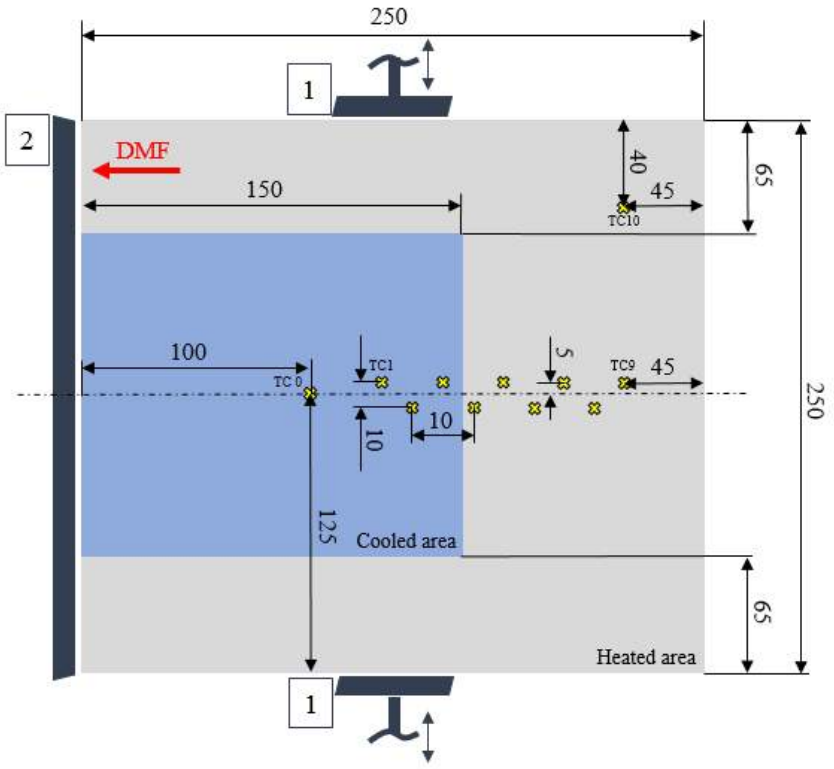

Figure 36: Thermocouples covering the hot and pre-cooled zones of the blank

Afterwards, the critical transfer times $t_{700\_crit\_i}$, which are part of the second phase of the entire process, are determined using these thermocouples-equipped blanks. The 250x250x1mm respectively the 250x250x2mm blanks are again exposed to the already fixed heat treatment cycles tabulated in table 16 before the glowing blanks finally get cooled in air until they reach ambient temperature T_a. The results of these tests enable the determination of exact time-temperature curves with respect to the unevenly heated areas of the blanks. This then helps identifying the critical transfer times $t_{700\_crit\_i}$. These time periods $t_{700\_crit\_i}$ are crucial for determining possible process windows until a minimum allowable hot zone insertion temperature of approximately 700°C is reached. The relevant figures of these preliminary tests with infinite air cooling are listed in table 17.

ID	s_b	T_f	$t_{i\_j\text{-}pt}$	$t_{i\_pt\text{-}700}$	$t_{700\_crit\_i}$
[-]	[mm]	[°C]	[sec]	[sec]	[sec]
PTAF1	1	890	14	32	5
PTAF2	2	890	12	19	11
PTAF3	1	930	21	35	5
PTAF4	2	930	20	29	11

Table 17: Preliminary tests with infinite air cooling

Figure 37 shows the time-temperature curves of the various thermocouples as the PTAF2 steel blank indefinitely cools in the air.

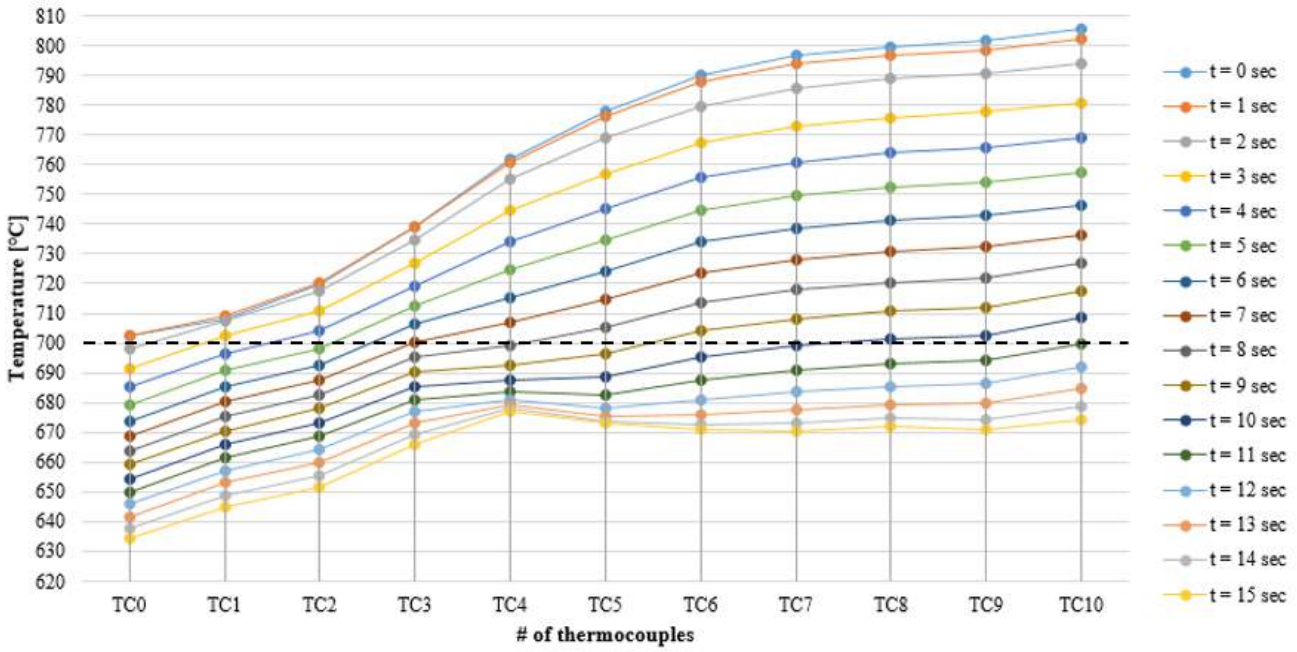

Figure 37: Time-temperature curves of all thermocouples of the PTAF2 blank

It can be seen, that the blank is removed from the trial furnace after the pre-cooled zone (TC0) is reheated to a temperature of about 700°C. It takes about eleven seconds for the hot zone of the blank to reach a temperature of 700°C (dashed line) during the cooling process in the air. In Appendix A4, all location-dependent temperature curves after the steel sheets are removed from the trial furnace are listed.

Figure 38 illustrates the entire heat treatment cycle of the sample PTAF2. As already mentioned, the thermocouple TC10, which is located in the hot area of the blank, defines a process window of eleven seconds until a blank temperature of 700°C is reached while the blank is cooled in air indefinitely.

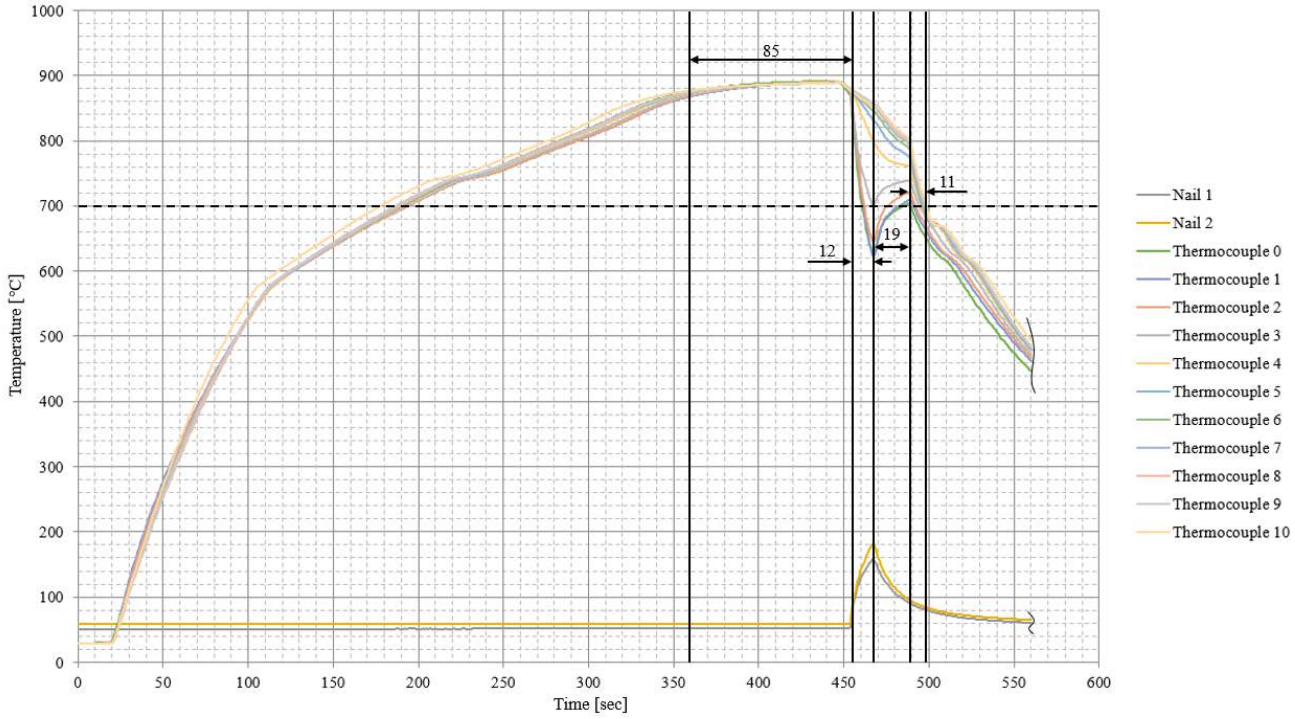

Figure 38: Determination of the critical transfer time of the sample PTAF2

All curves to determine the critical transfer times $t_{700\_crit\_i}$ are shown in Appendix A5.

Another major point of this work is the exact definition of the cooling rates $CR_{fqt\_750\text{-}200}$ during the quenching process in the flat tool as a function of the blank thickness. Therefore, a sheath thermocouple is placed in the middle of a 250x250x2mm sheet metal blank according to figure 39.

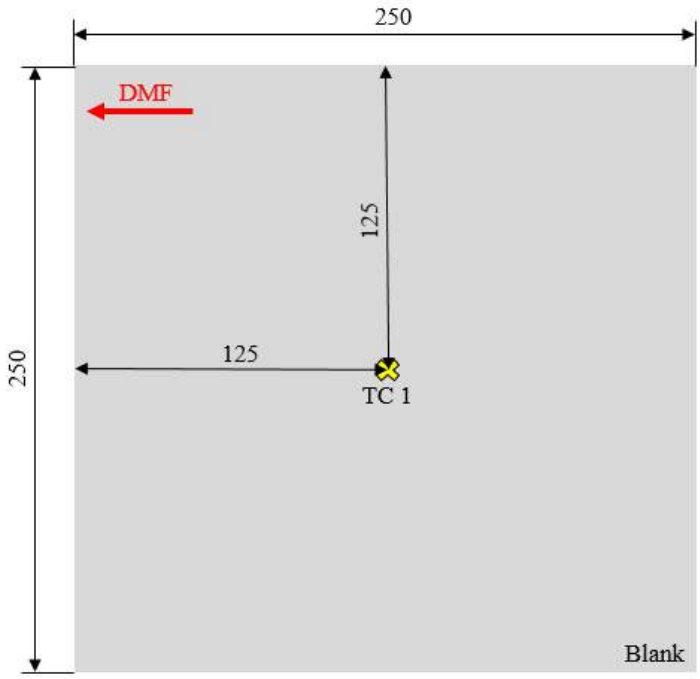

Figure 39: Position of the thermocouple to determine the cooling rate of the flat quenching tool $CR_{fqt\_750\text{-}200}$

For this type of experiment, the blanks are quenched in the flat tool after leaving the furnace without any pre-cooling. These process steps are repeated, and then, the temperature gradients between 750 and 200°C are analyzed to determine the average cooling rate $CR_{fqt\_750\text{-}200}$ with the temperature evaluation software 'GLdat NT'.

Thereafter, the investigated heat treatment cycles are used for further experimental studies with the trial furnace. Based on the resulting critical transfer times $t_{700\_crit\_i}$ tabulated in table 17, it is assumed, that lower and upper transfer times define the tailored tempering process window in the most precise way. After the specimens are cut out of the blanks according to the dimensions shown in Appendix A1, they are taken for hardness measurements in the cross-section, for tensile tests, and for a metallographic investigation, showing whether the results achieved meet the performance requirements listed in chapter 3.

The final tests represented in table 18 are performed using the trial furnace. In addition to the set values of the transfer times $t_{700\_i\_j\_sv}$, table 18 also shows the values of the actual lower and upper transfer times $t_{700\_i\_j\_av}$. The exponents of $t_{700\_i\_j\_sv}$ indicate the time period that can be used to calculate the reference value at which the hot zone of the blank reaches a temperature about 700°C whilst being transported from the trial furnace to the flat tool.

ID	s_b	T_f	$t_{i\_j\text{-}pt}$	$t_{i\_pt\text{-}700}$	$t_{700\_i\_j\_sv}$	$t_{700\_i\_j\_av}$
[-]	[mm]	[°C]	[sec]	[sec]	[sec]	[sec]
FTF1_l	1	890	14	32	5^{0}	5.5
FTF1_u1	1	890	14	32	7^{+2}	7
FTF1_u2	1	890	14	32	9^{+4}	9
FTF2_l	2	890	12	19	9^{-2}	8.5
FTF2_u1	2	890	12	19	13^{+2}	13
FTF2_u2	2	890	12	19	15^{+4}	15
FTF3_l	1	930	21	35	5^{0}	5
FTF3_u1	1	930	21	35	7^{+2}	7
FTF3_u2	1	930	21	35	9^{+4}	9
FTF4_l	2	930	20	29	9^{-2}	9
FTF4_u1	2	930	20	29	13^{+2}	13
FTF4_u2	2	930	20	29	15^{+4}	15

Table 18: Final tests with lower and upper transfer times using the trial furnace

Figure 40 illustrates a blank for the final tests with the trial furnace where the thermocouple TC1 is placed in the pre-cooled area of the blank.

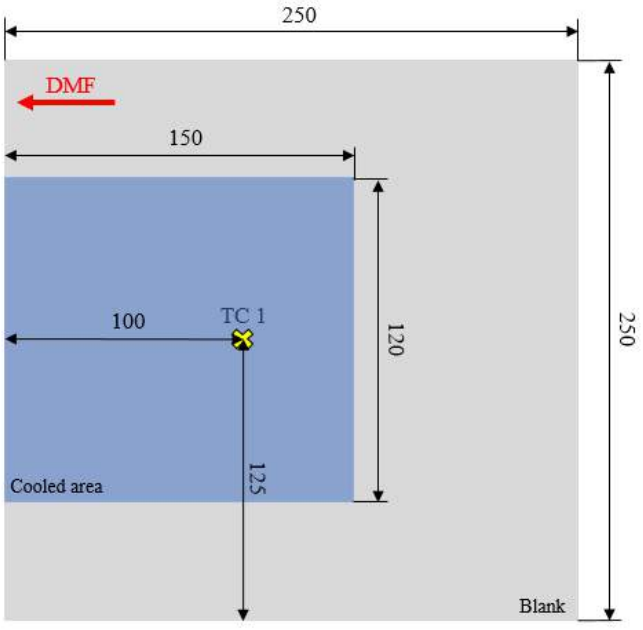

Figure 40: Position of the thermocouple for the final tests

All time-temperature curves of the final tests with lower and upper transfer times can be found in Appendix A6.

Table 19 summarizes all process parameters that are relevant for the entire experimental test procedure. As already mentioned, the main goal is to create possible process windows depending on the necessary part properties. On the one hand, the blank thickness s_b, the blank heating time t_h, the furnace temperature T_f, the ideal contact time of the contact cooler $t_{i\_j\text{-}pt}$, the ideal furnace dwell time after the contact cooler $t_{i\_pt\text{-}700}$, and the transfer time $t_{700\_i\_j\_sv}$ are specified as variables.

On the other hand, the press force of the flat quenching tool F_p, the quenching time of the flat quenching tool t_{fqt}, the cooling medium flow in the contact cooler $\dot{v}_W$, and the nitrogen flow in the upper area of the contact cooler $\dot{v}_N$ are considered to remain constant during all tests.

variable						**fixed**			
s_b	**t_h**	**T_f**	**$t_{i\_j\text{-}pt}$**	**$t_{i\_pt\text{-}700}$**	**$t_{700\_i\_j\_sv}$**	**F_p**	**t_{fqt}**	**$\dot{v}_W$**	**$\dot{v}_N$**
[mm]	**[sec]**	**[°C]**	**[sec]**	**[sec]**	**[sec]**	**[kN]**	**[sec]**	**[lpm]**	**[m^3/h]**
1	85	890	14	32	5	162	30	11	5
2	100	930	12	19	7				
			21	35	9				
			20	29	13				
					15				

Table 19: Variable and fixed process parameters

The following paragraphs will give a brief overview of the procedural steps during the test enforcement using the SimCAL 3.0 and, in addition, the trial furnace.

Tests with EBNER's SimCAL 3.0

When heating samples, SimCAL 3.0 uses a resistance heating application, whereas conventional furnaces use burners. This allows rapid heating of sheet metal blanks whilst producing similar temperature profiles compared to conventional furnaces. While the blanks are pre-cooled with nails and quenched with the flat quenching tool according to tests with the trial furnace of EBNER, SimCAL 3.0 uses N to simulate the slow cooling rates of the nails and He which simulates the fast quenching part of the process. The tanks are located next to the simulator (position 1a). This He-approach allows a similar cooling performance compared to realistic conditions, without neglecting security concerns. The pressure in the He-tank is maintained at a constant level of about 10bar. The gas reaches the slits (position 3b) after passing the control unit (position 1d). These small slits, which are part of the frame (position 2b), are visible under the heated blank and are used as a jet-cooling device, which simulates the quenching process. For each single test, a spot-welded thermocouple (position 3a) is placed on a 1mm respectively 2mm 22MnB5 blank. The position of the thermocouple was placed close to the front end of the blank to avoid being in the relevant testing area. The blank then is fixed in the SimCAL 3.0 application with a clamping cylinder to compensate possible arising strain (position 2e).

Figure 41 illustrates the entire SimCAL 3.0 testing apparatus.

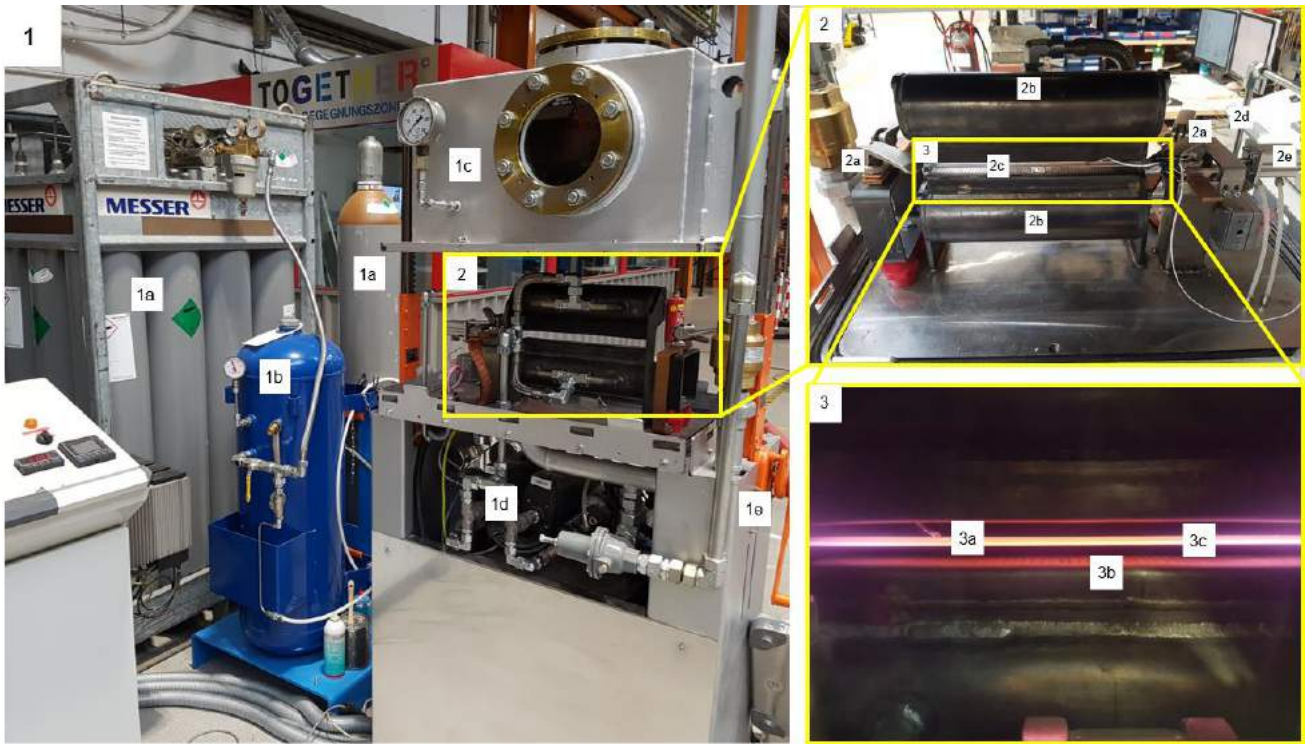

Figure 41: EBNER's SimCAL 3.0 continuous heat treatment simulation tool (1a: gas bottles, 1b: puffer tank, 1c: cover, 1d: control unit, 1e: crank handle, 2a: Cu brackets, 2b: frame, 2c: cold steel stripe, 2d: N purging tube, 2e: clamping cylinder, 3a: thermocouple, 3b: slits, 3c: heated steel stripe)

After the blank (position 2c, 3c) is fixed between the two brackets made of Cu (position 2a), the cylinder (position 2e) is clamped at about 0.3MPa to avoid any bending of the sample during the entire process. Then, the cover (position 1c) is firmly closed by using the crank handle (position 1e) and the chamber is purged

through the nitrogen tube (position 2d) to remove any O in the chamber. The usage of a N-based atmosphere makes it possible to avoid any oxidation of the sheet metal blanks during the entire heating and cooling procedure. After flushing the chamber, the purging remains active at low flow rates throughout the entire process. Figure 41 also shows a fixed blank whilst being heated inside the SimCAL 3.0 application (position 3c). During the heat treatment, the controlling software takes the input generated by the thermocouple on the blank (position 3a) to follow the predetermined temperature profile. In addition, a thyristor controls the process of adjusting the current. After the process is completed, the cover is opened, and the samples are extracted manually.

Tests with EBNER's trial furnace

First, the sheet metal blank is placed on the feeding table. Depending on the type of experiment, different amounts of thermocouples are spot-welded on the surface of the blank. Figure 42 shows an example of nine thermocouples placed on the blank's surface to determine the heat uniformity of the trial furnace, as explained in chapter 6.2.1.

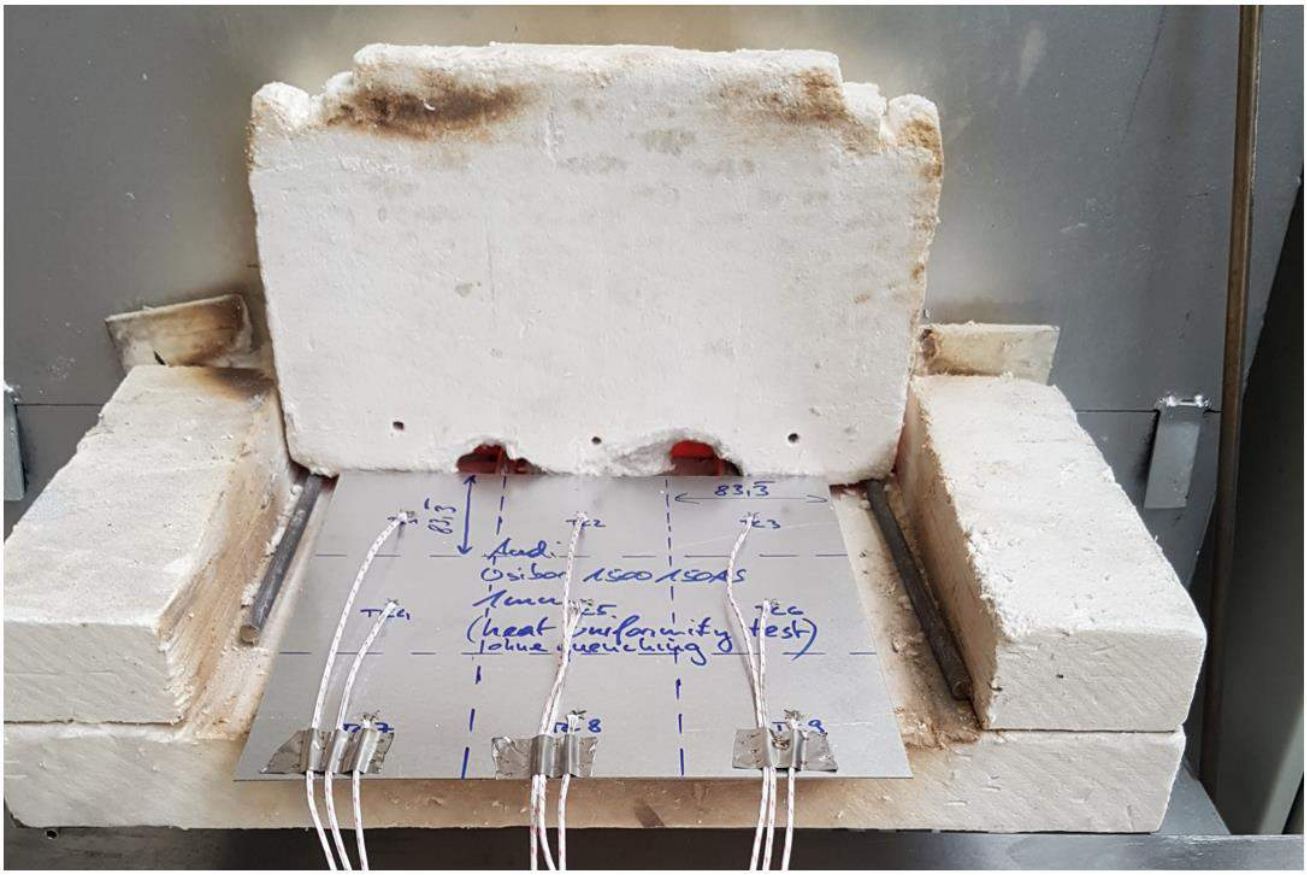

Figure 42: Blank on the feeding table

The next step is to insert the blanks (position b) with a charging rod into the furnace. The test pieces are placed exactly under the first burner (position a) where they are heated with the fastest heating gradient according to the information given in chapter 5.3. The temperature in this area is monitored and controlled by a thermocouple located on the upper side of the furnace chamber (position c).

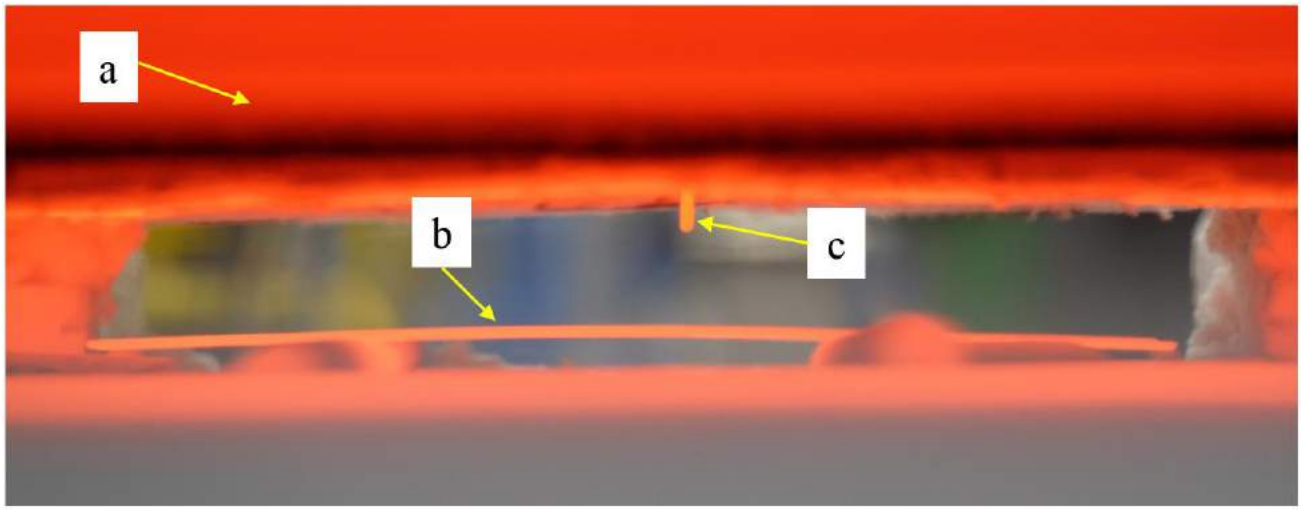

Figure 43: Blank placed under the first burner

Depending on the sheet thickness, the steel blanks remain under the first burner for different periods of time until they are completely austenitized before the solid rollers made of fused silica are turned on. The blanks are automatically transported towards the contact cooler, where they get centered and pre-cooled. The moment in which the blanks are pre-cooled is illustrated in figure 44.

Figure 44: Pre-cooling of a sheet metal blank

After the pre-cooling phase is completed, the blanks are transported to the furnace outlet. Once there, the glowing samples are grasped with a gripper and handed over to the flat quenching tool. The thermocouple gets removed from each blank before the sheet reaches the flat quenching tool. The actual values of the lower and upper transfer times $t_{700\_i\_j\_av}$ are measured using a stopwatch.

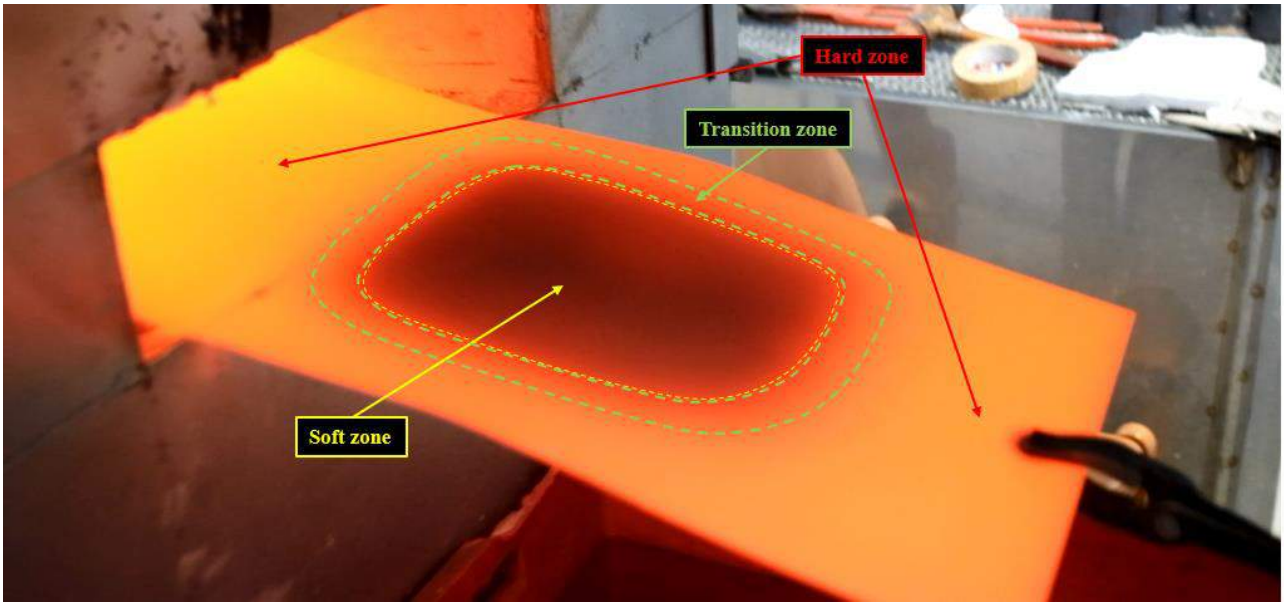

Figure 45: Grasping the blank

The blank (position b) gets positioned in the flat quenching tool (position a) in a way that no complete contact cooling does occur before the tool is entirely closed. Closing the tool takes an average of 2.5 seconds, with the lifting height constantly set to 210mm. After the tool is fully closed, the blanks are quenched for 30 seconds to return to ambient temperature T_a. The flat tool consists of two main parts with internal cooling channels. The contact pressure is kept constant at F_p = 162kN for all tests to be carried out. Thus, the flatness of the blanks produced is ensured. With the waterjet cutter, therefore, the necessary sample geometries can be easily cut out. Figure 46 shows a schematic positioning of a blank with a gripper (position c) in the flat tool.

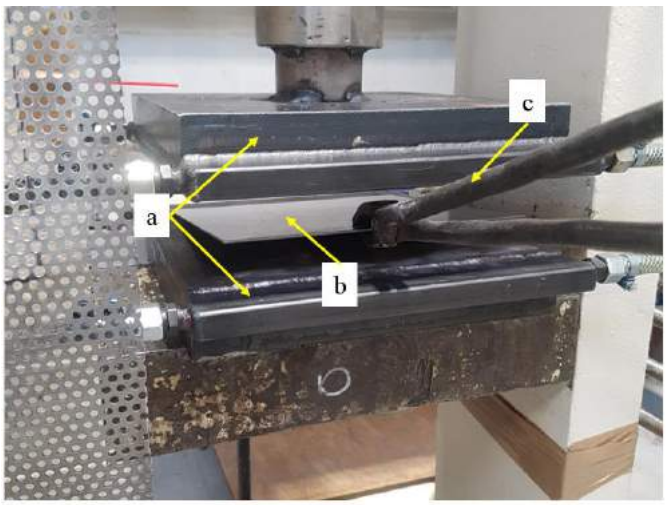

Figure 46: Press hardening by using the flat quenching tool

6 Results and discussion

The following sections of the final part of the thesis contain detailed information on the findings of various experiments conducted with EBNER's SimCAL 3.0 and the trial furnace. The findings are summarized and discussed.

6.1 Tests with EBNER's SimCAL 3.0

The first tests are performed with EBNER's SimCAL 3.0 to get a batch-dependent CCT diagram. An appropriate CCT diagram is the basis for understanding the production of different mechanical properties in one and the same component. The different mechanical properties are generated by targeted control of the blank temperature before the quenching process step is conducted. Therefore, the SimCAL 3.0 is taken to create a batch-dependent CCT diagram that shows the exact phase boundaries while examining different cooling rates. In other words, this CCT diagram is absolutely necessary in order to be able to determine the beginning and the end of each phase transformation during the pre-cooling process in the most accurate way.

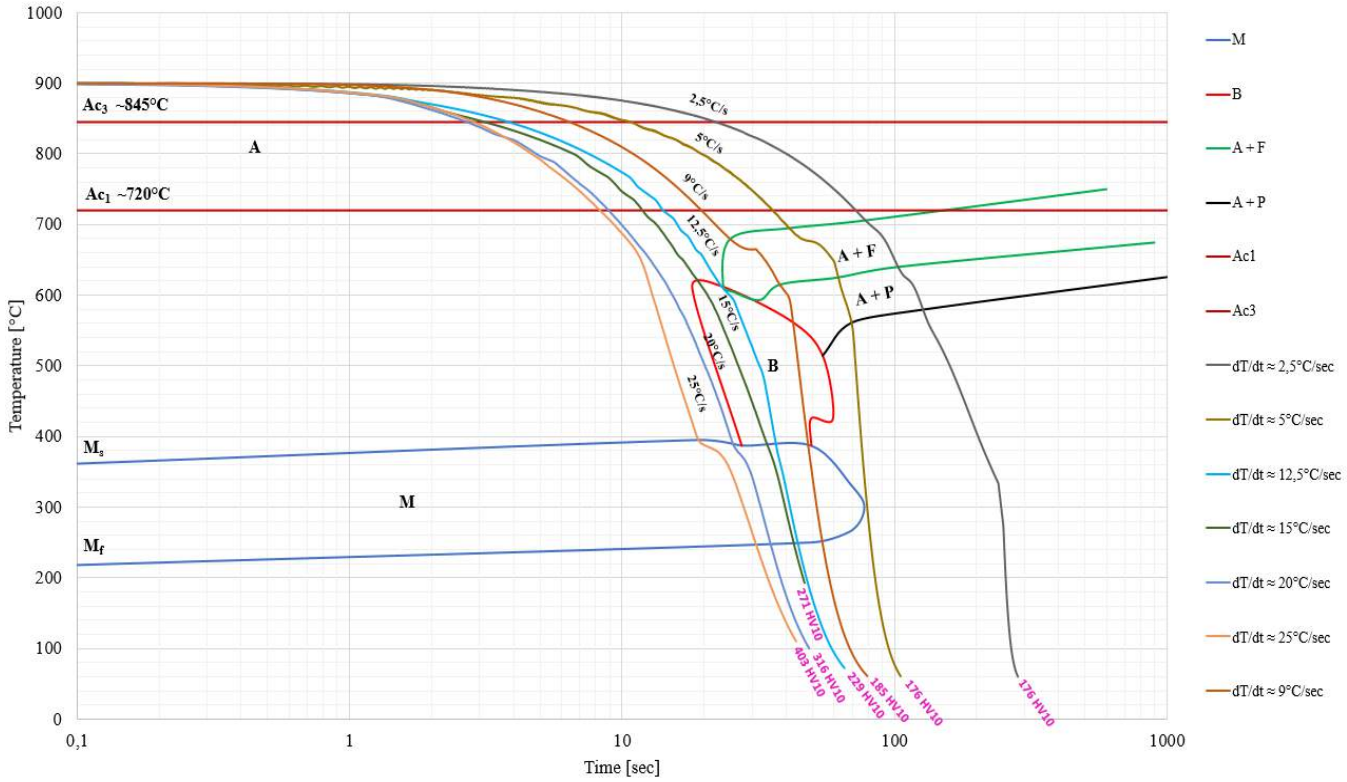

Figure 47: Batch-dependent CCT diagram (based on: [44])

For this test series, every single sheet metal blank is austenitized to a temperature of T_f = 900°C. The tempered stripes are then cooled to simulate different cooling gradients between 2.5°C/s and 25°C/s. The mean hardness value of the blank, cooled at a cooling rate of 2.5°C, is about 176HV10 due to its ferritic-pearlitic microstructure. Instead, 403HV10 are generated with a cooling gradient of 25°C/s.

These different time-temperature curves provide crucial information regarding the exact points at which the phase transformations of the 22MnB5 steel blanks occur. On the one hand, this helps determining the phase boundaries more accurately. On the other hand, knowing the exact position of each phase helps estimating and optimizing the blank thickness-dependent ideal contact times of the contact cooler $t_{i\_j\text{-}pt}$. This is important for the adjustment of the process parameters of phase 1, as already discussed in chapter 5.3. In addition, this batch-dependent CCT diagram is also used to evaluate the cooling performance of various nail materials tested in a preliminary series of experiments.

The exact values generated by the hardness measurements in the cross-section of the blanks can be found in Appendix A7.

6.2 Tests with EBNER's trial furnace

Chapter 6.2 contains the result of the test to determine the heat uniformity of the trial furnace. Then, the cooling performance of the contact cooler is examined to simulate series production. The following paragraphs also provide a comprehensive overview of the mechanical properties of the test pieces obtained by using the DoE. First, insights on the results of the hardness measurements in relevant cross-sectional areas of the blanks are given. Second, the results of the tensile tests are discussed before explaining the outcomes of the EDX-analysis respectively the optical microscopy (OM).

6.2.1 Temperature uniformity of the trial furnace

To ensure reproducible material properties of heat-treated blanks, sufficient knowledge about the temperature distribution in the trial furnace is of utmost importance as it has a direct impact on the uniformity of all final specimens. To validate this, the detection of any temperature variations during the heat treatment in the trial furnace is carried out whilst simulating and recording a conventional thermal heating cycle without any pre-cooling step. The thermal cycle is schematically illustrated in figure 48. Positions 1 and 2 represent the points at which the temperatures of various thermocouples are compared at a furnace temperature of $T_f = 900°C$.

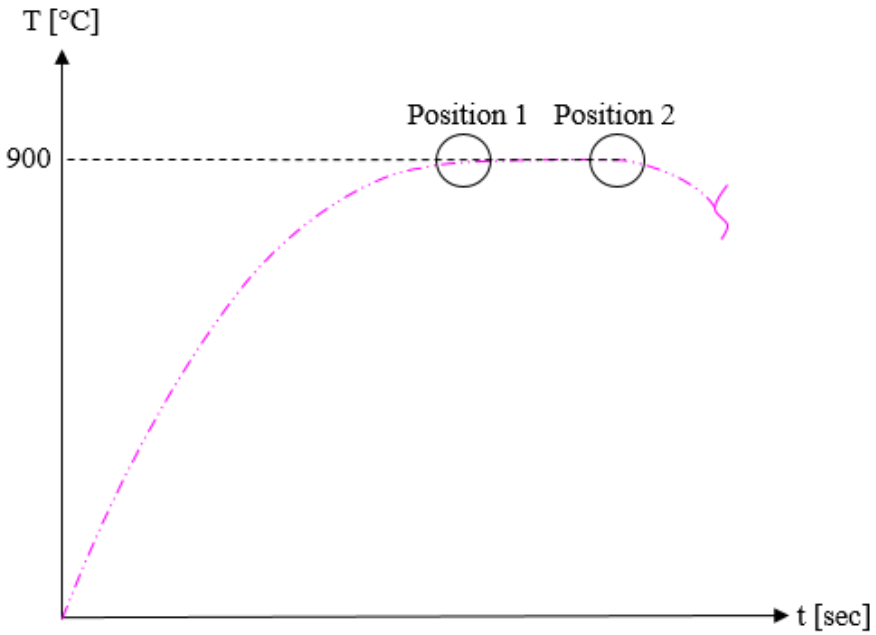

Figure 48: Heating cycle with points for temperature comparison

The yellow crosses in figure 49 represent the nine thermocouples placed on the surface of a 250x250x1mm steel metal blank. This is done to monitor and compare the temperatures that occur in the different areas of the blank during the whole heating process. The thermocouple in the middle can be considered as a reference. The distances between each thermocouple and the direction of material flow are also shown in figure 49.

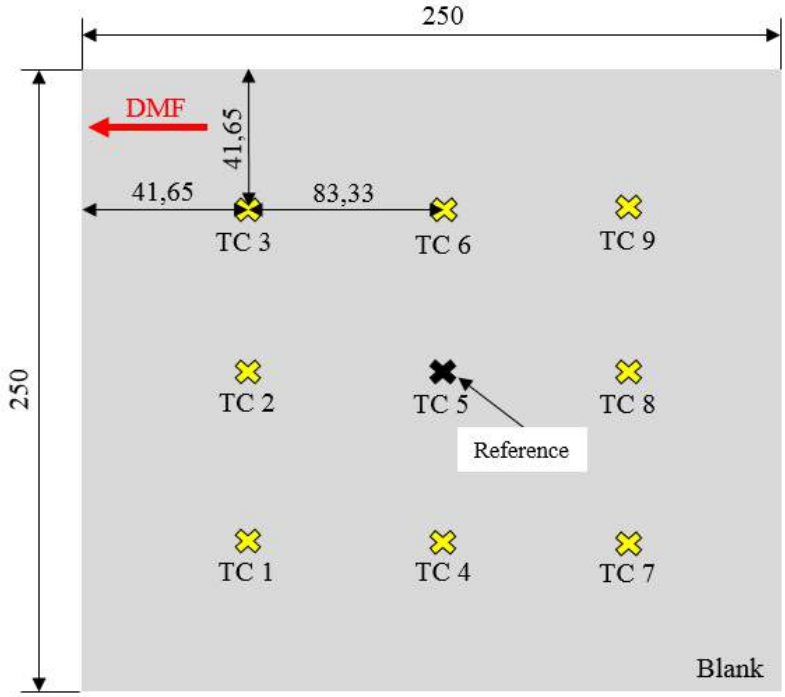

Figure 49: Heat uniformity testing blank for the trial furnace

Before starting the experiment, the blank is turned, which means that the thermocouples are located on the underside of the blank as it is transported through the trial furnace. The temperature deviations of the different areas of the blank in position 1 respectively position 2 are tabulated within table 20.

	TC 1	**TC 2**	**TC 3**	**TC 4**	**TC 5**	**TC 6**	**TC 7**	**TC 8**	**TC 9**
Position 1 [Δ°C]	+0.5	+2	-0.1	-1.7	0	-2.1	-9.4	-9.1	-9.3
Position 2 [Δ°C]	-4.9	-2.7	-3.9	-2.8	0	-5.1	-11.9	-10.5	-12.5

Table 20: Appearing temperature deviations during different phases of a conventional blank heating process

According to the results of the temperature comparison between the different areas of the blank, all temperature deviations are ranging between 0.1 and 12.5°C. The temperature deviations of the thermocouples placed on the front side of the blank (TC 1 – TC 6) remain below 5.1°C. The achieved temperature uniformity due to the small temperature deviations is thus the proof that uniform material properties can be produced.

6.2.2 Cooling performance of the contact cooler

With this experiment, the resulting nail temperature is examined in a simulated series operation. For this purpose, four sheath thermocouples are mounted on the front and back end of a 750x250x2mm sheet steel blank according to the dimensions given in figure 50.

The blank is attached to a rod at the rear end to be able to move it forwards and backwards during the entire experiment.

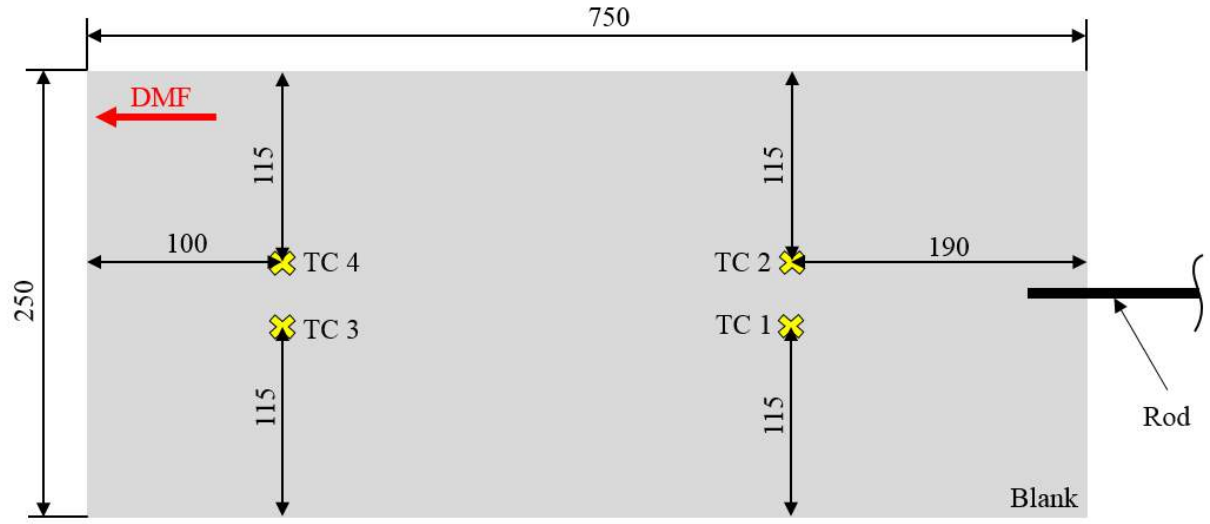

Figure 50: Cooling performance testing blank for the trial furnace

In addition, two Cu nails (position a) are equipped with sheath thermocouples. As shown in figure 51, these thermocouples are located inside the Cu nails (position b). This spot is exactly 2mm above the point of contact with the blank (position c).

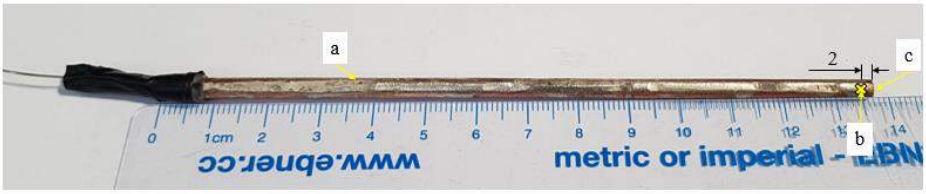

Figure 51: Sheath thermocouple placed on the inside of a Cu nail

The blue area in figure 52 represents the cooling geometry. Black crosses show the exact position of the thermocouples-equipped Cu nails (TC1 and TC2).

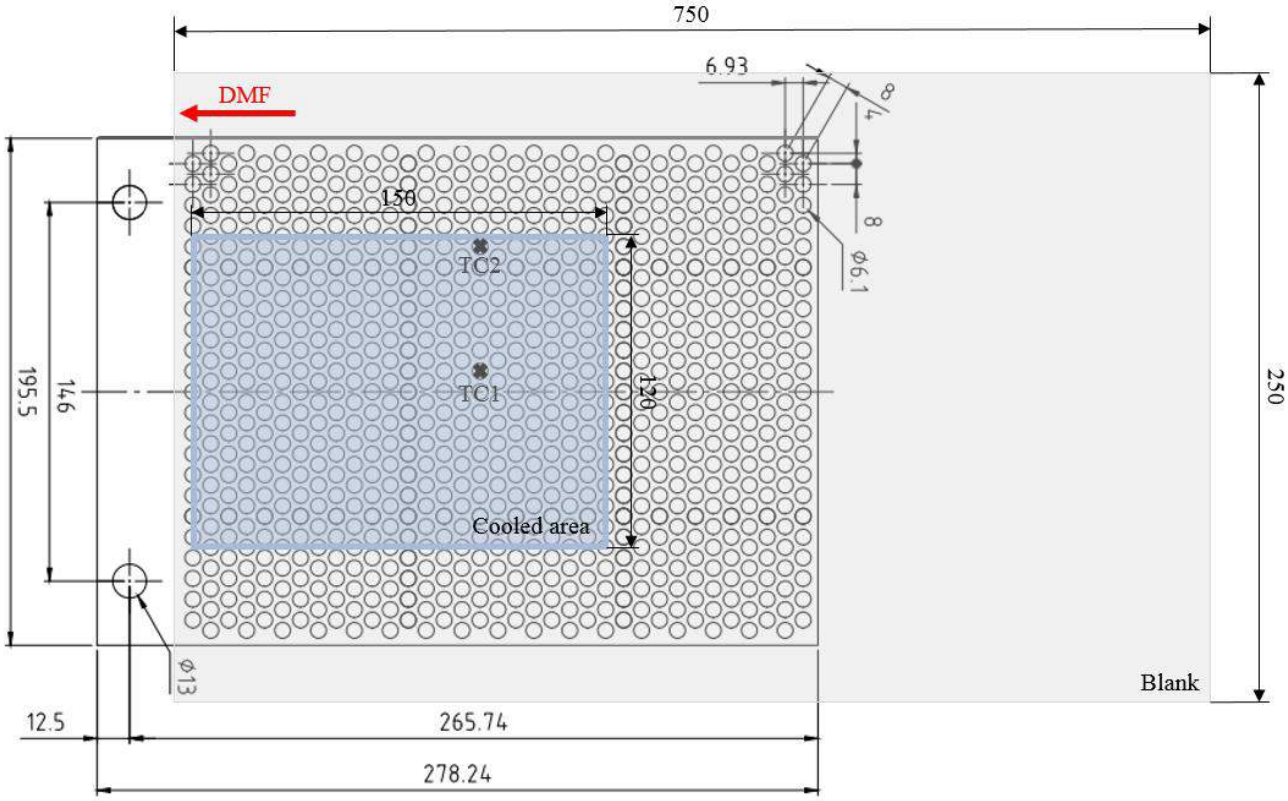

Figure 52: Positions of Cu nails equipped with sheath thermocouples

To prove that the sheath thermocouples on the inside of the nails are exactly in the same position, the following tests, as shown in figure 53, are performed.

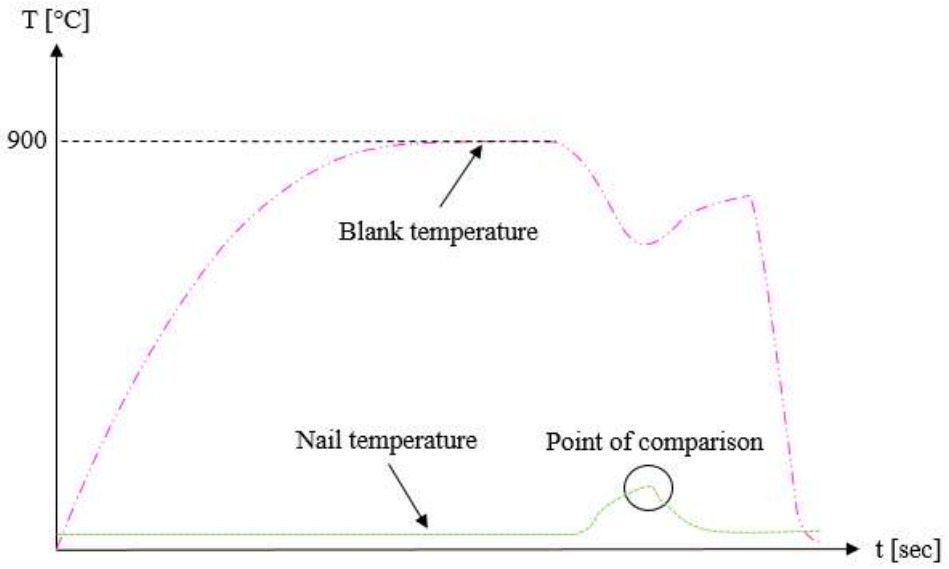

Figure 53: Heating cycle with point for comparing nail temperatures

After the first heat treatment cycle has been carried out, the position of the two thermocouples-equipped nails is swapped and the same process with the same parameters is repeated. The resulting temperature difference, referring to the point of comparison, is below 10°C. This ensures reliable and comparable temperature measurements of both thermocouples-equipped Cu nails.

The test simulating a series production in which the entire blank first is fully heated to about 920°C then follows. The 750x250x2mm sample is alternately cooled with a cooling gradient between 10 and 13°C/sec and reheated with a similar heating rate between 10 and 13°C/sec at the front and rear ends, taking into account a constant time interval of $21^{\pm 1}$ seconds. The average temperature after cooling the blank is about 630°C, while the blank temperature rises up to approximately 880°C after being reheated again. In this way, realistic cycle times for this blank thickness (2mm) are simulated. The result of this experiment is shown in figure 54.

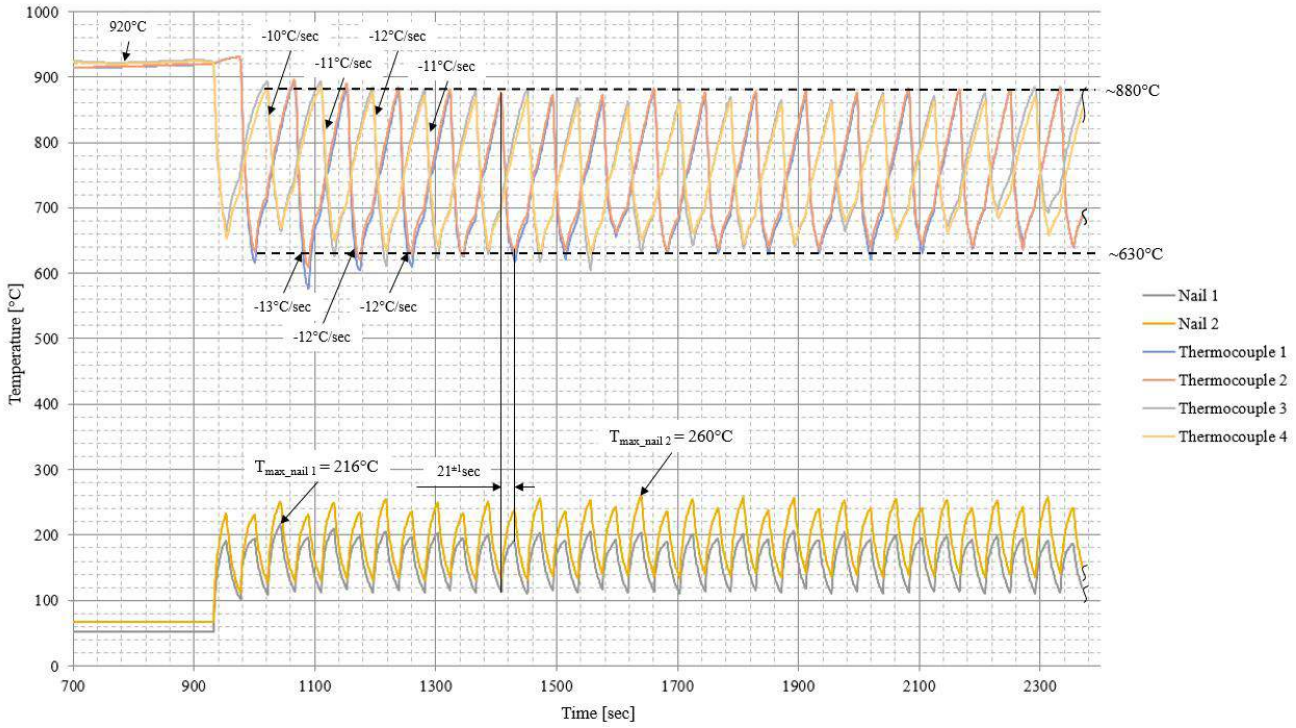

Figure 54: Nail temperature depending on the number of cooling contacts

After the first contact with the contact cooler a quasi-stationary temperature state of the nails sets in. Nail 1, which is located in the middle of the cooling zone, reaches an average temperature of about 159°C. The average temperature of the second thermocouple-equipped nail 2 rises to about 193°C. The maximum temperature level of nail 1 is about $T_{max\_nail\ 1}$ = 216°C, whereas the highest temperature of nail 2 is about $T_{max\_nail\ 2}$ = 260°C.

In summary, it can be said that, starting from the second cooling process, a quasi-stationary state ensues, which subsequently leads to a constant cooling behavior of the contact cooler. Thus, the series capability of the entire re-cooling system of the nails is approved.

6.2.3 Mechanical characterization

Hardness tests

Since the blanks are coated with an AlSi layer, the hardness measurements are carried out in the cross-section of the polished specimens. Otherwise, the coating would have a significant impact on the accuracy of the hardness values generated, as the measurement on the AlSi layer results in a reduction in hardness. The exact geometric properties and the positioning of these specimens are shown in Appendix A1.

The hardness measurements are carried out to specify the hardness distribution between the soft and hard zones of the blanks. This especially makes it possible to detect any changes in the size of the transition zones. Figure 55 shows the sizes of the transition areas of all samples with a sheet thickness of 1mm. The ideal hardness profile would be if the transition zone between the hard and soft regions is less than or equals to 30mm, as indicated by the dashed line. The maximum allowable hardness value for the soft zone is 220HV10, while the values for the hard areas should exceed 420HV10.

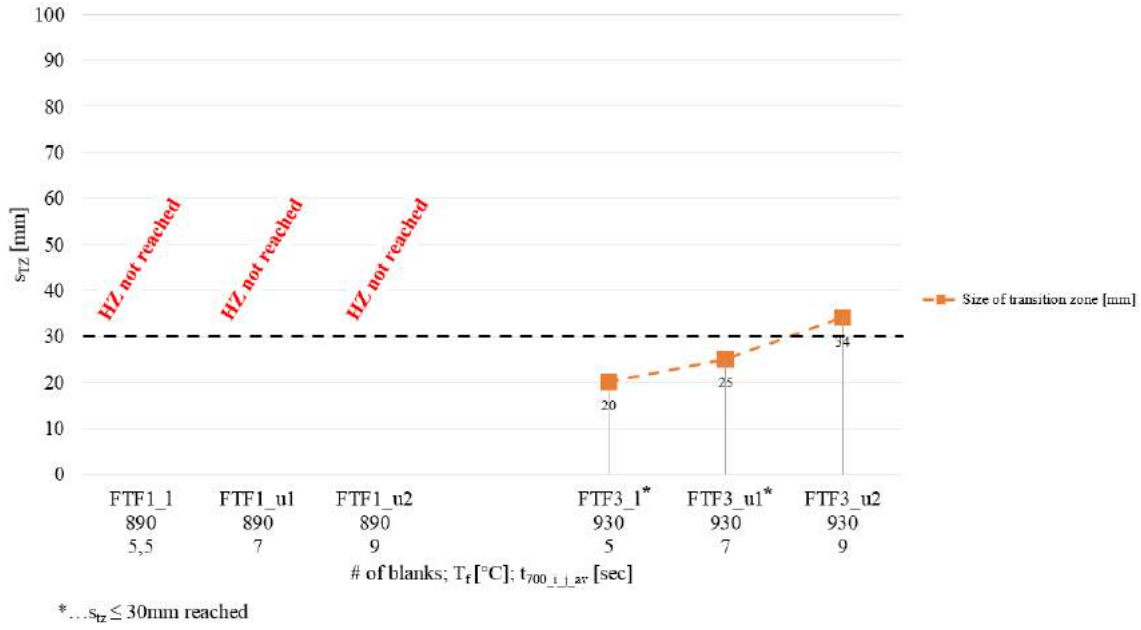

Figure 55: Size of the transition zones of 1mm sheet metal blanks

It is obvious that at a furnace temperature of T_f = 890°C, none of the three FTF1 samples reach the values required for the hard zone. The rapid cooling of blanks with 1mm thickness during the transfer to the flat quenching tool can be counteracted by raising the furnace temperature to T_f = 930°C.

The sizes of the transition zones s_{tz} of the samples FTF3_l and FTF3_u1 correspond to the required target specified in chapter 3. Figure 56 shows the hardness mapping of the sample FTF3_l.

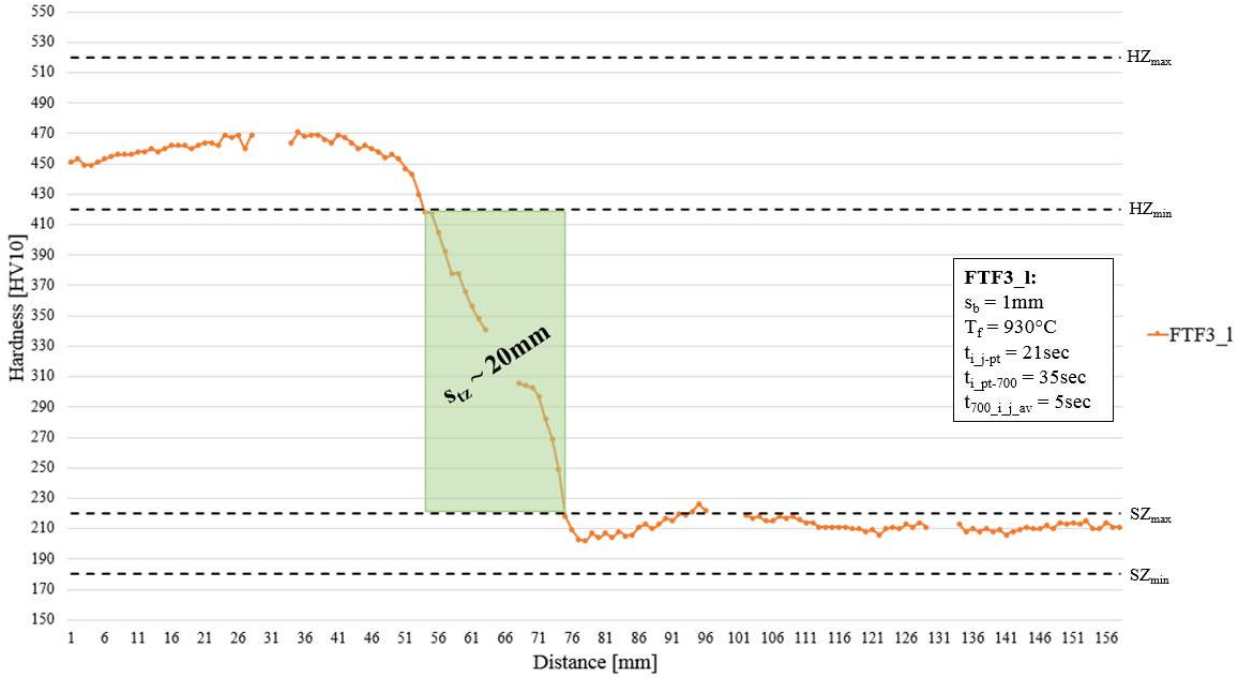

Figure 56: Hardness mapping of FTF3_l

According to the hardness profile shown in figure 56, the aim of eliminating discontinuous changes in hardness by producing homogeneously polished surface properties has been achieved. After comparing all hardness profiles, it can be assumed that the transfer time has a significant impact on the final hardness values and the size of the transition areas s_{tz}. While the hardness values of the soft zones remain similar, the hardness values of the hard zones decrease with an extension of the transfer time.

For example, the size of the transition zone of FTF3_u2 increases to an unacceptable level, although the hardness values achieved in the two zones meet the target specifications.

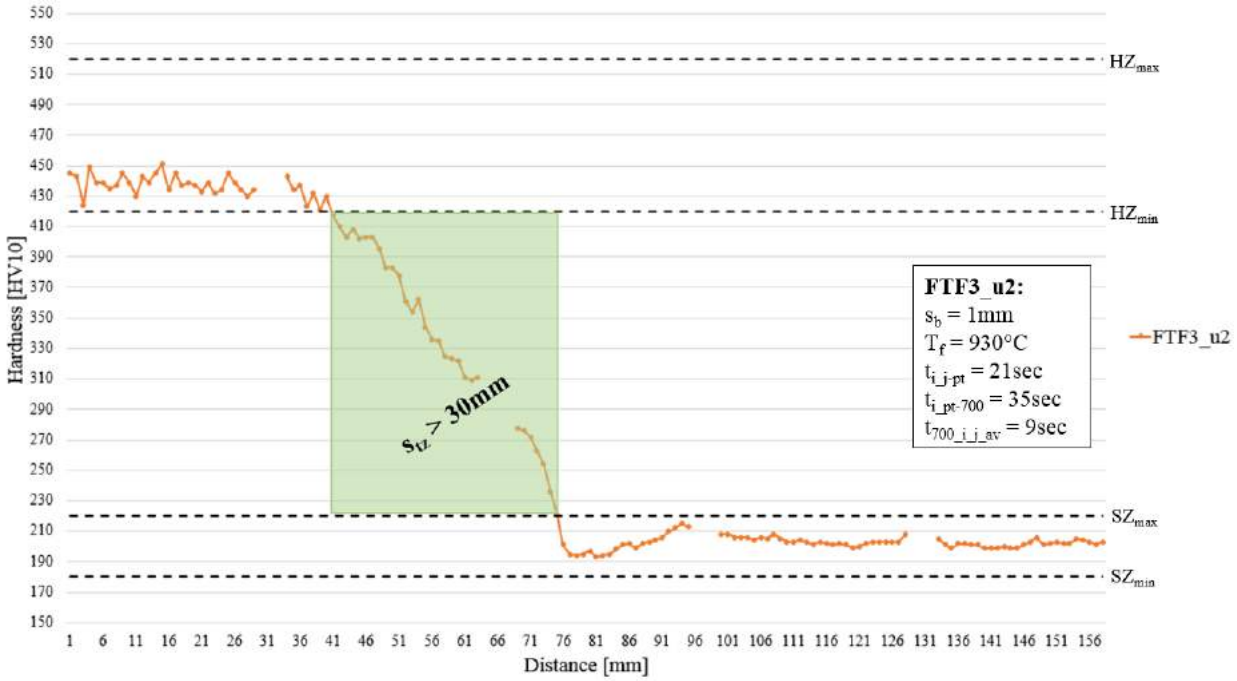

Figure 57: Hardness mapping of FTF3_u2

Figure 58 represents the sizes of the transition zones of boron blanks with a sheet thickness of 2mm. All samples tempered with a furnace temperature of T_f = 890°C again do not meet the target size s_{tz} of the transition area, since some areas do not reach the required values for the hard or the soft zone. The encouraging results of the samples FTF4_l and FTF4_u1, which are austenitized at a temperature of T_f = 930°C, are far more satisfactory.

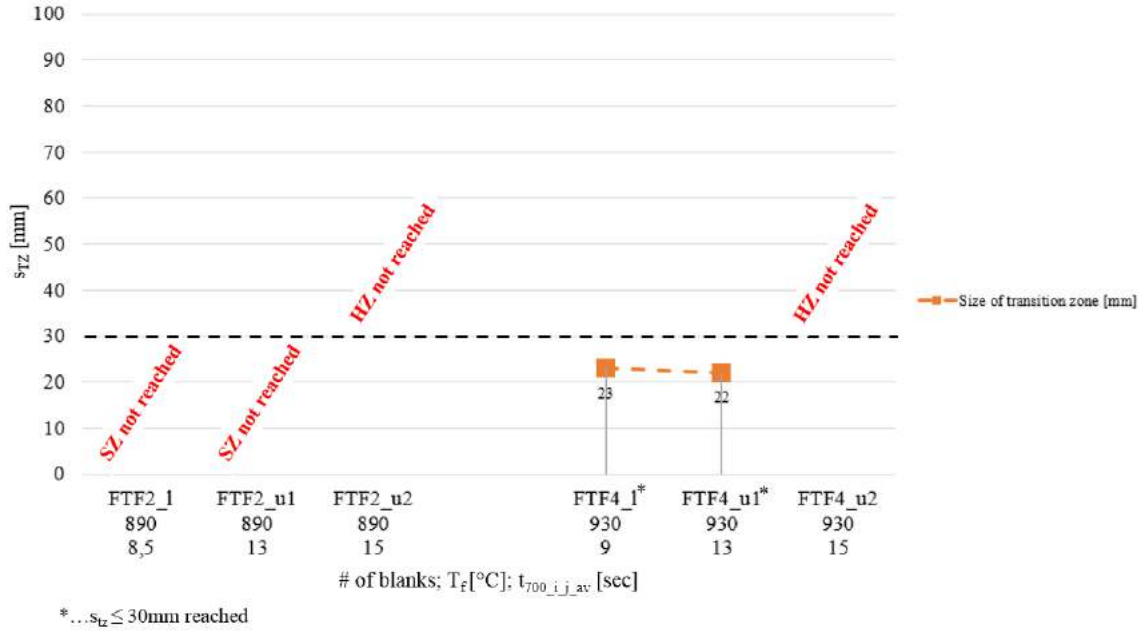

Figure 58: Size of the transition zones of 2mm sheet metal blanks

The size of the transition zone s_{tz} of sample FTF4_l reaches approximately 23mm, whereas the transition area of FTF4_u1 is about 22mm.

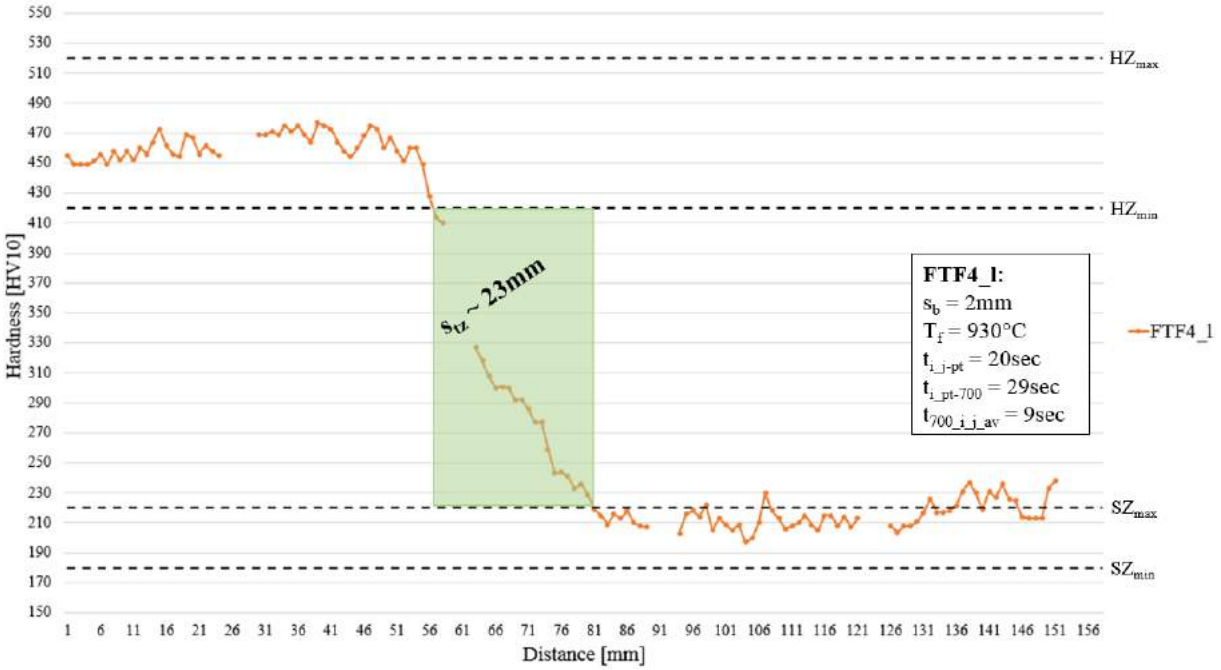

Figure 59: Hardness mapping of FTF4_l

As shown in figure 59, the sample FTF4_l reaches maximum hardness values of up to 480HV10 compared to the approximately 440HV10 of the blank FTF4_u1. The values in the soft region are on average 200HV10 and 210HV10, respectively, which could still be slightly lower for the sample FTF4_l.

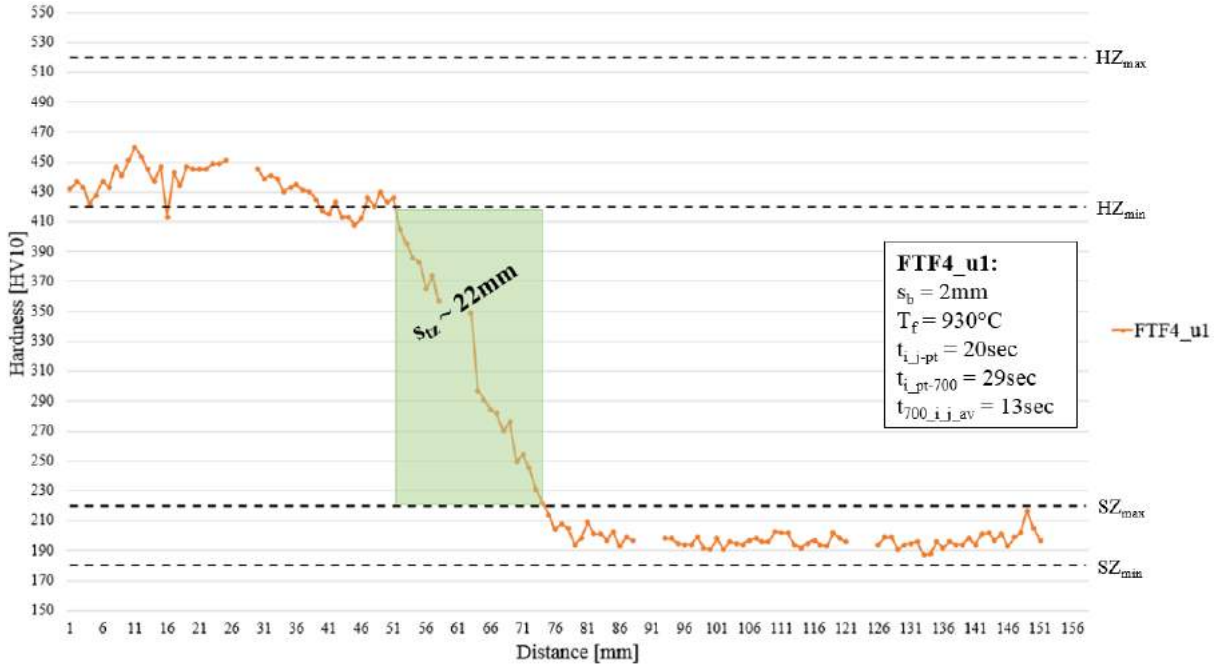

Figure 60: Hardness mapping of FTF4_u1

Further hardness profiles are attached in Appendix A7.

Tensile tests

With the tensile tests carried out in accordance to the method explained in chapter 4.3.3, various characteristics of the heat-treated material are determined to be able to compare and discuss them afterwards.

The results shown in figure 61 demonstrate various UTS values deriving from heat-treated 1mm thick blanks. It can be said that the furnace temperature T_f has a significant impact on the final mechanical properties. For example, at a furnace temperature of T_f = 890°C, it is not possible to achieve the predetermined target values of R_m in the hard zones. Nevertheless, two R_m values in the soft zone meet the target achieved at a furnace temperature of T_f = 890°C. The increase of the furnace temperature to T_f = 930°C makes it possible to maintain the required mechanical strength target values of R_m. The R_m values of the dog bone samples in the hot zones are ranging between 1427 up to 1507MPa, while the R_m levels in the pre-cooled areas are between 668 and 682MPa.

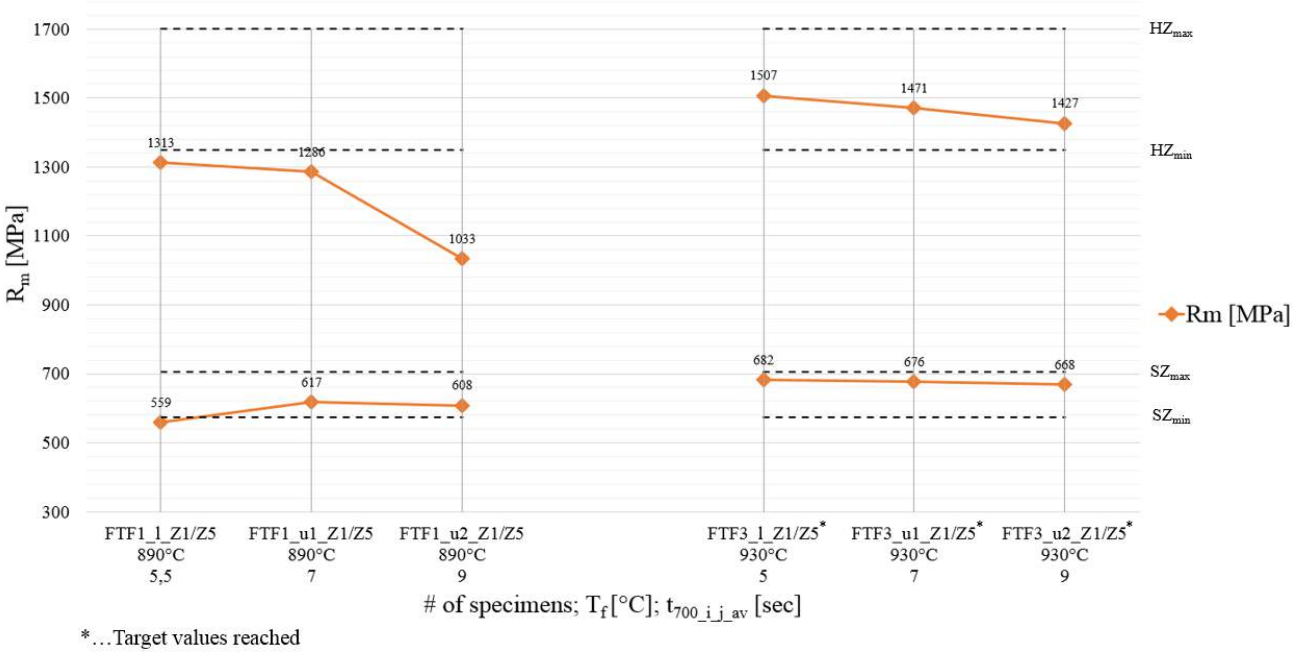

Figure 61: Comparison of R_m levels in the hot and pre-cooled zones of 1mm sheet metal blanks

Figure 62 shows the resulting mechanical properties of the sample FTF3_l across the entire transition area. This tempered test piece is considered to be the most promising result of the 1mm thick sheet metal blanks, since longer transfer times than 5 seconds have negative effects on the size of the transition zone and the insertion temperature of the blanks when finally being settled in the quenching device. As can be seen from the graph, the hard region reaches UTS values above R_m > 1500MPa, with values in the soft region falling to about R_m = 680MPa. The values for the YS drop down from $R_{p0,2}$ = 985MPa in the hard zone to $R_{p0,2}$ = 541MPa in the soft area of the blank.

In addition, the elongation at fracture A_{50} shows promising results. While the FTF3_l_Z1 specimen, which is located in the hard zone, has an elongation at fracture of A_{50} = 3.1%, strain values of about A_{50} = 10% occur in the ductile region of the boron-alloyed manganese steel. It can be said that by an increase of the ductility and therefore the elongation at fracture A_{50}, the absolute values of the UTS (R_m) and the YS ($R_{p0,2}$) are decreasing.

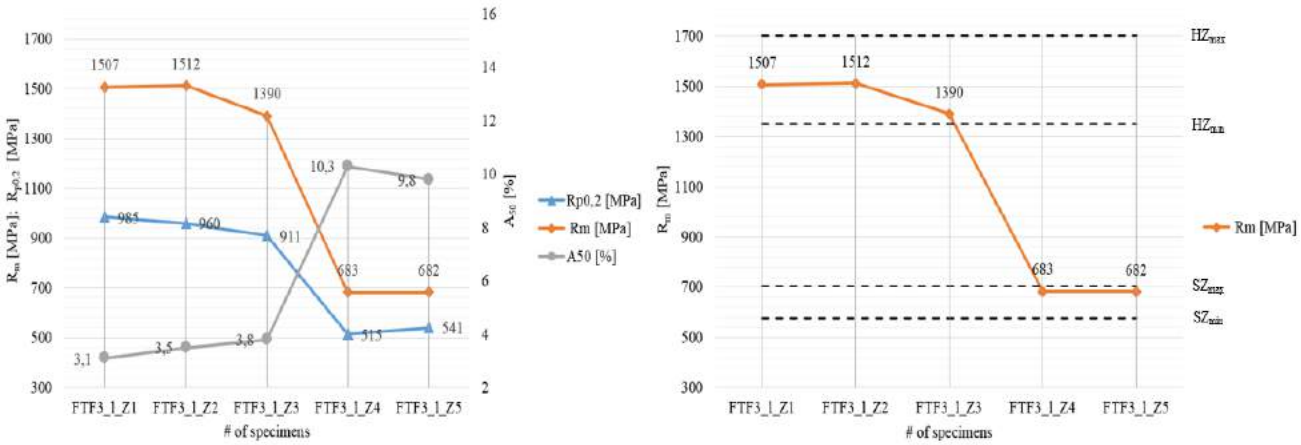

Figure 62: UTS-, YS-, and elongation at fracture-values of FTF3_l

Compared to the results discussed above, figure 63 displays the R_m values obtained by experiments with 2mm thick sheet metal blanks. The results show that the values achieved in both the soft and hard zones of the samples heated to a furnace temperature of T_f = 930°C better meet the target values than those blanks heated to a temperature of T_f = 890°C.

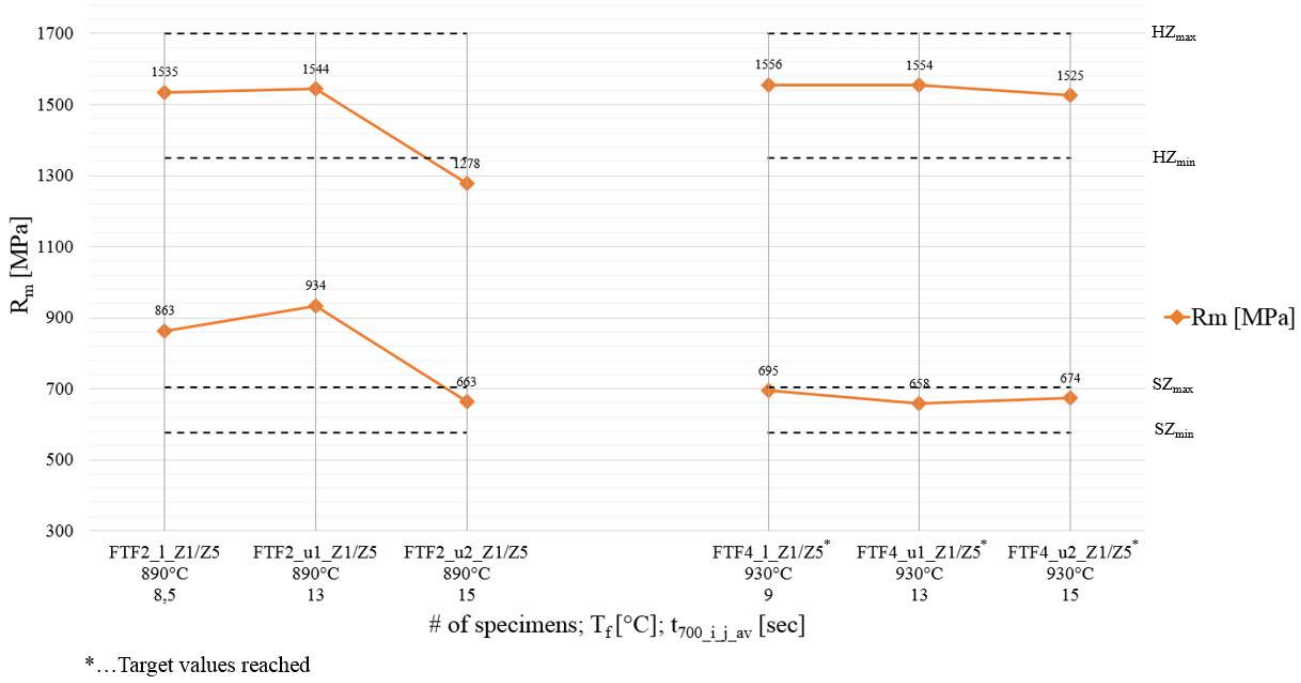

Figure 63: Comparison of R_m levels in the hot and pre-cooled zones of 2mm sheet metal blanks

The encouraging results of the sample FTF4_l are illustrated in figure 64.

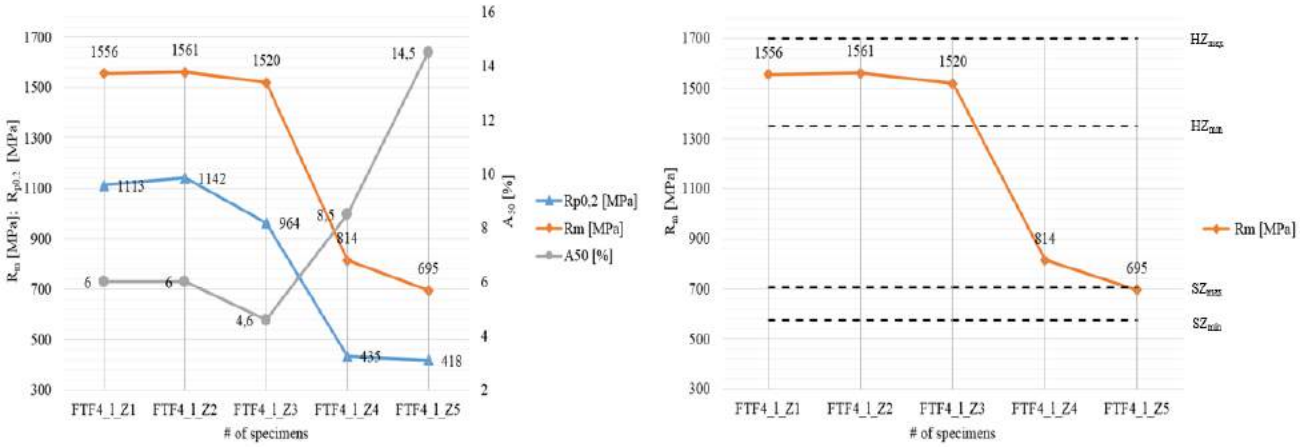

Figure 64: UTS-, YS-, and elongation at fracture-values of FTF4_l

While the values in the hard area are higher than R_m = 1550MPa, the R_m values of about 690MPa from the pre-cooled area are also within the specified target range. The elongation at fracture values of FTF4_l are also excellent. While the hard area has an elongation at fracture of A_{50} = 6%, A_{50} values in the soft zone of more than 14% are accomplished.

Table 21 summarizes the main results and findings of the tempered test pieces. The red areas point out that the results do not meet the targets, whereas the values of the green areas are matching.

In total, four different process-setups emerged, in which the findings meet the specified objectives with regard to the desired mechanical properties and the size of the transition zones s_{tz}. While the parameter set of 1mm thick blanks provided optimum results for the samples FTF3_l and FTF3_u1, the samples FTF4_l and FTF4_u1 with a blank thickness of 2mm lead to considerable results. However, only two different parameter sets of the entire DoE remain, which are relevant for a customer of EBNER due to stricter specifications regarding the hard zone insertion temperature before quenching T_{bi_h} of the blanks.

FTF3_l and FTF4_l best meet the additional target where the insertion temperature of the hard zone before quenching T_{bi_h} should be above 700°C. In addition, it can be said that FTF4_l delivers a much more realistic result since the transfer time of this sample is nine seconds compared to the five seconds of sample FTF3_l. While the temperature in the hot zone T_{bi_h} of sample FTF3_l is exactly 700°C, the temperature in the pre-cooled area T_{bi_s} is measured to be 661°C before the quenching is carried out. Furthermore, the temperature in the hot zone T_{bi_h} of the probe FTF4_l is about 717.2°C before quenching, which is definitely providing a better formability behavior and less die wear during the hot forming process compared to the previously mentioned sample FTF3_l. The temperature in the pre-cooled area T_{bi_s} is measured to be 660.4°C before quenching.

s_b	T_f	ID	$t_{700\_i\_j\_av}$	T_{bi_s}	$T_{bi\_h} \geq 700$	$575 \leq R_{m\_s} \leq 705$	$1350 \leq R_{m\_h} \leq 1700$	$s_{tz} \leq 30$
[mm]	[°C]	[-]	[sec]	[°C]	[°C]	[MPa]	[MPa]	[mm]
1	890	FTF1_l	5.5	669	693.2	559	1313	78
		FTF1_u1	7	654.4	675.2	617	1286	73
		FTF1_u2	9	635.2	662.8	608	1033	70
	930	FTF3_l	5	661	700	682	1507	20
		FTF3_u1	7	640.3	668.6	676	1471	25
		FTF3_u2	9	620.7	641.8	668	1427	34
2	890	FTF2_l	8.5	661.5	722.1	863	1535	89
		FTF2_u1	13	641.7	684.7	934	1544	96
		FTF2_u2	15	634.3	674.1	663	1278	75
	930	FTF4_l	9	660.4	717.2	695	1556	23
		FTF4_u1	13	642.1	684	658	1554	22
		FTF4_u2	15	633.7	669.1	674	1525	62

Table 21: Summary of all results of the tailor tempered samples

6.2.4 EDX-analysis and OM

EDX-analysis

The inspection of crucial surfaces on selected nails from the contact cooling system and a steel blank reveals the residues of any Cu respectively of any AlSi. This is done by using detectors for SEs and BEs, where the results are displayed and analyzed using different magnifications. In addition, the composition of the different phases is determined by the chemical analysis method EDX, which is, as already mentioned in chapter 4.3.5, an additional function of the SEM.

First, the contact surfaces of two Cu nails (position 1) are analyzed for any AlSi residues according to figure 65. It should be emphasized that these nails already count about 1000 contacts with heated AlSi-coated sheet metal blanks.

Thereafter, the surface of a tailor tempered blank (position 2) is checked for any Cu residues. The surfaces that had no contact with the Cu nails are compared with the surfaces on which the pre-cooling was performed.

As a preparatory step, the samples are cut to the desired size according to figure 65 before being installed in the SEM test chamber. It should be noted, that the cooled area (position 2a and 2b) of these preliminary tests, which are carried out in order to optimize the entire cooling system, slightly deviates from the cooled area of the other tests performed during this study.

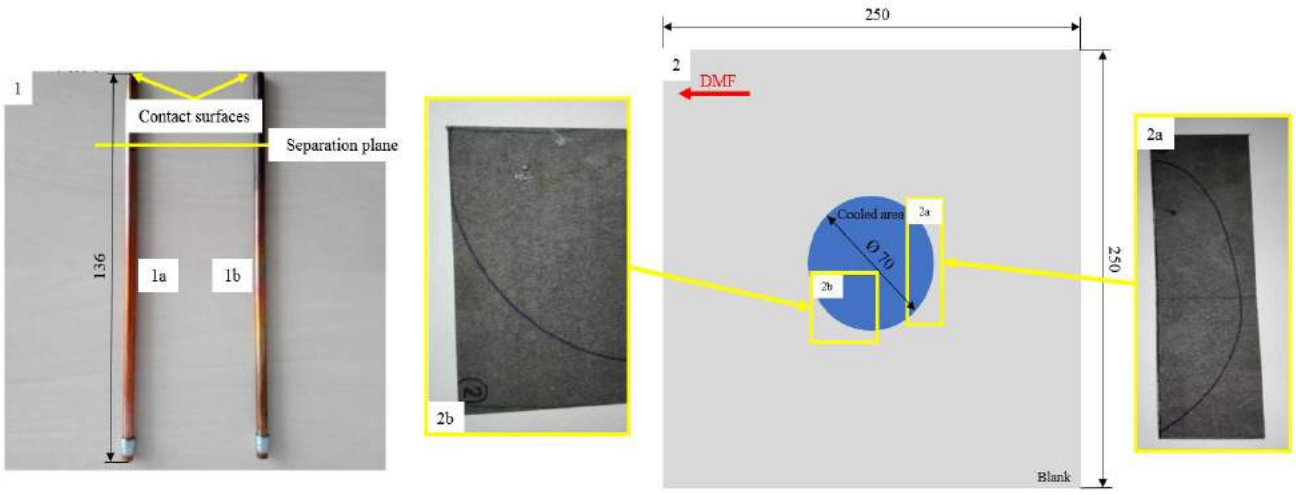

Figure 65: Contact areas (1a: nail 1, 1b: nail 2, 2: 22MnB5 blank)

The first part of the investigation deals with the analysis of the contact areas of the two Cu nails. The following figures show a comparison of the two nail surfaces. Nail 2 (position 1b_1, 1b_2) has less residues than nail 1 (position 1a_1, 1a_2). These residues especially are characterized by their lower density compared to the base material Cu.

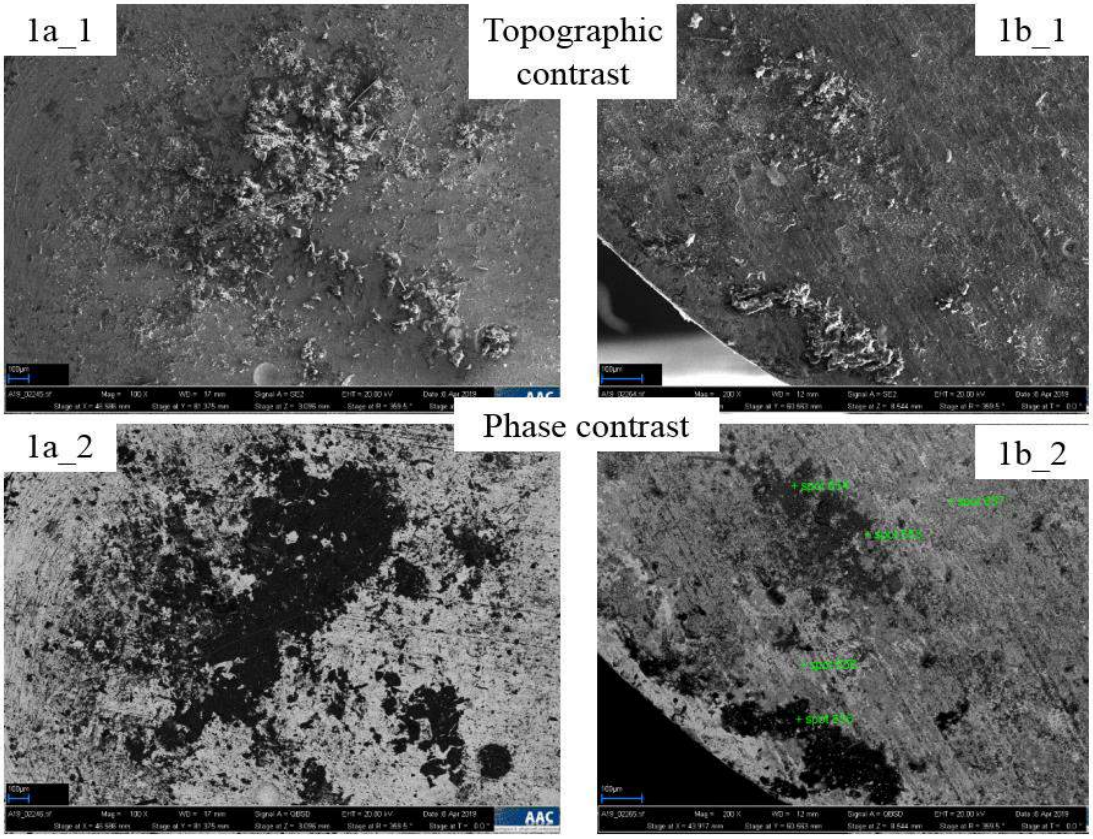

Figure 66: Residues on the contact surfaces (1a_1 and 1a_2: nail 1, 1b_1 and 1b_2: nail 2)

There are voluminous and dried residues visible on both nails, on which also fibrous structures appear. On the contact surface of nail 1, most of the residues occur in the middle, whereas those on the second nail are piled up on the edge. Figure 66 shows various EDX-spots on the contact surface of nail 2 (highlighted in green). In addition, the main elements of these points are listed and explained.

EDX-spots	Main elements	Comments
653	Fe, O, C, Cr, Mn, Ni, Si	Fe-rich particles
654	Si, Ca, O, C, Cl, Fe	Si-rich particles
655	C, O, Cu, Cl, Na, Si, Ca, K, S	C-rich and dried film
656	C, O, Cl, Si, Ca	Thin C-rich film
657	C, O, Cu, Cl, Si, Ca	C-rich and dried film
658	C, O, Cu, Cl, Si	Thin C-rich film

Table 22: Chemical composition and morphological properties of particles on the contact surface of nail 2

Figure 67 shows some magnifications of the contact surface of nail 1.

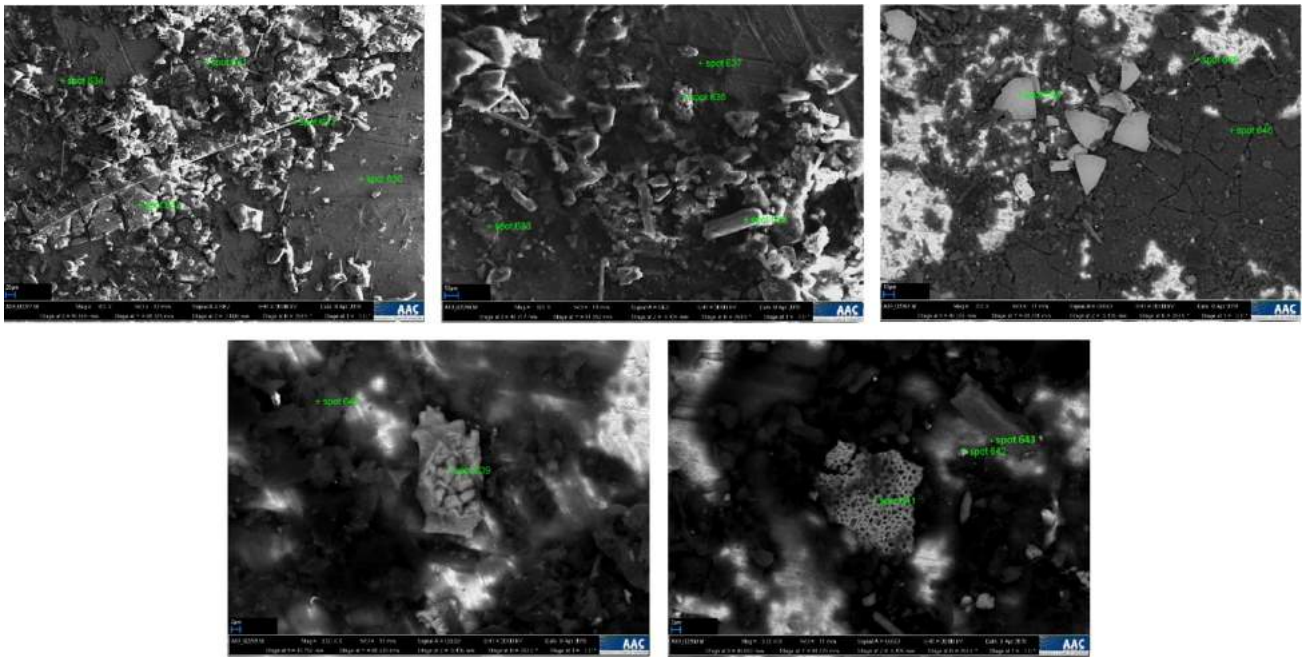

Figure 67: Morphological properties of particles on the contact surface of nail 1

The chemical and morphological characteristics of the EDX-spots are tabulated in table 23.

EDX-spots	Main elements	Comments	EDX-spots	Main elements	Comments
630	Cu, O	Oxidized Cu-surface	639	Cr, O, C, Mn, Si	Irregular particle
631	C, O, Si, Cl, Ca	C-rich and dried coating	640	C, O, Cu, Cl, Ca, Si, Fe	Dried coating
632	C, O, Cu, Cl, Si, Ca	C-rich and dried coating	641	Fe, O, C	Sharp-edged porous particle
633	Al, Si, O, C	Long fiber	643	Si, Ca, C, O	Long particle
634	C, O, Cu, Cl, Si, Ca	C-rich and dried coating	644	Fe, O, C	Sharp-edged particle
636	Si, Ca, C, O	Long particle	645	C, Cu, Cl, Ca, Si	C-rich and dried coating
637	C, O, Cu, Cl, Si, Ca, S	C-rich and dried coating	646	Al, Si, O, C	Short fiber
638	Fe, C, O	Sharp-edged porous particle			

Table 23: Chemical composition and morphological properties of particles on the contact surface of nail 1

The high concentration of O indicates that most of the elements are in an oxidized state. In addition, the detection of small amounts Al, Si and Fe is very likely due to the material transfer of the AlSi-coated 22MnB5 sheet blanks.

Figure 68 gives an overview of the different elements that were detected when performing an EDX-mapping of the contact surface of nail 2.

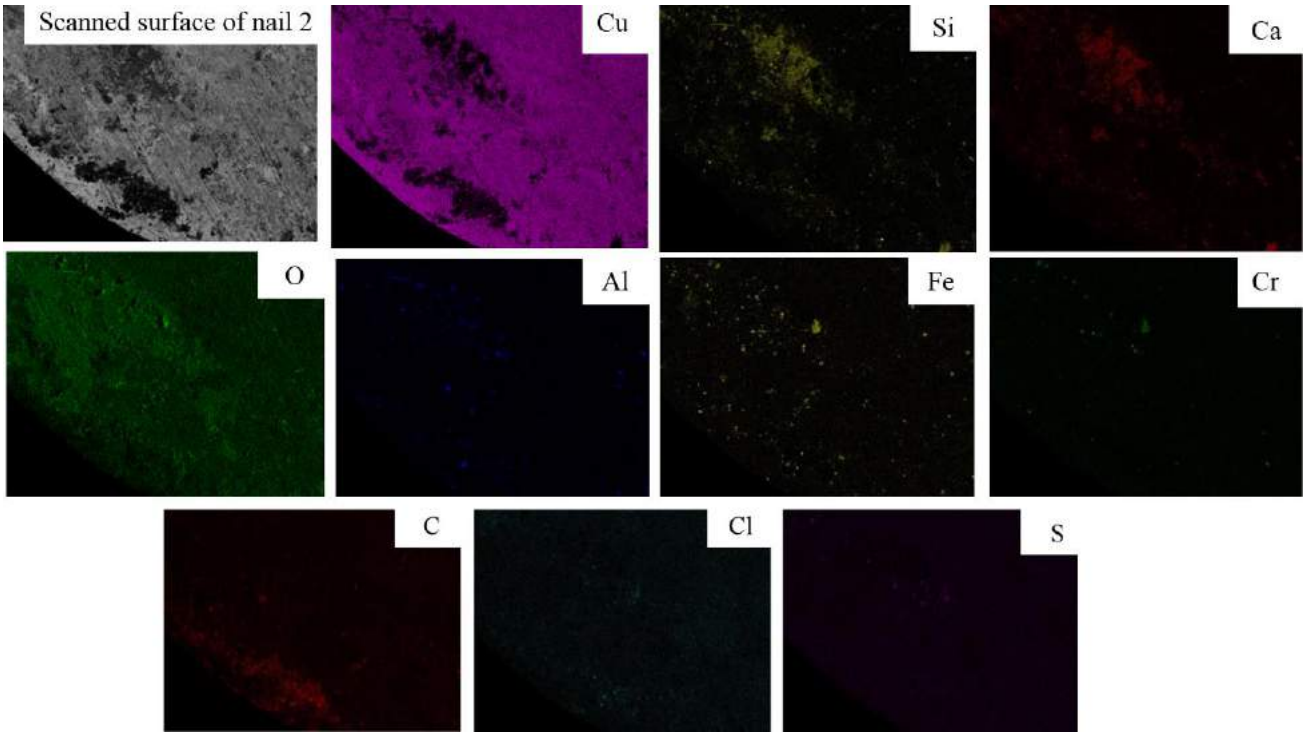

Figure 68: EDX-mapping of nail 2

After an approximate number of about 1000 contacts between the nails and the blanks, the contact areas of the Cu nails are continuously covered with a film mainly containing C, O, Cl, Si, and Ca. This film forms thick and cracked residues in some areas of the surface. The detected elements are present at least partially in the form of Cu-containing phases. Al-, Si-, and Fe-containing oxide particles on the contact surface indicate a material transfer of the steel blank. In addition, Al- and Si-fibers and Cr- and Mn-particles with a size of about 20µm are detected. It can be assumed that the thermal conductivity of the Cu-contact surfaces is impaired by the formation of the phases found respectively by the transfer of material between the nails and the sheet metal blanks. Therefore, it is advisable to replace these nails or to grind the contact surfaces of these nails according to a well-defined period of operation.

The second part of the EDX-analysis deals with a detailed investigation of the cooled area from a tailor tempered blank. As shown in figure 65, the blank is cut into several parts to determine if there are any differences according to their surface topography and chemical composition.

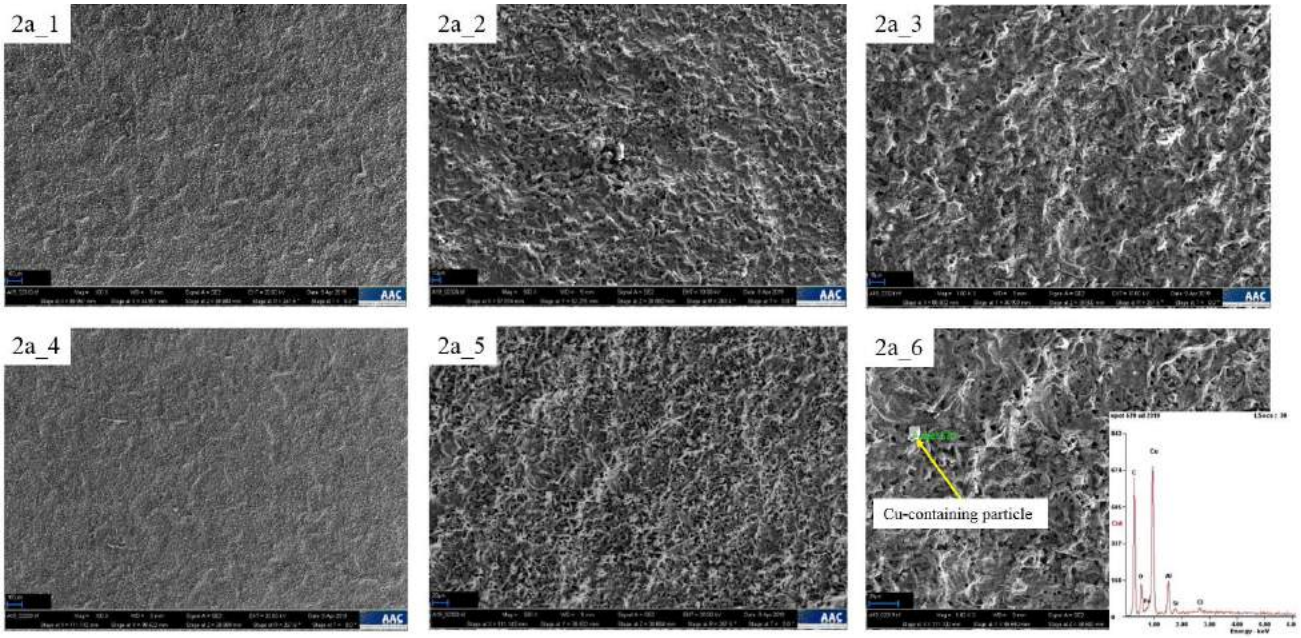

Figure 69: Comparison of the blank surface (2a_1, 2a_2, and 2a_3: pre-cooled area, 2a_4, 2a_5, and 2a_6: hot area)

As highlighted in figure 69, only one Cu-containing particle with a size of about 10µm is spotted. Nevertheless, no significant difference can be detected between the pre-cooled and uncooled area of this specimen (position 2a). Further investigations with detailed magnifications of these areas show that similar chemical and morphological properties can also be detected.

Figure 70 shows images that allow the comparison between the pre-cooled and hot area of the second specimen (position 2b). As can be seen, outbreaks in the coating occur in both the pre-cooled and hot zone (position 2b_3 and 2b_6). In the pre-cooled area, even crack-like structures (position 2b_2) occur.

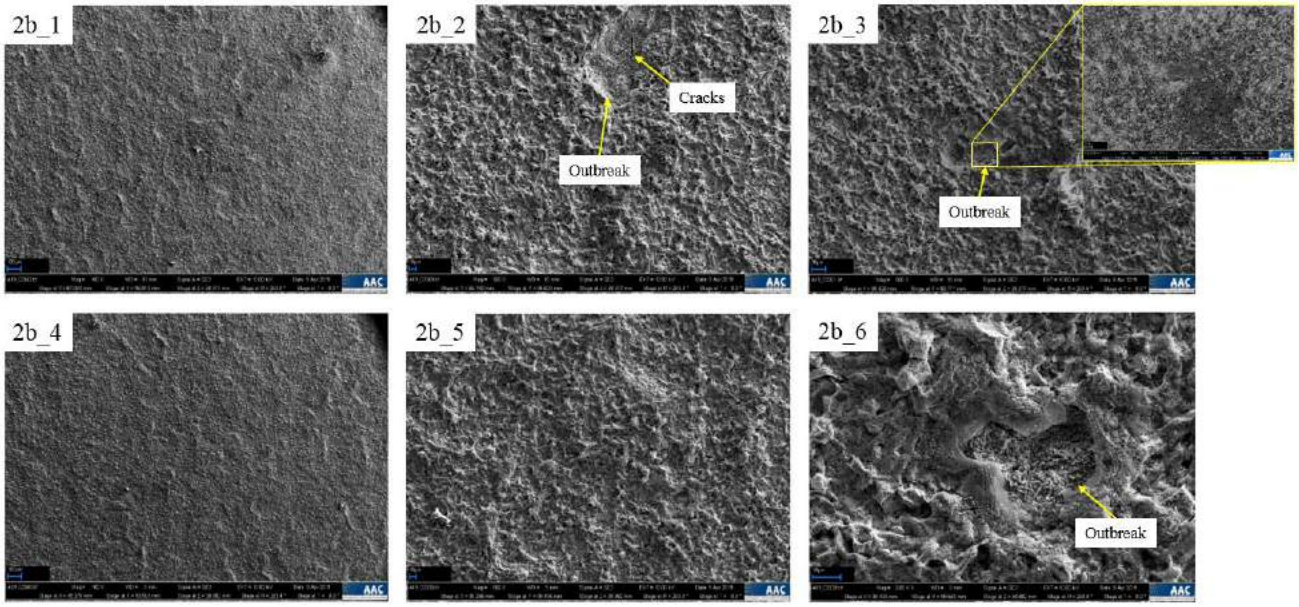

Figure 70: Comparison of the blank surface (2b_1, 2b_2, and 2b_3: pre-cooled area, 2b_4, 2b_5, and 2b_6: hot area)

Figure 71 gives an overview of the element distribution of the pre-cooled zone. The elements with the largest share are Fe, O, Si, and Al. The Cu-share in this area is insignificant and below the detection limit.

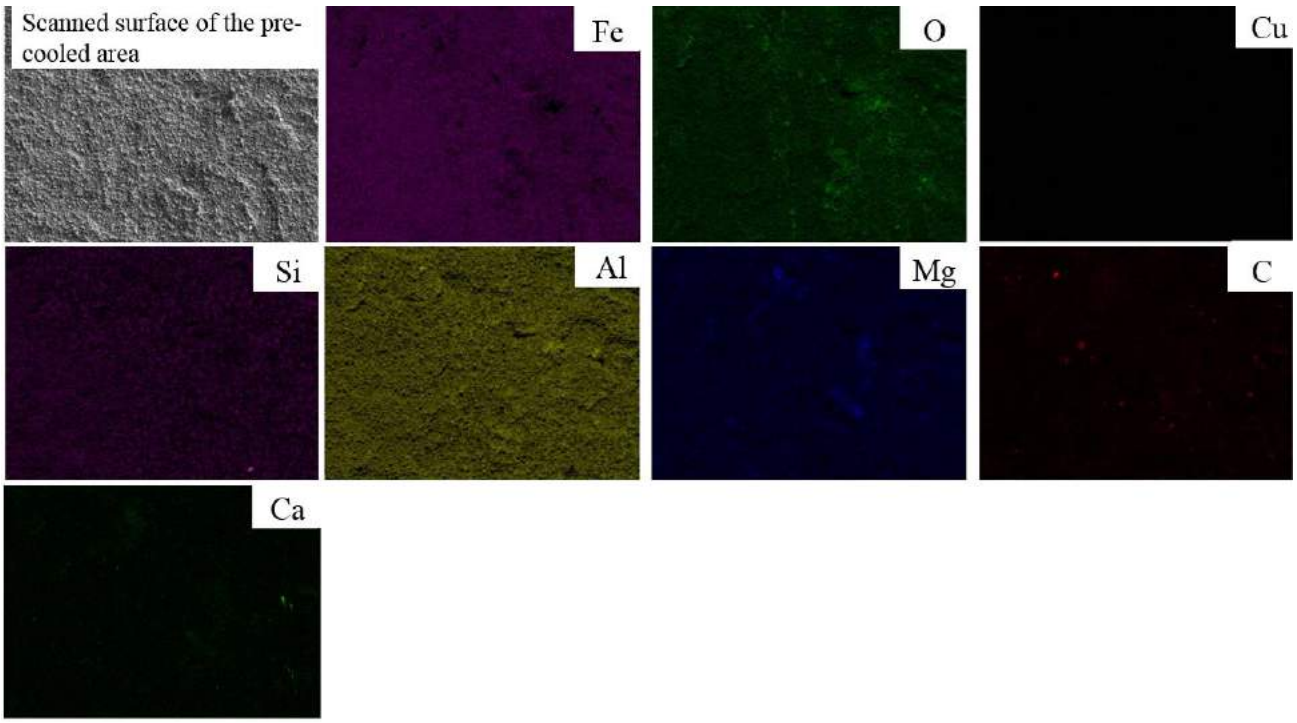

Figure 71: EDX-mapping of the pre-cooled area of the blank

It is noticeable, that the pre-cooled and hot areas of the entire blank barely differ according to their topography and their chemical composition. No Cu is found in the entire pre-cooled area, whereas a small Cu-containing particle is detected in the hot area. The high concentration of O indicates that the elements Al, Si, Fe, and Mg are present in an oxidized form.

OM

On the one hand, figure 72 exhibits a metallographic investigation of a sample in its original state (as-delivered condition). Before the heat treatment, the sample has a distinct ferritic-pearlitic matrix (position 1). In addition, the AlSi coating can be seen. Right at the interface to the base material, a ternary alloy layer can be seen, above which the binary AlSi layer can be detected. On the other hand, the image on the right represents a sample with its dominant martensitic microstructure after hot stamping and its AlFeSi alloy layers (position 2).

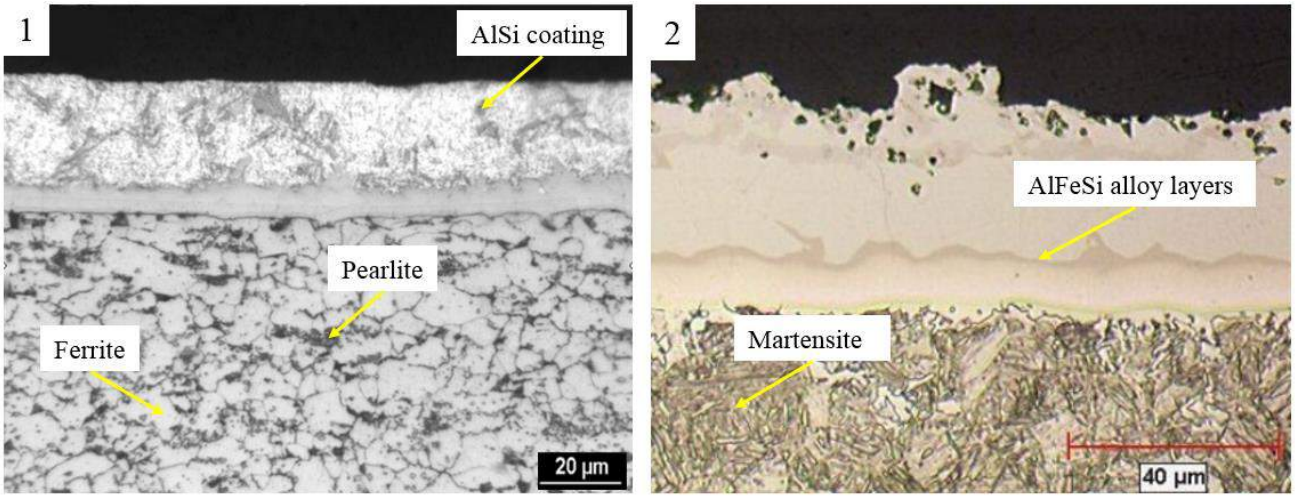

Figure 72: AlSi-coated 22MnB5 (1: prior to hot forming, 2: after hot forming (based on: [30]))

Figure 73 shows the obtained microstructure of the sample FTF3_l. After being exposed for 100 seconds to a furnace temperature of T_f = 930°C this test piece is pre-cooled for 21 seconds. After pre-cooling is complete, the blank remains under the second burner for about 35 seconds before being transferred to the flat quenching tool within five seconds.

After press hardening, a comparison of the average layer thickness of the soft zone and the hard area is performed. As illustrated in the magnified images generated by a light OM, the thickness of the coating in the pre-cooled zone is about 32.6µm, while the thickness in the hard region is approximately 43.5µm.

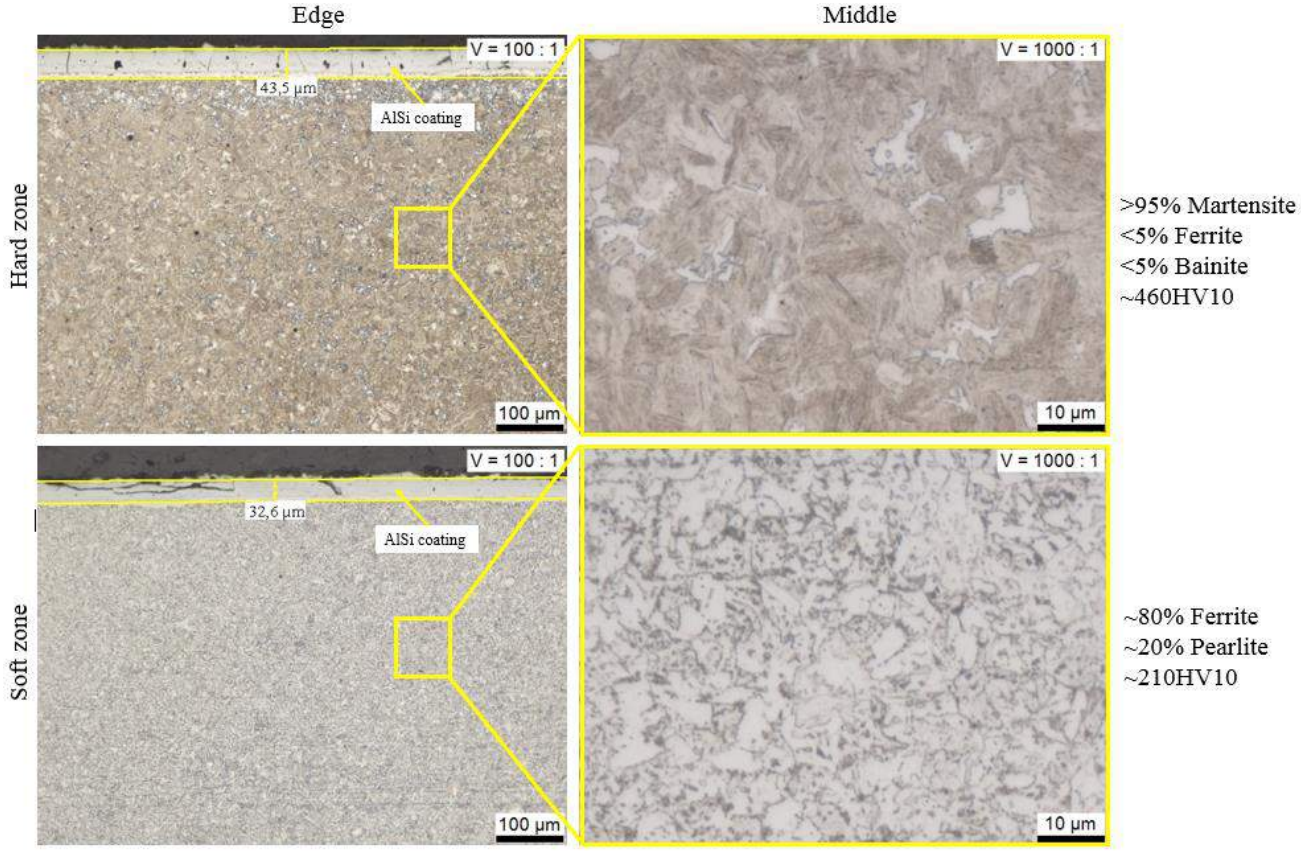

Figure 73: Microstructure of FTF3_l

As illustrated in figure 73, the average hardness value in the pre-cooled zone is approximately 210HV10 compared to 460HV10 in the hot area of this blank with a sheet thickness of s_b = 1mm. On the one hand, the metallographic analysis reveals that most of the soft zone of the partially cooled blank has a ferritic-pearlitic microstructure that correlates to the hardness values of about 210HV10. On the other hand, the hot zone develops a dominant martensitic content of more than 95%.

Nevertheless, the actual transfer time of five seconds from the sample FTF3_l is difficult to implement in practice. Conventional transfer times of a customer of EBNER are about twelve seconds. Therefore, the entire process cycle of the sample FTF4_l provides a more realistic alternative with its transfer time of nine seconds compared to the sample FTF3_l.

Figure 74 represents the microstructure of the sample FTF4_u1 with a sheet thickness of 2mm. Similar to the test piece FTF3_l, this sample is exposed to a furnace temperature of 930°C for 100 seconds. Afterwards, FTF4_u1 is pre-cooled for 20 seconds. The furnace dwell time is set to 29 seconds before the blank is transferred to the flat quenching tool within 13 seconds.

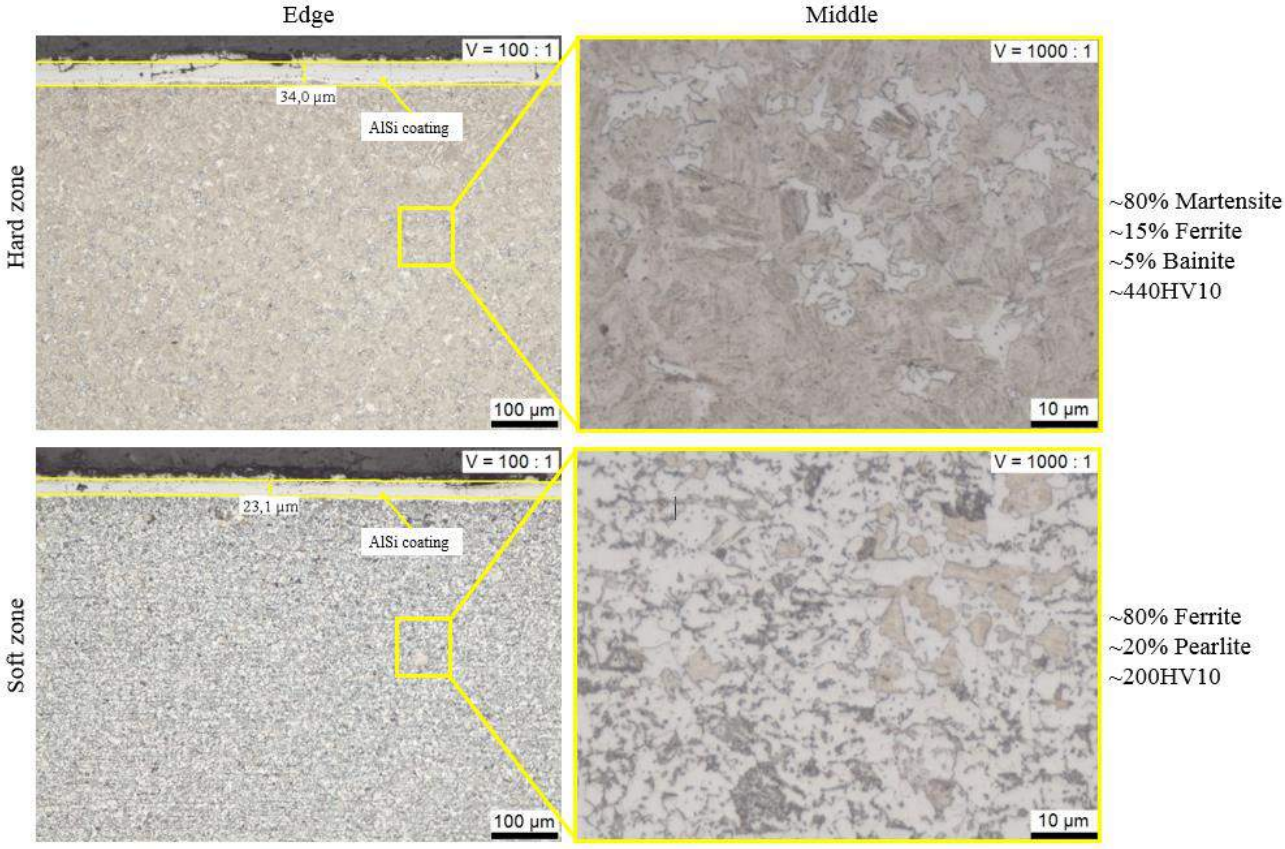

Figure 74: Microstructure of FTF4_u1

The mean hardness value of this metallic test piece is about 200HV10 in the soft region and about 440HV10 in the hard area. The soft zone again consists mainly of a ferritic-pearlitic microstructure, while the hardened zone is almost entirely transformed into a martensitic state.

7 Conclusion

In this work, the influence of various process parameters in the fabrication of tailor tempered steel blanks is investigated with the target to realize high strength automotive parts which also provide the required energy absorption potential in certain customizable areas of one and the same component. This can be considered as the first important step towards overcoming the technological challenges of creating diverging material properties in a single steel blank using the new contact cooling method developed by EBNER. In addition, results of this work represent ideal prerequisites for further investigations to optimize the partial cooling process on the next level.

After finally finding ideal process parameters for phase 1 (inside the furnace) and phase 2 (outside the furnace), the simulation of the material flow properties during the forming process plays an important role when designing the entire tailored tempering solution. The diverging blank temperatures between the ductile and the hard areas of the blanks determined in this work can be used as a basis for further computer-aided simulation. Taking this data under account, the hot forming process thus can be simulated. This helps avoiding possible problems effectively that may occur during the hot stamping process in the press. Increased tool wear, problems with dimensional accuracy of the parts produced, cracks appearing in critical areas of the hot-formed components, etc. can thus be minimized with regard to the temperature-dependent formability behavior of the tempered blanks.

With the parameter sets used for the experiments carried out in the trial furnace, blanks with the required material properties can be produced. The partial hardening system, which allows cycle times of less than 25 seconds, can also be retrofitted in press hardening furnaces already sold by EBNER, without requiring any furnace extension. The rapid cooling of all 1mm blanks only allows a critical transfer time of $t_{700\_crit\_i}$ = 5 seconds, until a hot zone insertion temperature of approximately T_{bi_h} = 700°C is reached. The usage of 2mm thick blanks, such as the sample FTF4_l, seems to be more constructive. Longer transfer times than nine seconds between the end of the furnace and the insertion of the blank into the press are possible, resulting from the higher energy storage potential of thicker blanks.

In order to check the process stability and quality of the parameter sets discovered in this study, the mechanical properties should be checked for their standard deviation in a further series of experiments. On the one hand, this can be done under laboratory conditions by means of the already used trial furnace or under realistic conditions at production facilities of EBNER's customers.

The encouraging results of the cooling performance of the contact cooler after simulating cycle times of approximately $21^{\pm1}$ seconds have shown that the serial capability of the cooling system can be confirmed. The next step is to verify and compare those results with tests that simulate mass production with a furnace of EBNER’s customers under more realistic conditions.

The analysis of the grinding surface patterns in this work revealed interesting results regarding the various microstructures in the hot and pre-cooled areas of the blanks. Higher furnace temperatures of T_f = 930°C result in better mechanical properties and sharper transition zones of the steel blanks produced. This means that the hard zones represent a high amount of martensite whereas the soft areas primarily have a ferritic-pearlitic microstructure.

The investigation of the mutual material transfer also showed that the contact between the nails and the blank during the pre-cooling process leaves only a very small amount of Cu on the surface of the tempered blanks. The residues that have been detected on the contact surfaces of the nails may permanently affect the thermal conductivity. Therefore, it is advisable to perform maintenance activities in a well-defined time interval to guarantee optimal cooling properties of the entire pre-cooling system. Another EDX-analysis of the contact surfaces between the nails and the blanks after 5000 or 10000 contacts could provide important information about the period of time after which such nail maintenance activities would be necessary.

Finally, the execution of a further experimental matrix with pre-diffused AlSi-coated 22MnB5 blanks from POSCO could provide further insights into the optimization of the partial cooling process for the economic production of hot-formed ultra-high strength steel blanks in the automotive industry. In addition to the reduction of AlSi residues on the rollers, the use of this new material enables rapid heating rates. This pre-diffused material is expected to be available on the market at the beginning of 2020.

List of references

[1] Green Car Reports (publ.); 1.2 Billion Vehicles On World's Roads Now, 2 Billion By 2035: Report, https://www.greencarreports.com/news/1093560_1-2-billion-vehicles-on-worlds-roads-now-2-billion-by-2035-report, (07.01.2019)

[2] Thaden, Georg; Mogge, Felix; Riederle, Stefan; Automotive metal components for car bodies and chassis, Global market study, Roland Berger, 2017

[3] Autoform Engineering GmbH (publ.); Leichtbau in der Automobilindustrie, https://www.autoform.com/de/glossar/leichtbau/, (07.01.2019)

[4] Skrikerud, Martin; Friberg, Johan; Press Hardening, Process Design and Tool Systems, in: Hot Sheet Metal Forming of High-Performance Steel, ed. by Oldenburg, Mats; Prakash, Braham; Steinhoff, Kurt; 4th ed., Verlag Wissenschaftliche Scripten, 2013, pp.423-430

[5] ICCT-The International Council on Clean Transportation (publ.); CO_2 emissions from new passenger cars in the EU: Car manufacturers' performance in 2016, https://www.theicct.org/sites/default/files/publications/PV-EU-OEM_ICCT-Briefing_03072017_vF.pdf, (15.01.2019)

[6] Fonstein, Nina; Advanced High Strength Sheet Steels, Physical Metallurgy, Design, Processing, and Properties, Springer, 2015

[7] Chiriac, Constantin; Sohmshetty, Raj; The Effects of the Heating Rate and the Incoming Microstructure on the Phase Transformation Temperatures of 22MnB5 Steel, in: Hot Sheet Metal Forming of High-Performance Steel, ed. by Oldenburg, Mats; Prakash, Braham; Steinhoff, Kurt; 6th ed., 2017, pp.403-414

[8] Schönherr, Julia; Landgrebe, Dirk; Polubinski, Swetlana; Entwicklungen beim Presshärten, Ein Update; Carl Hanser Verlag, Chemnitz, 2017, pp.33-36

[9] ArcelorMittal (publ.); Hot Stamped Door Ring, https://automotive.arcelormittal.com/tailoredblanks/1864/doorring2017, (09.01.2019)

[10] Schuler Pressen GmbH (publ.); HOT STAMPING WITH PCH FLEX – FAST, FLEXIBLE, COST EFFECTIVE, pp.1-20

[11] Aspacher, Jens; Tools and Technologies for Processing Ultra High Strength Materials, Schuler Equipment for Press Hardening, Verlag der Technischen Universität Graz, 2013, pp.37-48

[12] WorldAutoSteel (publ.); ADVANCED HIGH STRENGTH STEEL APPLICATION GUIDELINES, 2005

[13] Billur, Eren; Çetin, Bariş; Gürleyik, Murat; New generation advanced high strength steels: developments, strengths and constraints, International Journal of Scientific and Technological Research **2**, 2016, pp.50-62

[14] Billur, Eren; Introduction, in: Hot Stamping of Ultra High-Strength Steels, From a Technological and Business Perspective, ed. by Billur, Eren; Springer, 2019, pp.1-18

[15] Kim, C.; Kang, M.J.; Park, Y.D.; Laser welding of Al-Si coated hot stamping steel, in: Procedia Engineering **10**, Elsevier, 2011, pp.2226-2231

[16] So, H.; Faßmann, D.; Hoffmann, H.; et al.; An investigation of the blanking process of the quenchable boron alloyed steel 22MnB5 before and after hot stamping process, in: Journal of Materials Processing Technology **212**(2), 2012, pp.437-449, quoted from Billur, Eren; Introduction, in: Hot Stamping of Ultra High-Strength Steels, From a Technological and Business Perspective, ed. by Billur, Eren; Springer, 2019, pp.1-18

[17] Oppermann, A.; Seemann, P.; Experiences with Press Hardening Furnaces and Tailored Tempering Systems, in: 13. Erlanger Workshop Warmblechumformung, ed. by Merklein, M.; 13th ed., Lehrstuhl für Fertigungstechnologie-Friedrich-Alexander Universität Erlangen-Nürnberg, 2018, pp.51-58

[18] Porter, M.E.; Wettbewerbsvorteile (Competitive Advantage), Spitzenleistungen erreichen und behaupten, Campus Verlag Frankfurt/New York, 2014

[19] Lehmann, Harald; Challenges in Heat Treatment for Press Hardening, in: Hot Sheet Metal Forming of High-Performance Steel, ed. by Oldenburg, Mats; Prakash, Braham; Steinhoff, Kurt; 6th ed., 2017, pp.525-542

[20] Taylor, T.; Clough, A.; Critical review of automotive hot-stamped sheet steel from an industrial perspective, in: Materials Science and Technology, 2018, pp. 809-861

[21] Fan, D.W.; Kim, Han S.; Birosca, S.; et al.; Critical Review of Hot Stamping Technology for Automotive Steels, in: Proc. from the Materials Science & Technology Conference MS&T, 2007, pp.1-12

[22] Berglund, G.; The history of hardening of boron steel in northern Sweden, in: 1st International Conference on Hot Sheet Metal Forming of High-Performance Steel, 2008, pp.175-177, quoted from Taylor, T.; Clough, A.; Critical review of automotive hot-stamped sheet steel from an industrial perspective, in: Materials Science and Technology, 2018, pp. 809-861

[23] Behrens, B.A.; Hot stamping, in: CIRP, ed. by Laperriere, Luc; Reinhart, Gunther; CIRP Encyclopedia of Production Engineering, Berlin, 2014, pp.1-7, quoted from Taylor, T.; Clough, A.; Critical review of automotive hot-stamped sheet steel from an industrial perspective, in: Materials Science and Technology, 2018, pp. 809-861

[24] Steinhoff, Kurt; From spades to functionally graded automotive components, compact training on hot stamping technology, 2nd GM PHS Suppliers Forum, GM, 2014, pp.7-32, quoted from Taylor, T.; Clough, A.; Critical review of automotive hot-stamped sheet steel from an industrial perspective, in: Materials Science and Technology, 2018, pp. 809-861

[25] Wurzer, A.J.; Wettbewerbsvorteile durch Patentinformationen, 2nd ed., FIZ-Karlsruhe, 2003, quoted from Schönherr, Julia; Landgrebe, Dirk; Polubinski, Swetlana; Entwicklungen beim Presshärten, Ein Update; Carl Hanser Verlag, Chemnitz, 2017, pp.33-36

[26] Naderi, M.; Hot stamping of ultra high strength steels, Doctoral Thesis, RWTH Aachen, 2007 quoted from H., Karbasian; A.E. Tekkaya; A review on hot stamping, in: Journal of Materials Processing Technology **210**, Elsevier, 2010, pp.2103-2118

[27] Zs., Lukacs; M., Tisza; Application and development trends in high strength steel and aluminium, in: Material Science and Engineering **448**, 2018, pp.1-7

[28] Billur, Eren; Son, Hyun-Sung; Blank Materials, in: Hot Stamping of Ultra High-Strength Steels, From a Technological and Business Perspective, ed. by Billur, Eren; Springer, 2019, pp.45-76

[29] Salzgitter-Flachstahl (publ.); Boron-alloyed quenched and tempered steel, https://www.salzgitter-flachstahl.de/en/products/hot-rolled-products/steel-grades/boron-alloyed-quenched-and-tempered-steel.html, (04.02.2019)

[30] ArcelorMittal (publ.); Steels for hot stamping - Usibor® and Ductibor®, https://automotive.arcelormittal.com, (04.02.2019)

[31] ThyssenKrupp Steel (publ.), Produktinformation Mangan-Bor-Stähle für die Warmumformung, https://www.thyssenkrupp-steel.com/de/download?p=497872A2A1336C33BB2485AA205A71E30634C75A178E1C0C2D89F3E13E54BDF9D910976B1D22061DDC9EF18010014AB0DCB2EA3CBD0133F378F94B6CF90B96DEA30EBD83656D54633D2B7A9A1D35356C362F9DAE9CBA5538DB25AF2254AFAF1CDBBD71A05565EAA7AC4B543B54548DB49621D36EF98FBBD7123C5849C14171AA, (04.02.2019)

[32] SSAB (publ.), Docol® PHS 1500 – Härtbarer Borstahl für die Automobilindustrie, https://www.ssab.de/produkte/warenzeichen/docol/products/docol-phs-1500, (04.02.2019)

[33] Voestalpine (publ.), phs-ultraform®, https://www.voestalpine.com/stahl/content/download/4714/file/phs-ultraform-voestalpine-DE-20180828.pdf, (04.02.2019)

[34] Hwang, B.; Suh, D.; Kim, S.; Austenitizing temperature and hardenability of low-carbon boron steels, Scr Mater, 2011, pp.1118–1120, quoted from T., Taylor; A., Clough; Critical review of automotive hot-stamped sheet steel from an industrial perspective, in: Materials Science and Technology, 2018, pp. 809-861

[35] Paar, U.; Becker, H.H.; Alsmann, M.; Press-hardened components from Kassel – chances and challenges, Proceedings of the 1st International Conference in Hot Sheet Metal Forming of High-performance Steel CHS², 2008, pp.153-163, quoted from Veit, Robert; Hofmann, Harald; Kolleck, Ralf; et al.; Phase Formation of Al/Si-Coatings during Induction Heating of Boron Alloyed Steel Sheets, Verlag der Technischen Universität Graz, 2011, pp.225-234

[36] Lenze, F.J.; Sikora, S.; Banik, J.; et al.; Development tendencies as to processing of press hardening under application of coated steel, Proceedings of the 1st International Conference in Hot Sheet Metal Forming of High-performance Steel CHS², 2008, pp.15-21, quoted from Veit, Robert; Hofmann, Harald; Kolleck, Ralf; et al.; Phase Formation of Al/Si-Coatings during Induction Heating of Boron Alloyed Steel Sheets, Verlag der Technischen Universität Graz, 2011, pp.225-234

[37] Schrenk, Mario; Peuker, Christian; Franek, Friedrich; et al.; Oxidation of Uncoated 22MnB5 Steel Grades for Hot Stamping Applications, in: Hot Sheet Metal Forming of High-Performance Steel, ed. by Oldenburg, Mats; Prakash, Braham; Steinhoff, Kurt; 4th ed., Verlag Wissenschaftliche Scripten, 2013, pp.161-166

[38] Veit, Robert; Hofmann, Harald; Kolleck, Ralf; et al.; Phase Formation of Al/Si-Coatings during Induction Heating of Boron Alloyed Steel Sheets, Verlag der Technischen Universität Graz, 2011, pp.225-234

[39] Banik, Janko; Etzold, Ulrich; Rössler, Norbert; Hydrogen in Hot Forming Steels – Mechanisms and Coating Design, in: Hot Sheet Metal Forming of High-Performance Steel, ed. by Oldenburg, Mats; Prakash, Braham; Steinhoff, Kurt; 6th ed., 2017

[40] Lehmann, H.; Furnaces for press hardening, Presented at AP&T Press Hardening, Next Step Seminar, 2010, quoted from Billur, Eren; Berglund, Göran; Gustafsson, Tord; History and Future Outlook of Hot Stamping, in: Hot Stamping of Ultra High-Strength Steels, From a Technological and Business Perspective, ed. by Billur, Eren; Springer, 2019, pp.31-44

[41] Jinkeun, Oh; Seongwoo, Kim; Yeol-Rae, Cho; Development of New Al Coating for Press Hardening, in: Hot Sheet Metal Forming of High-Performance Steel, ed. by Oldenburg, Mats; Prakash, Braham; Steinhoff, Kurt; 6th ed., 2017, pp.131-132

[42] Merklein, Marion; Wieland, Michael; Lechner, Michael; et al.; Hot stamping of boron steel sheets with tailored properties: A review, in: Journal of Materials Processing Technology **228**, Elsevier, 2016, pp.11-24

[43] Karbasian, H.; Tekkaya, A.E.; A review on hot stamping, in: Journal of Materials Processing Technology **210**, Elsevier, 2010, pp.2103-2118

[44] Neugebauer, R.; Schieck, F.; Polster, S.; et al.; Press hardening – An innovative and challenging technology, in: Archives of Civil and Mechanical Engineering **12**, 2012, pp.113-118

[45] Kelsch, Reiner; Sommer, Andreas; Schwinghammer, Harald; et al.; Hot Forming of Zinc Coated Press Hardening Steel. Characterization of Forming Behaviour and New Process Routes for Mass Production, in: Hot Sheet Metal Forming of High-Performance Steel, ed. by Oldenburg, Mats; Prakash, Braham; Steinhoff, Kurt; 6th ed., 2017, pp.337-344

[46] Reini, Luke A.; Choi, Minyoung; Wendorf, Axel; Development of Zn-Coated PHS Components for Automotive Applications, in: Hot Sheet Metal Forming of High-Performance Steel, ed. by Oldenburg, Mats; Prakash, Braham; Steinhoff, Kurt, 4th ed., Verlag Wissenschaftliche Scripten, 2013, pp.223-230

[47] Kim, Seongwoo; Son, IIryong; Kim, Dongjin; et al.; Cracking Issues of Zn Coated Press Hardening Steel in Direct Hot Press Forming, in: Hot Sheet Metal Forming of High-Performance Steel, ed. by Oldenburg, Mats; Prakash, Braham; Steinhoff, Kurt; 4th ed., Verlag Wissenschaftliche Scripten, 2013, pp.537-544

[48] Drillet, P.; Grigorieva, R.; Leuillier, G.; et al.; Study of cracks propagation inside the steel on press hardened steel zinc based coatings, in: La Metallurgia Italiana **1**, 2012, pp.3-8

[49] Frenzer, G.; Nano-x Gmbh x-tec® and alsi® coat products against scale formation on steel, 2015, quoted from Billur, Eren; Son, Hyun-Sung; Blank Materials, in: Hot Stamping of Ultra High-Strength Steels, From a Technological and Business Perspective, ed. by Billur, Eren; Springer, 2019, pp.45-76

[50] Fan, D.W.; De Cooman, B.C.; State-of-the-Knowledge on Coating Systems for Hot Stamped Parts, Wiley Online Library, 2012, pp.412-433

[51] Schwing Technologies GmbH (publ.); Fluidized Bed Heat Treatment, https://www.heat--treatment.com/en.html, (05.05.2019)

[52] J., Dietrich; Praxis der Umformtechnik, 12th ed., Springer Vieweg, 2018, quoted from Oppermann, A.; Seemann, P.; Experiences with Press Hardening Furnaces and Tailored Tempering Systems, in: 13. Erlanger Workshop Warmblechumformung, ed. by Merklein, M.; 13th ed., Lehrstuhl für Fertigungstechnologie-Friedrich-Alexander Universität Erlangen-Nürnberg, 2018, pp.51-58

[53] Çetin, Bariş; Halim, Meço; Metallurgy of Steels, in: Hot Stamping of Ultra High-Strength Steels, From a Technological and Business Perspective, ed. by Billur, Eren; Springer, 2019, pp.19-30

[54] G., Krauss; Deformation and fracture in martensitic carbon steels tempered at low temperatures, in: Metallurgical and Materials Transactions B **32**(2), 2001, pp 205-221, quoted from Çetin, Bariş; Halim, Meço; Metallurgy of Steels, in: Hot Stamping of Ultra High-Strength Steels, From a Technological and Business Perspective, ed. by Billur, Eren; Springer, 2019, pp.19-30

[55] D., Deng; FEM prediction of welding residual stress and distortion in carbon steel considering phase transformation effects, in: Materials and Design **30**(2), 2009, pp. 359-366, quoted from Çetin, Bariş; Halim, Meço; Metallurgy of Steels, in: Hot Stamping of Ultra High-Strength Steels, From a Technological and Business Perspective, ed. by Billur, Eren; Springer, 2019, pp.19-30

[56] Callister, W.D.; Rethwisch, D.G.; Fundamentals of Materials Science and Engineering, Vol.21, Wiley-New York, 2013, quoted from Çetin, Bariş; Halim, Meço; Metallurgy of Steels, in: Hot Stamping of Ultra High-Strength Steels, From a Technological and Business Perspective, ed. by Billur, Eren; Springer, 2019, pp.19-30

[57] Miklós, Tisza; Péter Z., Kovács; Zsolt, Lukács; Hot Press Forming in Sheet Metal Forming, International Multidisciplinary Scientific Conference, University of Miskolc, 2014

[58] Ademaj, Agim; Donis, Alexander, Weidig, Ursula; et al.; Hot Stamping of Multi-Material Composites, in: Hot Sheet Metal Forming of High-Performance Steel, ed. by Oldenburg, Mats; Prakash, Braham; Steinhoff, Kurt; 4th ed., Verlag Wissenschaftliche Scripten, 2013, pp.481-488

[59] AP&T (publ.); AP&T führt TemperBox® ein: eine neue zykluszeitneutrale Produktionslösung, die maßgeschneiderte Eigenschaften in pressgehärteten Bauteilen ermöglicht, https://www.aptgroup.com/de/das-unternehmen/neuigkeiten/apt-f%C3%BChrt-temperbox%C2%AE-ein-eine-neue-zykluszeitneutrale-produktionsl%C3%B6sung, (05.05.2019)

[60] Kurz, T.; Luckeneder, G.; Manzenreiter, T.; et al.; Zinc coated press-hardening steel – challenges and solutions, in: SAE Technical Paper, SAE International, 2015

[61] Billur, Eren; Bošković, Vladimir; Tailored Properties, in: Hot Stamping of Ultra High-Strength Steels, From a Technological and Business Perspective, ed. by Billur, Eren; Springer, 2019, pp.157-190

[62] Bostik (publ.); Automotive body in white (BIW) and a smart Solution, https://www.bostik-industrial.com/automotive-body-white-biw-smart-solution/, (07.01.2019)

[63] Horn, A.; Merklein, M.; Fertigung funktionsoptimierter Bauteile beim Presshärten, in: 13. Erlanger Workshop Warmblechumformung, ed. by Merklein, M.; 13th ed., Lehrstuhl für Fertigungstechnologie-Friedrich-Alexander Universität Erlangen-Nürnberg, 2018, pp.157-170

[64] Hilditch, T.B.; De Souza, T.; Hodgson, P.D.; Properties and automotive applications of advanced high-strength steels (AHSS), Deakin University, 2015, pp.9-28

[65] Field, Natalie N.; DiCiano, Massimo; D'Souza, Michael; et al.; Tailoring by Direct Contact Heating During HFDQ, in: Hot Sheet Metal Forming of High-Performance Steel, ed. by Oldenburg, Mats; Prakash, Braham; Steinhoff, Kurt; 6th ed., 2017, pp.473-480

[66] Klein, B.; Crichley, S.; Khang, K.; Hot Stamp Rear Frame Optimization, in: Great Designs in Steel, 2015

[67] Fernandez, B.; Zarate, J.; Garcia, I.; et al.; Tailor strategies in press hardening, in: Hot Sheet Metal Forming of High-Performance Steel, ed. by Oldenburg, Mats; Prakash, Braham; Steinhoff, Kurt; 3rd ed., 2011, pp.437-446, quoted from Billur, Eren; Bošković, Vladimir; Tailored Properties, in: Hot Stamping of Ultra High-Strength Steels, From a Technological and Business Perspective, ed. by Billur, Eren; Springer, 2019, pp.157-190

[68]Yokogawa Electric Corporation (publ.); Touch Screen GP10/GP20, https://www.yokogawa.com/solutions/products-platforms/data-acquisition/portable-data-acquisition/touch-screen-gp10-gp20/, (06.03.2019)

[69] Ebner Industrieofenbau GmbH, Internal Information, 2019

[70] Stöhr, T.; Lechler, J.; Merklein, M.; investigations on different strategies for influencing the microstructural properties with respect to partial hot stamping, in: 2nd International Conference on Hot Sheet Metal Forming of High-Performance Steel, pp.273–281, quoted from H., Karbasian; A.E. Tekkaya; A review on hot stamping, in: Journal of Materials Processing Technology **210**, Elsevier, 2010, pp.2103-2118

[71] Feuser, P.S.; Ein Ansatz zur Herstellung von pressgehärteten Karosseriekomponenten mit maßgeschneiderten mechanischen Eigenschaften: Temperierte Umformwerkzeuge. Prozessfenster, Prozesssimulation und funktionale Untersuchung, 2012, quoted from Horn, A.; Merklein, M.; Fertigung funktionsoptimierter Bauteile beim Presshärten, in: 13. Erlanger Workshop Warmblechumformung, ed. by Merklein, M.; 13th ed., Lehrstuhl für Fertigungstechnologie-Friedrich-Alexander Universität Erlangen-Nürnberg, 2018, pp.157-170

[72] Ebner Industrieofenbau GmbH, Hot Phase – Press Hardening Automotive Solutions by Ebner, Internal Presentation, 2017

[73] Ebner Industrieofenbau GmbH, Hot Phase – Basic knowledge for press hardening of steel, Internal Presentation, 2018

[74] Ebner, Fritz Josef; The HotPHASE Multi-Level Chamber Furnace – Concept, Advantages and Experiences from Production, in: Hot Sheet Metal Forming of High-Performance Steel, ed. by Oldenburg, Mats; Prakash, Braham; Steinhoff, Kurt, 4th ed., Verlag Wissenschaftliche Scripten, 2013

[75] Horn, A.; Merklein, M.; Identification of a process window for tailored carburization of sheet metals in hot stamping, in: AIP Conference Proceedings 1960, 2018, quoted from Horn, A.; Merklein, M.; Fertigung funktionsoptimierter Bauteile beim Presshärten, in: 13. Erlanger Workshop Warmblechumformung, ed. by Merklein, M.; 13th ed., Lehrstuhl für Fertigungstechnologie-Friedrich-Alexander Universität Erlangen-Nürnberg, 2018, pp.157-170

[76] PennState Eberly College of Science (publ.); A Quick History of the Design of Experiments (DoE), https://newonlinecourses.science.psu.edu/stat503/node/6/, (16.02.2019)

[77] J.M., Berasategi; C., Garbalena; B., Irazu; et al.; Past and future for tailor-made hot stamping lines, in: Hot Sheet Metal Forming of High-Performance Steel, ed. by Oldenburg, Mats; Prakash, Braham; Steinhoff, Kurt; 3rd ed., 2011, pp.255-261, quoted from Billur, Eren; Teague, Rick; Çetin, Bariş; Economics of Hot Stamping, in: Hot Stamping of Ultra High-Strength Steels, From a Technological and Business Perspective, ed. by Billur, Eren; Springer, 2019, pp.225-245

[78] Billur, Eren; Teague, Rick; Çetin, Bariş; Economics of Hot Stamping, in: Hot Stamping of Ultra High-Strength Steels, From a Technological and Business Perspective, ed. by Billur, Eren; Springer, 2019, pp.225-245

[79] Anton Schweizer (publ.); Formelsammlung und Berechnungsprogramme Anlagenbau, Wärmeleitfähigkeit – Metalle, https://www.schweizer-fn.de/stoff/wleit_metall/wleit_metall.php, (10.03.2019)

[80] Lumitos AG (publ.); Kupfer, http://www.chemie.de/lexikon/Kupfer.html, (10.03.2019)

[81] Lumitos AG (publ.); Baustahl, http://www.chemie.de/lexikon/Baustahl.html, (10.03.2019)

[82] Lumitos AG (publ.); Aluminium, http://www.chemie.de/lexikon/Aluminium.html, (10.03.2019)

[83] Lumitos AG (publ.); Schmelzpunkt, http://www.chemie.de/lexikon/Schmelzpunkt.html, (10.03.2019)

[84] OMAX Corporation (publ.); ProtoMAX, https://www.protomax.com/, (01.04.2019)

[85] Eggert, Frank; Standardfreie Elektronenstrahl Mikroanalyse, Mit dem EDX im Rasterelektronenmikroskop-Ein Handbuch für die Praxis, Books on Demand GmbH, 2005

[86] Technische Hochschule Ulm (publ.), Prinzip der EDX-Analyse im REM, https://www.hs-ulm.de/Institut/IFW/Abteilungen/IFW-WP/Laborversuche/DemoVersuch2/Ausstattung/EDXAnalysensystem/Prinzip-EDX/beschreibung_de.dbx, (20.04.2019)

[87] EMCO-TEST (publ.), Theory of hardness testing, https://www.emcotest.com/en/the-world-of-hardness-testing/hardness-know-how/theory-of-hardness-testing/vickers-52/categorisation-of-the-vickers-method-238/, (28.04.2019)

[88] Schwartz GmbH (publ.); Thermisches Printen (Tailored Tempering), https://schwartz-wba.com/produkte/thermisches-printen/, (28.04.2019)

List of figures

List of tables

Appendix

Appendix table of contents

Appendix A1: Geometric properties of the specimens

Geometric properties:

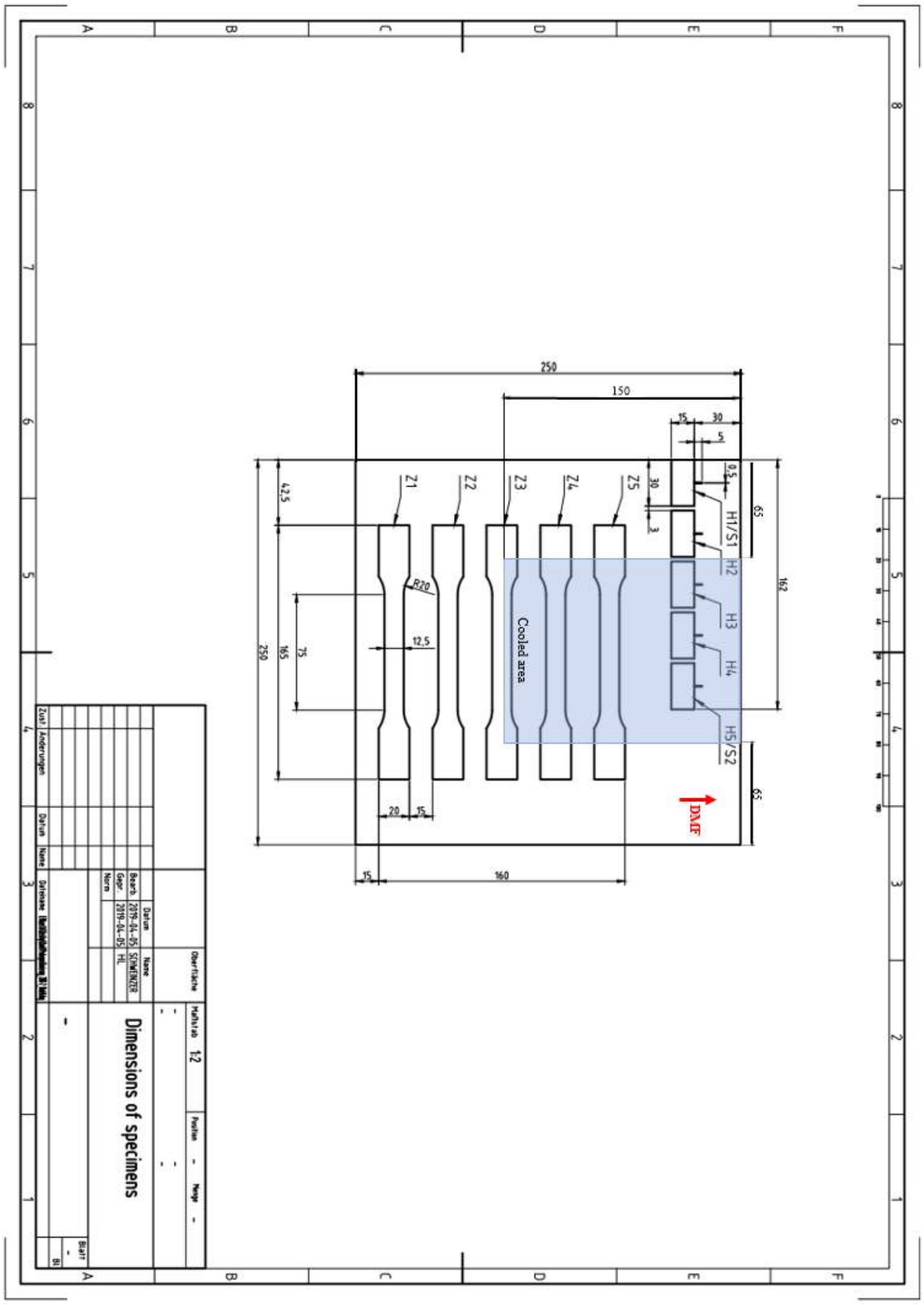

Appendix A2: Determination of the ideal contact times of the contact cooler $t_{i\_j\text{-}pt}$

Trial furnace

1.1_890-pt:

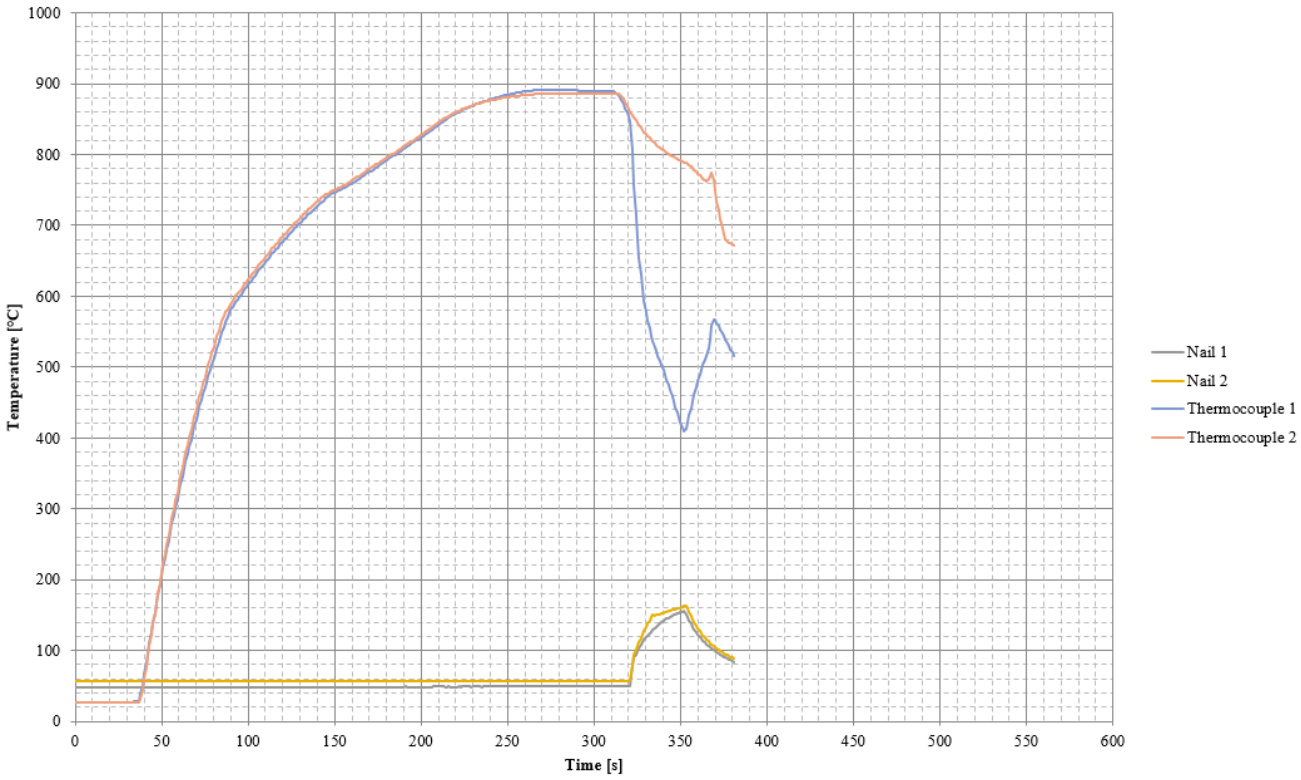

2.1_890-pt:

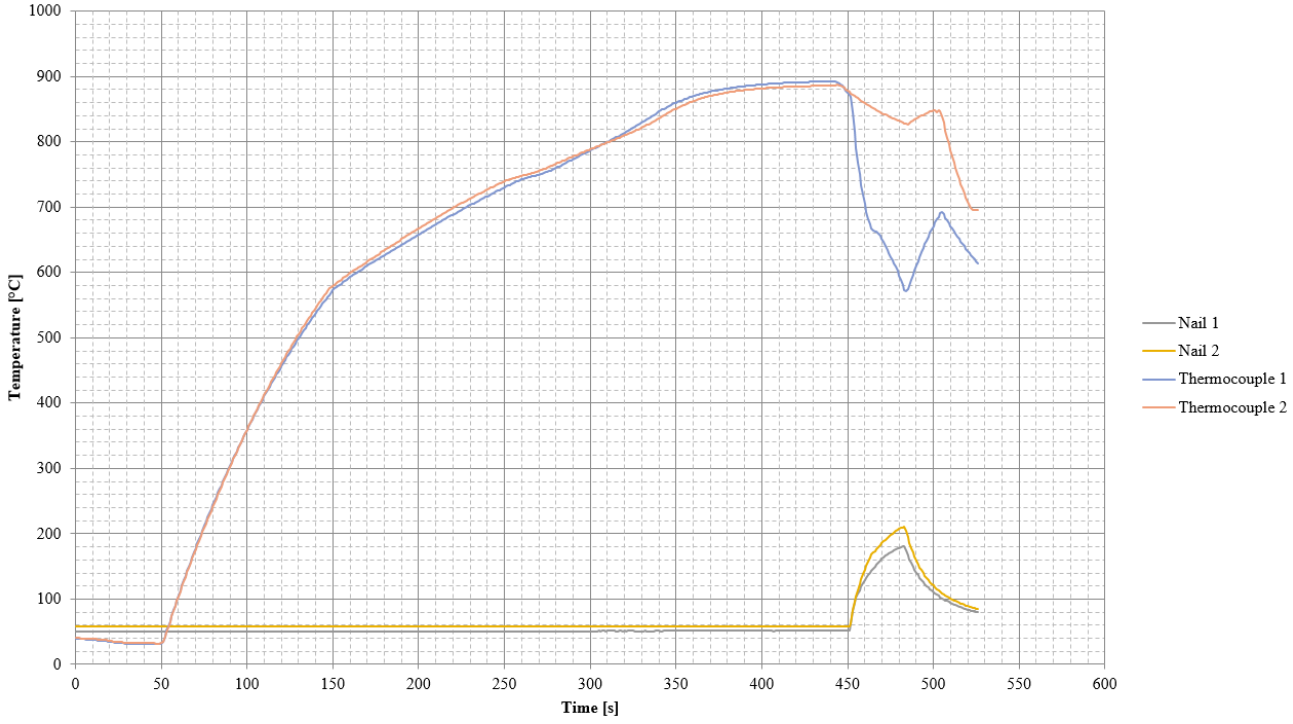

3.1_930-pt:

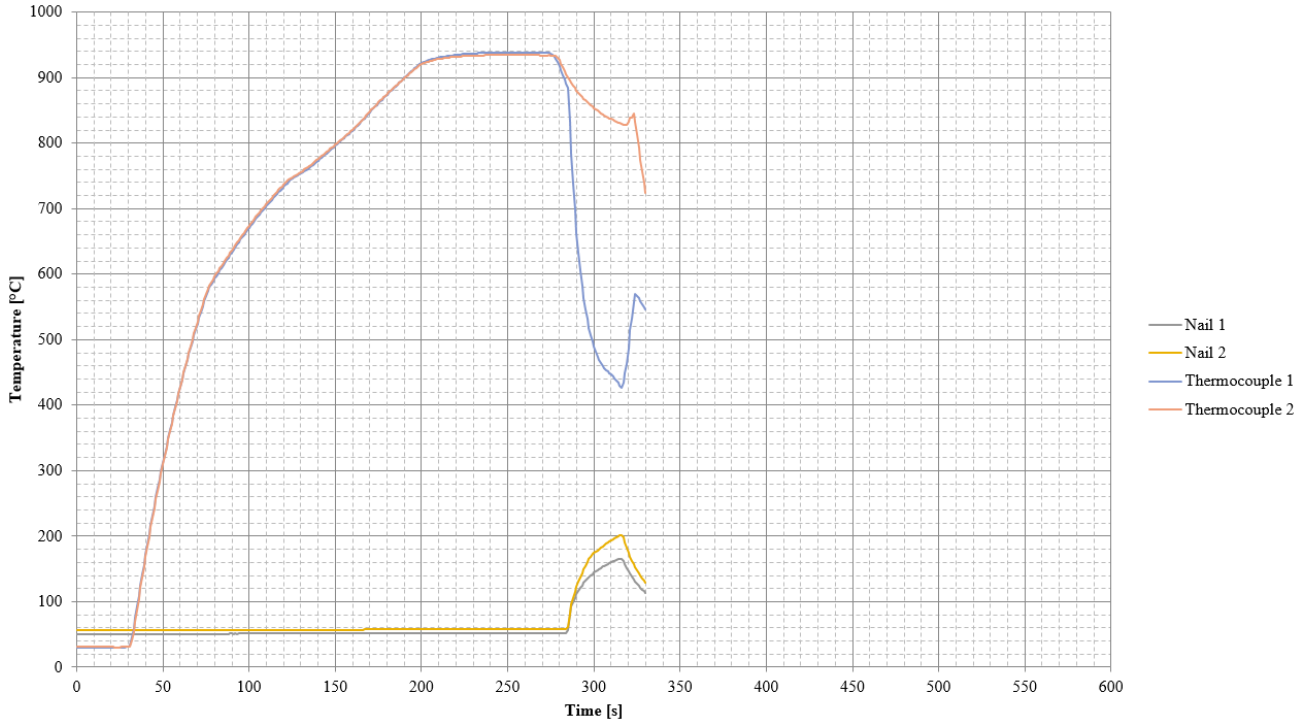

4.1_930-pt:

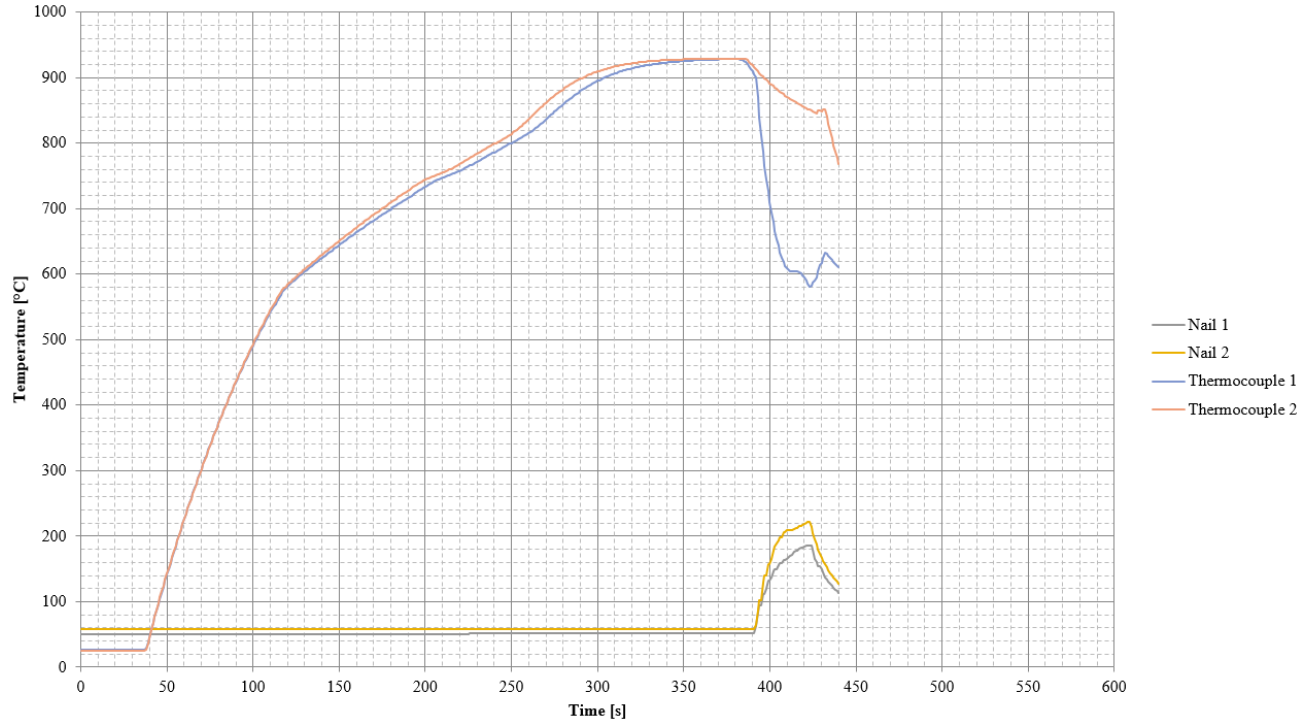

Appendix A3: Determination of the ideal furnace dwell times after the contact cooler $t_{i\_pt\text{-}700}$

Trial furnace

1.2_pt-700:

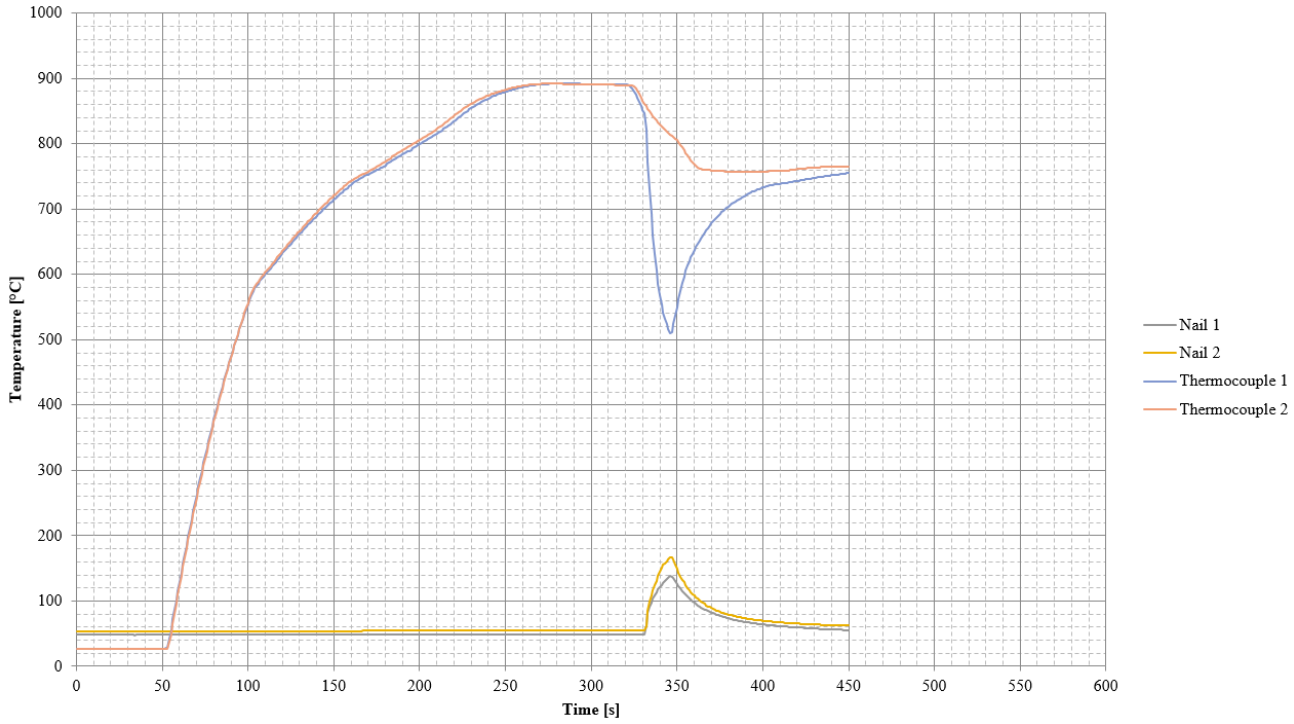

2.2_pt-700:

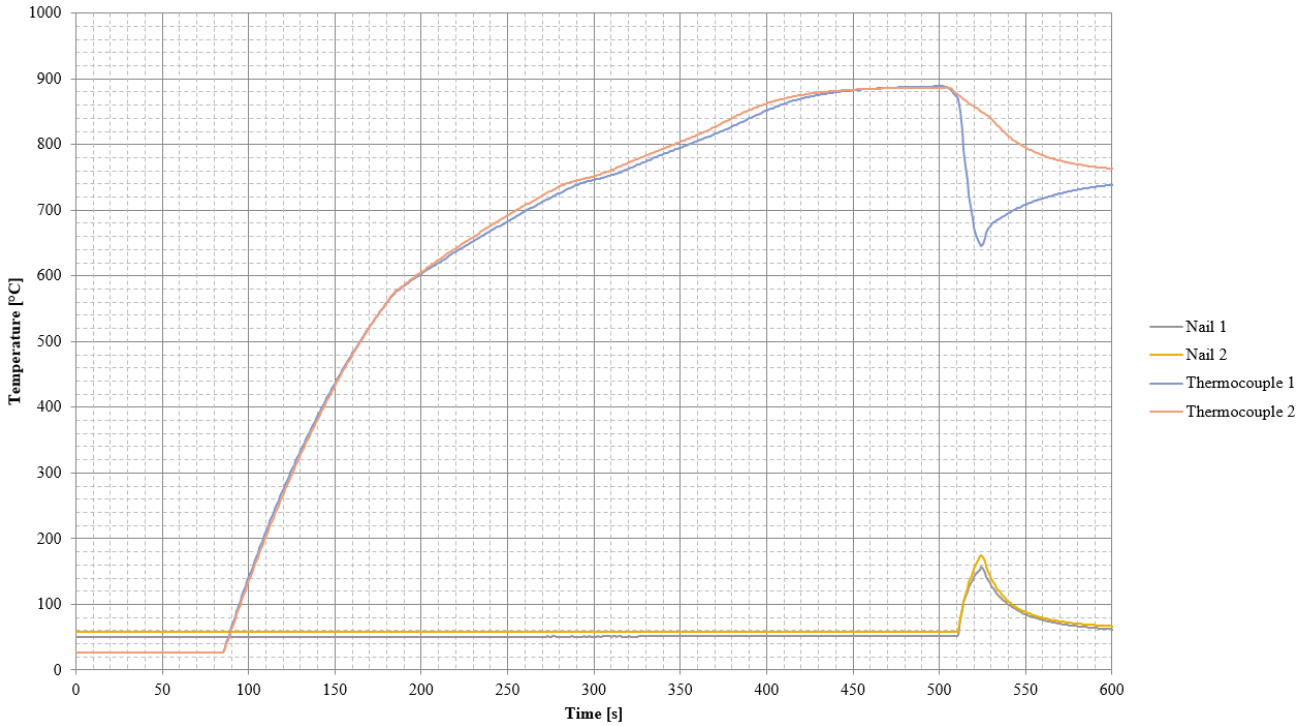

3.2_pt-700:

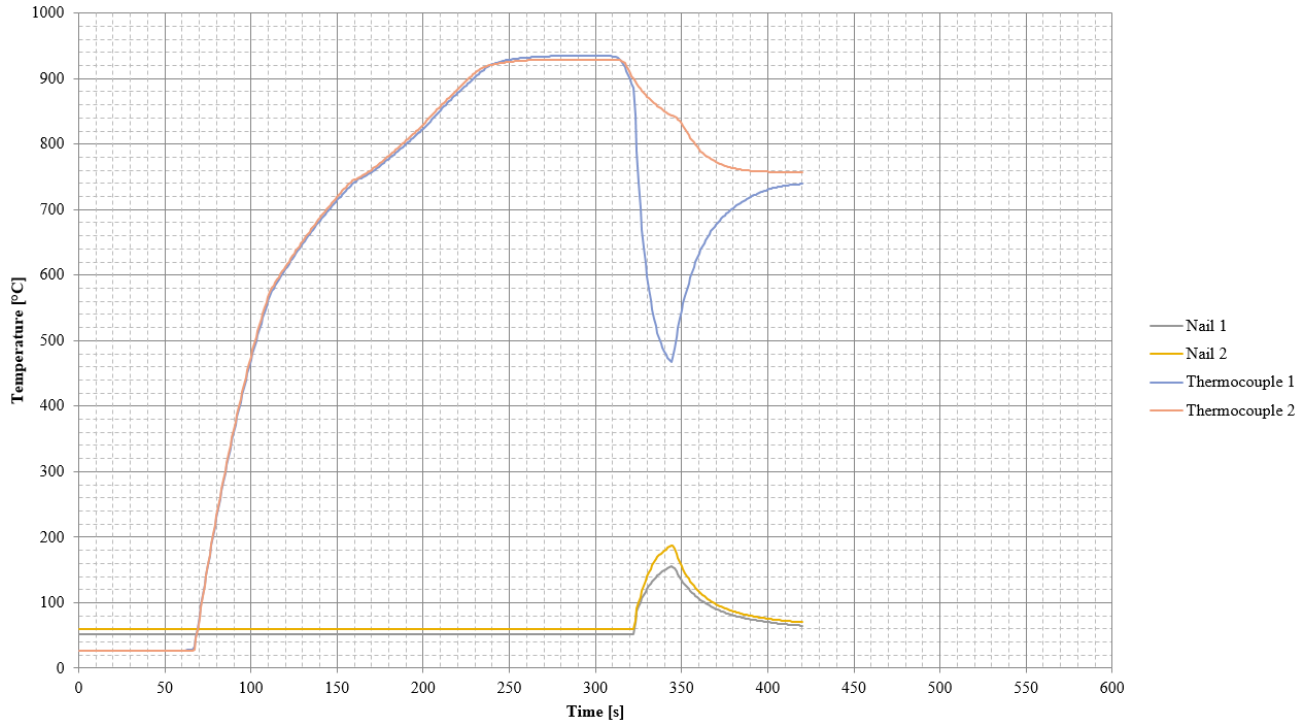

4.2_pt-700:

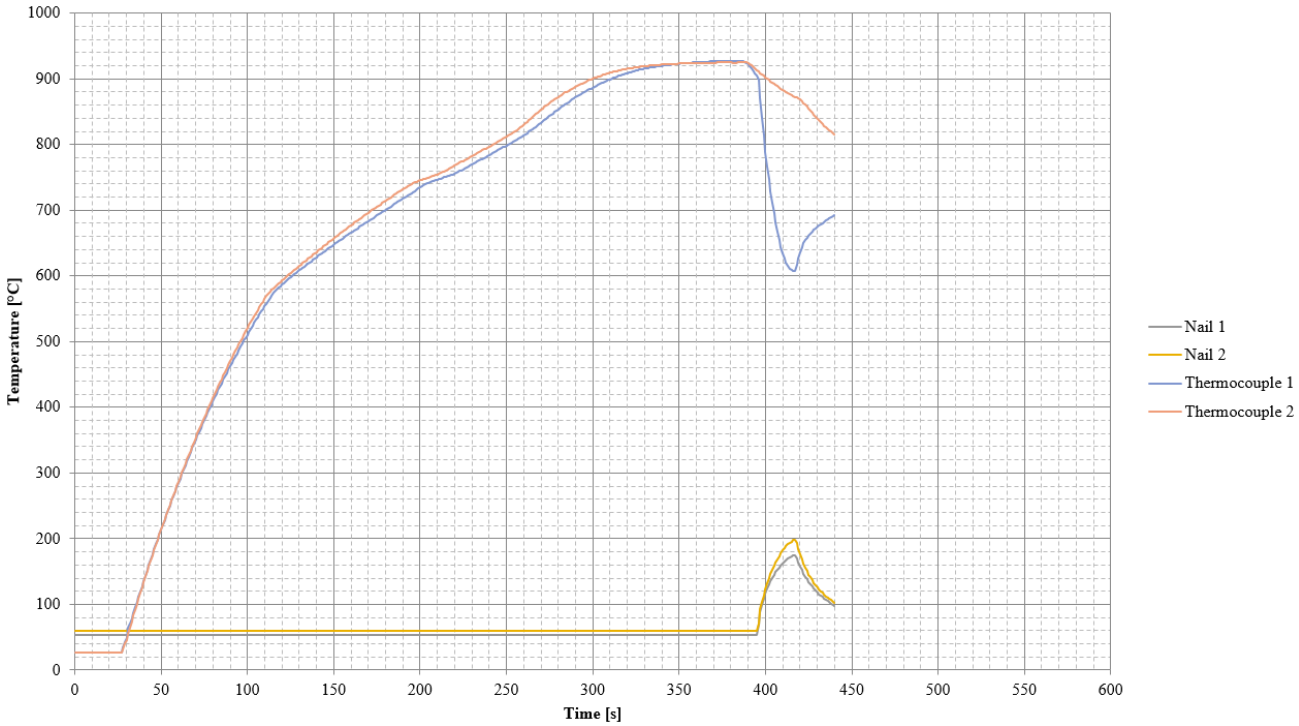

Appendix A4: Location-dependent temperature curves with indefinite air cooling

Trial furnace

PTAF1:

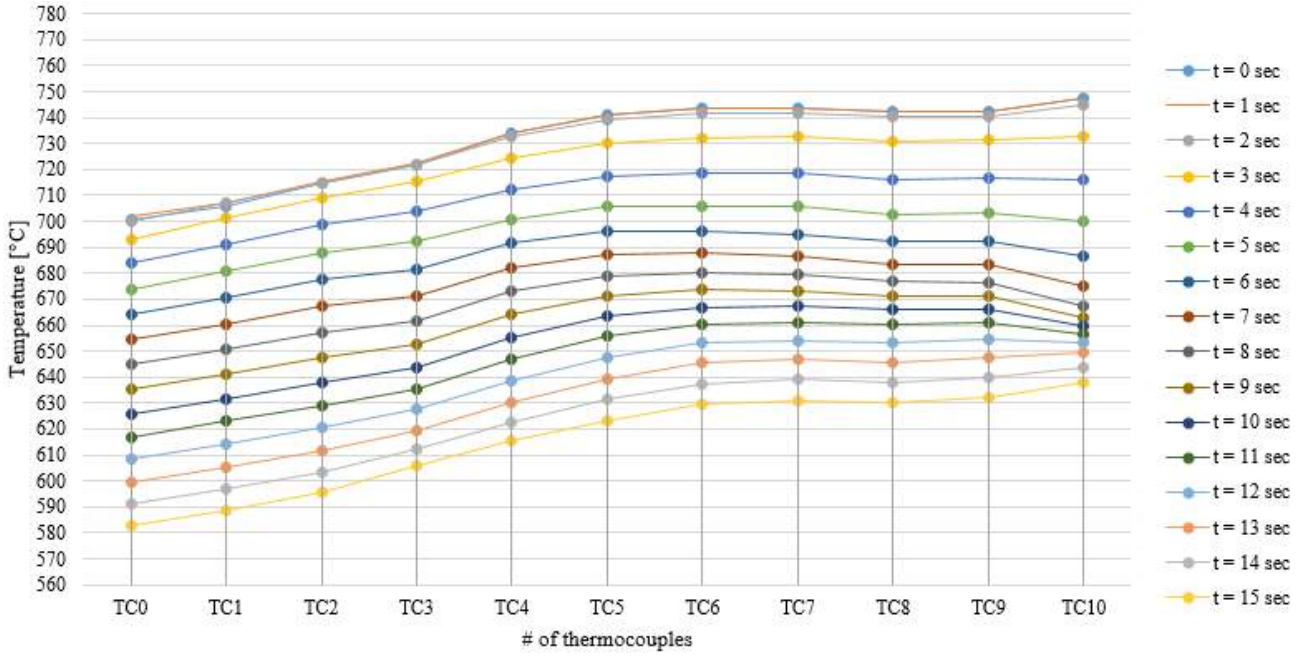

PTAF2:

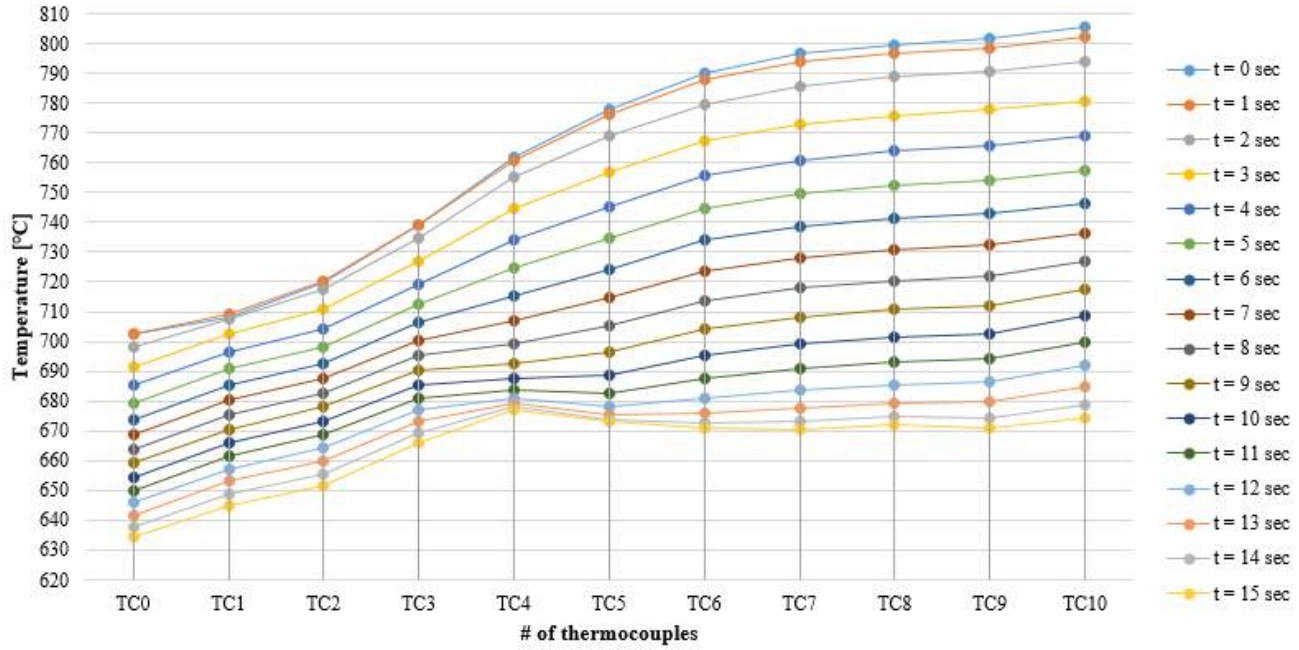

PTAF3:

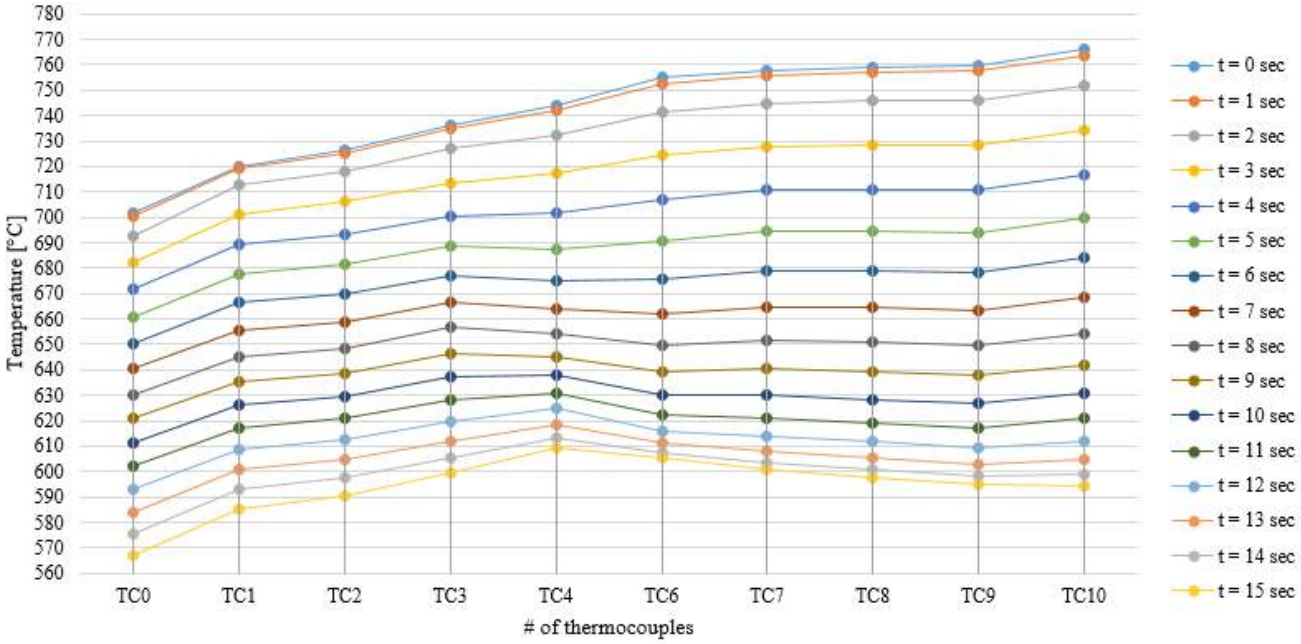
Temperature [°C]
780
770
760
750
740
730
720
710
700
690
680
670
660
650
640
630
620
610
600
590
580
570
560
TC0
TC1
TC2
TC3
TC4
TC6
TC7
TC8
TC9
TC10
# of thermocouples
t = 0 sec
t = 1 sec
t = 2 sec
t = 3 sec
t = 4 sec
t = 5 sec
t = 6 sec
t = 7 sec
t = 8 sec
t = 9 sec
t = 10 sec
t = 11 sec
t = 12 sec
t = 13 sec
t = 14 sec
t = 15 sec

PTAF4:

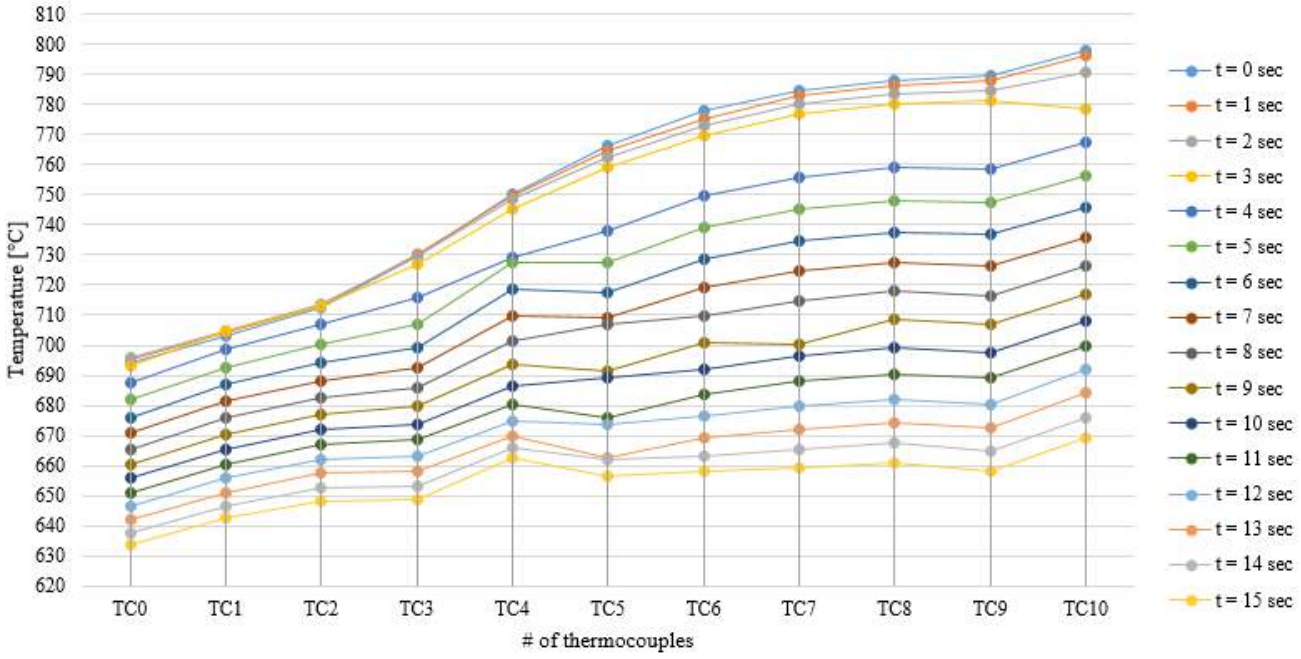
Temperature [°C]
810
800
790
780
770
760
750
740
730
720
710
700
690
680
670
660
650
640
630
620
TC0
TC1
TC2
TC3
TC4
TC5
TC6
TC7
TC8
TC9
TC10
# of thermocouples
t = 0 sec
t = 1 sec
t = 2 sec
t = 3 sec
t = 4 sec
t = 5 sec
t = 6 sec
t = 7 sec
t = 8 sec
t = 9 sec
t = 10 sec
t = 11 sec
t = 12 sec
t = 13 sec
t = 14 sec
t = 15 sec

Appendix A5: Determination of the critical transfer times $t_{700\_crit\_i}$

Trial furnace

PTAF1:

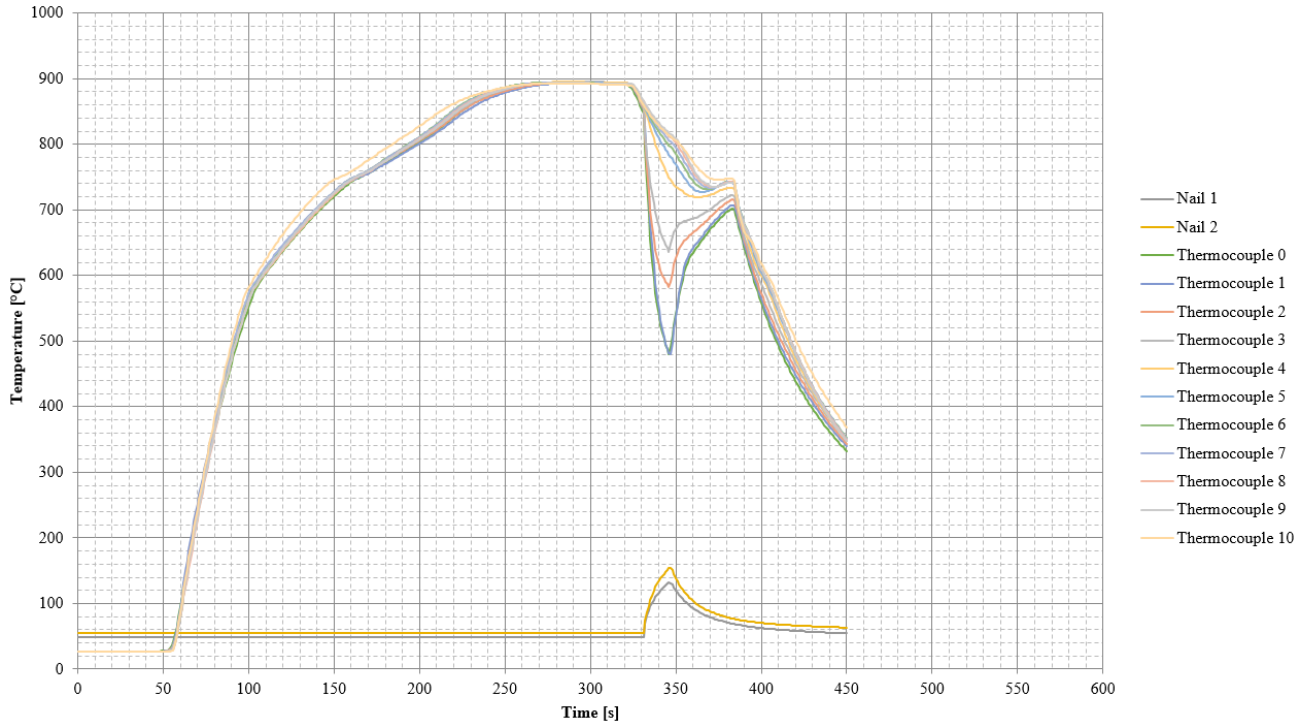

PTAF2:

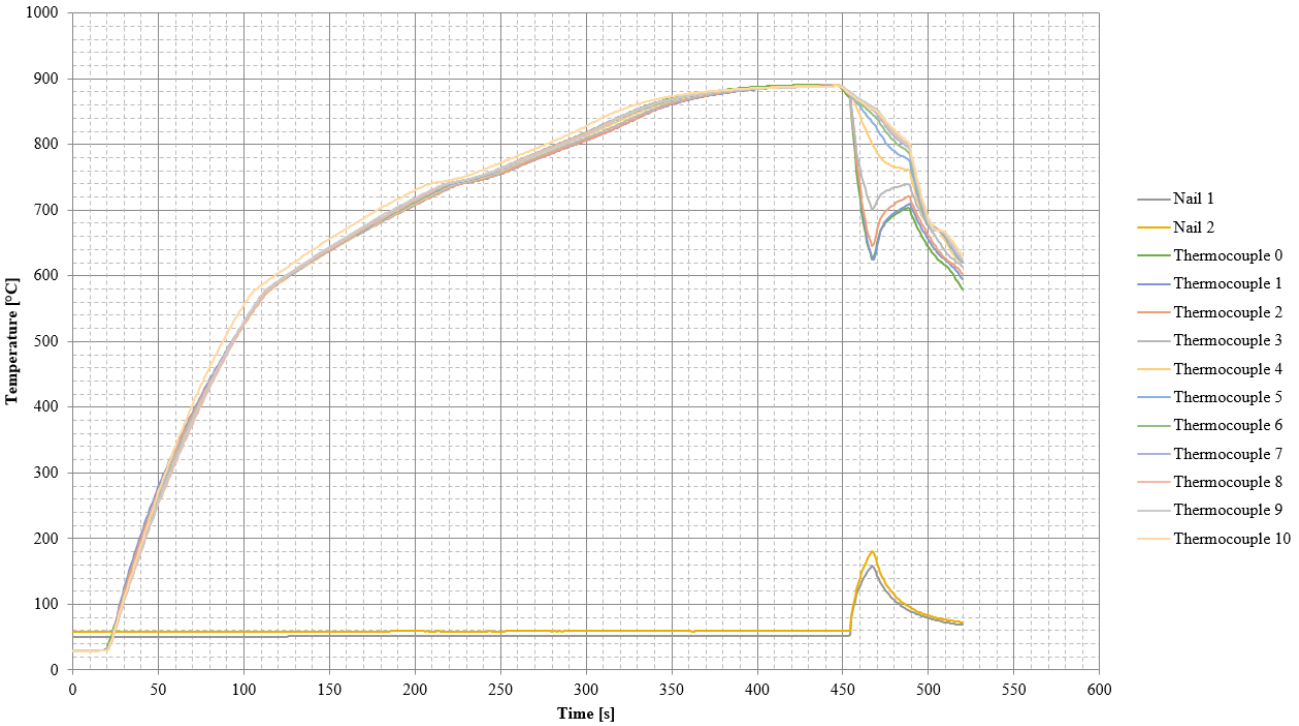

PTAF3:

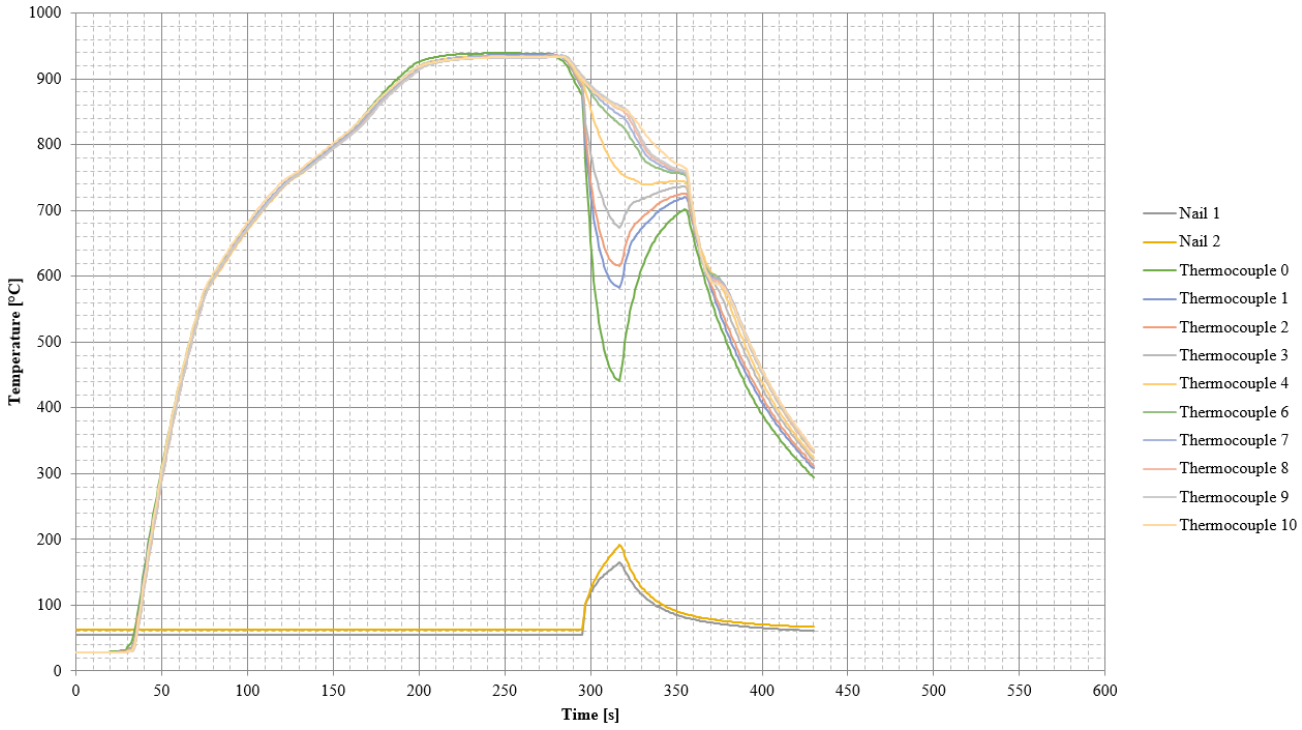
Temperature [°C]
Time [s]
Nail 1
Nail 2
Thermocouple 0
Thermocouple 1
Thermocouple 2
Thermocouple 3
Thermocouple 4
Thermocouple 6
Thermocouple 7
Thermocouple 8
Thermocouple 9
Thermocouple 10

PTAF4:

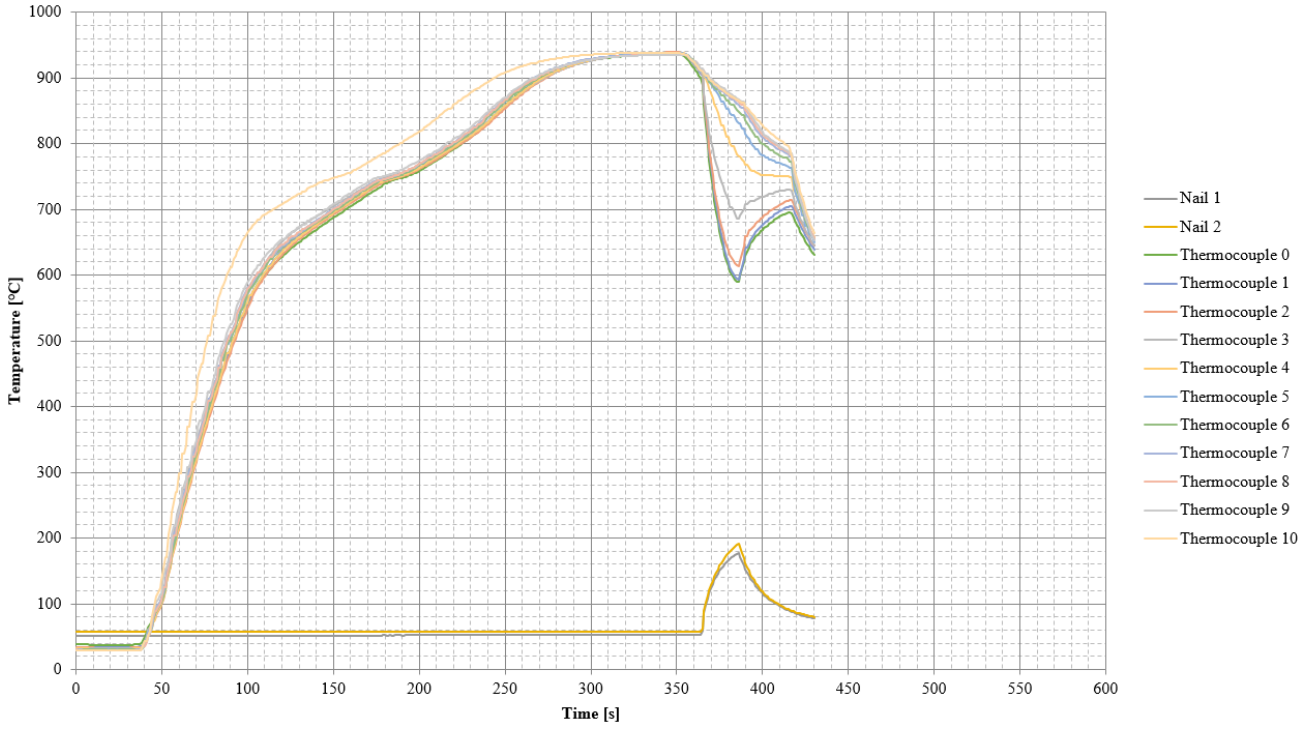
Temperature [°C]
Time [s]
Nail 1
Nail 2
Thermocouple 0
Thermocouple 1
Thermocouple 2
Thermocouple 3
Thermocouple 4
Thermocouple 5
Thermocouple 6
Thermocouple 7
Thermocouple 8
Thermocouple 9
Thermocouple 10

Appendix A6: Final tests with lower and upper transfer times

Trial furnace

FTF1_l:

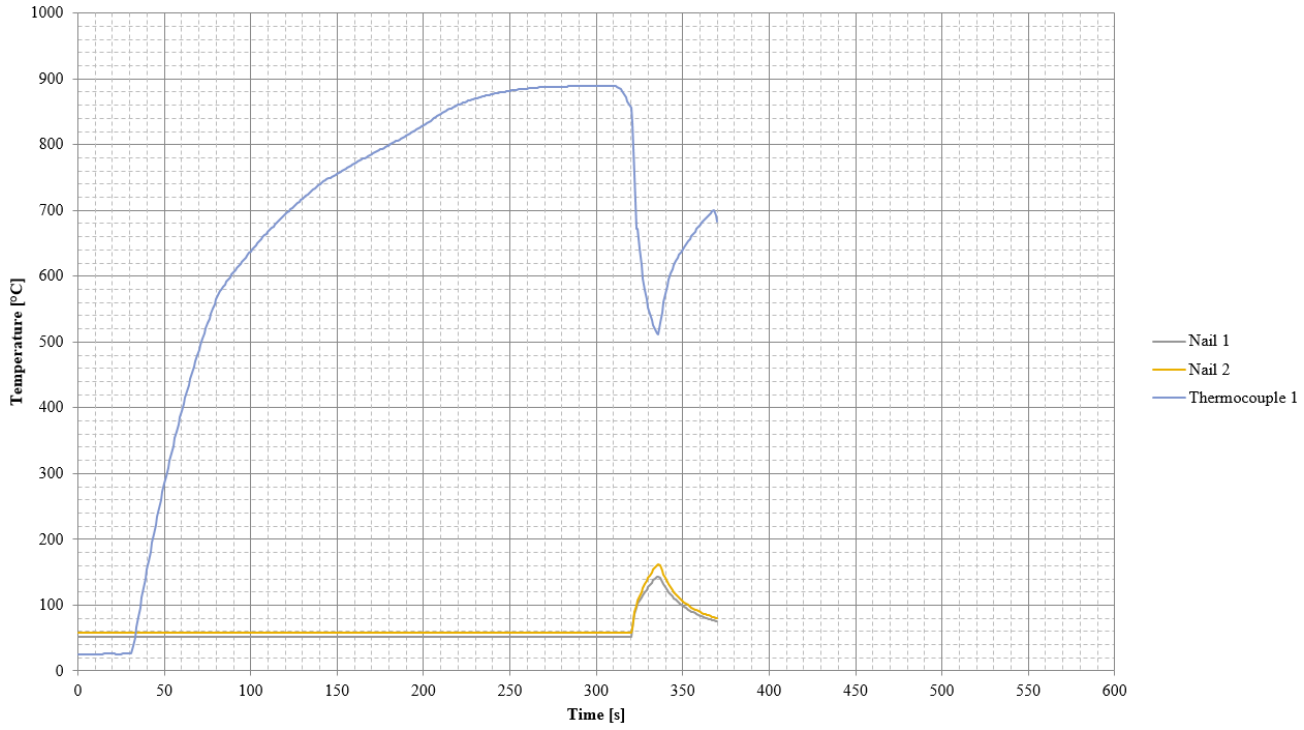

FTF1_u1:

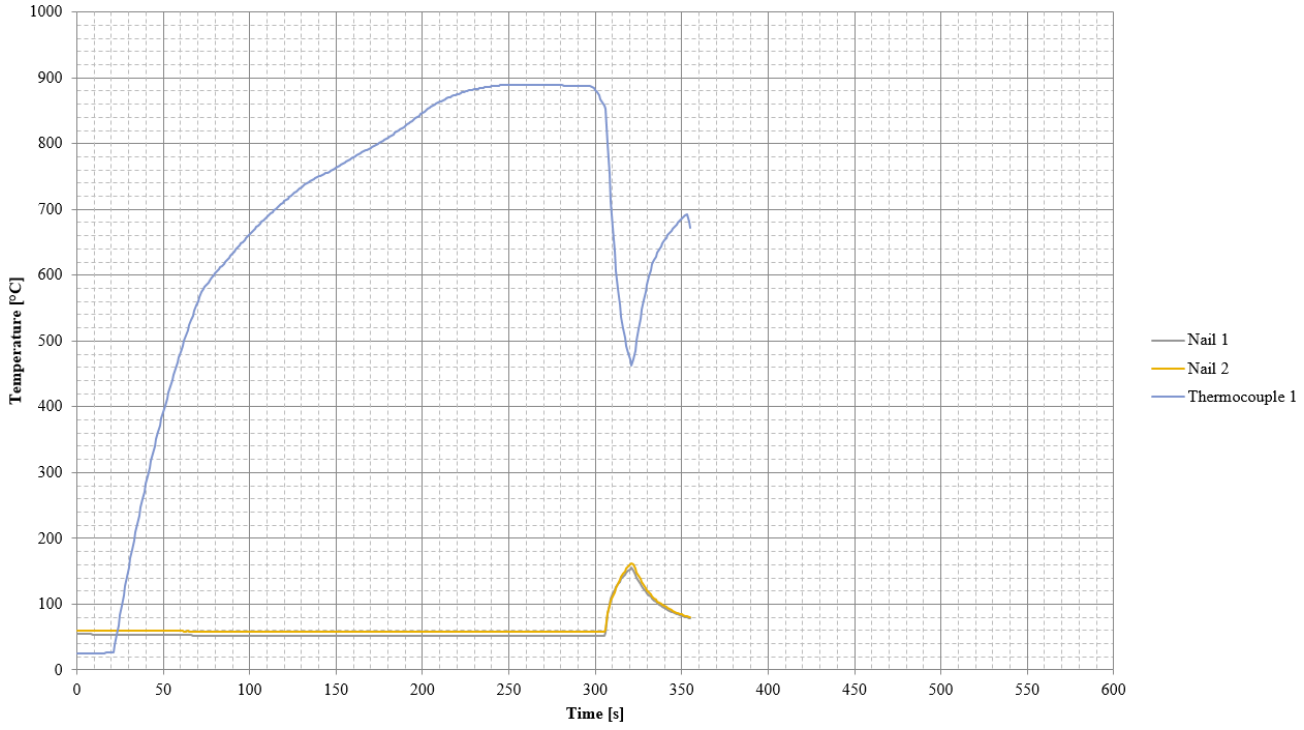

FTF1_u2:

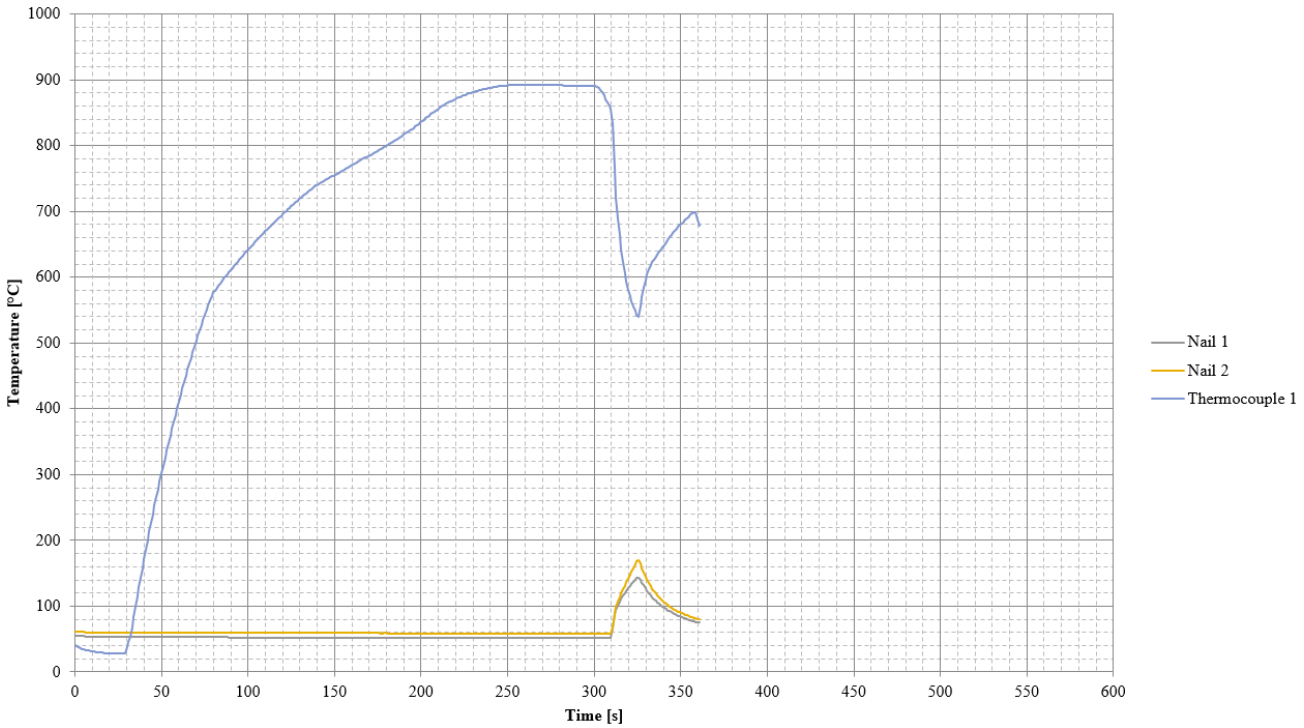

FTF2_l:

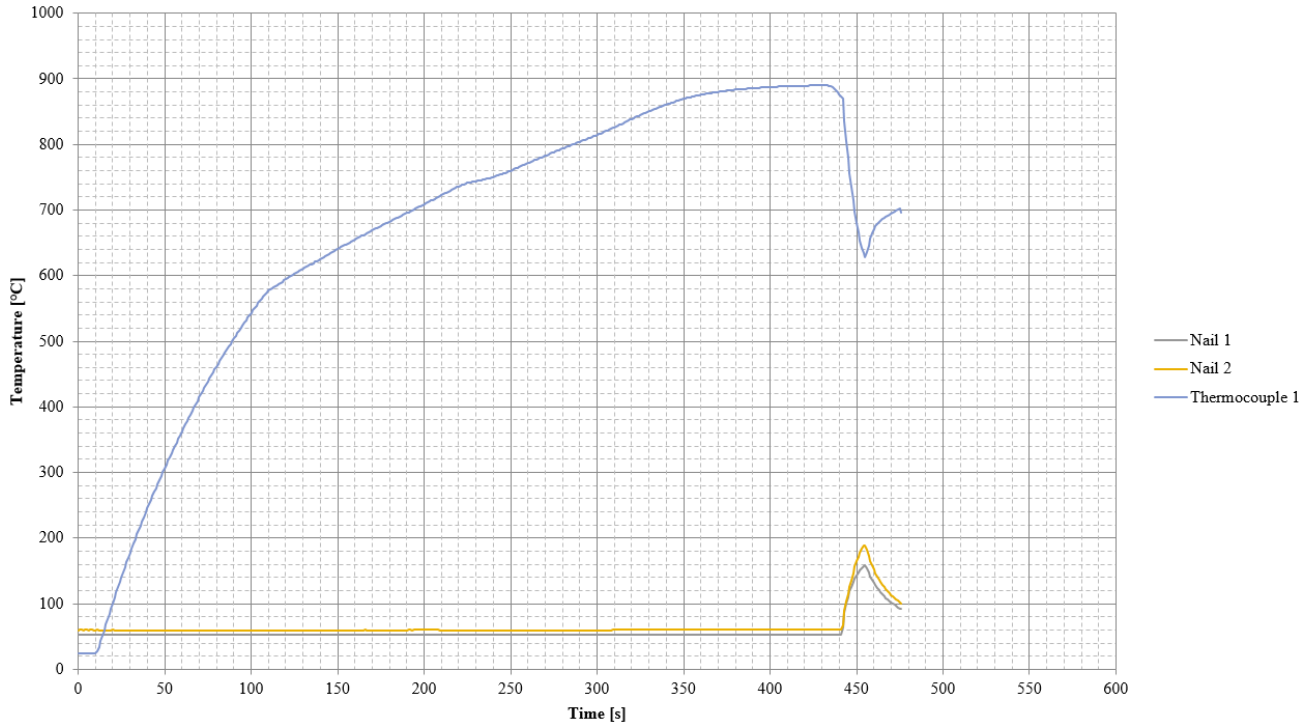

FTF2_u1:

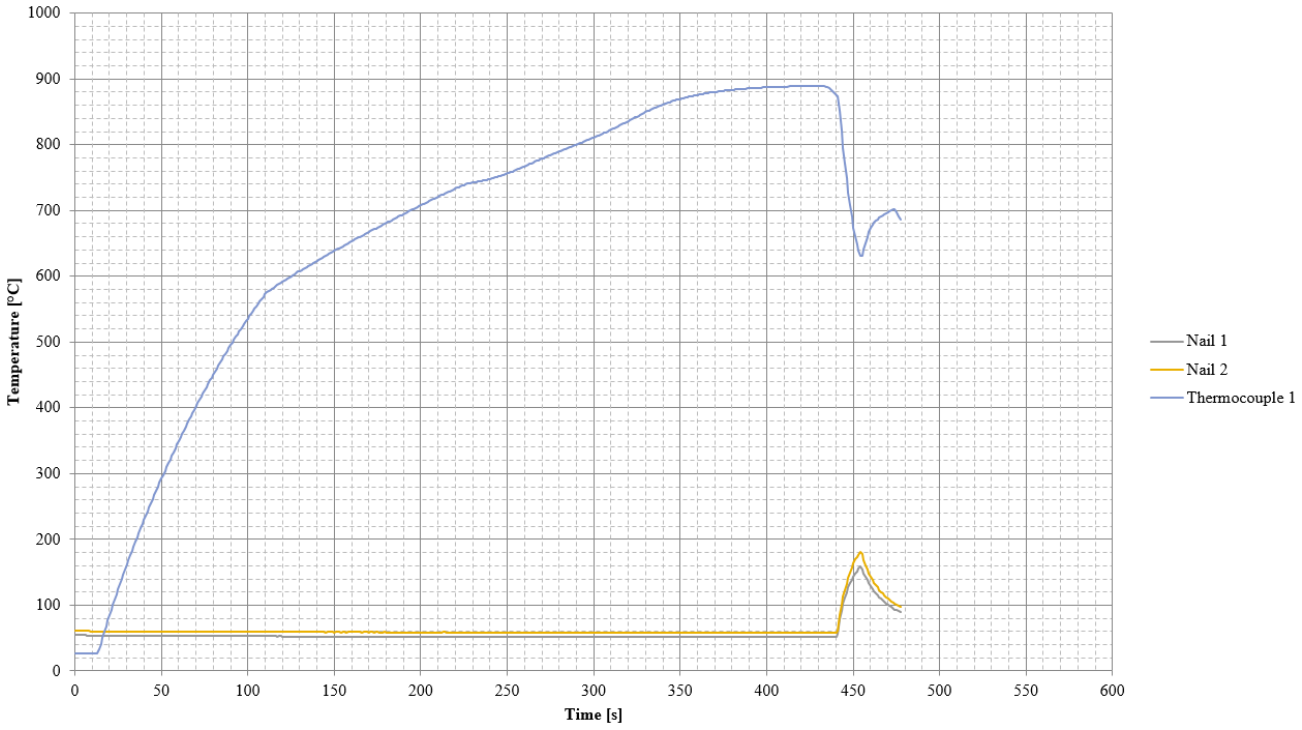

FTF2_u2:

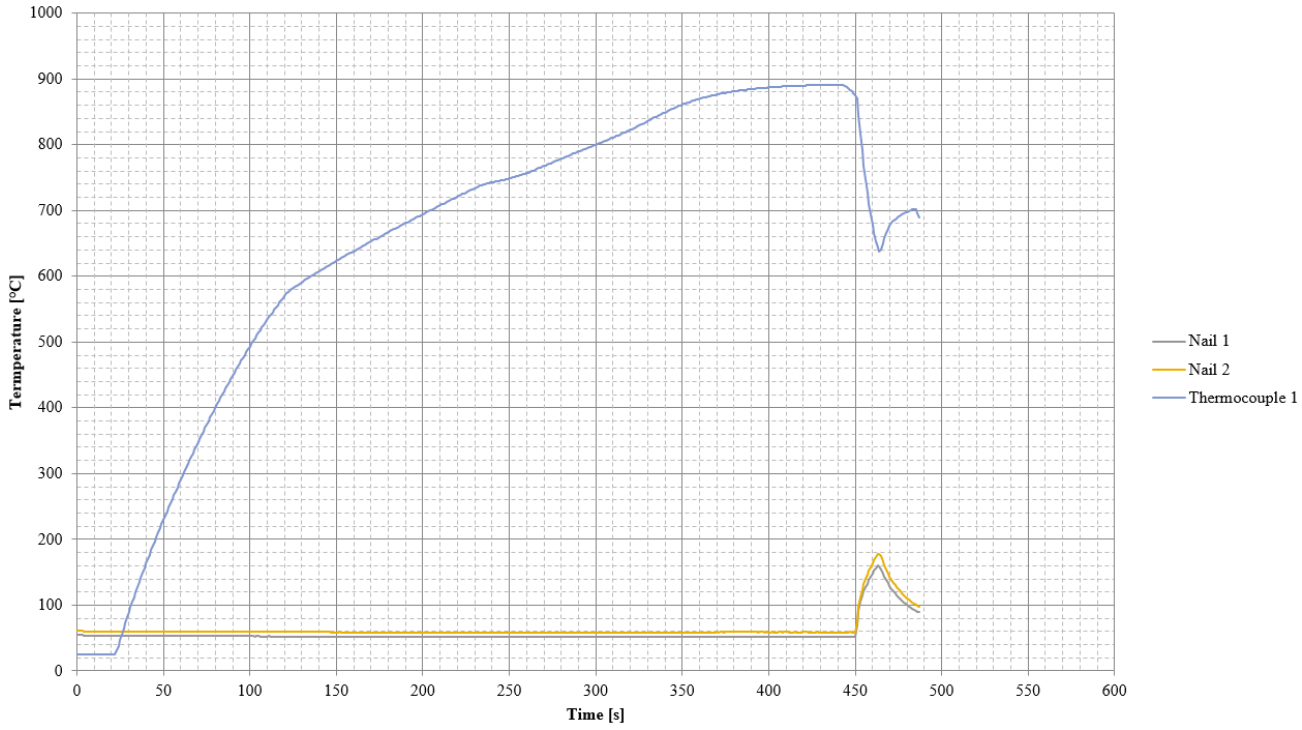

FTF3_l:

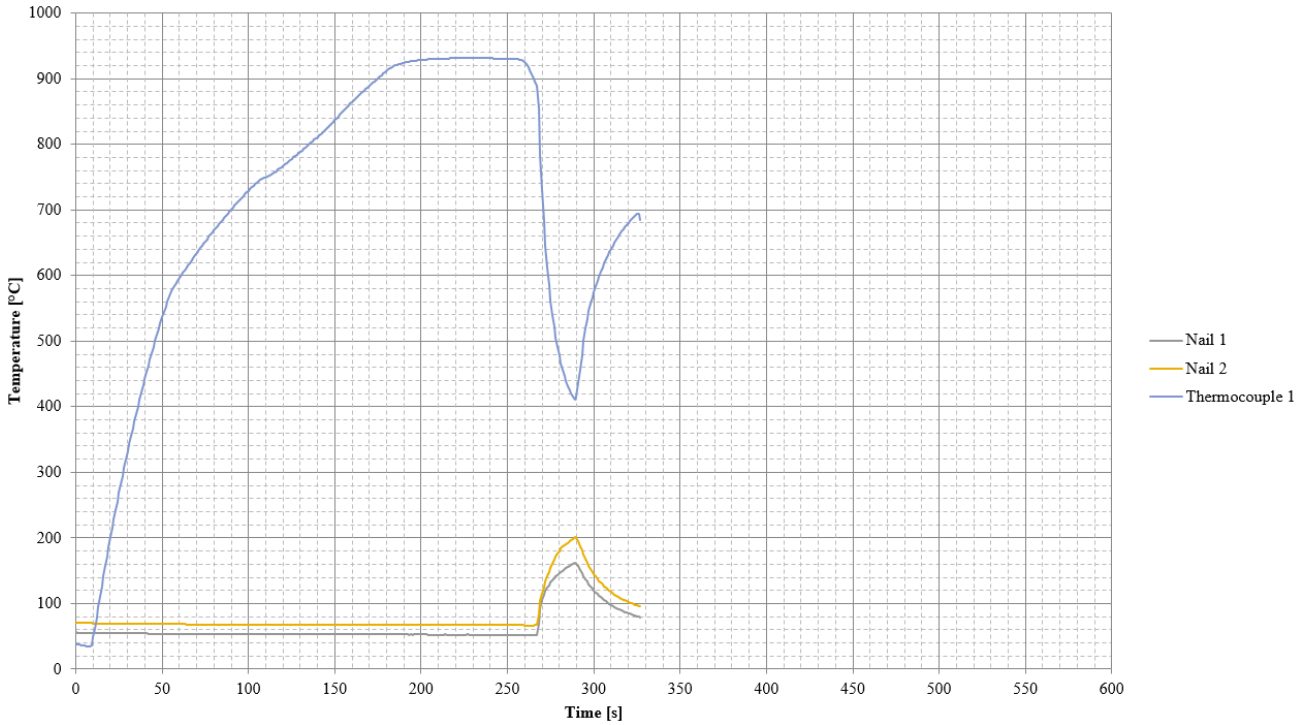

FTF3_u1:

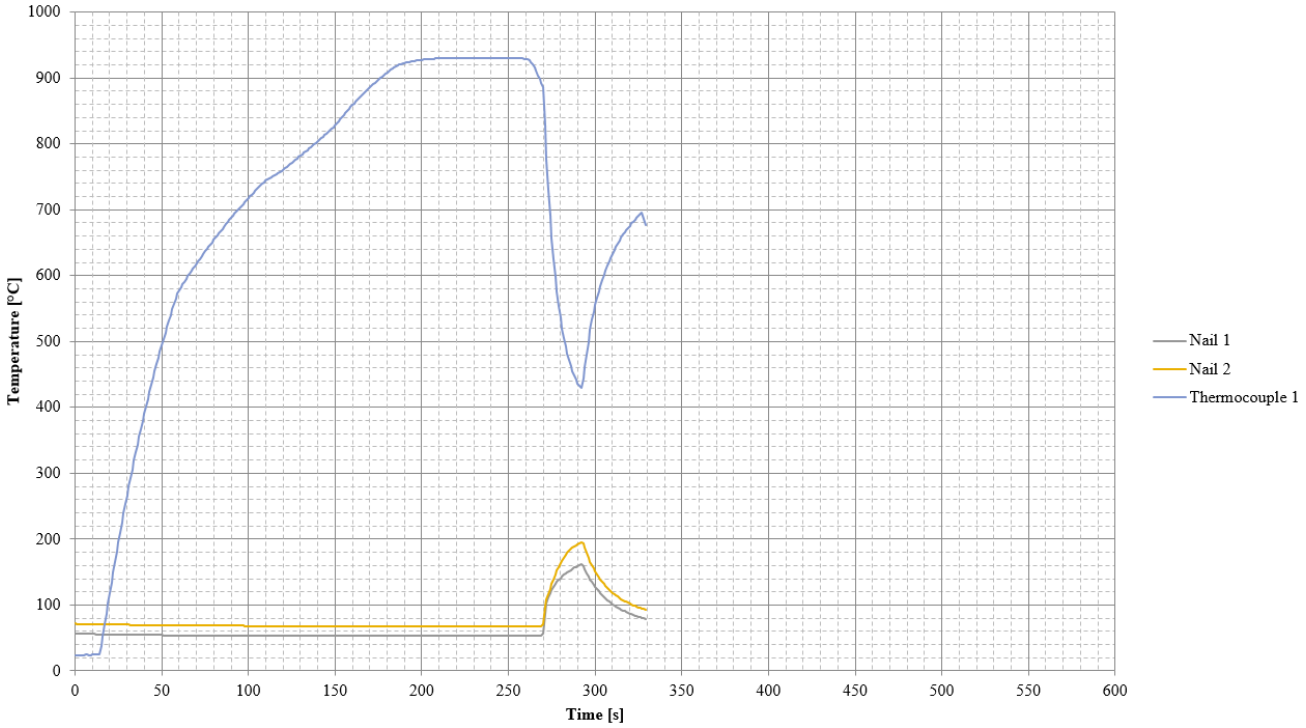

FTF3_u2:

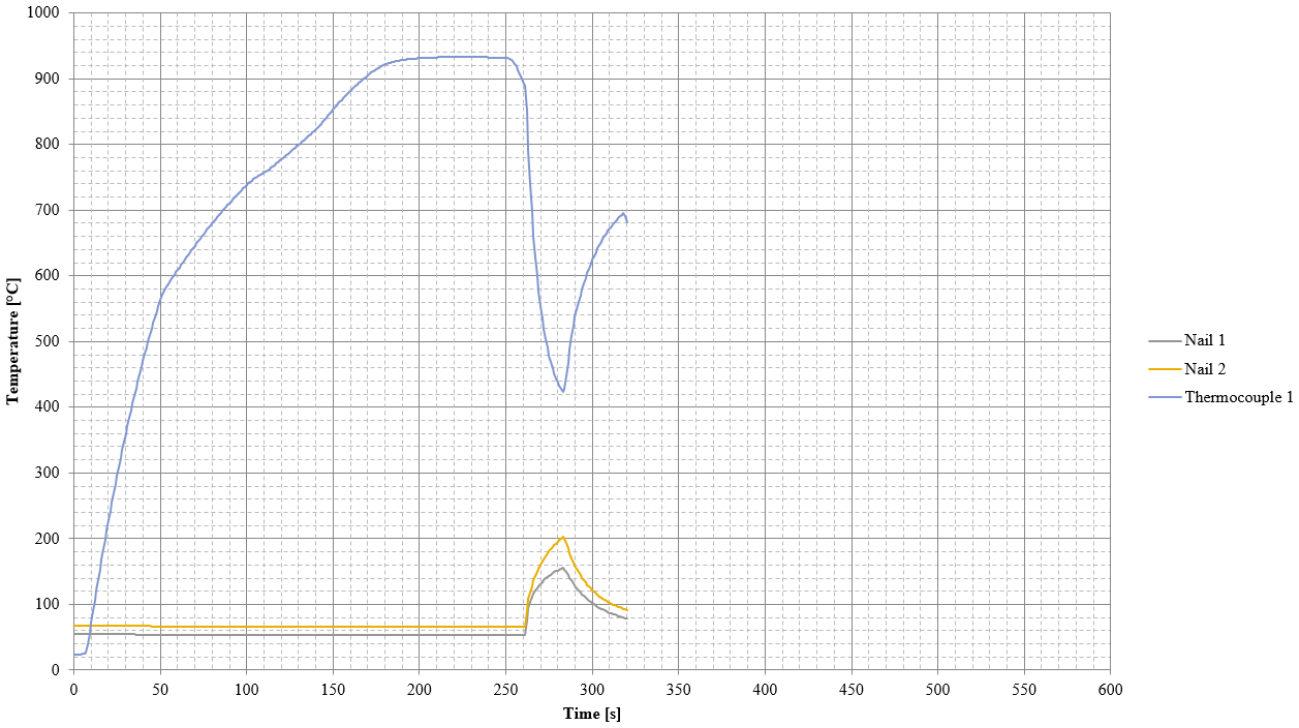

FTF4_l:

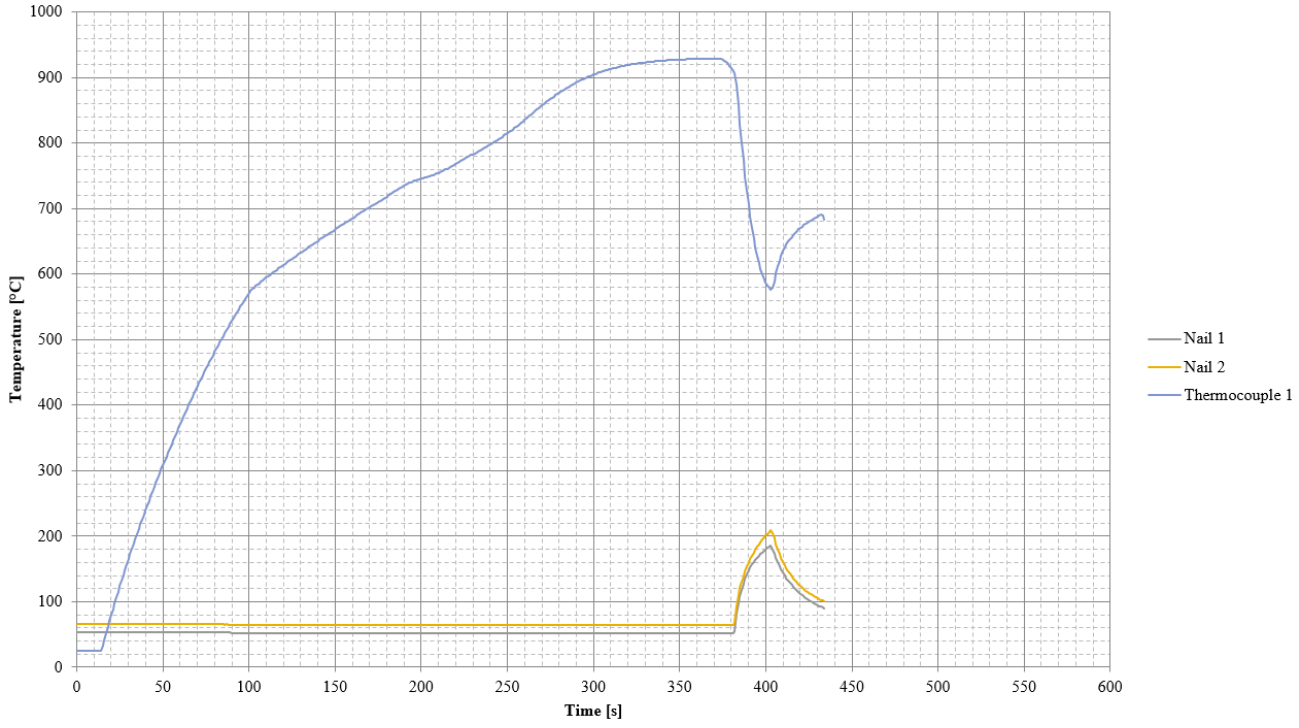

FTF4_u1:

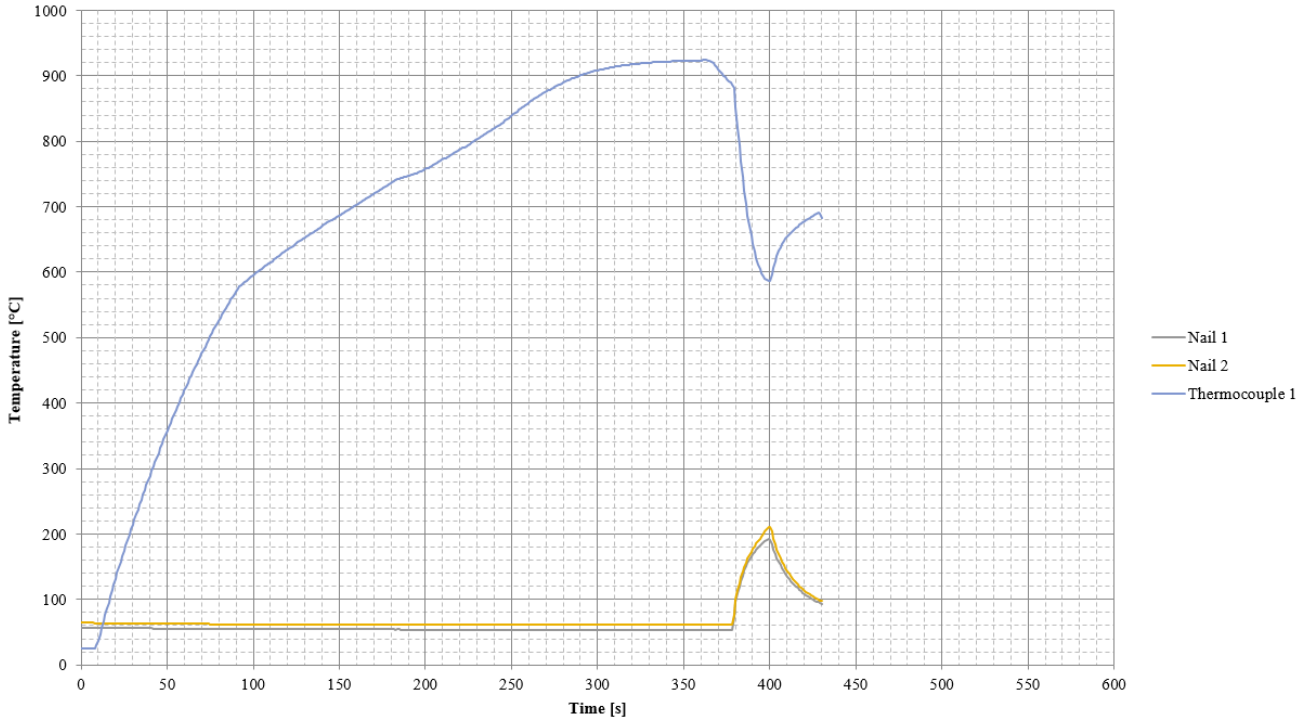

FTF4_u2:

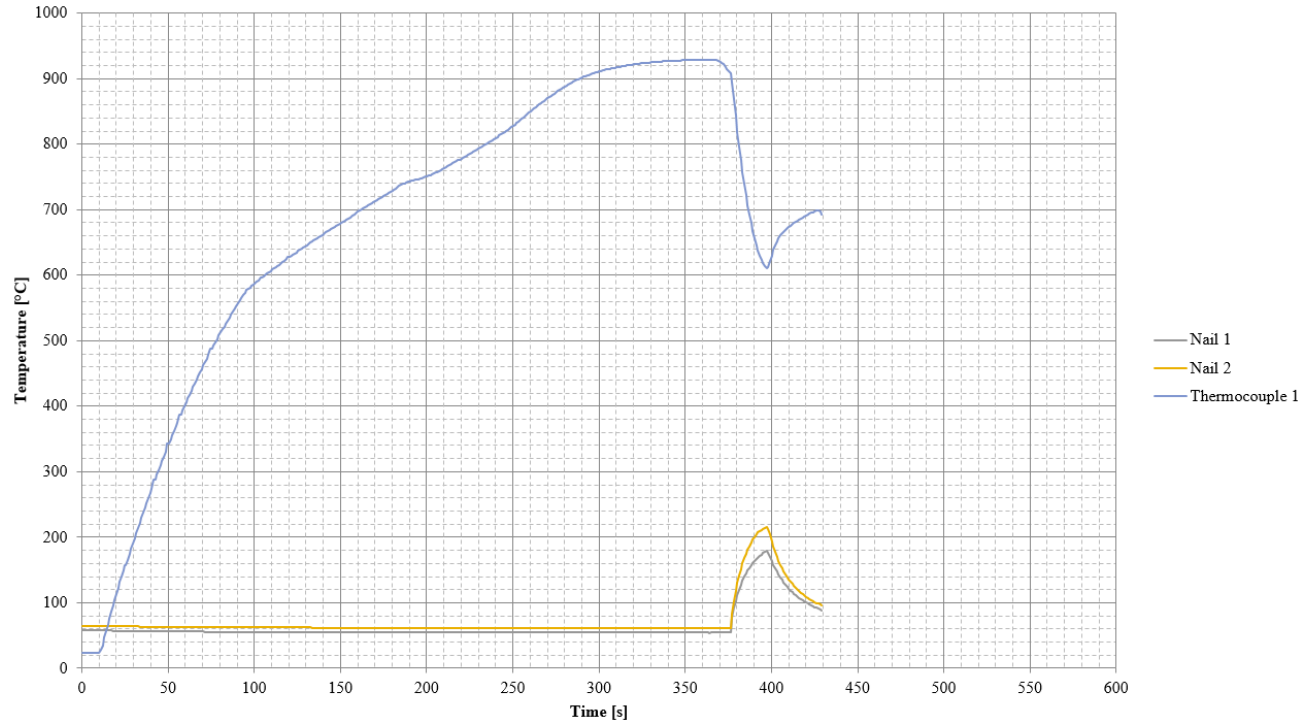

Appendix A7: Hardness tests

SimCAL 3.0

dT/dt ≈ 2,5°C/sec

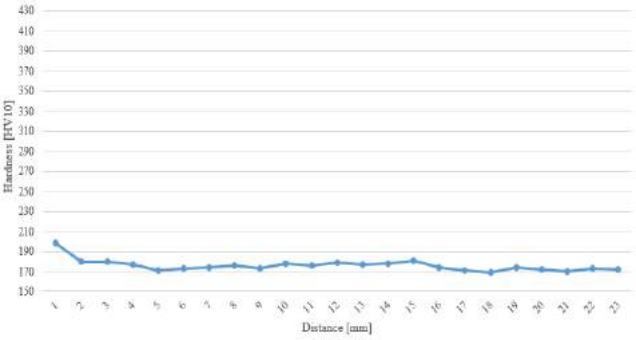

dT/dt ≈ 5°C/sec

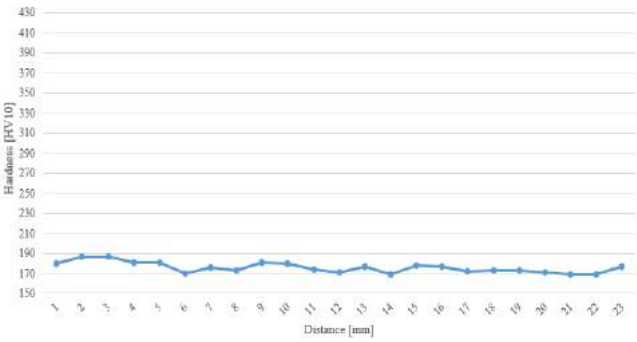

dT/dt ≈ 9°C/sec

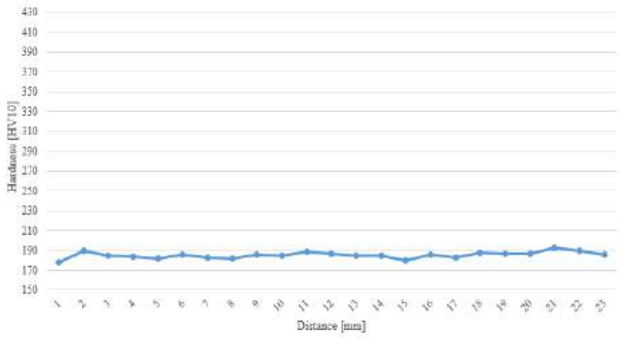

dT/dt ≈ 12,5°C/sec

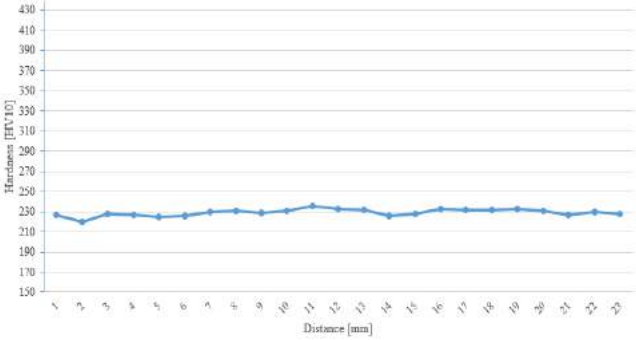

dT/dt ≈ 15°C/sec

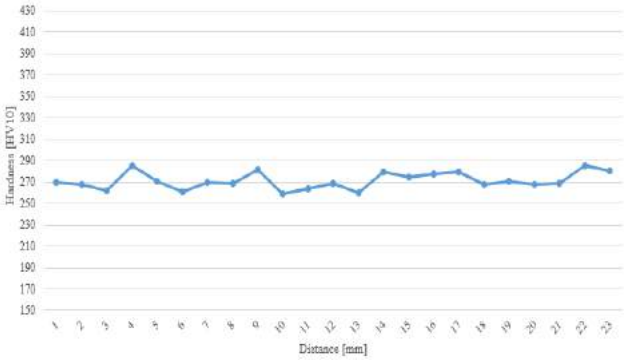

dT/dt ≈ 20°C/sec

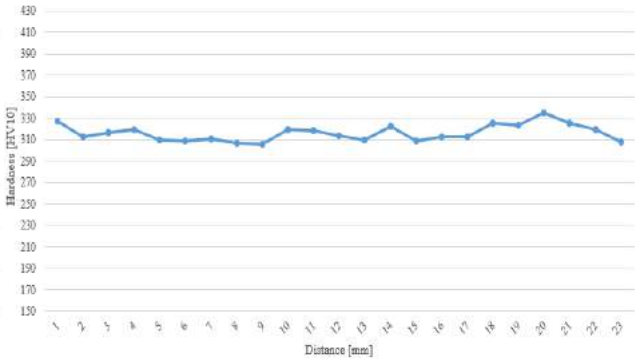

dT/dt ≈ 25°C/sec

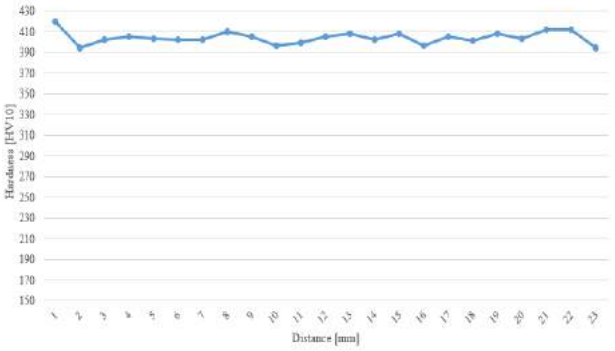

Trial furnace

FTF1:

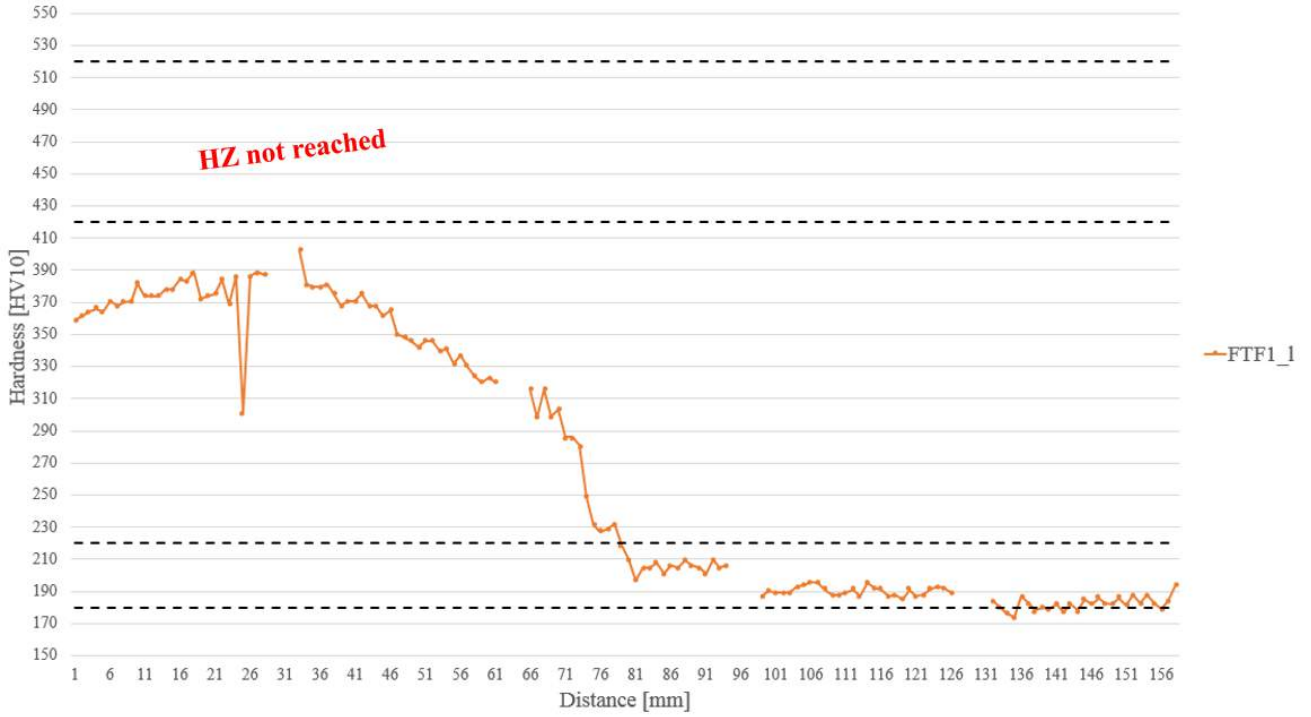


HZ not reached
Hardness [HV10]
Distance [mm]
FTF1_u2

FTF2:

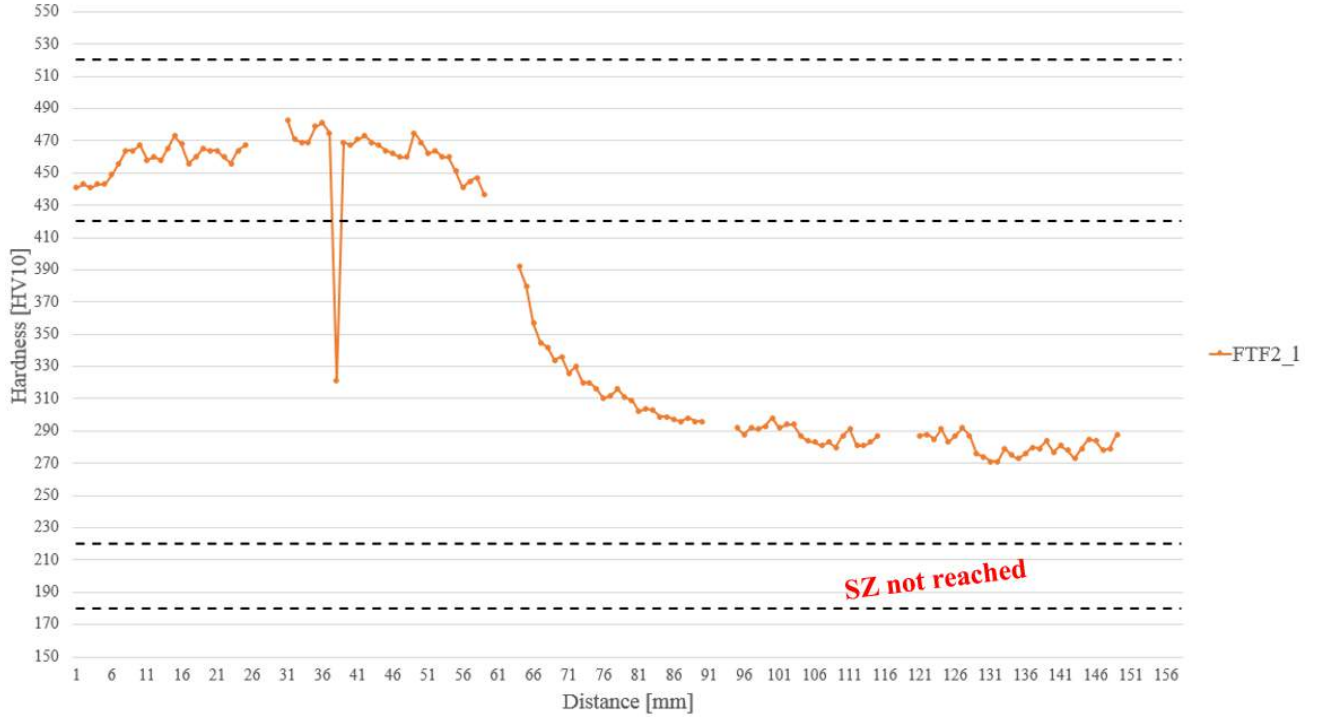
Hardness [HV10]
Distance [mm]
FTF2_1
SZ not reached

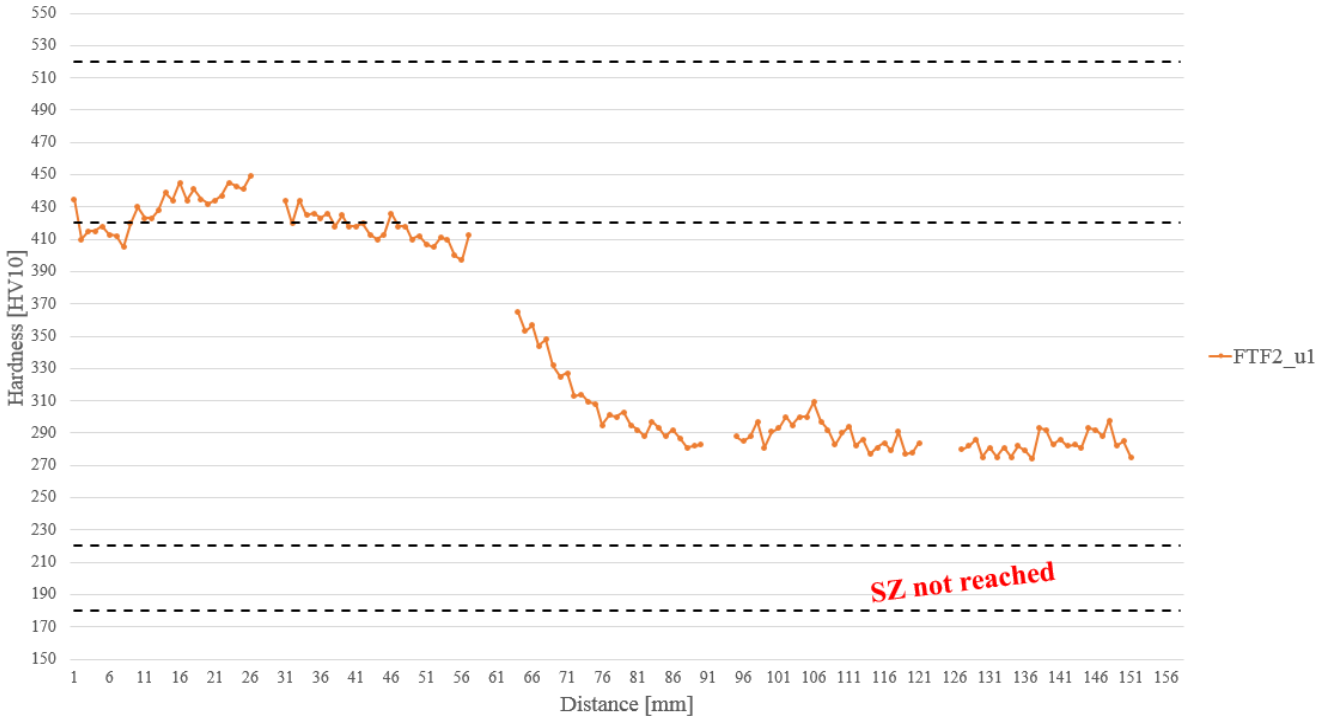
Hardness [HV10]
Distance [mm]
FTF2_u1
SZ not reached

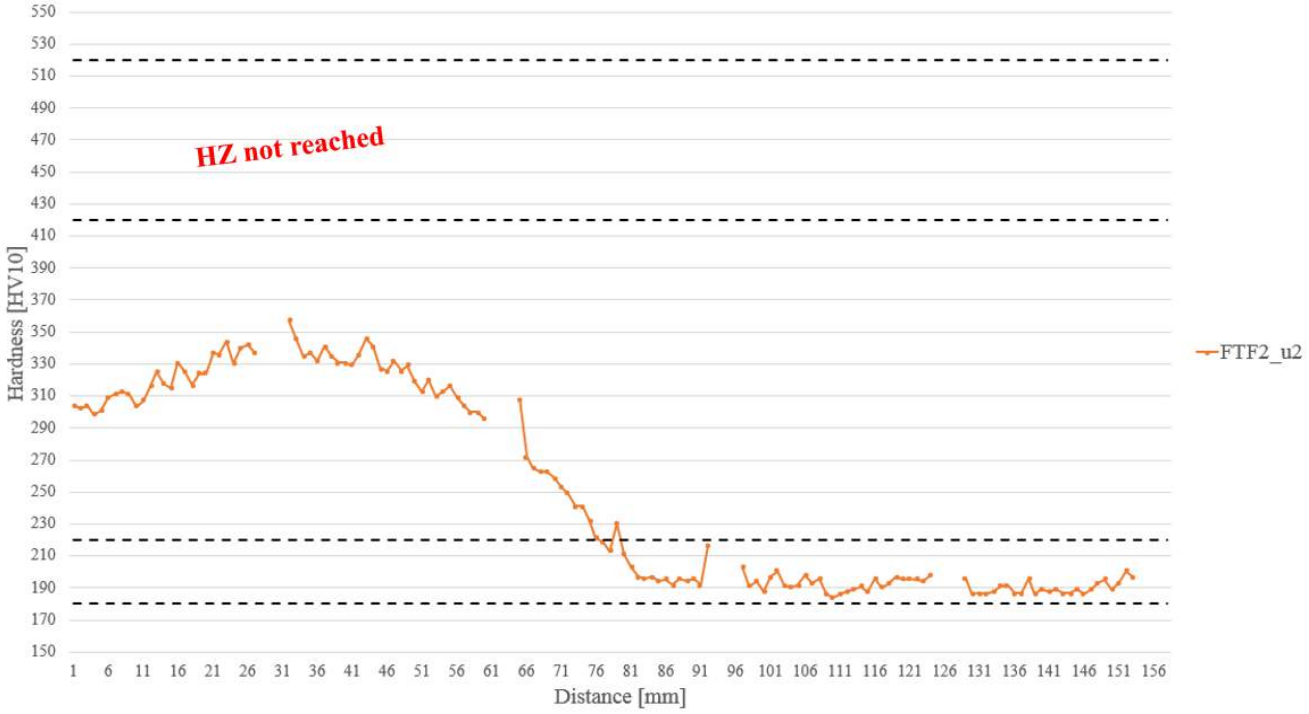
HZ not reached
Hardness [HV10]
Distance [mm]
FTF2_u2

FTF3:

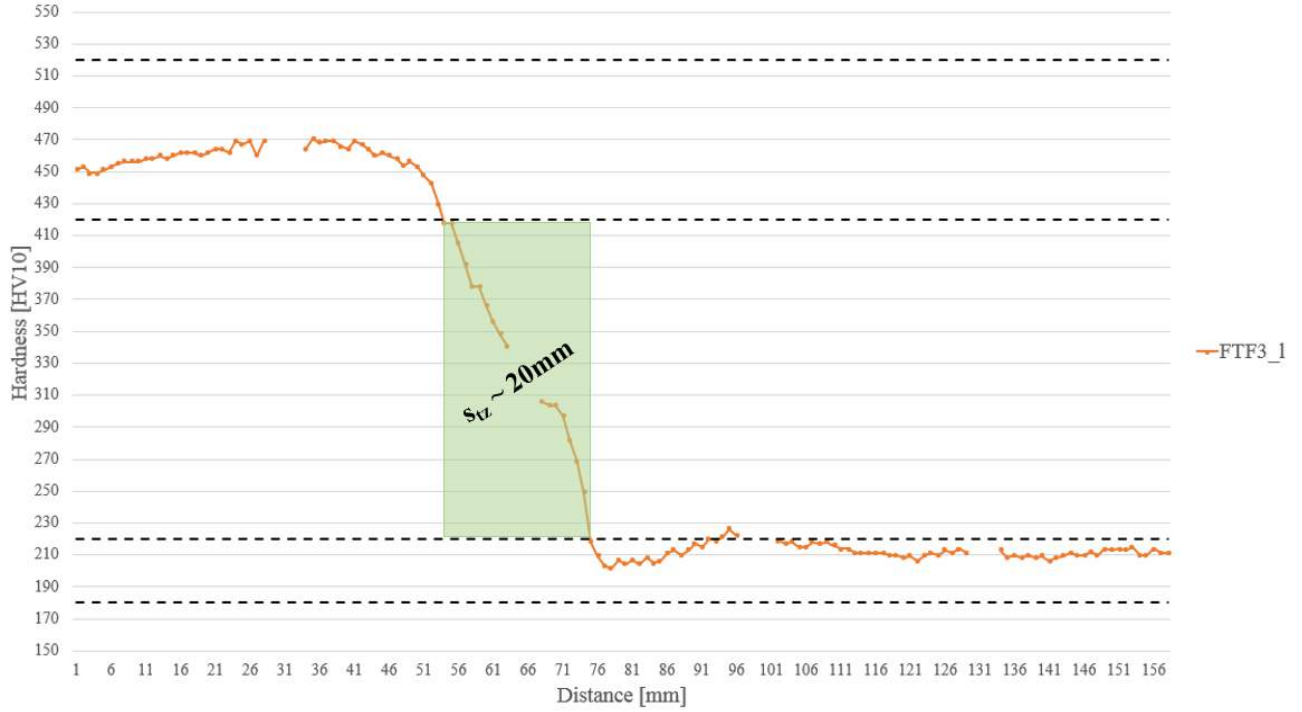
Hardness [HV10]
Distance [mm]
Sz ~ 20mm
FTF3_1

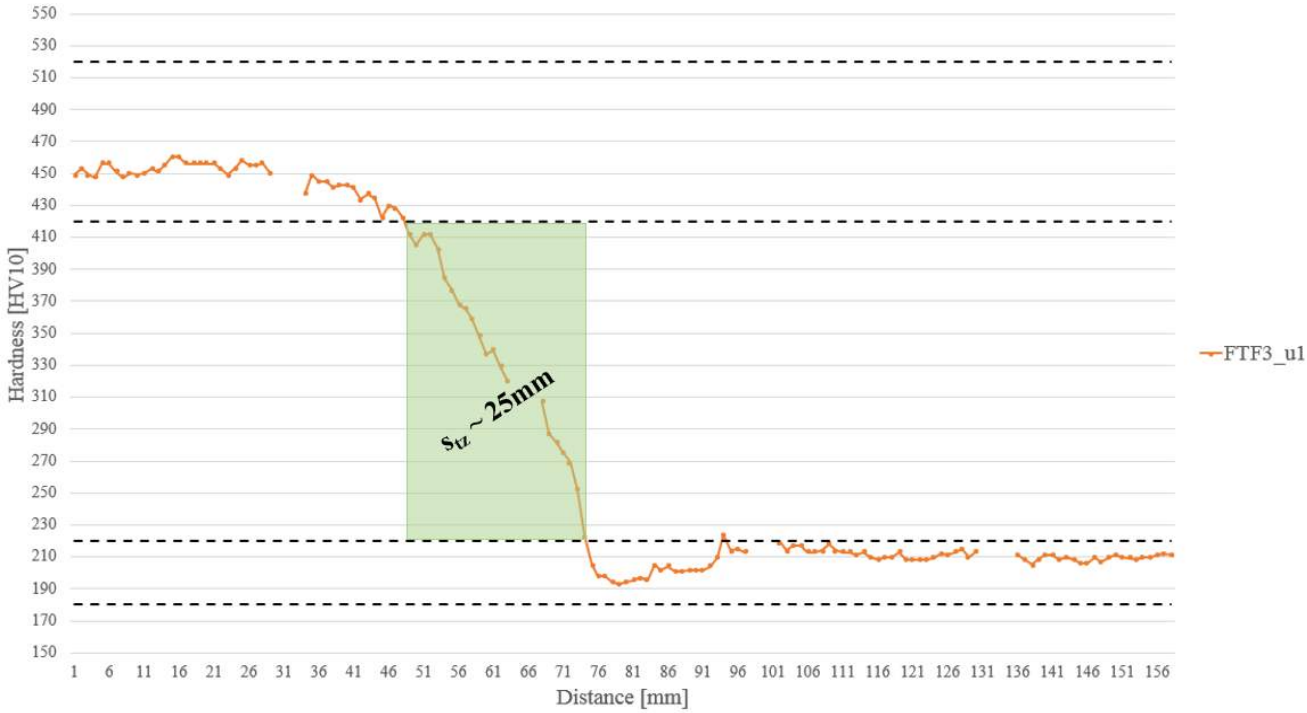
Hardness [HV10]
Distance [mm]
Sz ~ 25mm
FTF3_u1

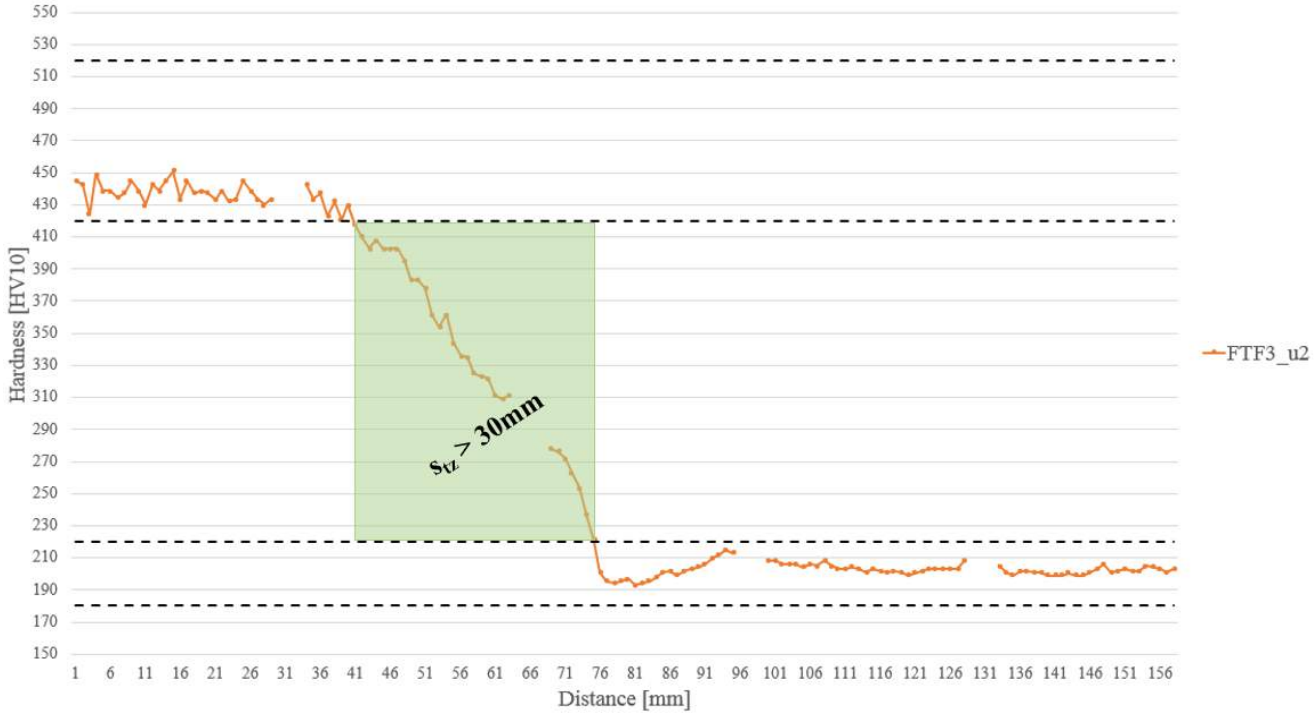
Hardness [HV10]
Distance [mm]
FTF3_u2
s_{HZ} > 30mm

FTF4:

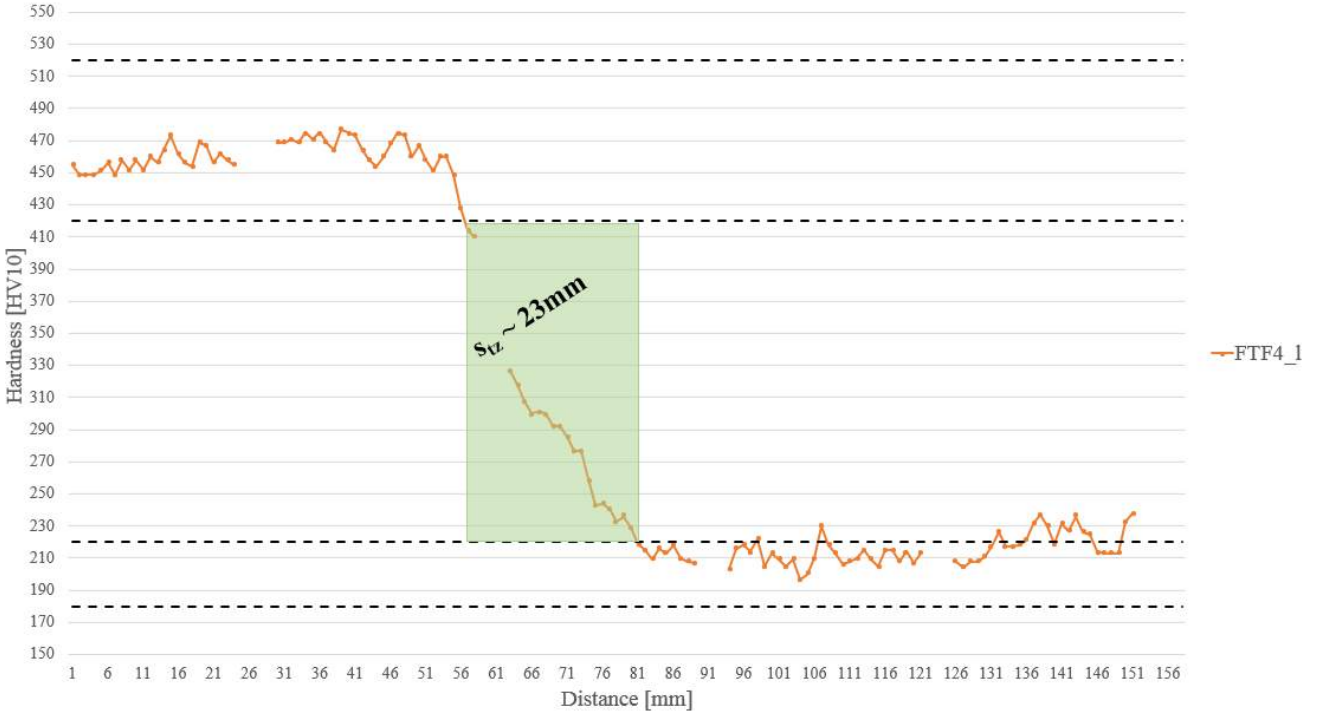
Hardness [HV10]
Distance [mm]
s_{tz} ~ 23mm
FTF4_l

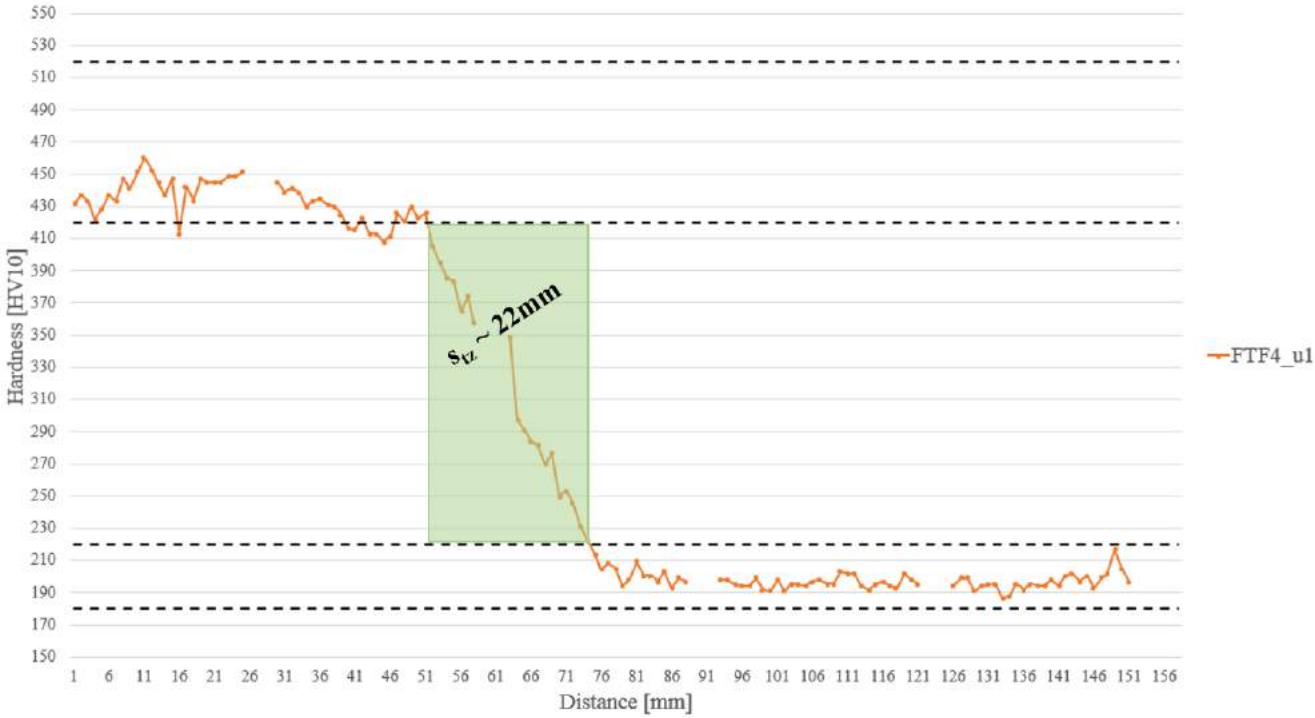
Hardness [HV10]
Distance [mm]
s_{tz} ~ 22mm
FTF4_u1


HZ not reached
Hardness [HV10]
Distance [mm]
FTF4_u2

Appendix A8: Tensile tests

Test protocols

As-delivered:

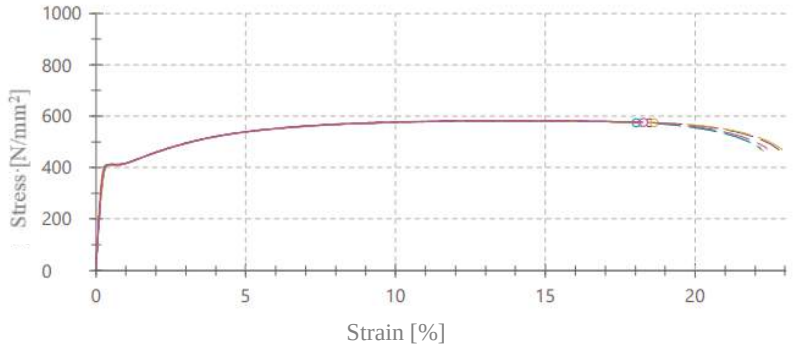

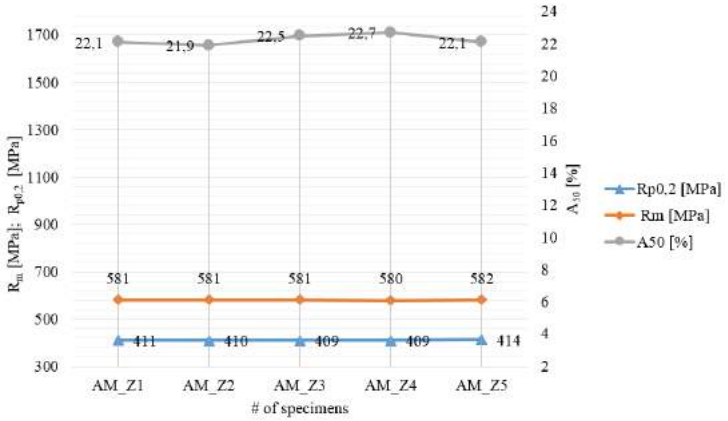

Hardened:

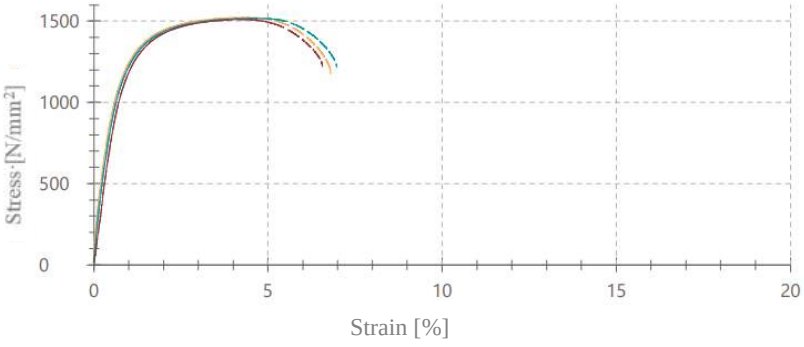

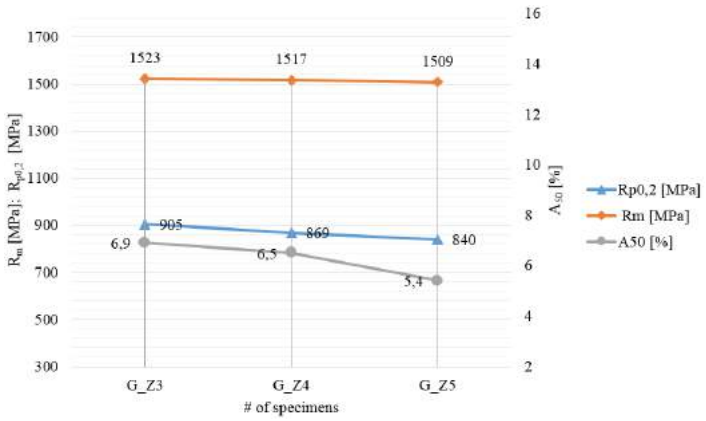

FTF1_l:

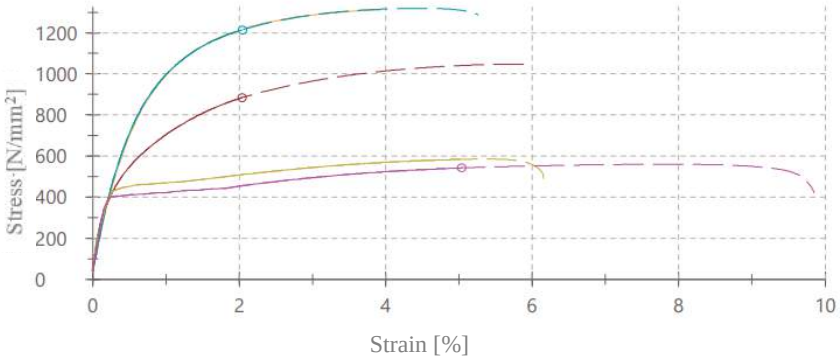

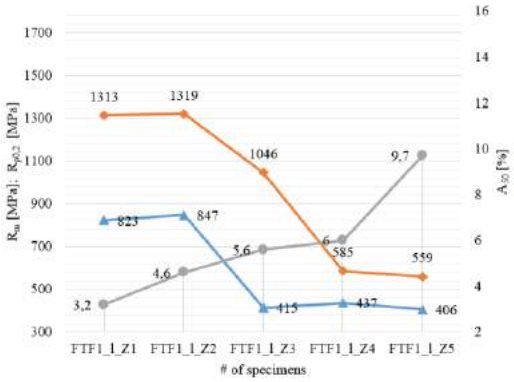

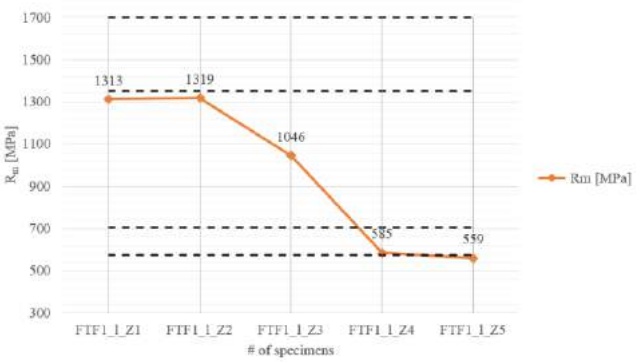

FTF1_u1:

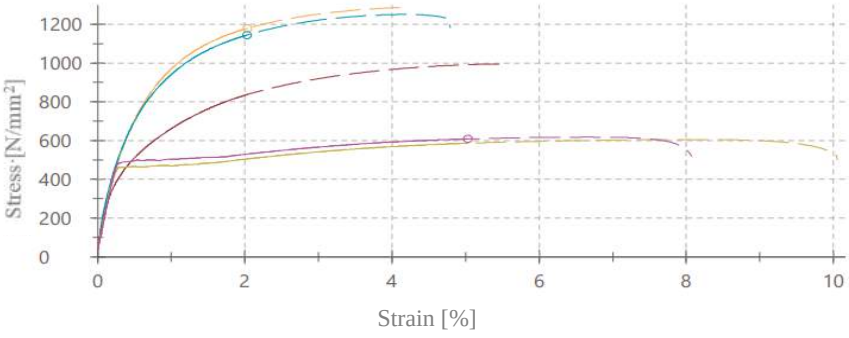

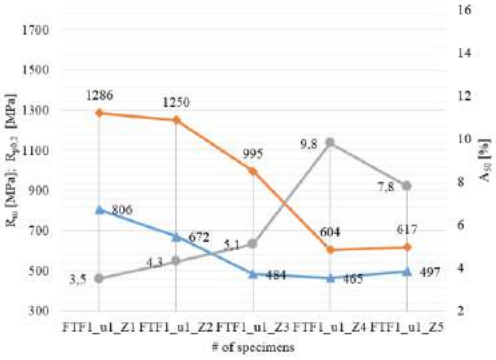

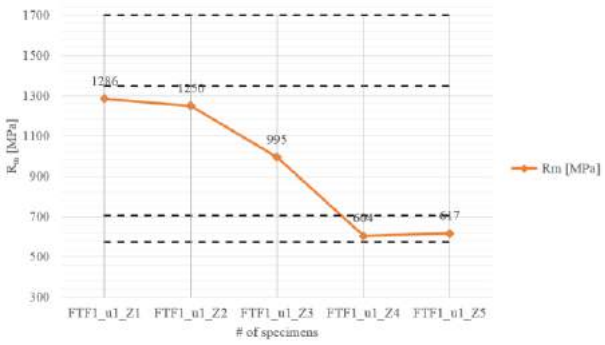

FTF1_u2:

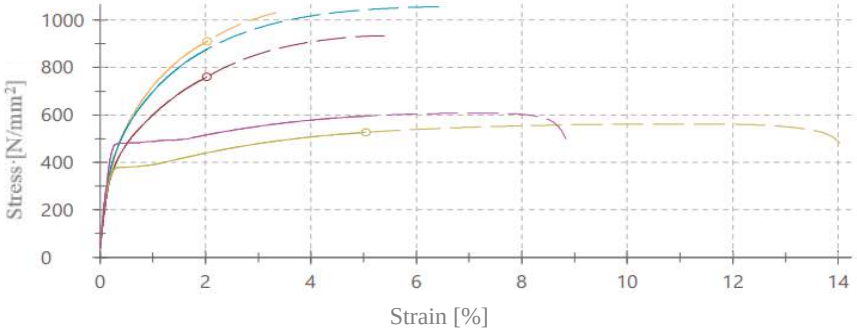

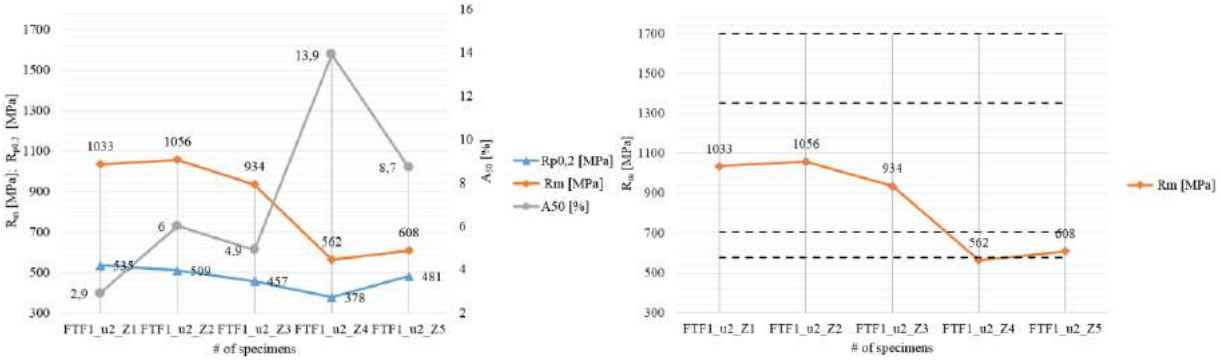

FTF2_l:

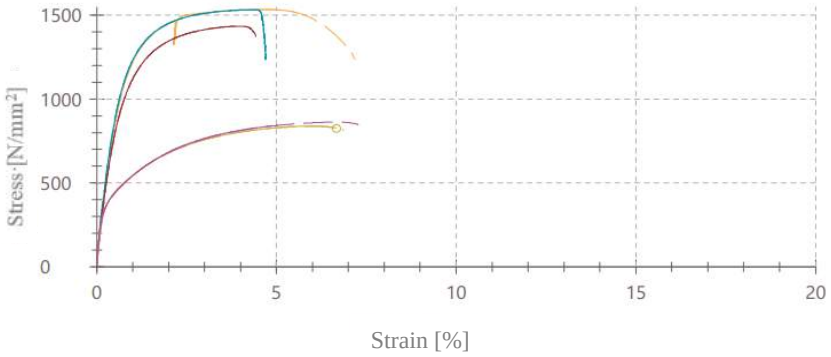

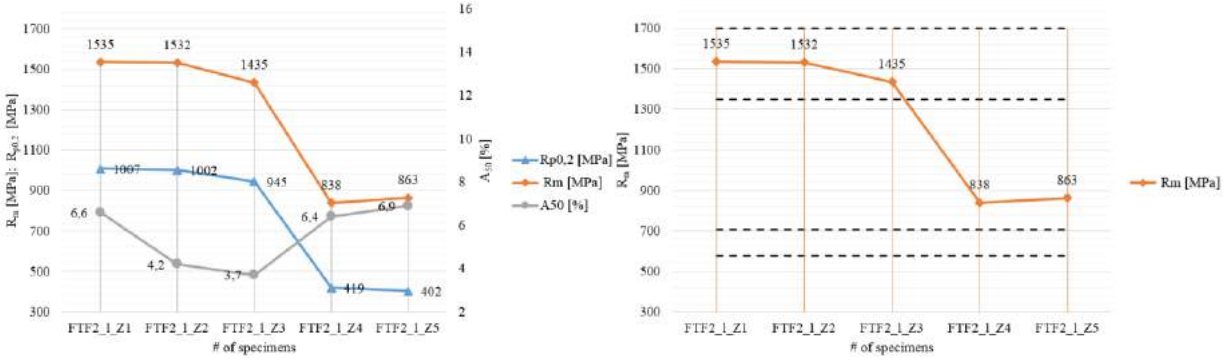

FTF2_u1:

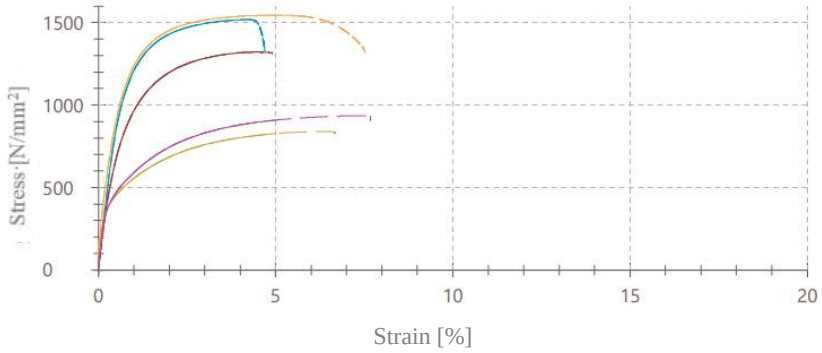

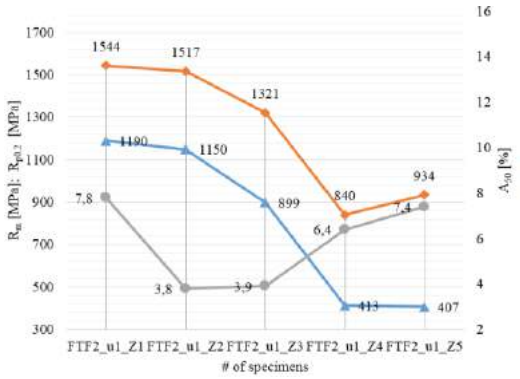

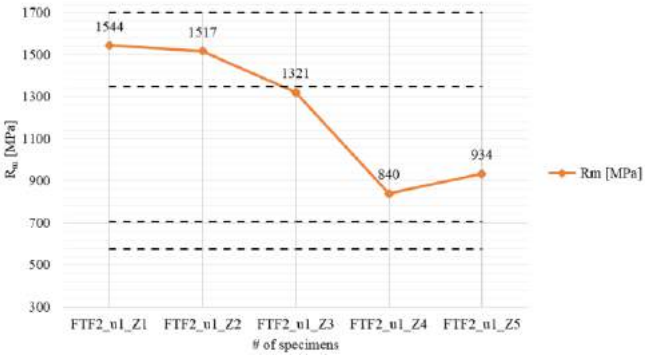

FTF2_u2:

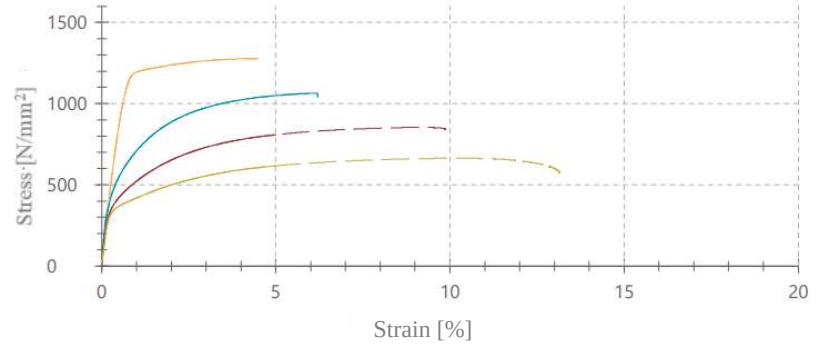

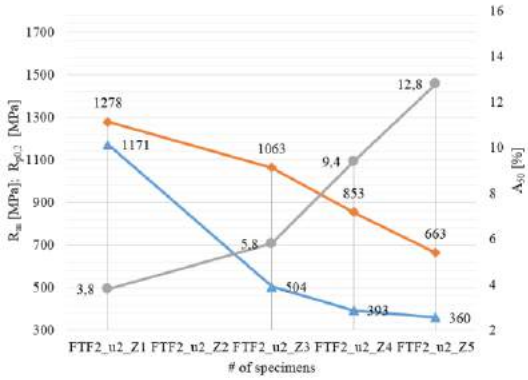

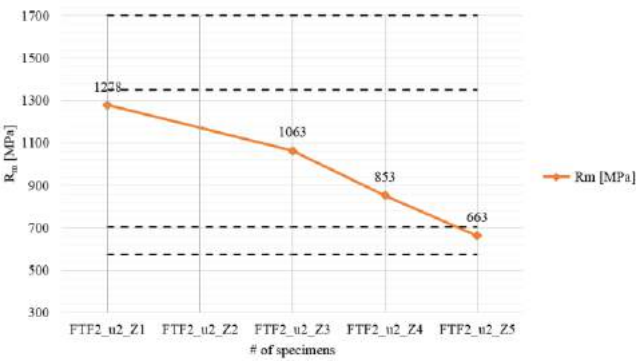

FTF3_l:

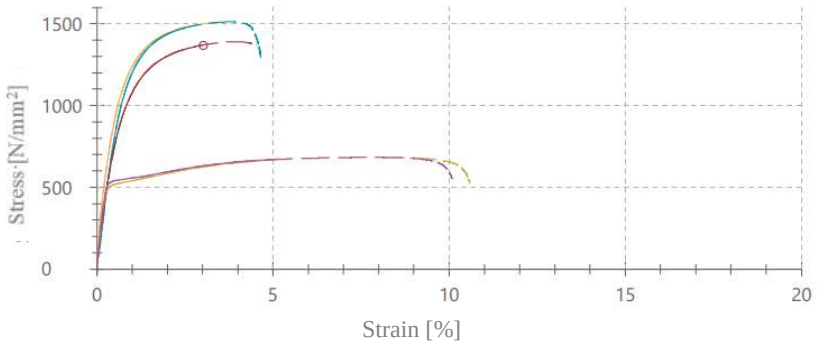

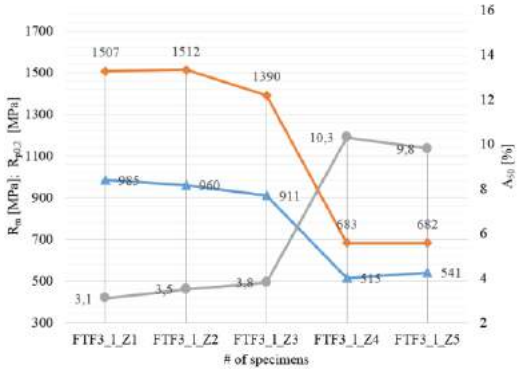

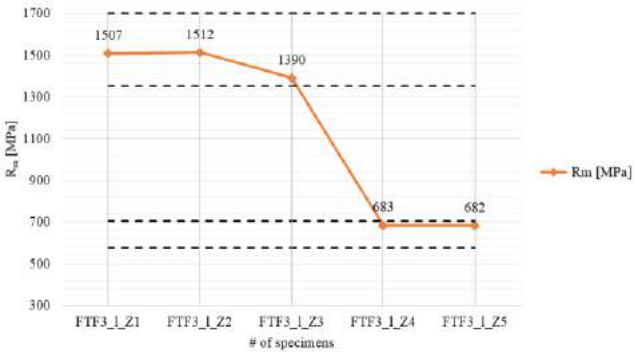

FTF3_u1:

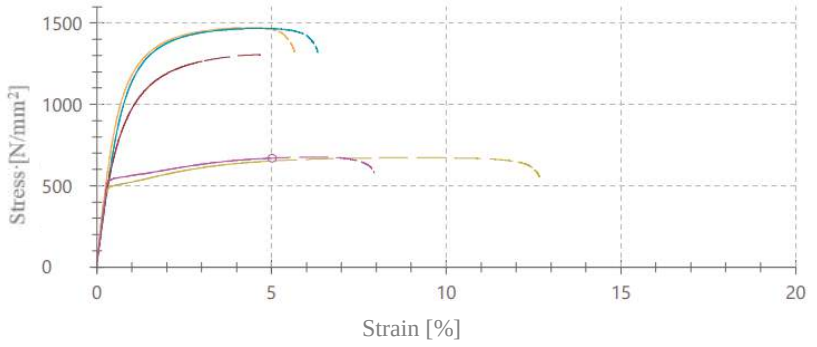

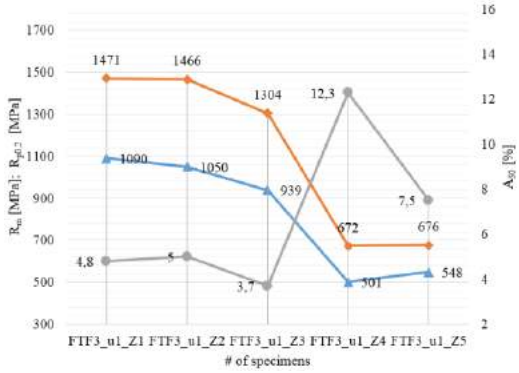

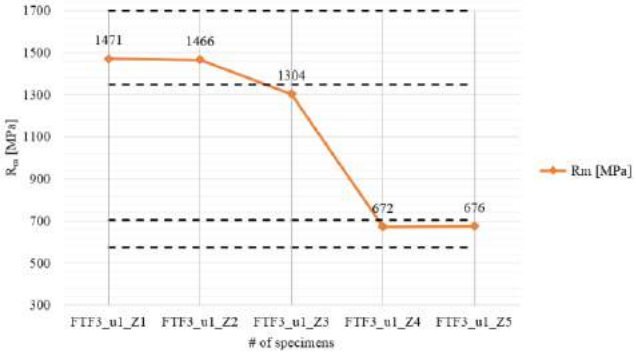

FTF3_u2:

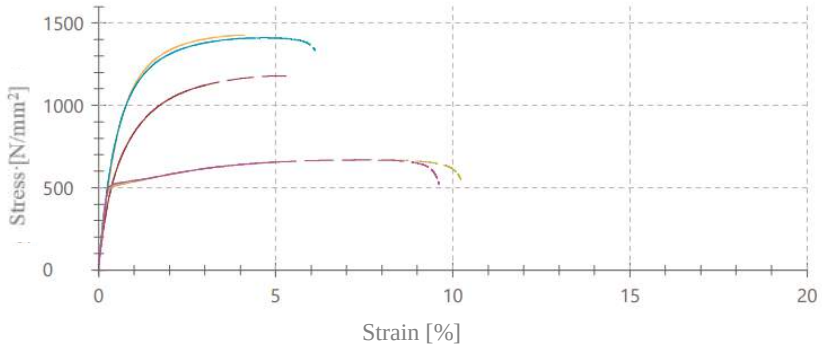

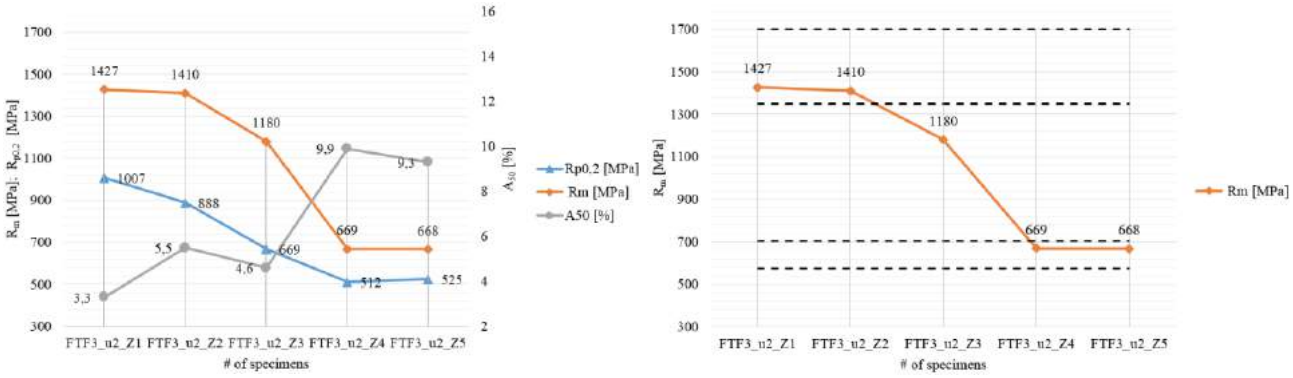

FTF4_l:

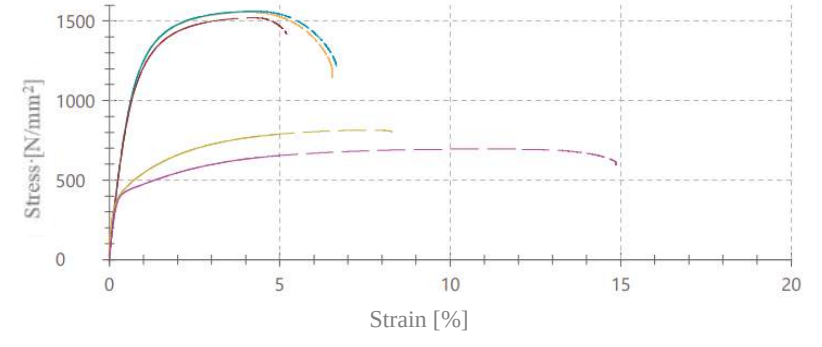

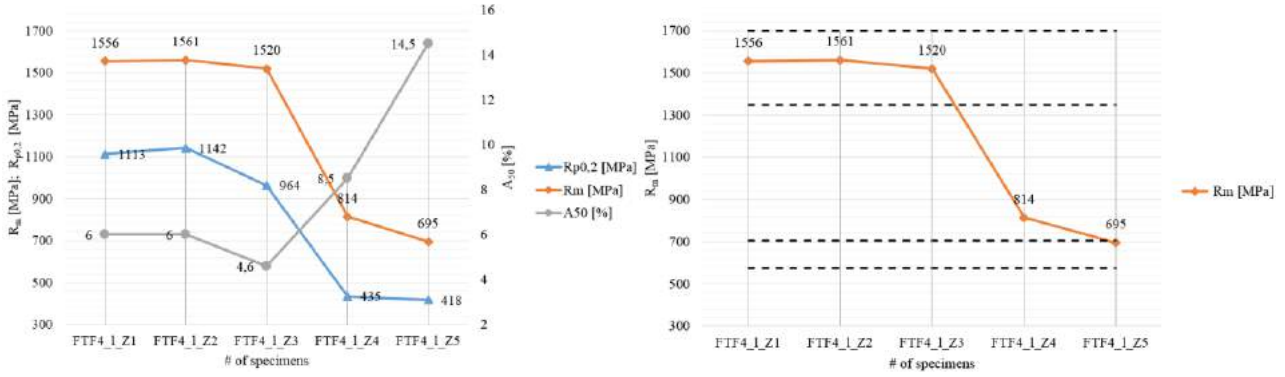

FTF4_u1:

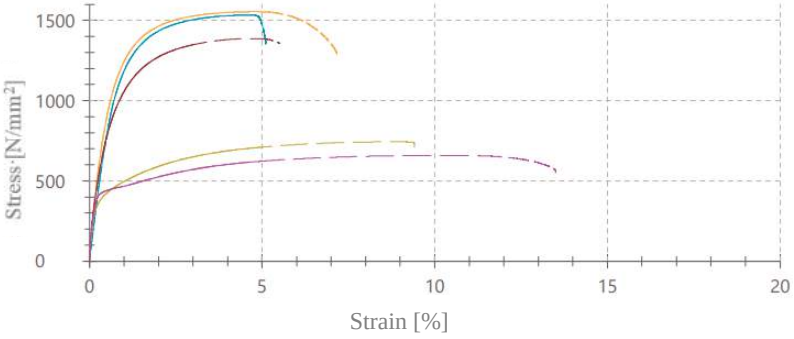

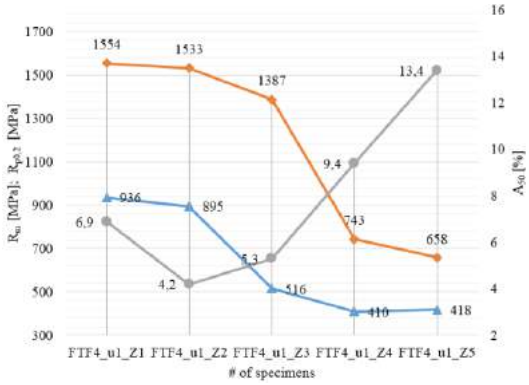

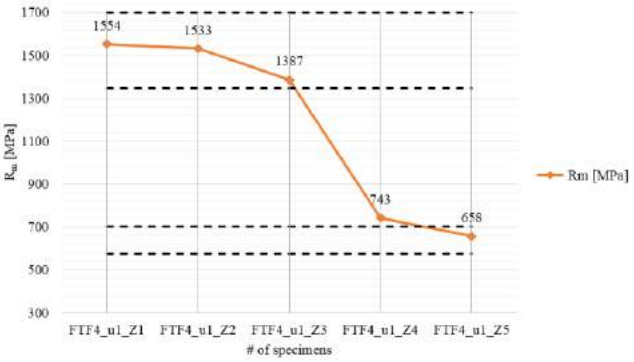

FTF4_u2:

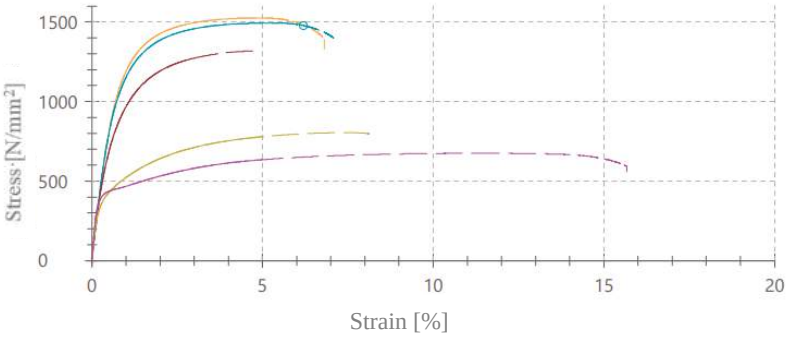

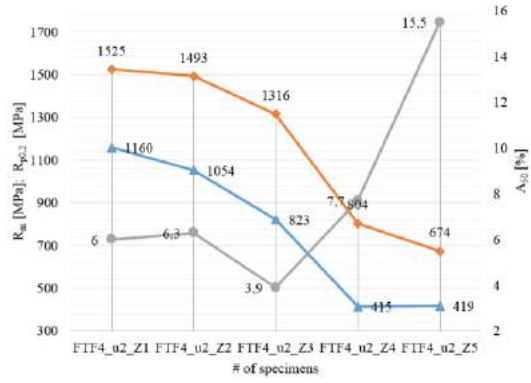

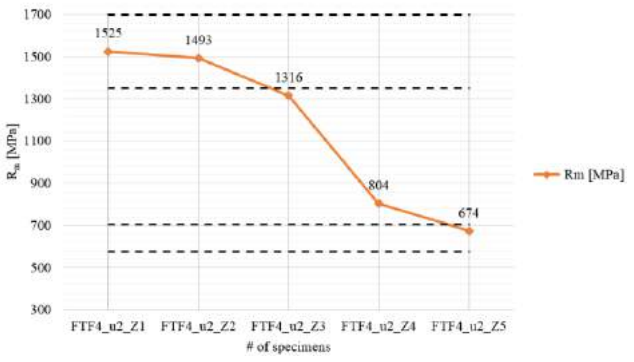

Appendix A9: Microstructural analysis

Hard zone

FTF1_l:

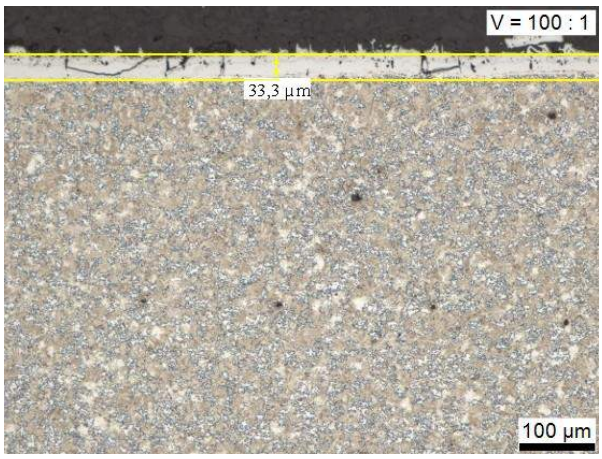

Fig.: 1 0007425
FTF1_l_S1
Edge x100

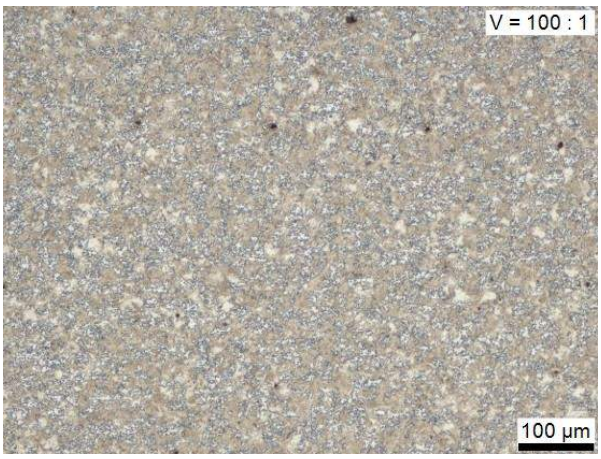

Fig.: 2 0007428
FTF1_l_S1
Middle x100

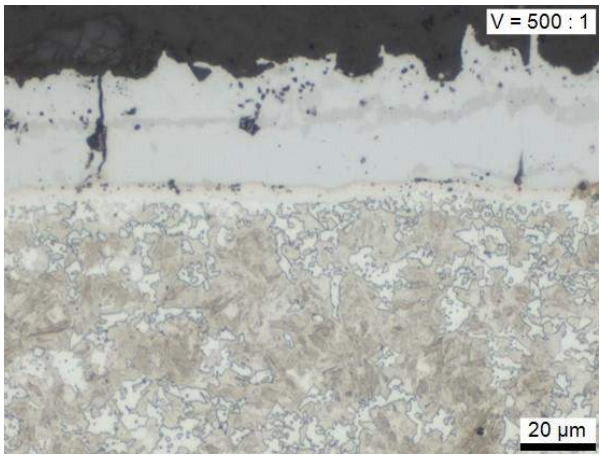

Fig.: 3 0007426
FTF1_l_S1
Edge x500

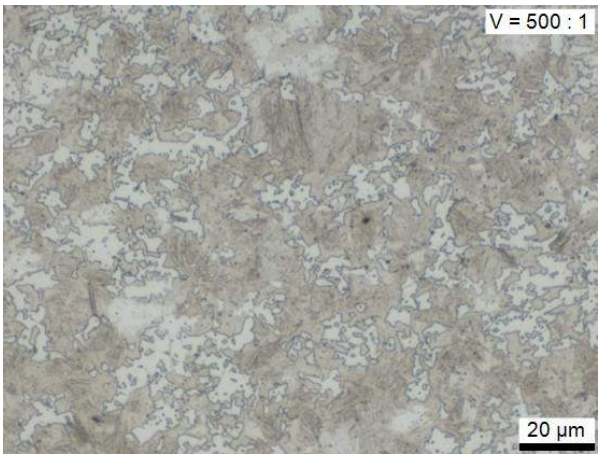

Fig.: 4 0007429
FTF1_l_S1
Middle x500

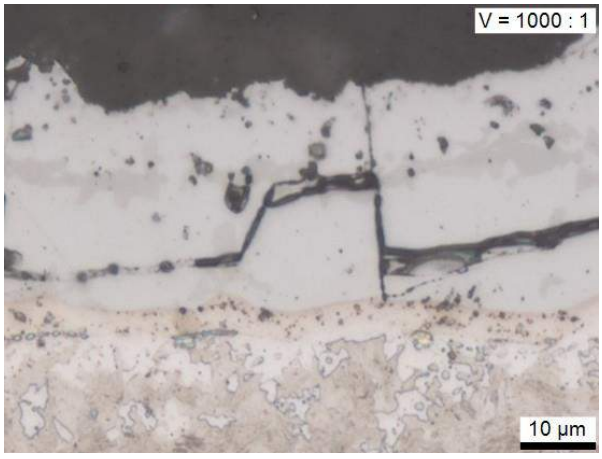

Fig.: 5 0007427
FTF1_l_S1
Edge x1000

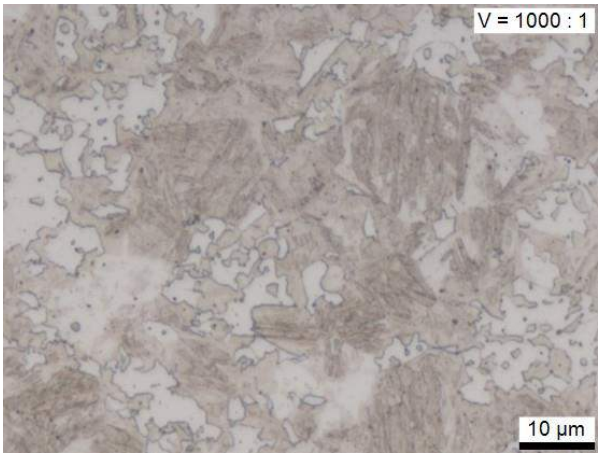

Fig.: 6 0007430
FTF1_l_S1
Middle x1000

FTF1_u1:

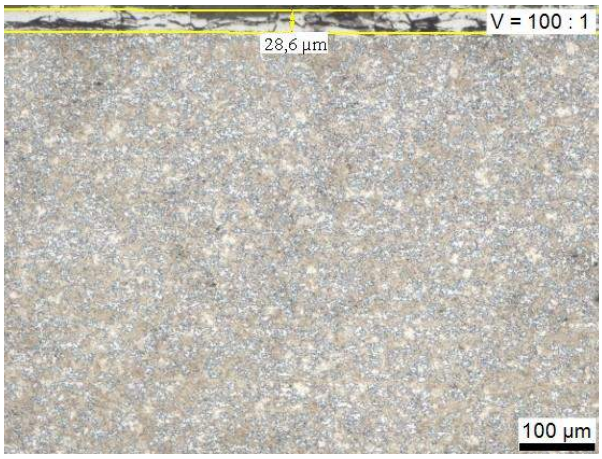

Fig.: 7 0007382
FTF1_u1_S1
Edge x100

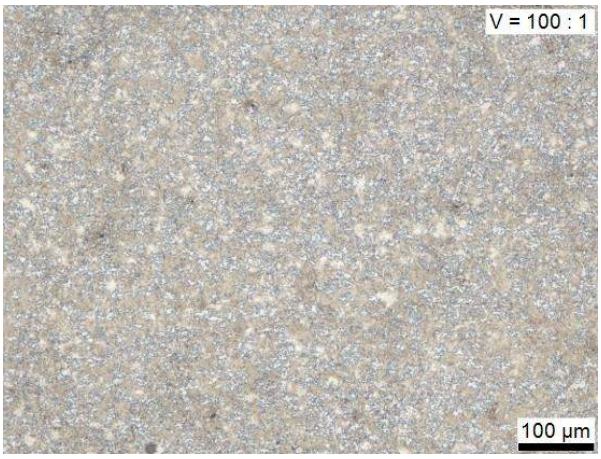

Fig.: 8 0007385
FTF1_u1_S1
Middle x100

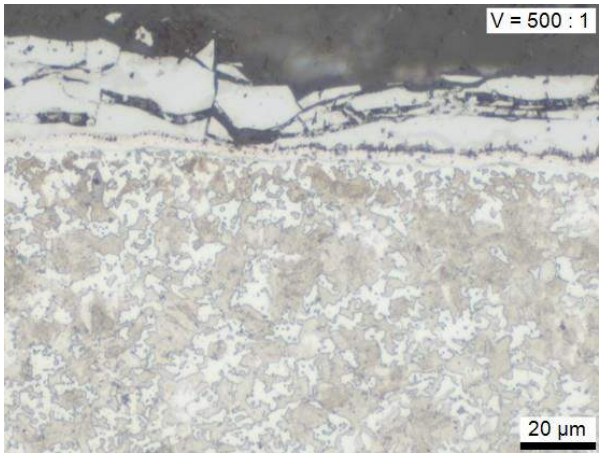

Fig.: 9 0007383
FTF1_u1_S1
Edge x500

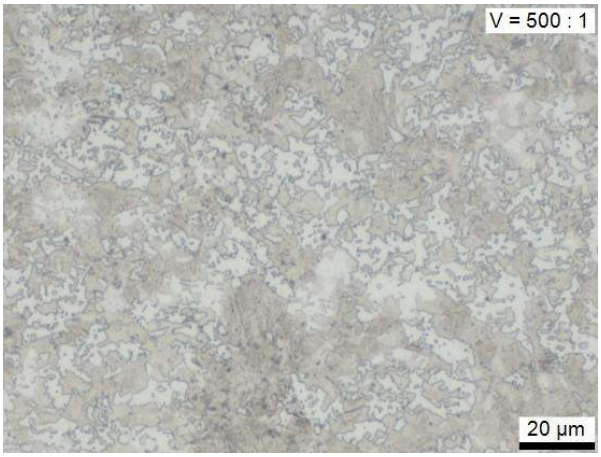

Fig.: 10 0007386
FTF1_u1_S1
Middle x500

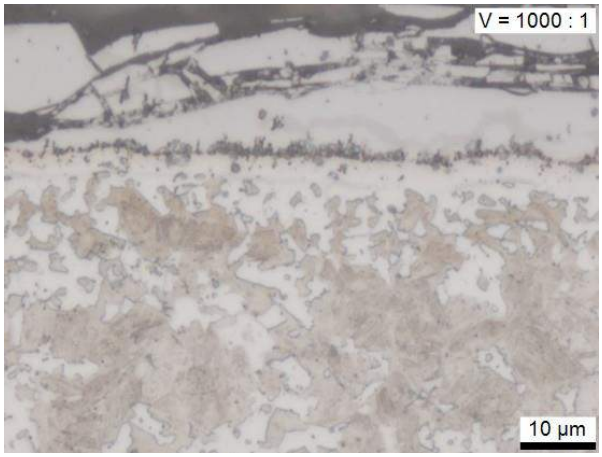

Fig.: 11 0007384
FTF1_u1_S1
Edge x1000

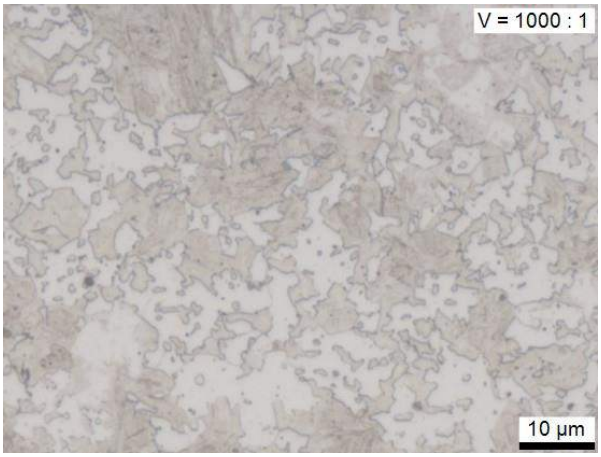

Fig.: 12 0007387
FTF1_u1_S1
Middle x1000

FTF1_u2:

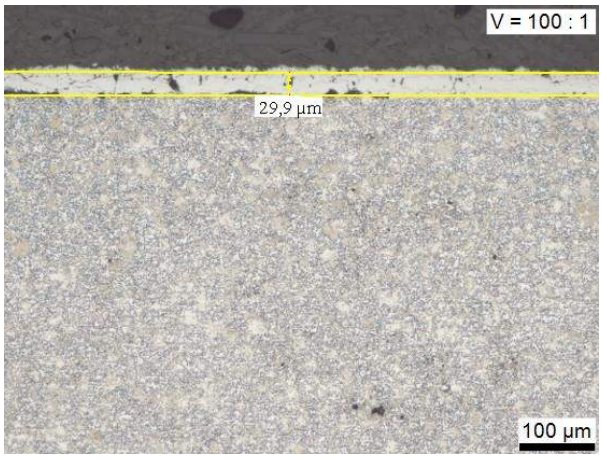

Fig.: 13 0007375
FTF1_u2_S1
Edge x100

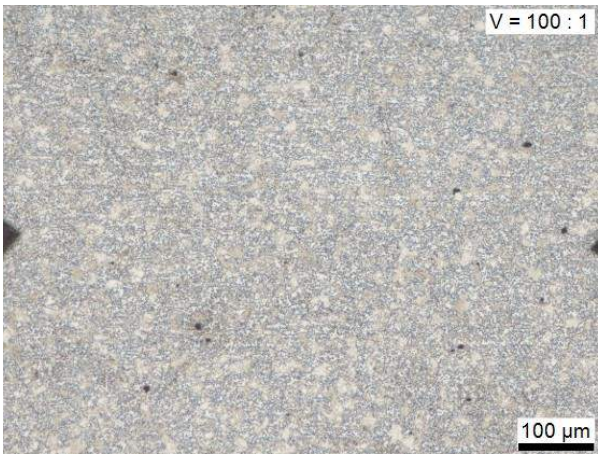

Fig.: 14 0007378
FTF1_u2_S1
Middle x100

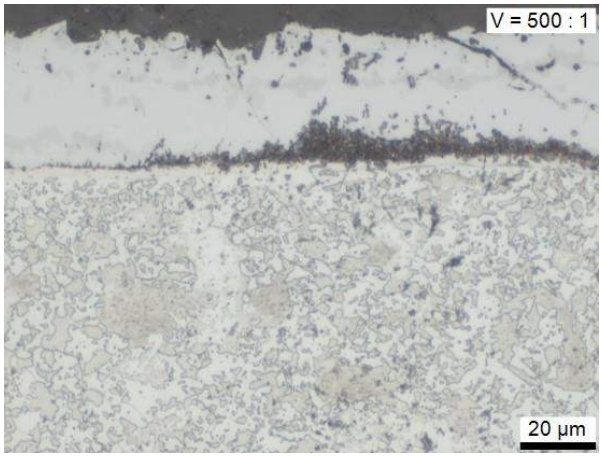

Fig.: 15 0007376
FTF1_u2_S1
Edge x500

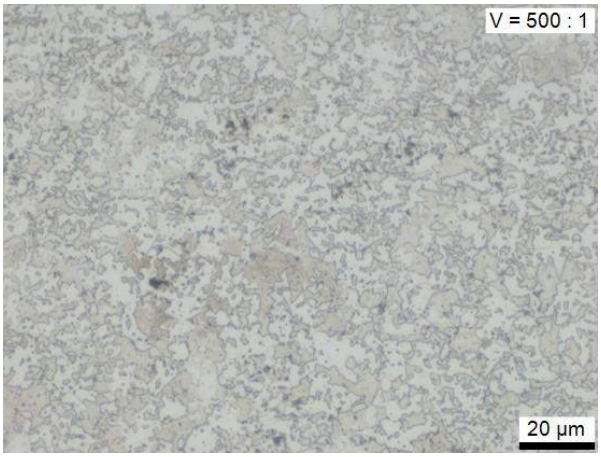

Fig.: 16 0007379
FTF1_u2_S1
Middle x500

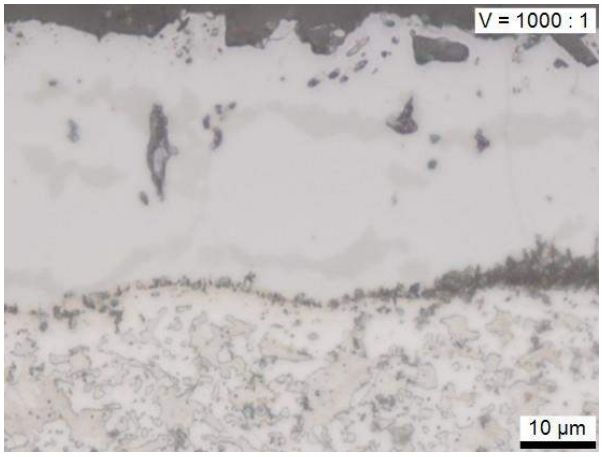

Fig.: 17 0007377
FTF1_u2_S1
Edge x1000

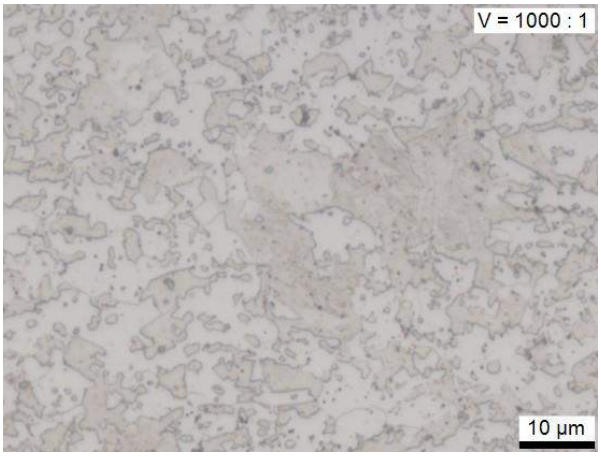

Fig.: 18 0007380
FTF1_u2_S1
Middle x1000

FTF2_l:

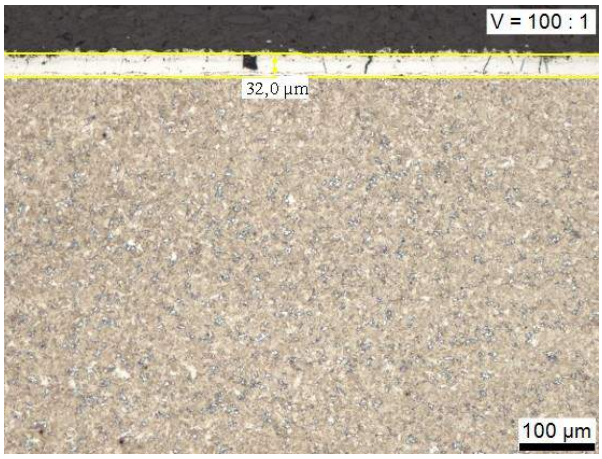

Fig.: 19 0007446
FTF2_l_S1
Edge x100

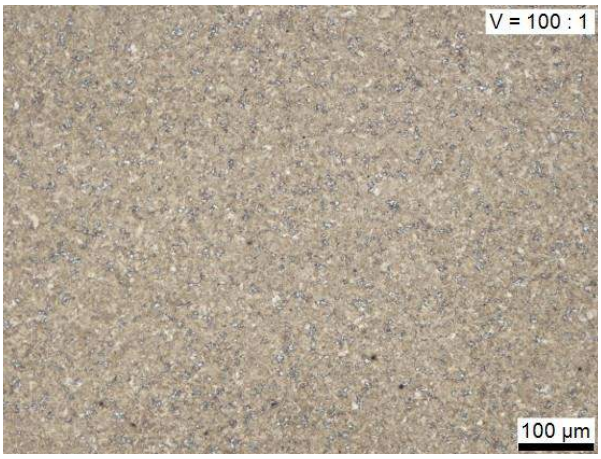

Fig.: 20 0007449
FTF2_l_S1
Middle x100

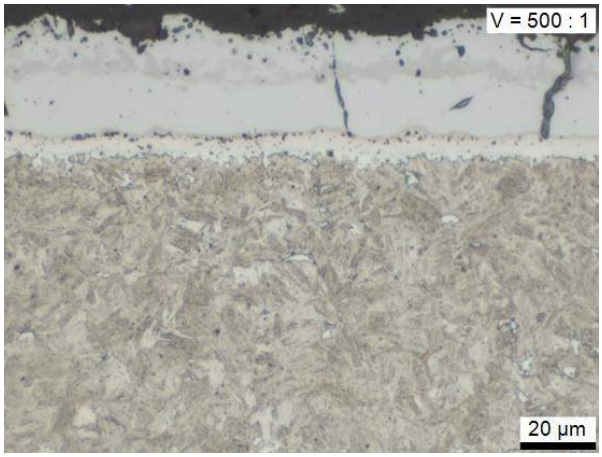

Fig.: 21 0007447
FTF2_l_S1
Edge x500

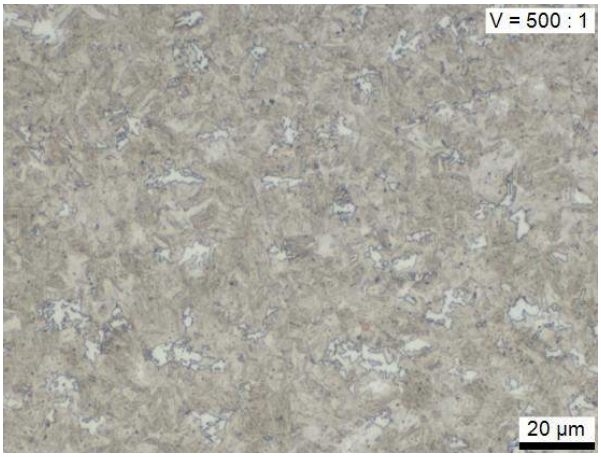

Fig.: 22 0007450
FTF2_l_S1
Middle x500

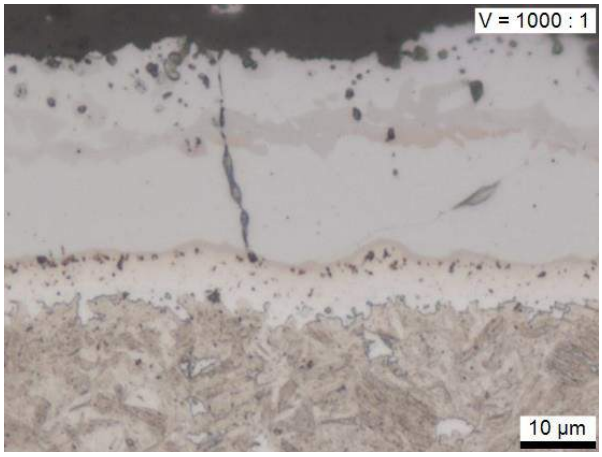

Fig.: 23 0007448
FTF2_l_S1
Edge x1000

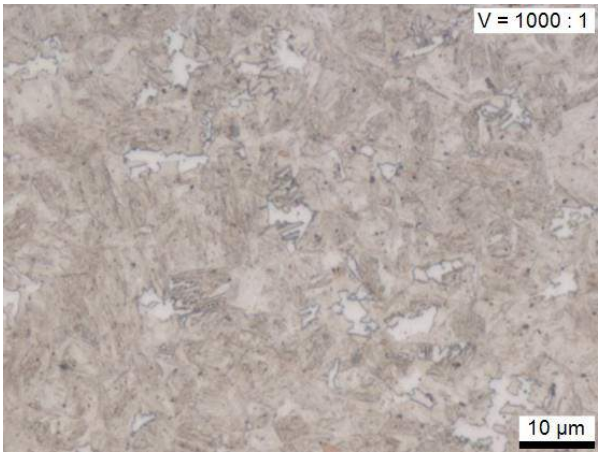

Fig.: 24 0007451
FTF2_l_S1
Middle x1000

FTF2_u1:

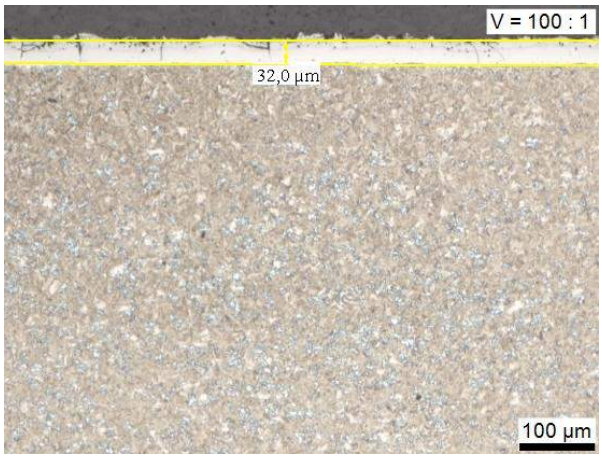

Fig.: 25 0007404_
FTF2_u1_S1
Edge x100

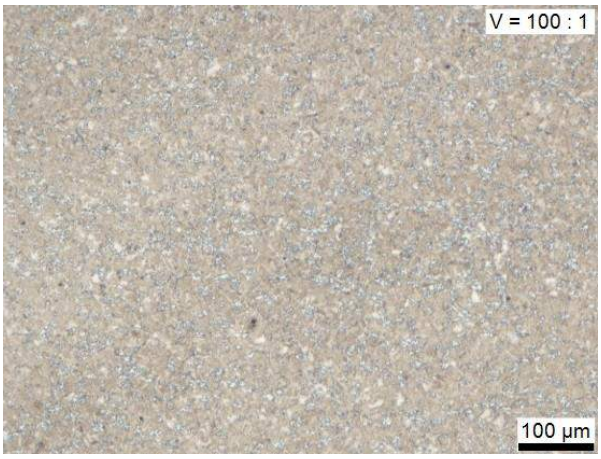

Fig.: 26 0007407_
FTF2_u1_S1
Middle x100

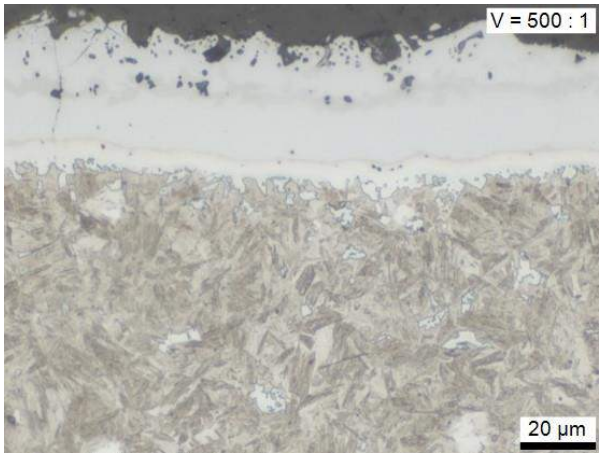

Fig.: 27 0007405
FTF2_u1_S1
Edge x500

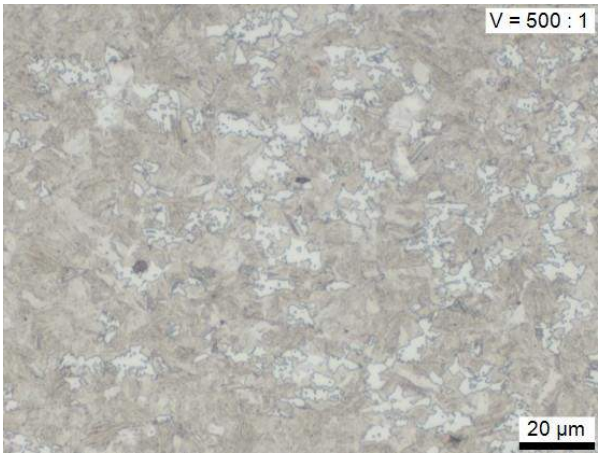

Fig.: 28 0007408
FTF2_u1_S1
Middle x500

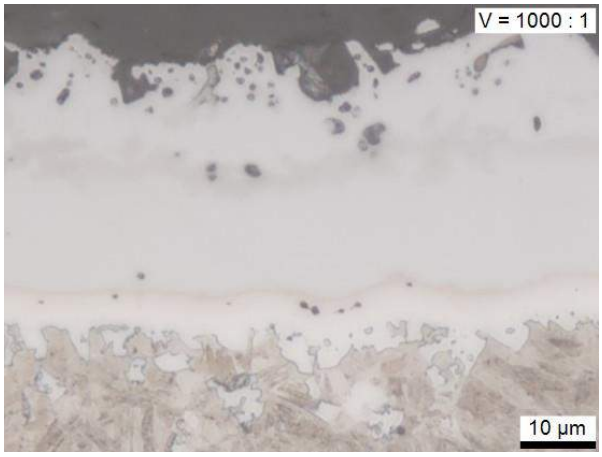

Fig.: 29 0007406
FTF2_u1_S1
Edge x1000

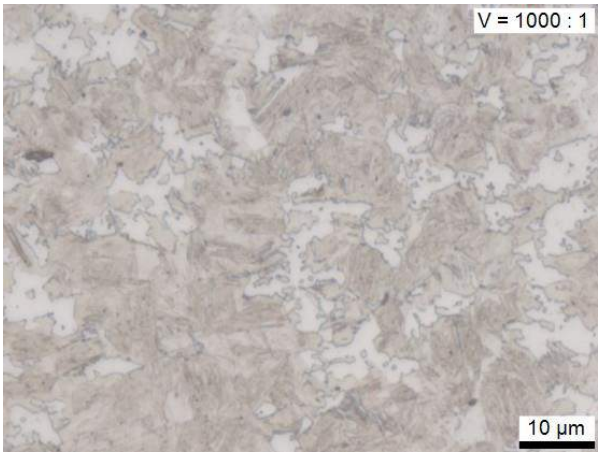

Fig.: 30 0007409
FTF2_u1_S1
Middle x1000

FTF2_u2:

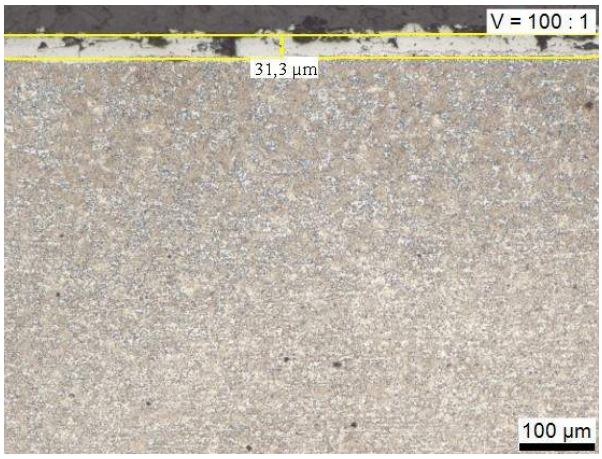

Fig.: 31 0007396
FTF2_u2_S1
Edge x100

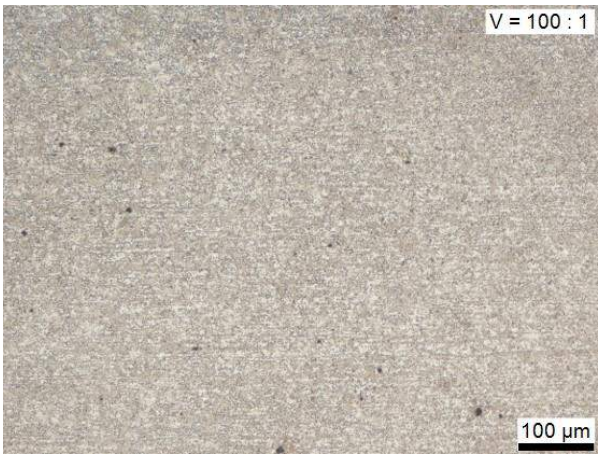

Fig.: 32 0007400
FTF2_u2_S1
Middle x100

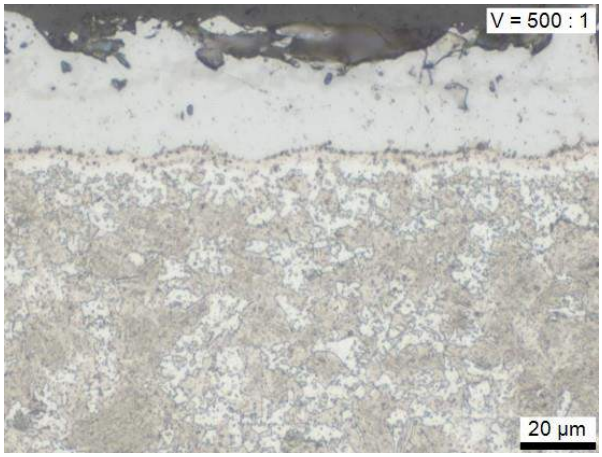

Fig.: 33 0007398
FTF2_u2_S1
Edge x500

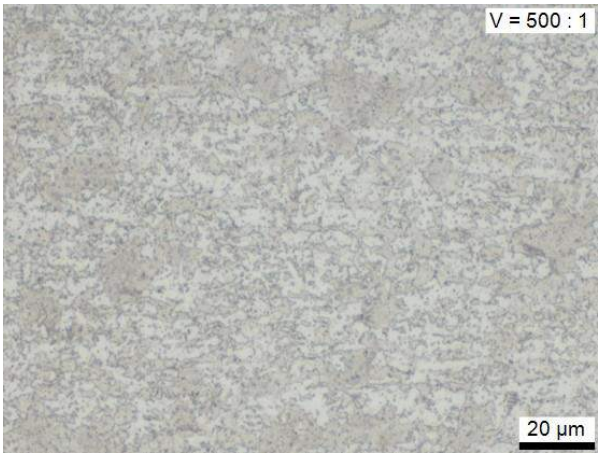

Fig.: 34 0007401_
FTF2_u2_S1
Middle x500

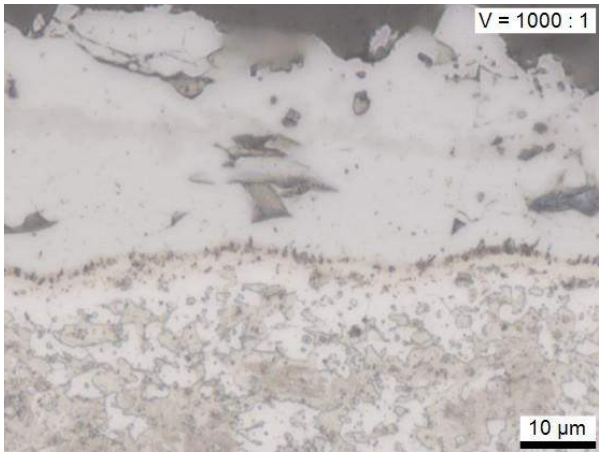

Fig.: 35 0007399
FTF2_u2_S1
Edge x1000

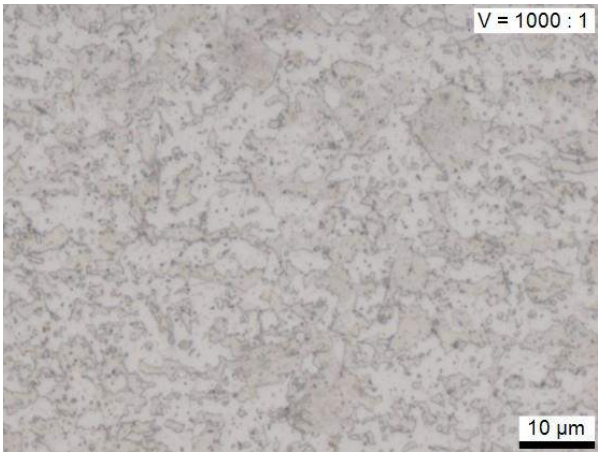

Fig.: 36 0007402
FTF2_u2_S1
Middle x1000

FTF3_l:

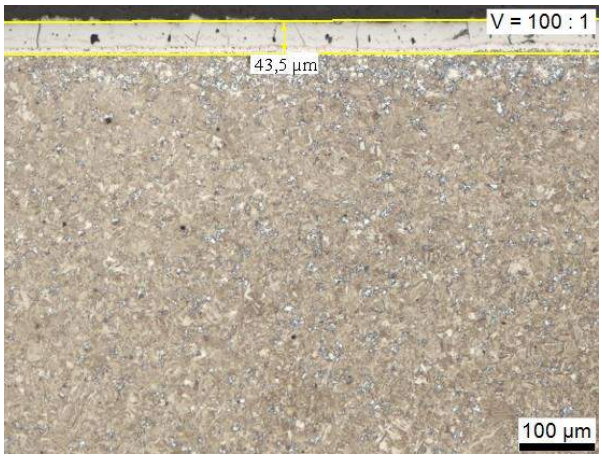

Fig.: 37 0007432
FTF3_l_S1
Edge x100

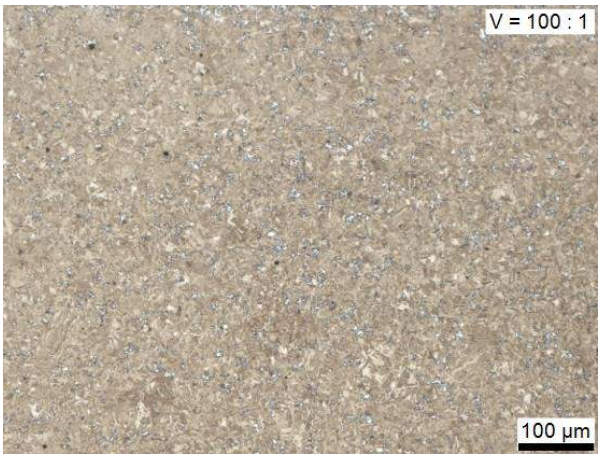

Fig.: 38 0007435
FTF3_l_S1
Middle x100

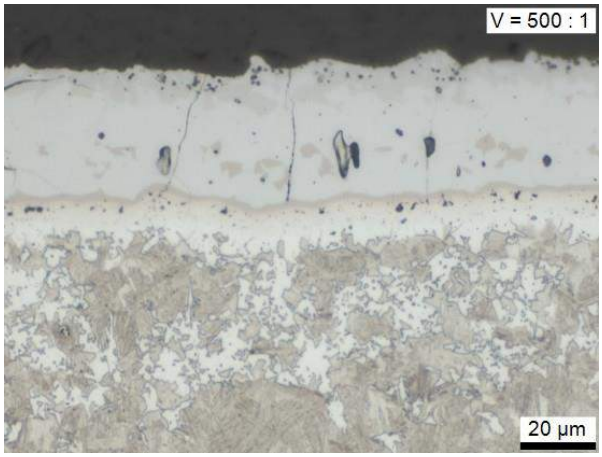

Fig.: 39 0007433
FTF3_l_S1
Edge x500

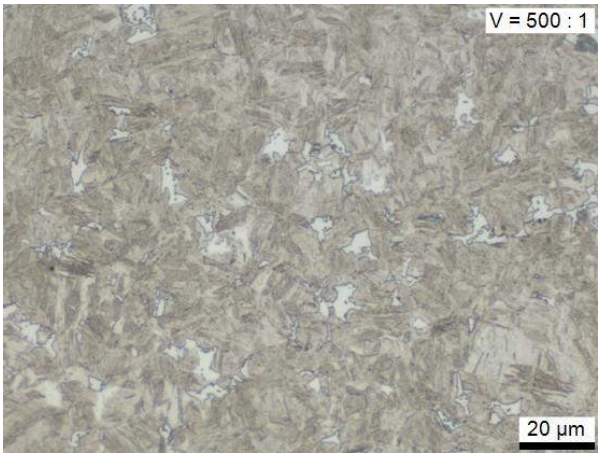

Fig.: 40 0007436
FTF3_l_S1
Middle x500

Fig.: 41 0007434
FTF3_l_S1
Edge x1000

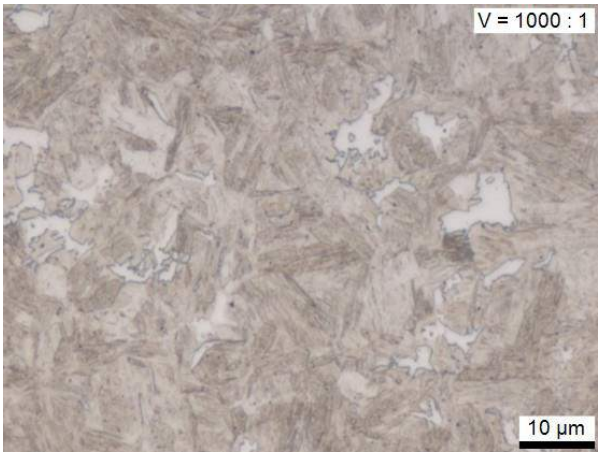

Fig.: 42 0007437
FTF3_l_S1
Middle x1000

FTF3_u1:

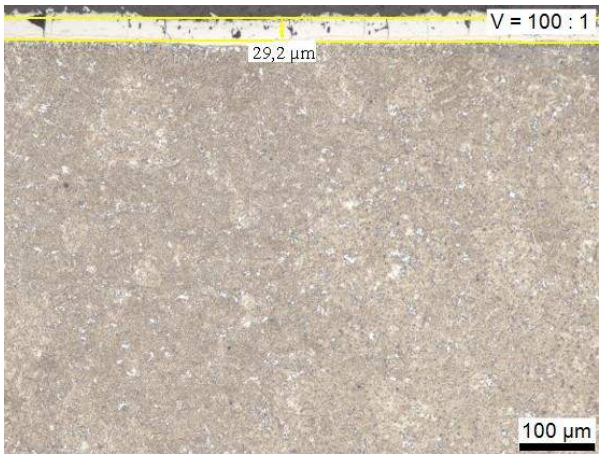

Fig.: 43 000738_
FTF3_u1_S1
Edge x100

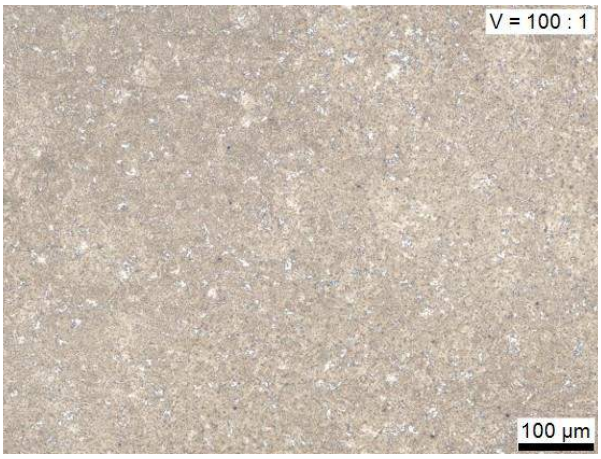

Fig.: 44 0007392
FTF3_u1_S1
Middle x100

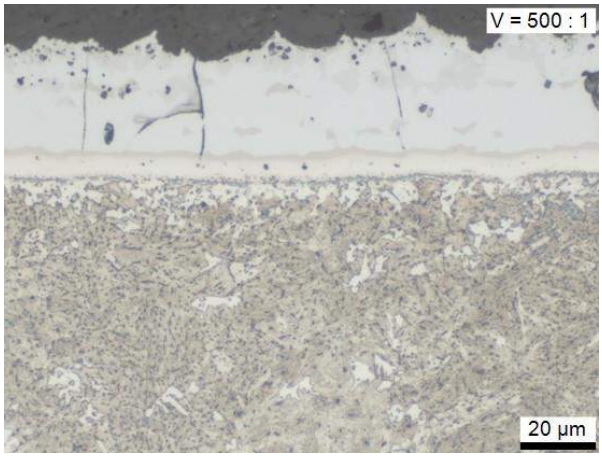

Fig.: 45 0007390
FTF3_u1_S1
Edge x500

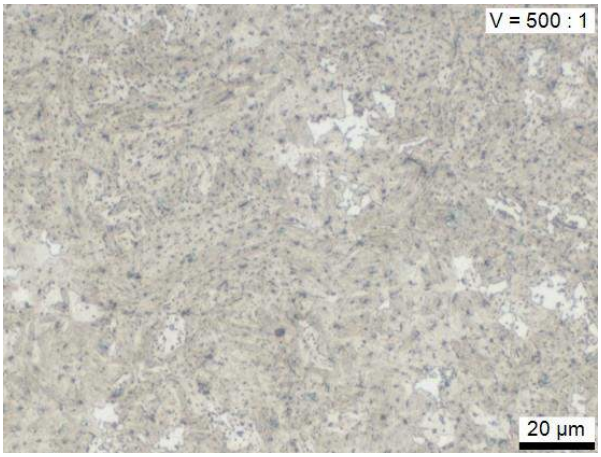

Fig.: 46 0007393
FTF3_u1_S1
Middle x500

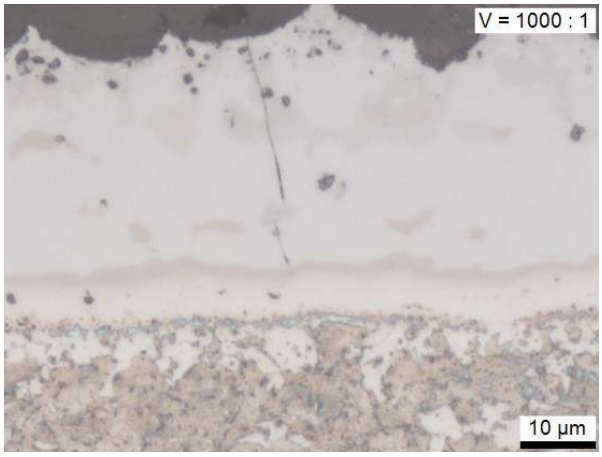

Fig.: 47 0007391
FTF3_u1_S1
Edge x1000

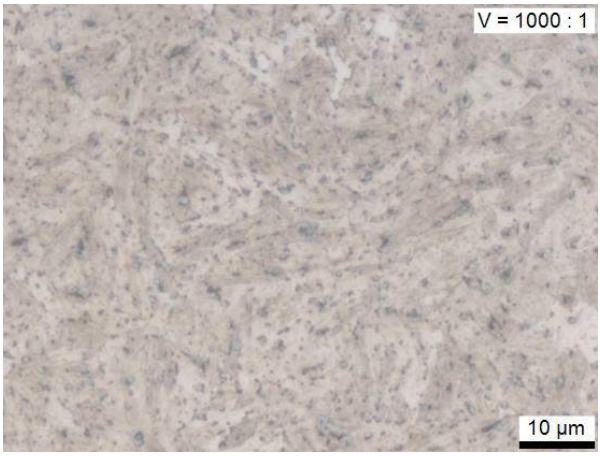

Fig.: 48 0007394
FTF3_u1_S1
Middle x1000

FTF3_u2:

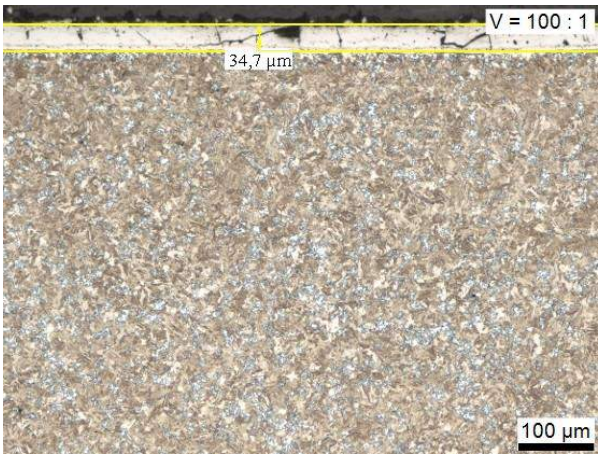

Fig.: 49 0007439
FTF3_u2_S1
Edge x100

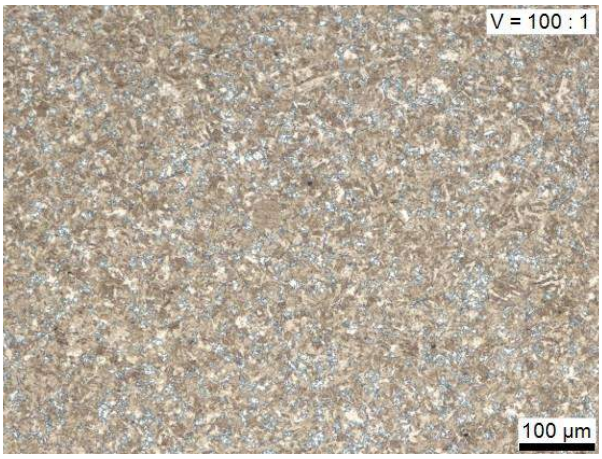

Fig.: 50 0007442
FTF3_u2_S1
Middle x100

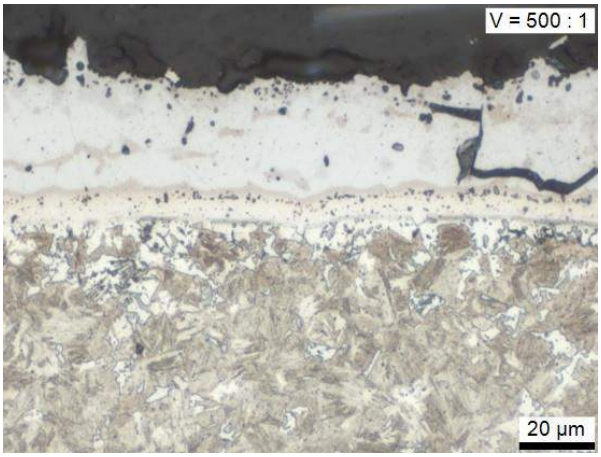

Fig.: 51 0007440
FTF3_u2_S1
Edge x500

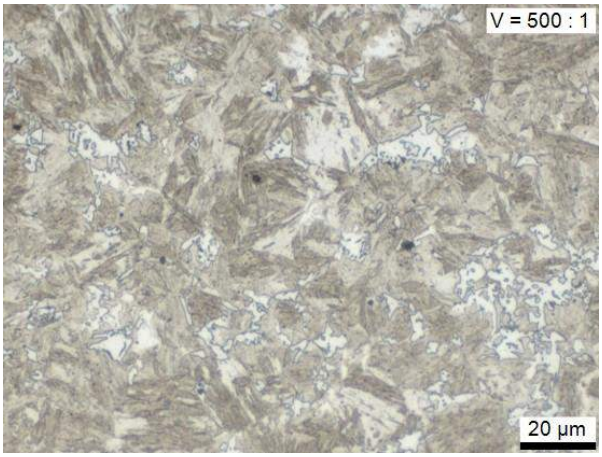

Fig.: 52 0007443
FTF3_u2_S1
Middle x500

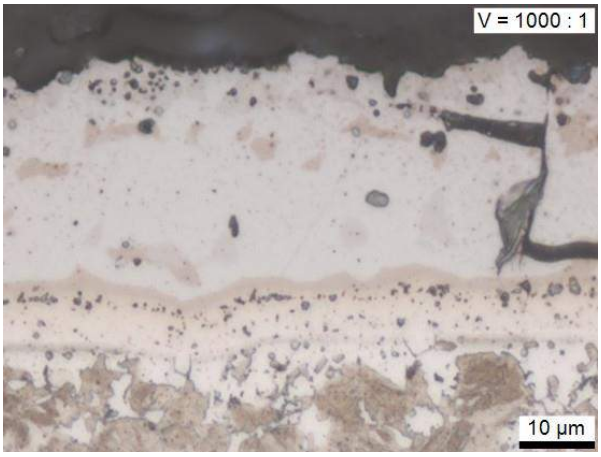

Fig.: 53 0007441
FTF3_u2_S1
Edge x1000

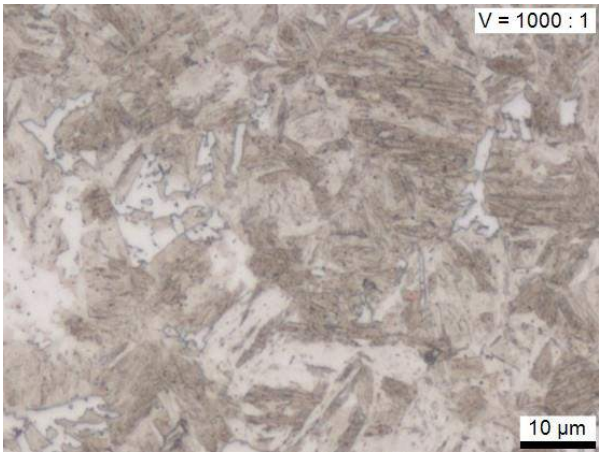

Fig.: 54 0007444
FTF3_u2_S1
Middle x1000

FTF4_l:

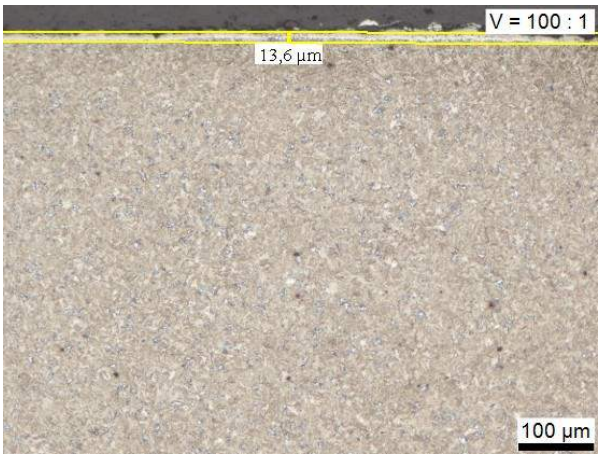

Fig.: 55 0007368
FTF4_l_S1
Edge x100

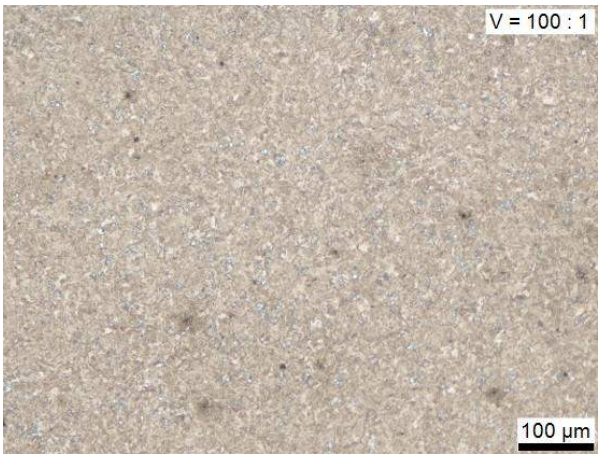

Fig.: 56 0007371
FTF4_l_S1
Middle x100

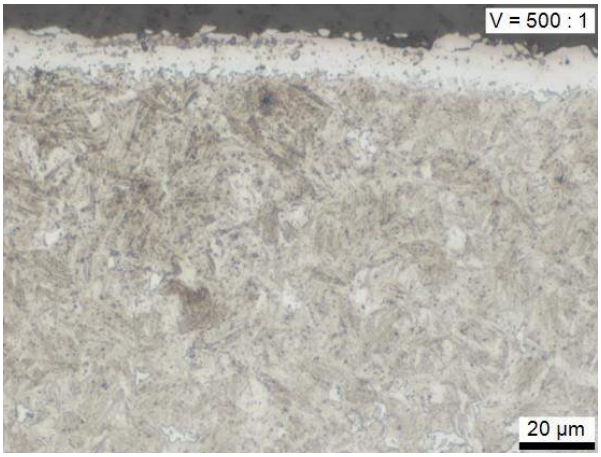

Fig.: 57 0007369
FTF4_l_S1
Edge x500

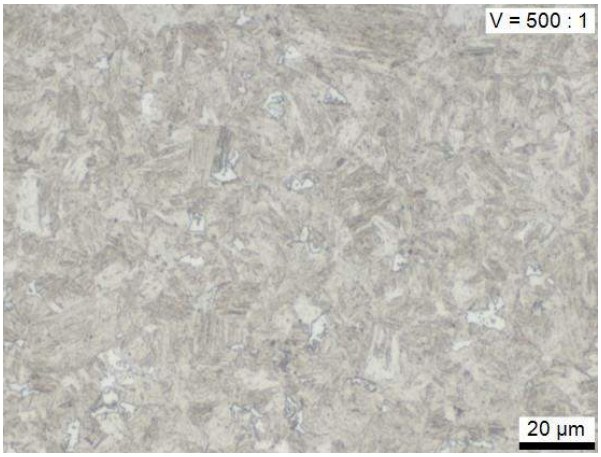

Fig.: 58 0007372
FTF4_l_S1
Middle x500

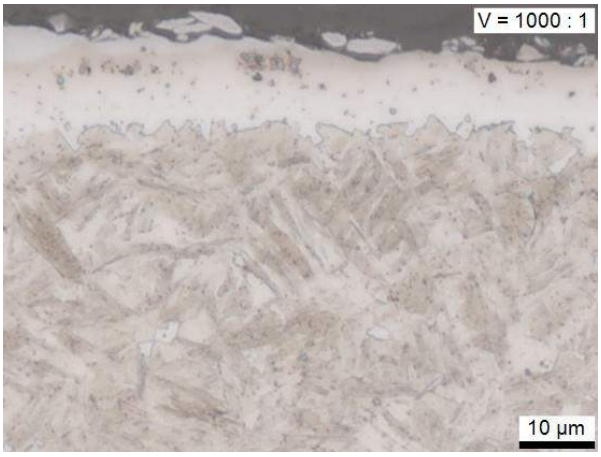

Fig.: 59 0007370
FTF4_l_S1
Edge x1000

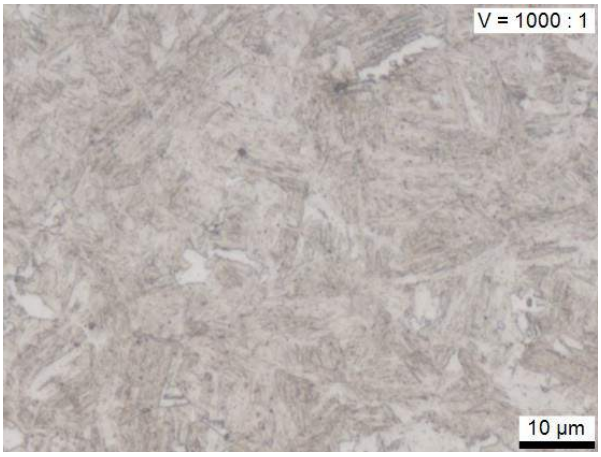

Fig.: 60 0007373
FTF4_l_S1
Middle x1000

FTF4_u1:

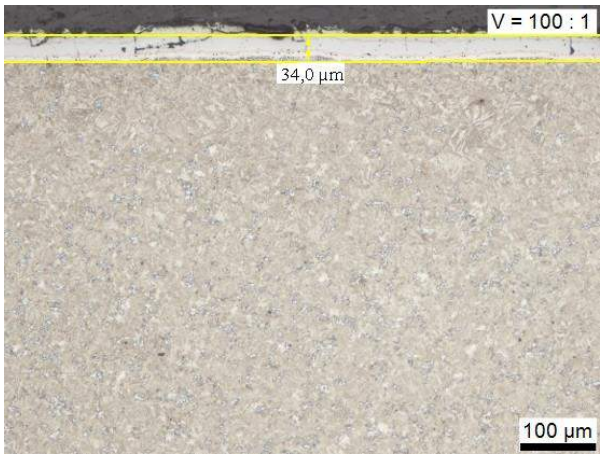

Fig.: 61 0007411_
FTF4_u1_S1
Edge x100

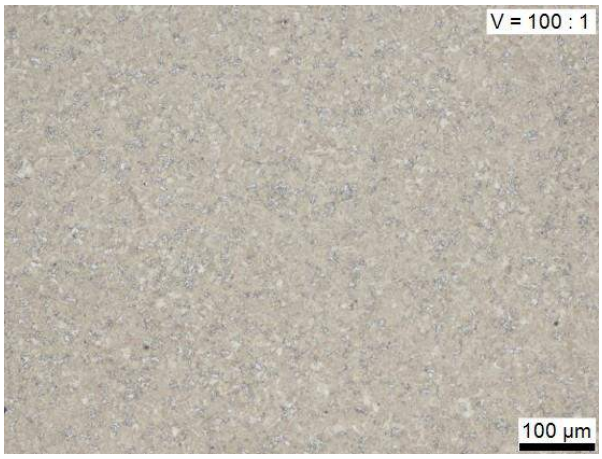

Fig.: 62 0007414
FTF4_u1_S1
Middle x100

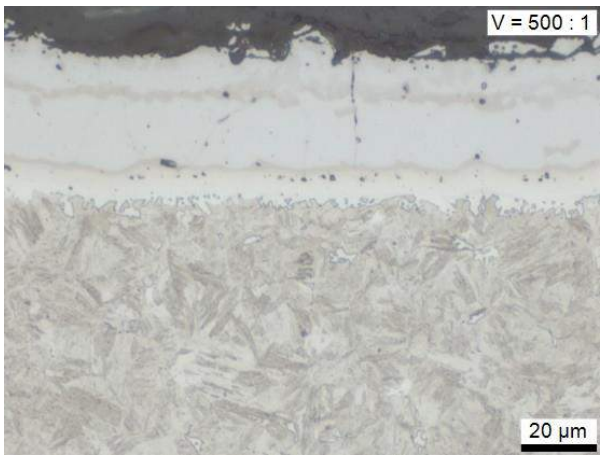

Fig.: 63 0007412
FTF4_u1_S1
Edge x500

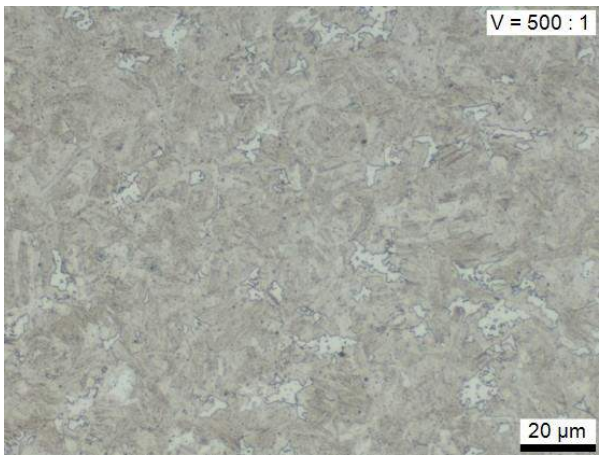

Fig.: 64 0007415
FTF4_u1_S1
Middle x500

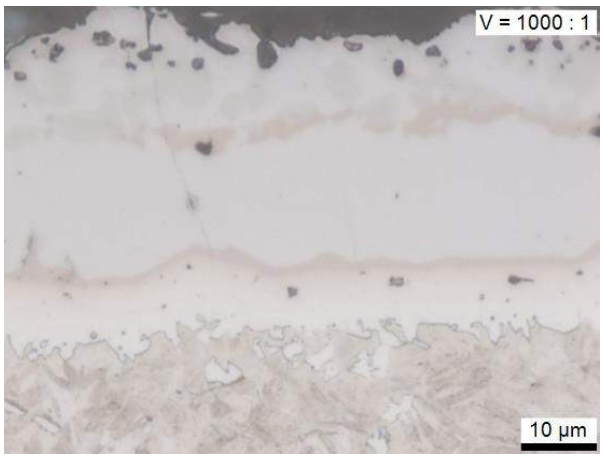

Fig.: 65 0007413
FTF4_u1_S1
Edge x1000

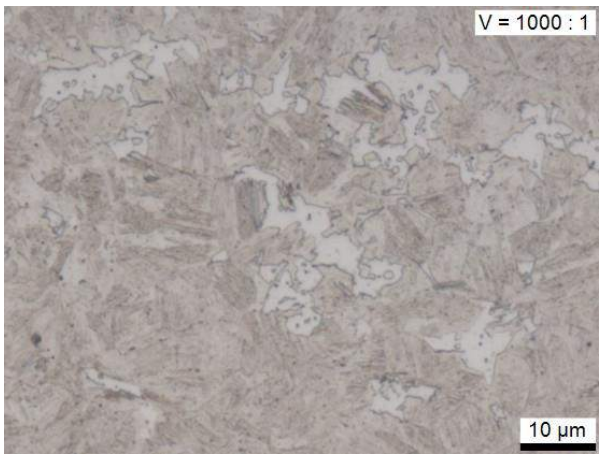

Fig.: 66 0007416
FTF4_u1_S1
Middle x1000

FTF4_u2:

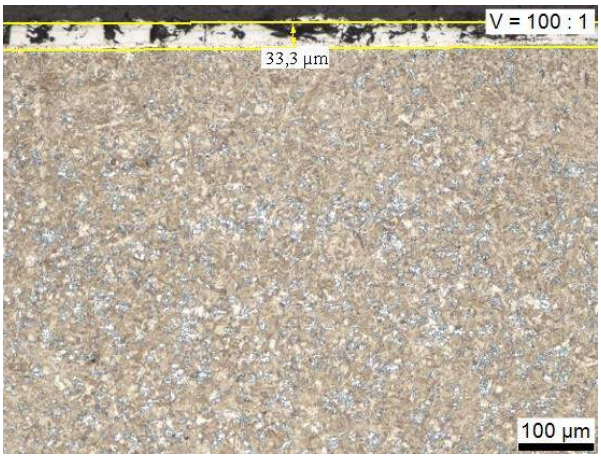

Fig.: 67 0007418
FTF4_u2_S1
Edge x100

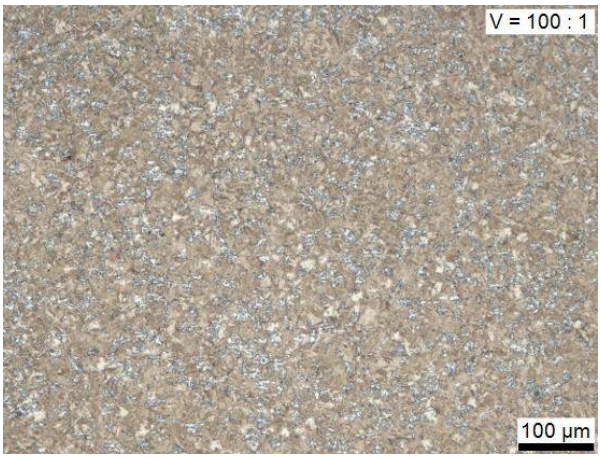

Fig.: 68 0007421
FTF4_u2_S1
Middle x100

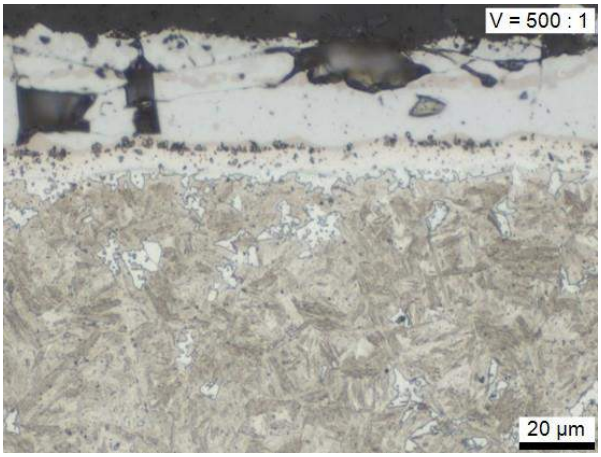

Fig.: 69 0007419
FTF4_u2_S1
Edge x500

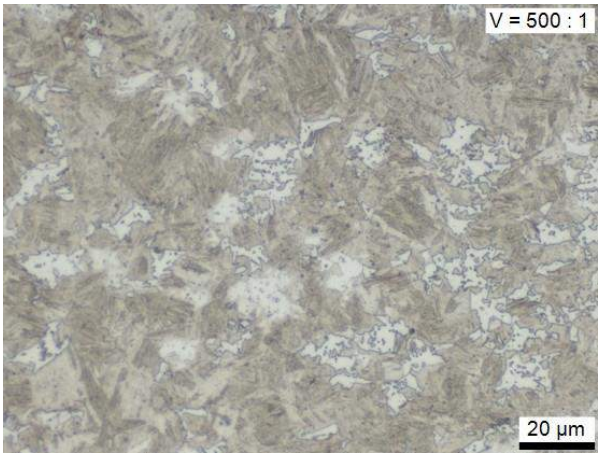

Fig.: 70 0007422
FTF4_u2_S1
Middle x500

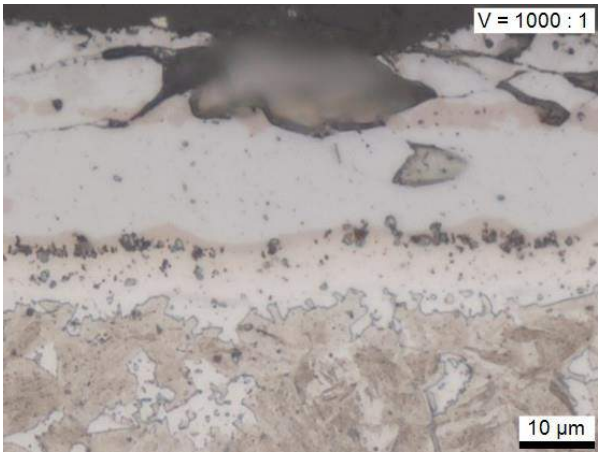

Fig.: 71 0007420
FTF4_u2_S1
Edge x1000

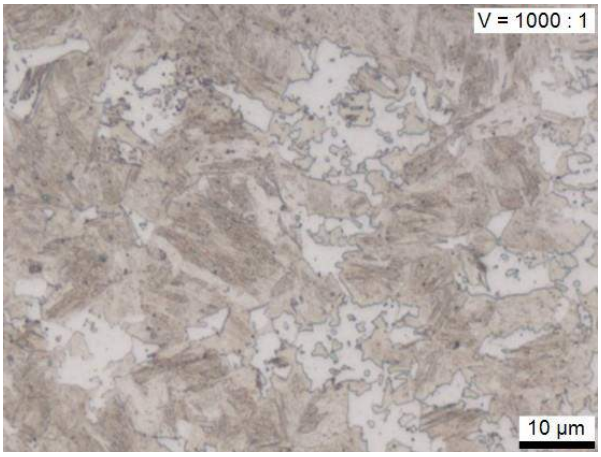

Fig.: 72 0007423
FTF4_u2_S1
Middle x1000

Soft zone

FTF1_l:

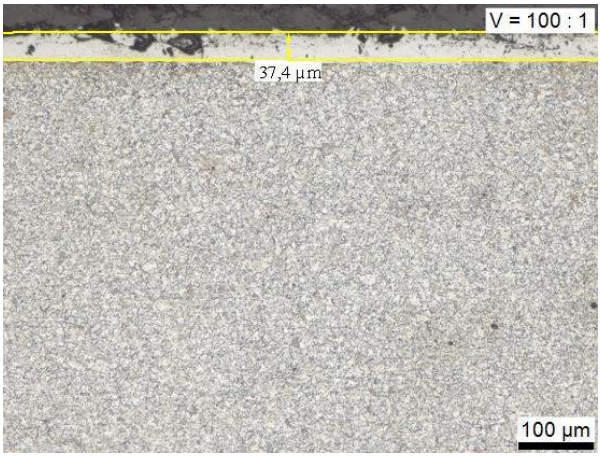

Fig.: 73 0007259
FTF1_l_S2
Edge x100

Fig.: 74 0007262
FTF1_l_S2
Middle x100

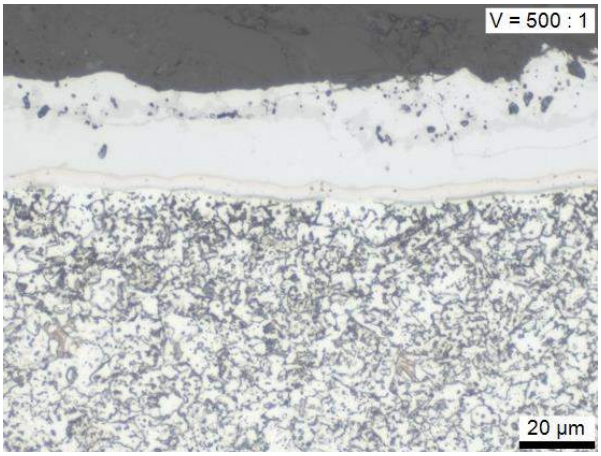

Fig.: 75 0007260
FTF1_l_S2
Edge x500

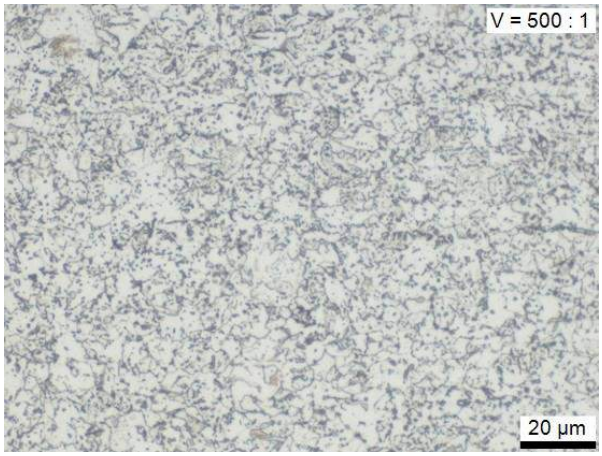

Fig.: 76 0007263
FTF1_l_S2
Middle x500

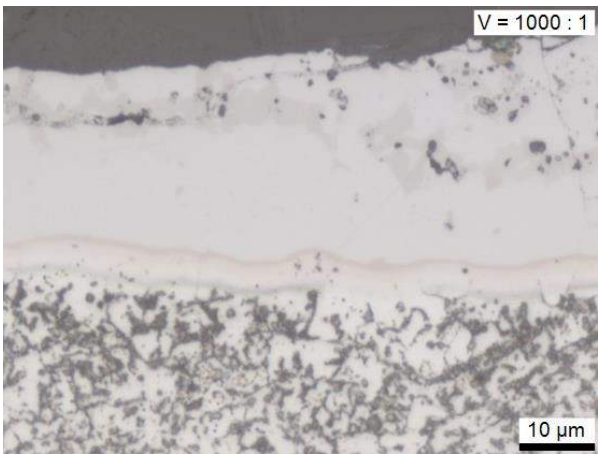

Fig.: 77 0007261
FTF1_l_S2
Edge x1000

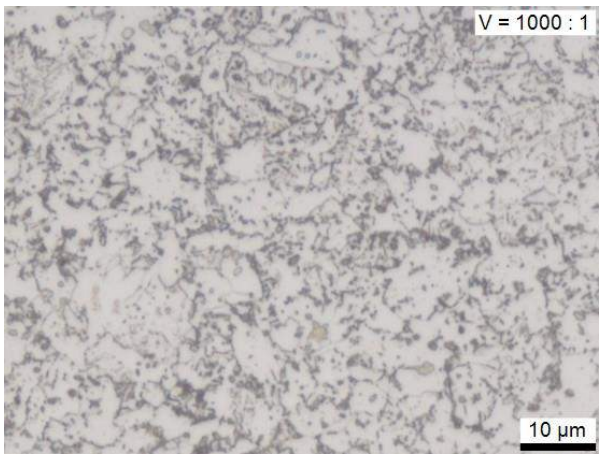

Fig.: 78 0007264
FTF1_l_S2
Middle x1000

FTF1_u1:

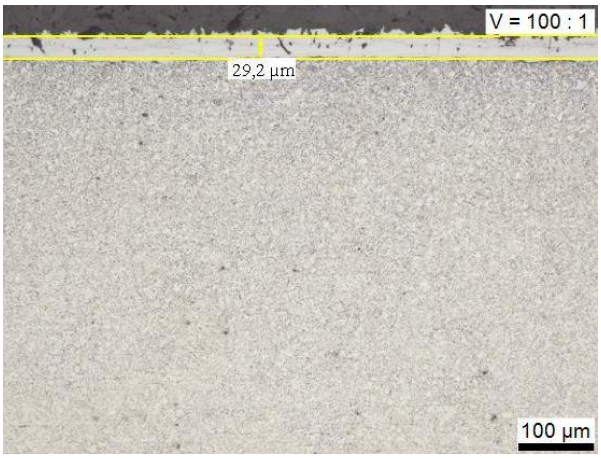

Fig.: 79 0007273
FTF1_u1_S2
Edge x100

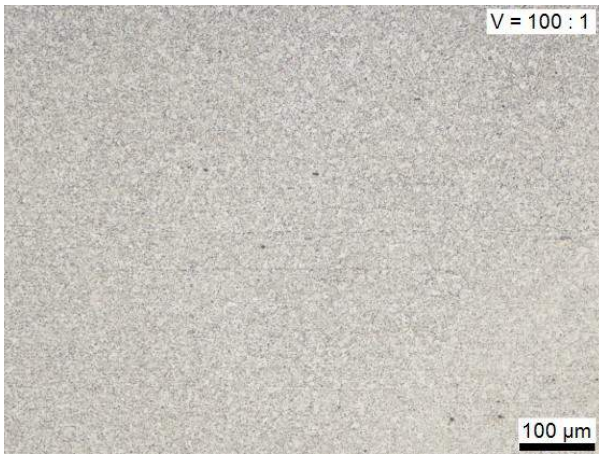

Fig.: 80 0007276
FTF1_u1_S2
Middle x100

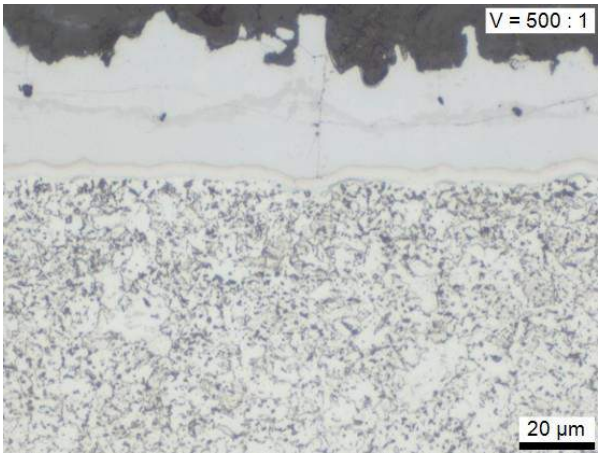

Fig.: 81 0007274
FTF1_u1_S2
Edge x500

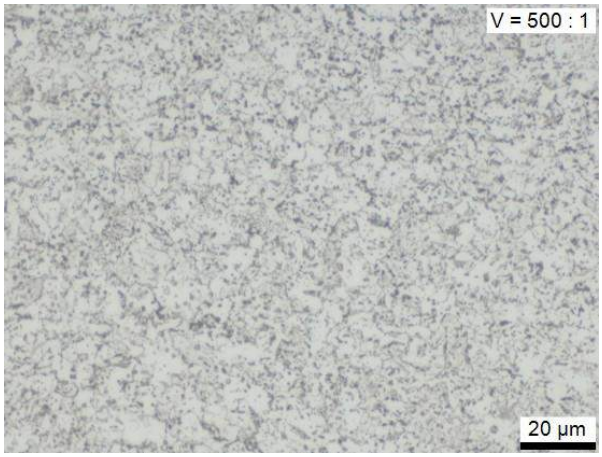

Fig.: 82 0007277
FTF1_u1_S2
Middle x500

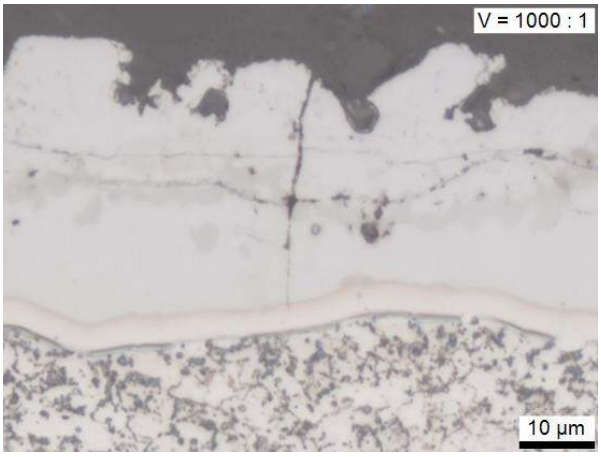

Fig.: 83 0007275
FTF1_u1_S2
Edge x1000

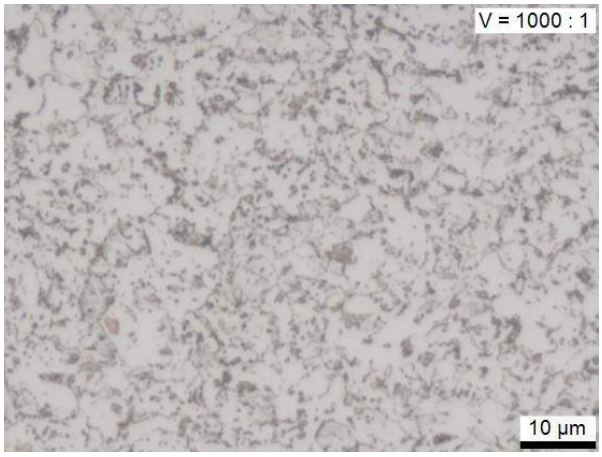

Fig.: 84 0007278
FTF1_u1_S2
Middle x1000

FTF1_u2:

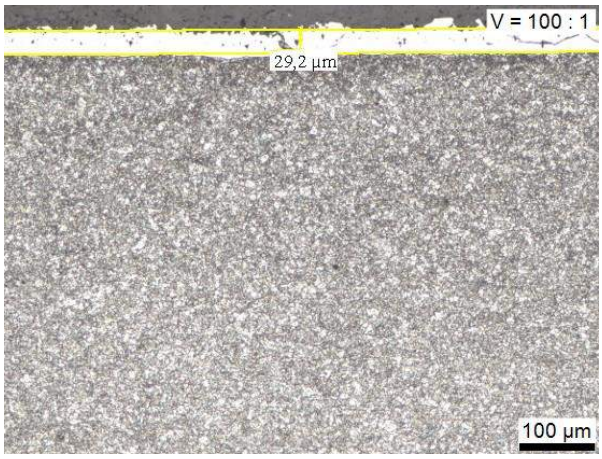

Fig.: 85 0007340
FTF1_u2_S2
Edge x100

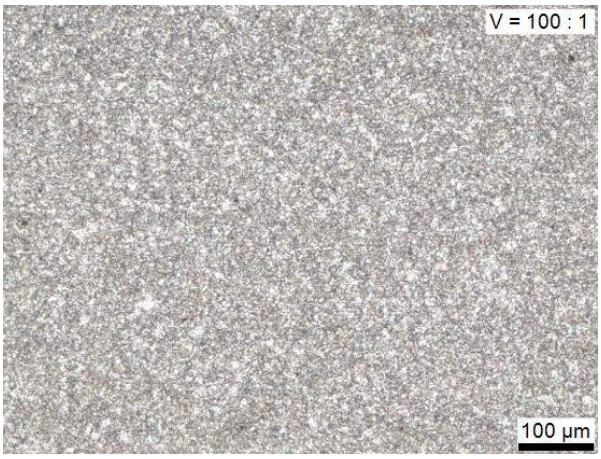

Fig.: 86 0007343
FTF1_u2_S2
Middle x100

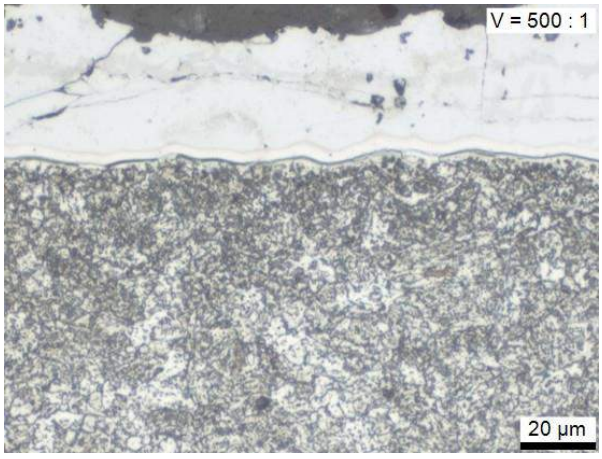

Fig.: 87 0007341
FTF1_u2_S2
Edge x500

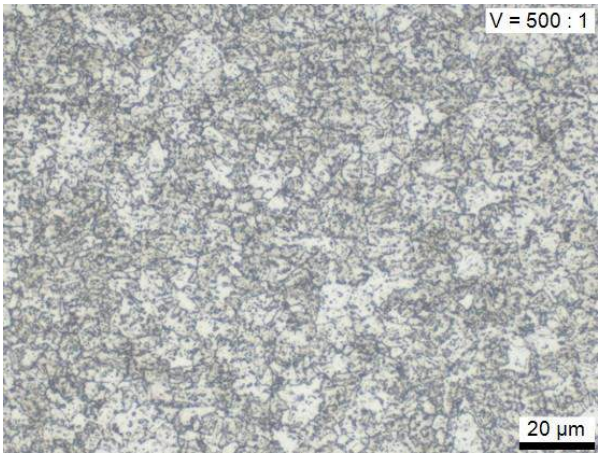

Fig.: 88 0007344
FTF1_u2_S2
Middle x500

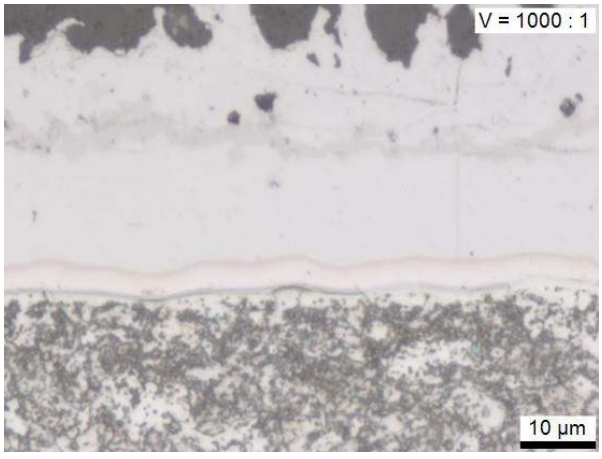

Fig.: 89 0007342
FTF1_u2_S2
Edge x1000

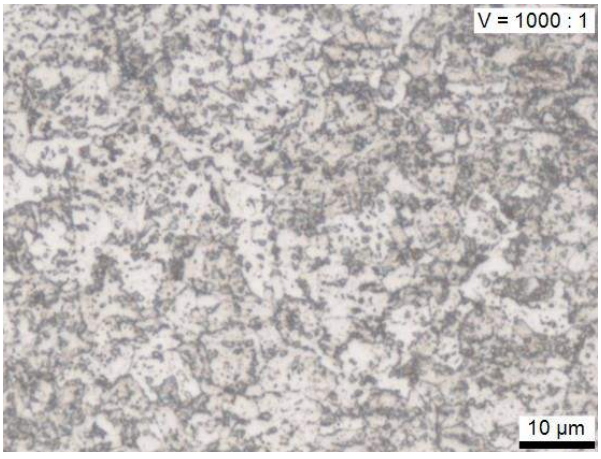

Fig.: 90 0007345
FTF1_u2_S2
Middle x1000

FTF2_l:

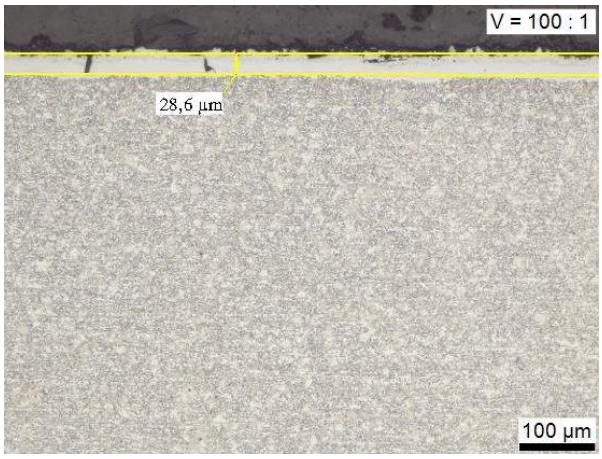

Fig.: 91 0007251
FTF2_l_S2
Edge x100

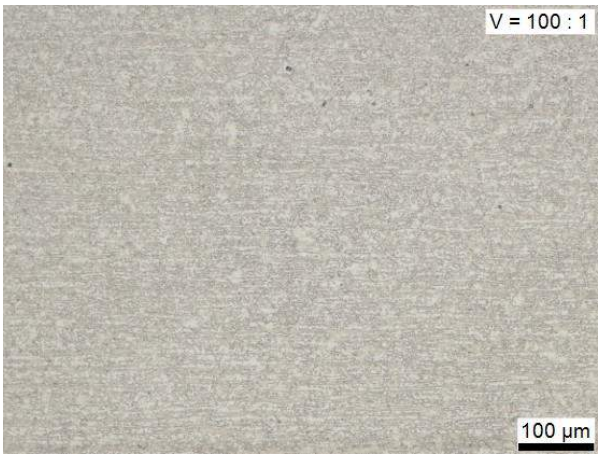

Fig.: 92 0007254
FTF2_l_S2
Middle x100

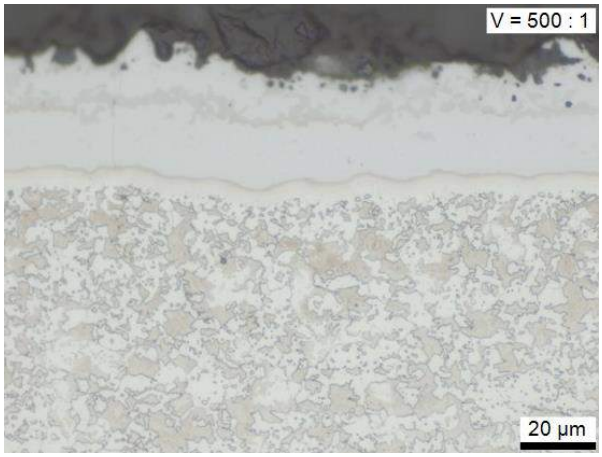

Fig.: 93 0007252
FTF2_l_S2
Edge x500

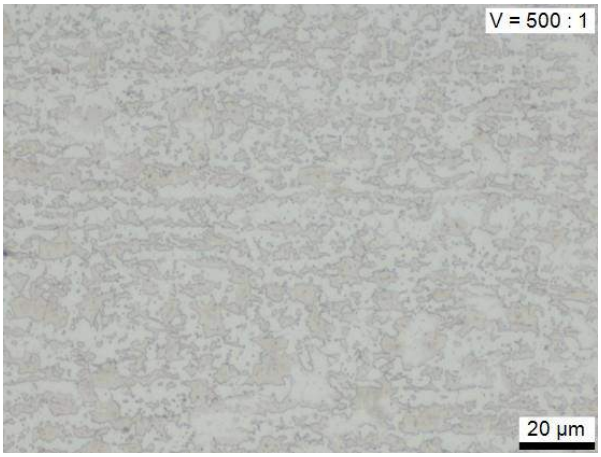

Fig.: 94 0007255
FTF2_l_S2
Middle x500

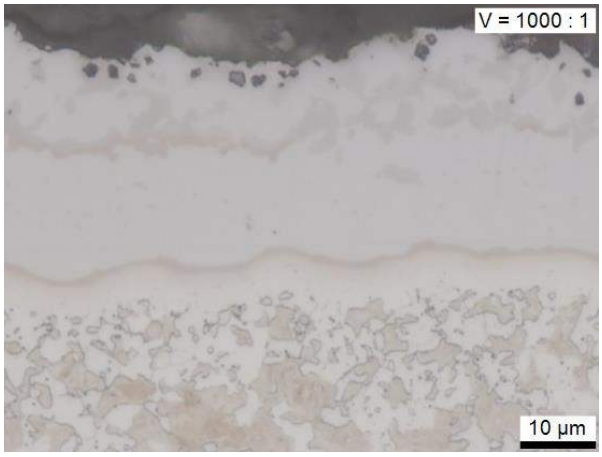

Fig.: 95 0007253
FTF2_l_S2
Edge x1000

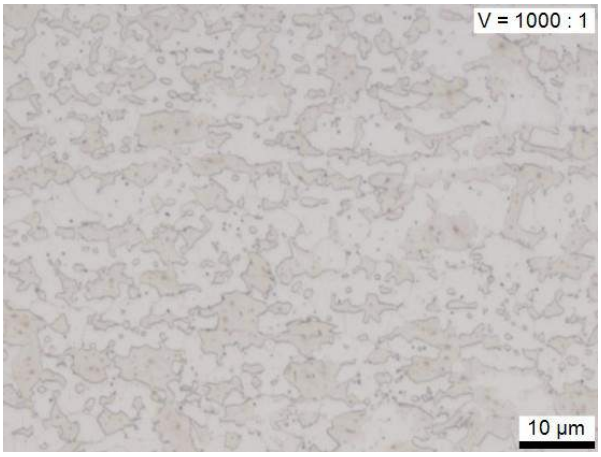

Fig.: 96 0007256
FTF2_l_S2
Middle x1000

FTF2_u1:

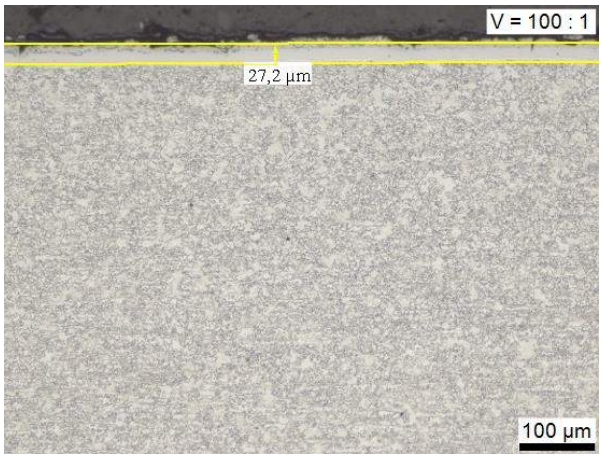

Fig.: 97 0007289
FTF2_u1_S2
Edge x100

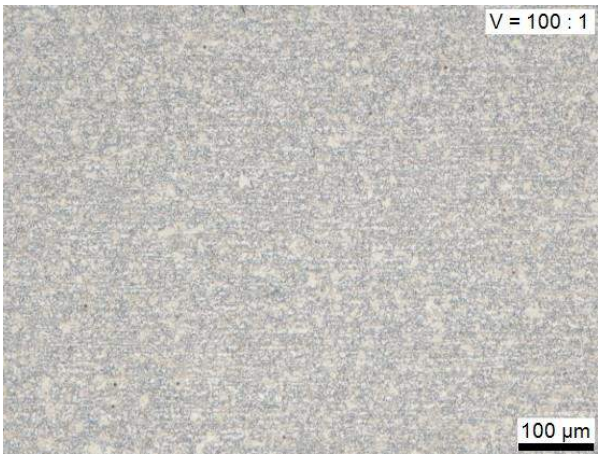

Fig.: 98 0007293
FTF2_u1_S2
Middle x100

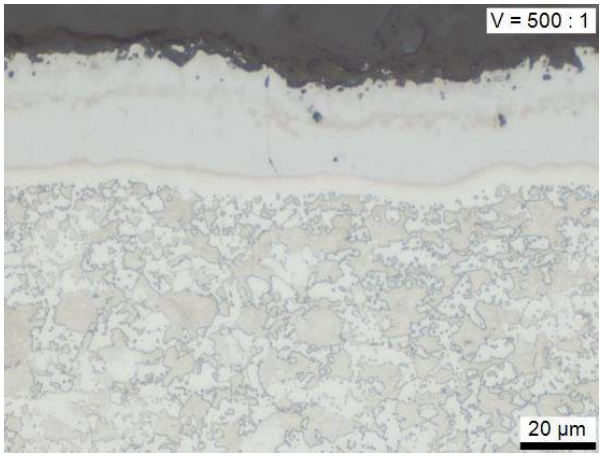

Fig.: 99 0007290
FTF2_u1_S2
Edge x500

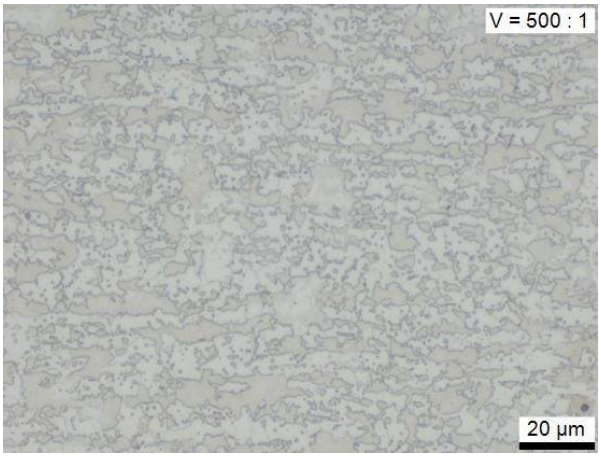

Fig.: 100 0007294
FTF2_u1_S2
Middle x500

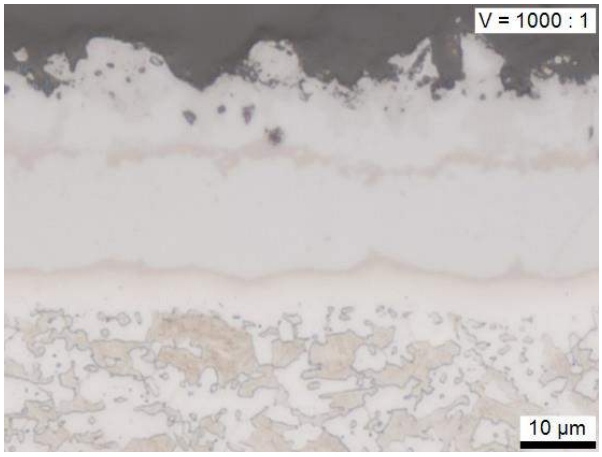

Fig.: 101 0007292
FTF2_u1_S2
Edge x1000

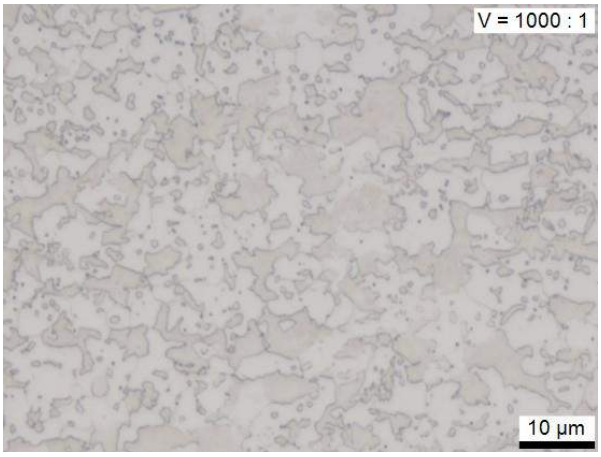

Fig.: 102 0007295
FTF2_u1_S2
Middle x1000

FTF2_u2:

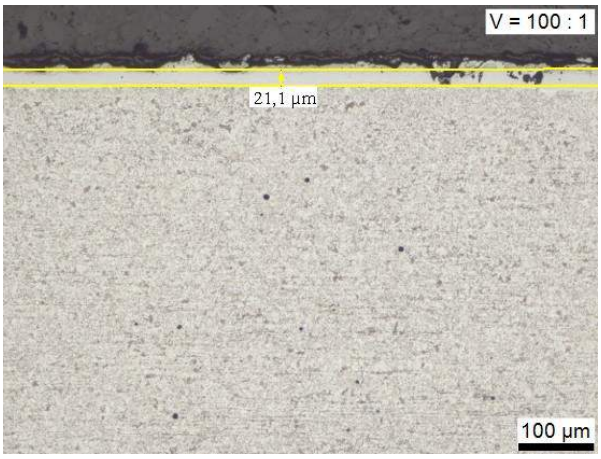

Fig.: 103 0007297
FTF2_u2_S2
Edge x100

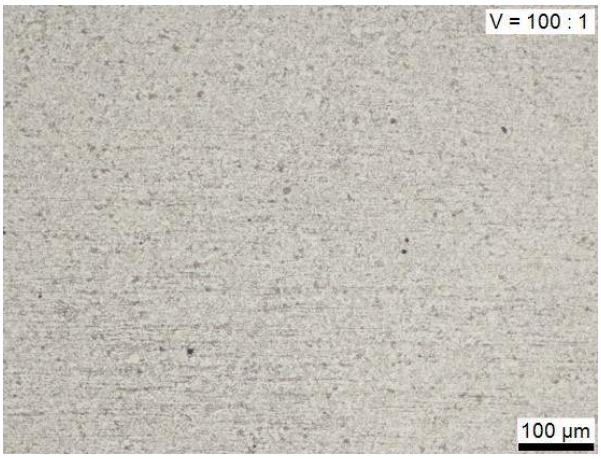

Fig.: 104 0007300
FTF2_u2_S2
Middle x100

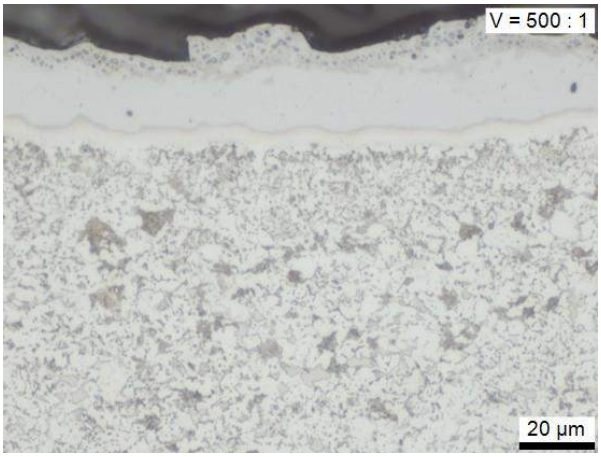

Fig.: 105 0007298
FTF2_u2_S2
Edge x500

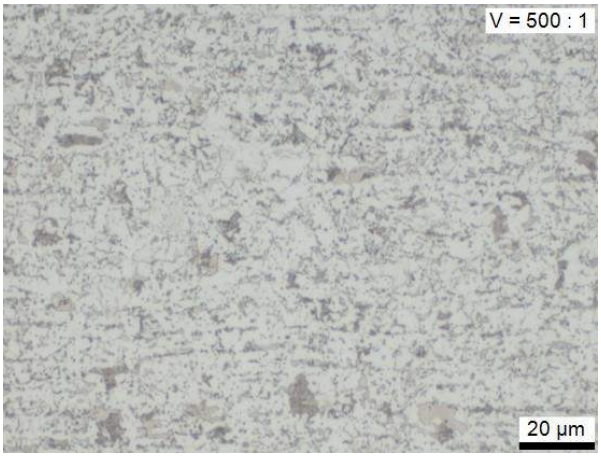

Fig.: 106 0007301
FTF2_u2_S2
Middle x500

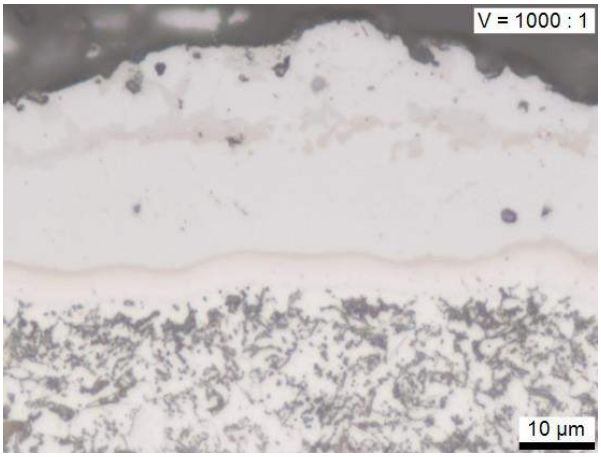

Fig.: 107 0007299
FTF2_u2_S2
Edge x1000

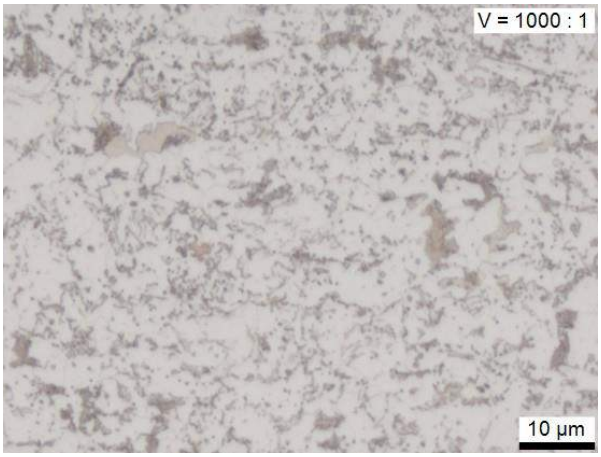

Fig.: 108 0007302
FTF2_u2_S2
Middle x1000

FTF3_l:

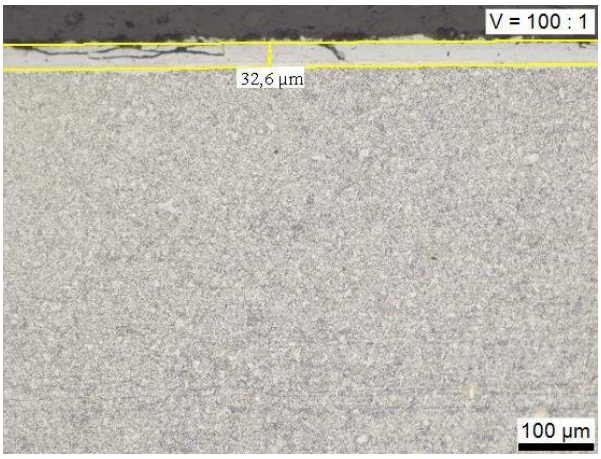

Fig.: 109 0007266
FTF3_l_S2
Edge x100

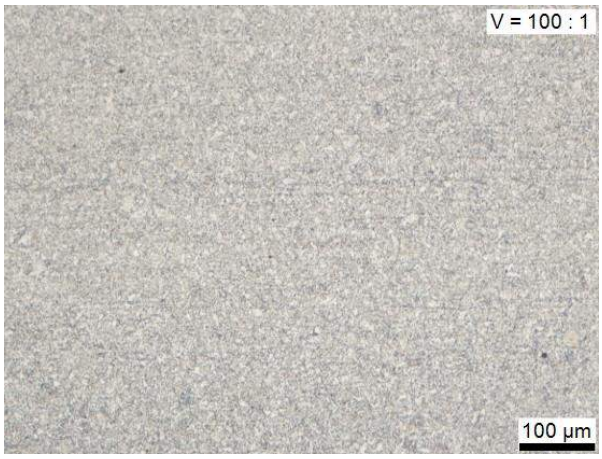

Fig.: 110 0007269
FTF3_l_S2
Middle x100

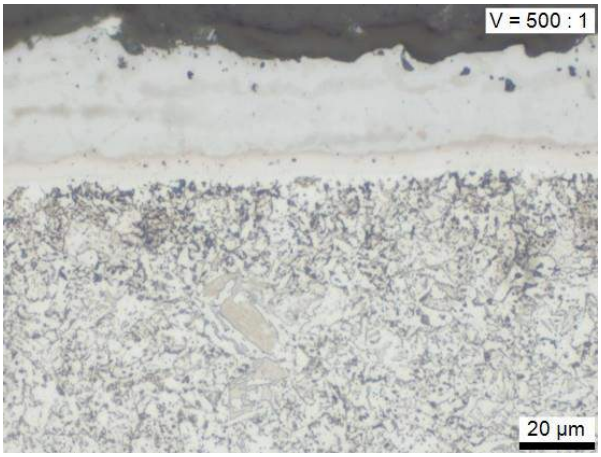

Fig.: 111 0007267
FTF3_l_S2
Edge x500

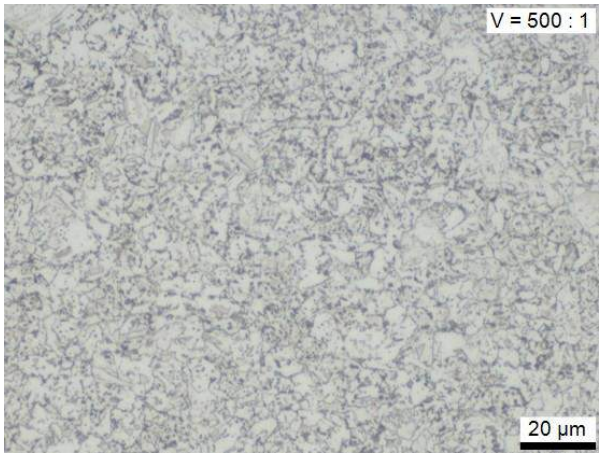

Fig.: 112 0007270
FTF3_l_S2
Middle x500

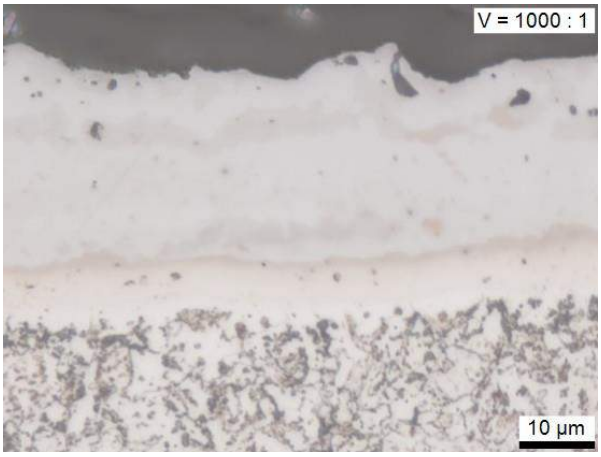

Fig.: 113 0007268
FTF3_l_S2
Edge x1000

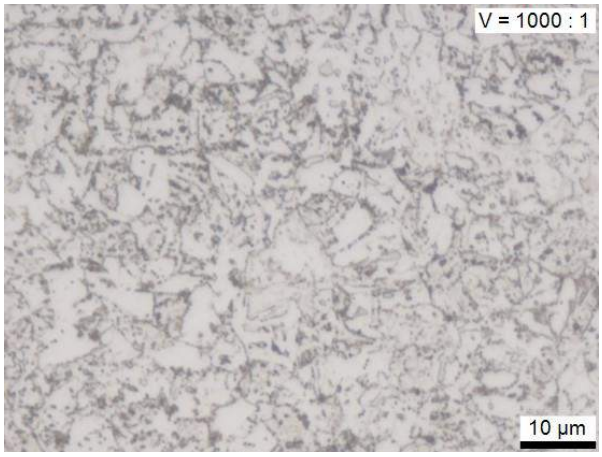

Fig.: 114 0007271
FTF3_l_S2
Middle x1000

FTF3_u1:

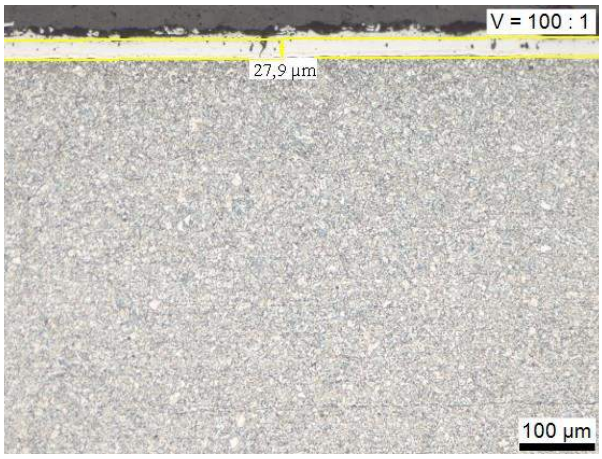

Fig.: 115 0007304
FTF3_u1_S2
Edge x100

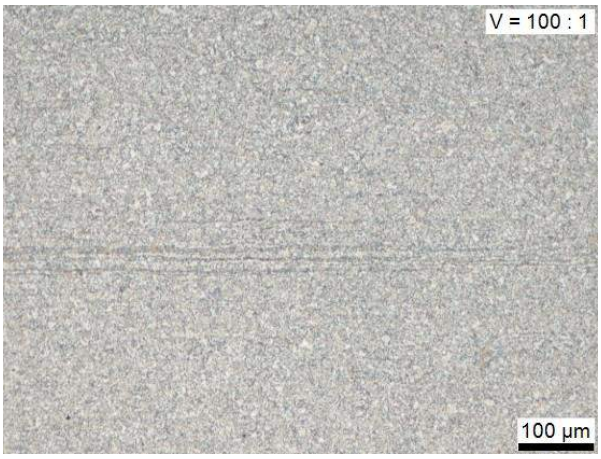

Fig.: 116 0007307
FTF3_u1_S2
Middle x100

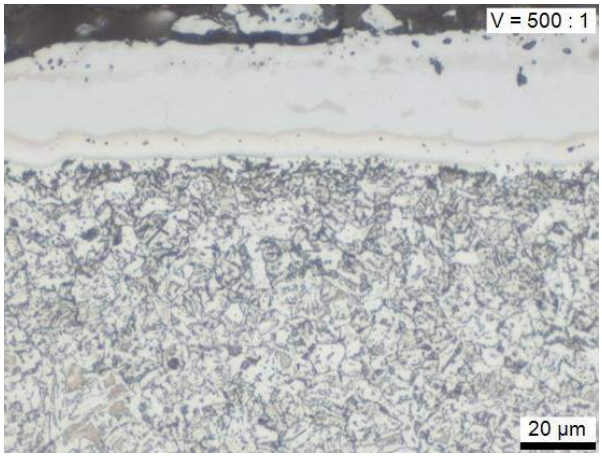

Fig.: 117 0007305
FTF3_u1_S2
Edge x500

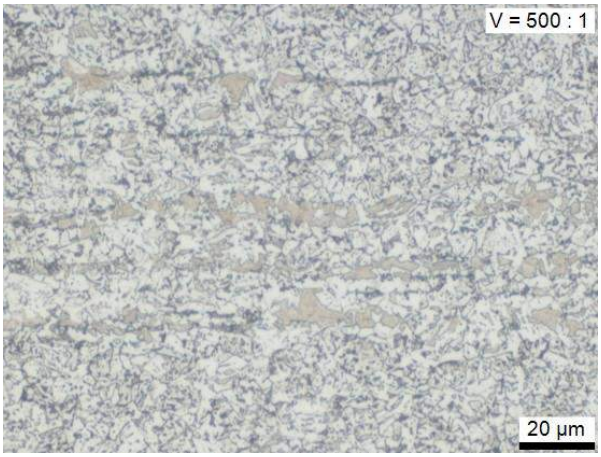

Fig.: 118 0007308
FTF3_u1_S2
Middle x500

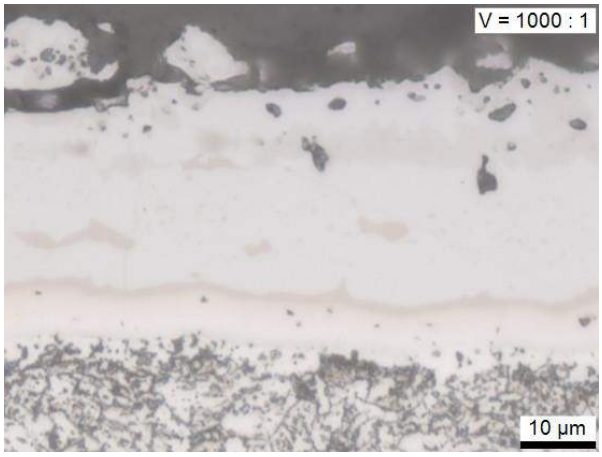

Fig.: 119 0007306
FTF3_u1_S2
Edge x1000

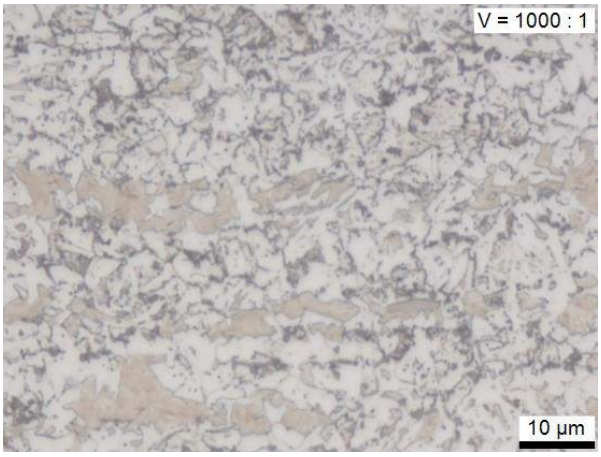

Fig.: 120 0007309
FTF3_u1_S2
Middle x1000

FTF3_u2:

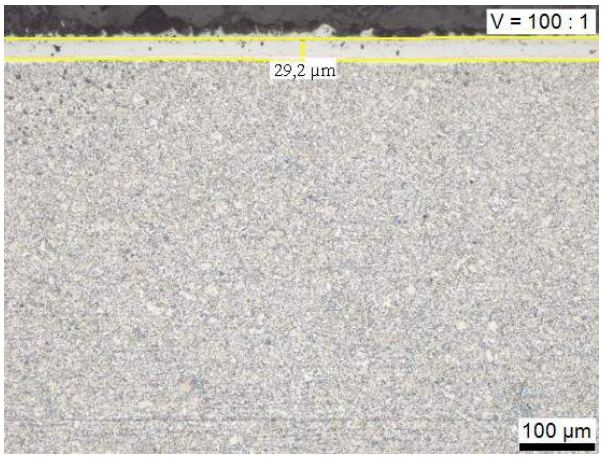

Fig.: 121 0007312
FTF3_u2_S2
Edge x100

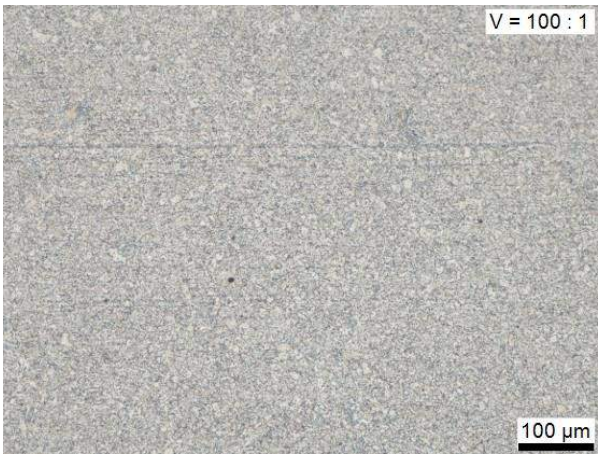

Fig.: 122 0007315
FTF3_u2_S2
Middle x100

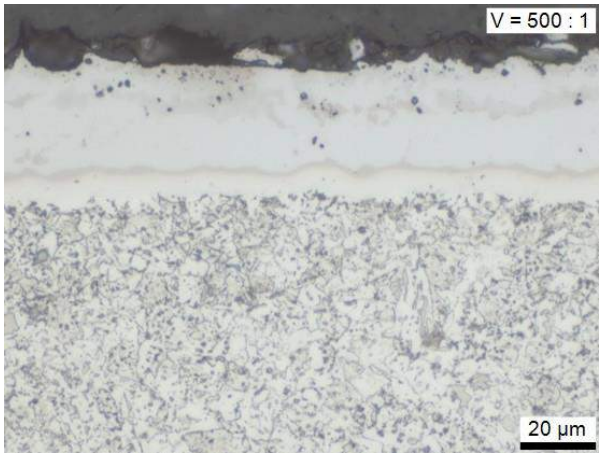

Fig.: 123 0007313
FTF3_u2_S2
Edge x500

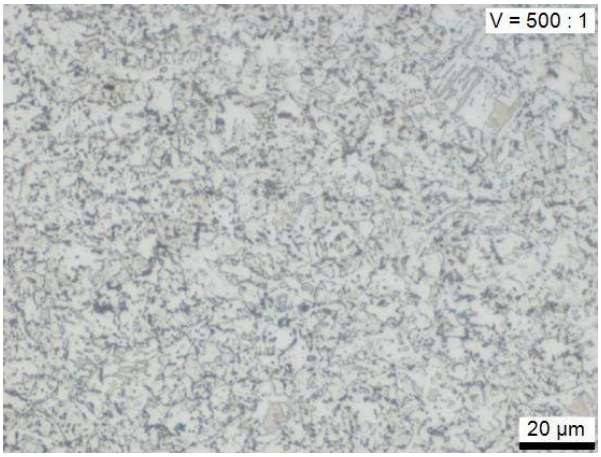

Fig.: 124 0007316
FTF3_u2_S2
Middle x500

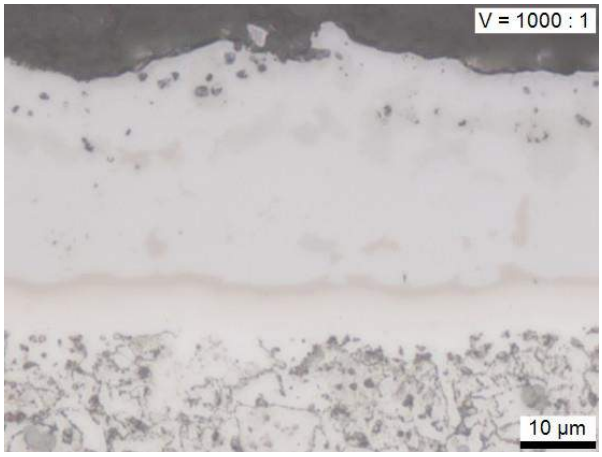

Fig.: 125 0007314
FTF3_u2_S2
Edge x1000

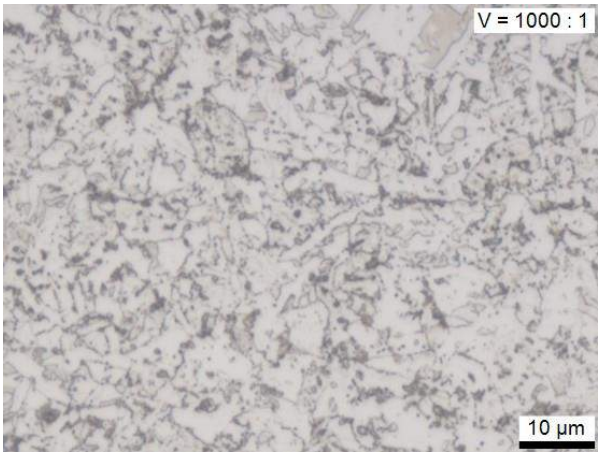

Fig.: 126 0007317
FTF3_u2_S2
Middle x1000

FTF4_l:

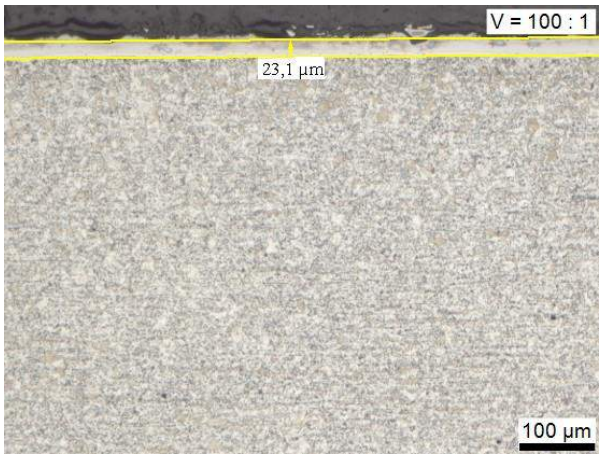

Fig.: 127 0007347
FTF4_l_S2
Edge x100

Fig.: 128 0007350
FTF4_l_S2
Middle x100

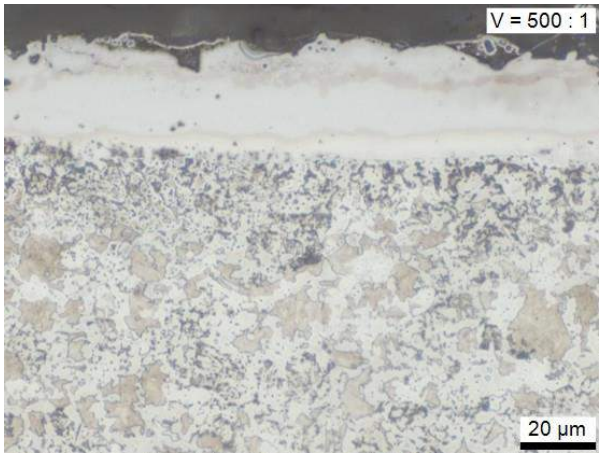

Fig.: 129 0007348
FTF4_l_S2
Edge x500

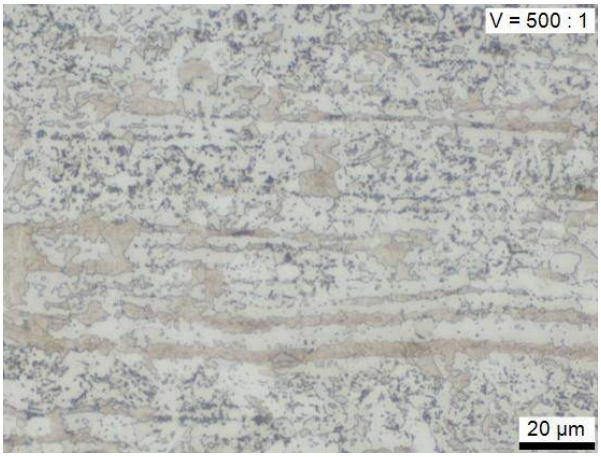

Fig.: 130 0007351
FTF4_l_S2
Middle x500

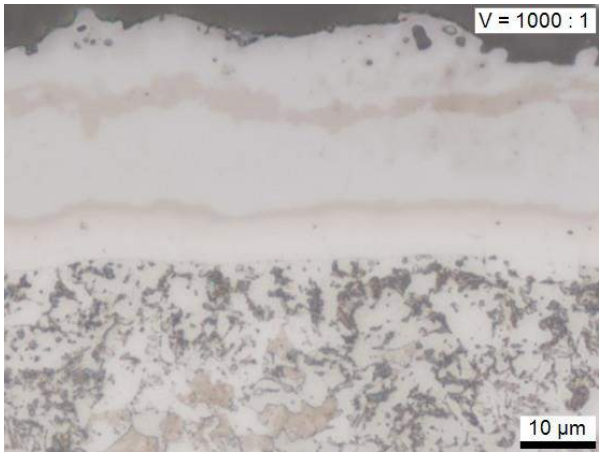

Fig.: 131 0007349
FTF4_l_S2
Edge x1000

Fig.: 132 0007352
FTF4_l_S2
Middle x1000

FTF4_u1:

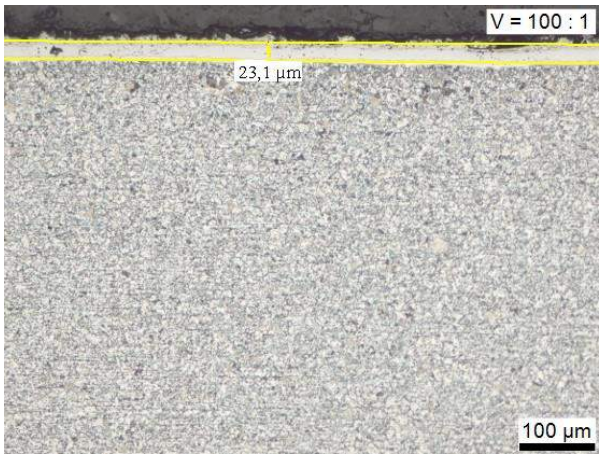

Fig.: 133 0007319
FTF4_u1_S2
Edge x100

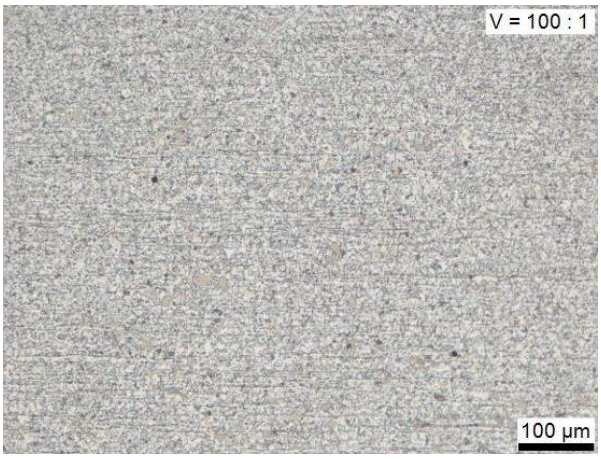

Fig.: 134 0007322
FTF4_u1_S2
Middle x100

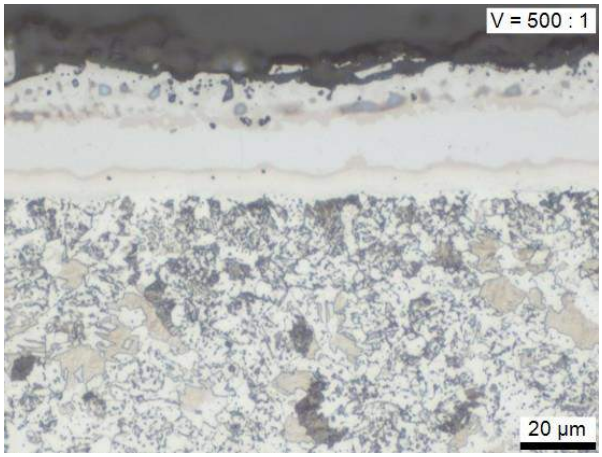

Fig.: 135 0007320
FTF4_u1_S2
Edge x500

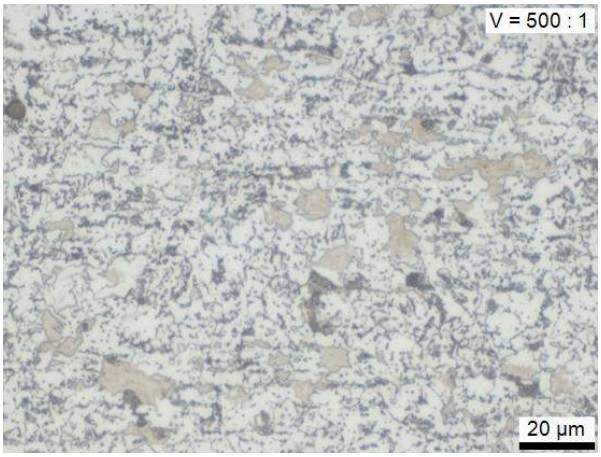

Fig.: 136 0007323
FTF4_u1_S2
Middle x500

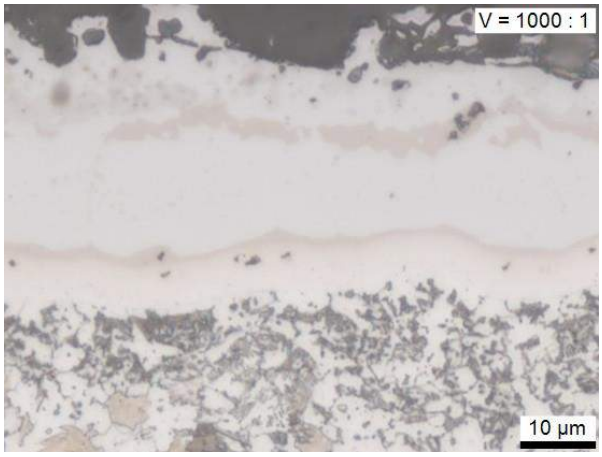

Fig.: 137 0007321
FTF4_u1_S2
Edge x1000

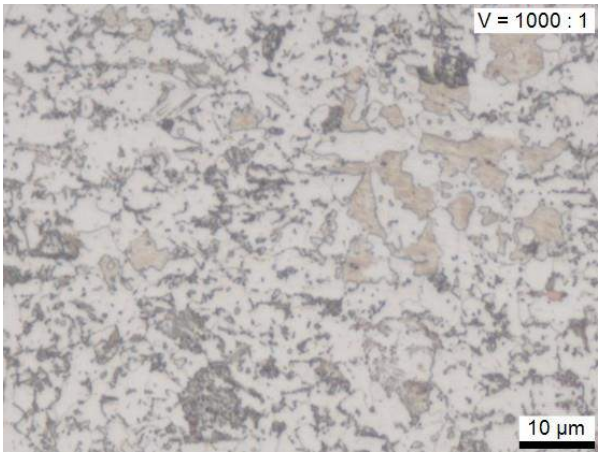

Fig.: 138 0007324
FTF4_u1_S2
Middle x1000

FTF4_u2:

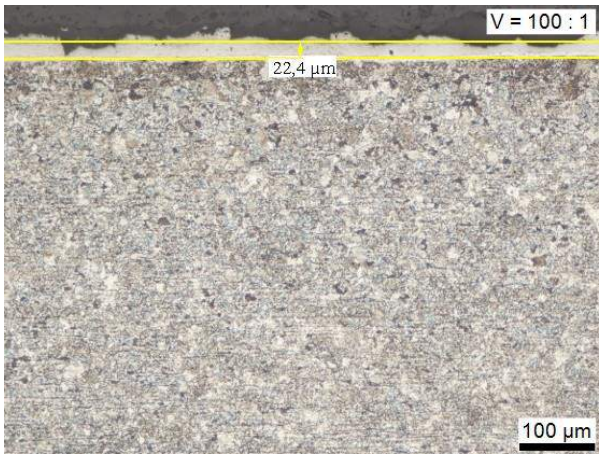

Fig.: 139 0007333
FTF4_u2_S2
Edge x100

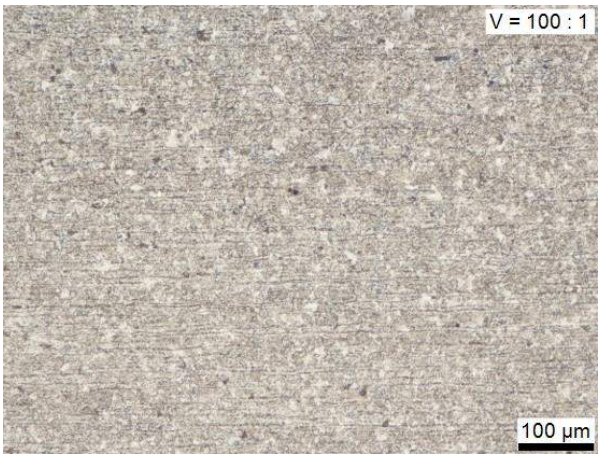

Fig.: 140 0007336
FTF4_u2_S2
Middle X100

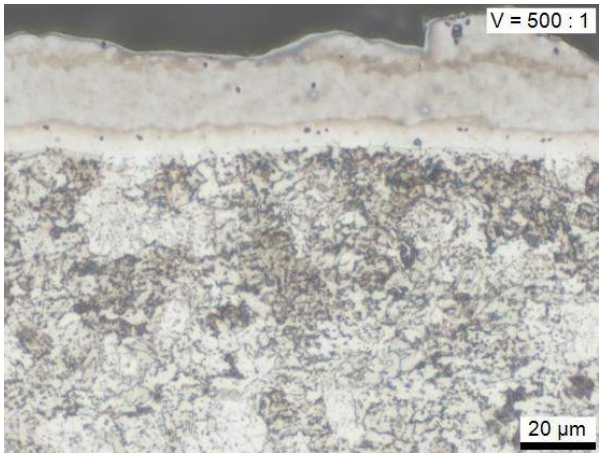

Fig.: 141 0007334
FTF4_u2_S2
Edge x500

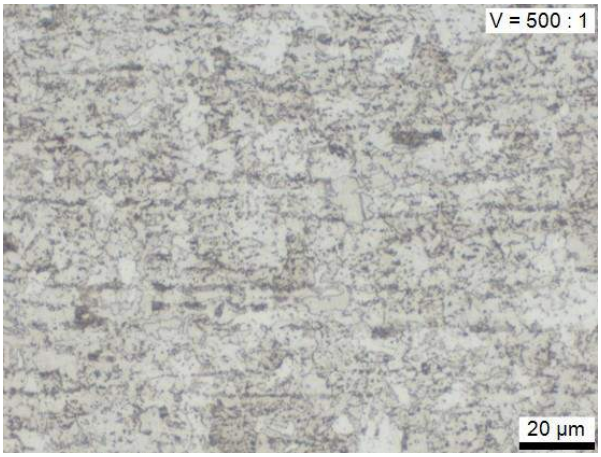

Fig.: 142 0007337
FTF4_u2_S2
Middle x500

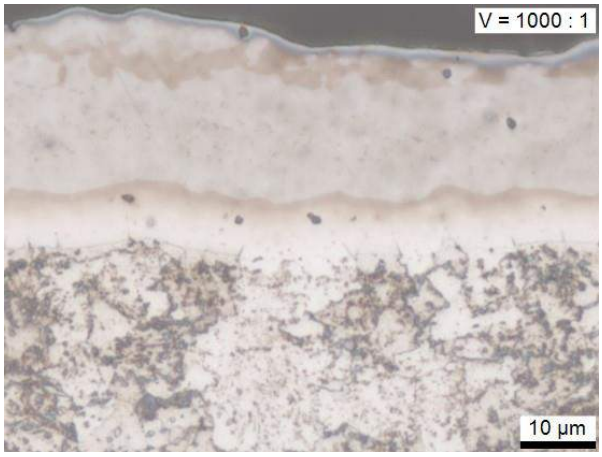

Fig.: 143 0007335
FTF4_u2_S2
Edge x1000

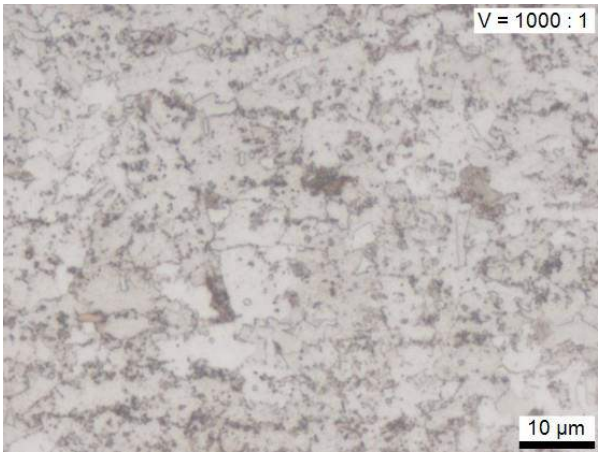

Fig.: 144 0007338
FTF4_u2_S2
Middle x1000